Contract Report 609

Investigations of Purposeful and Inadvertent Weather and Climate Modification and the Implications of Altered Atmospheric Conditions

by
Stanley A. Changnon, Robert R. Czys, Steven E. Hollinger,
Floyd A. Huff, Robert W. Scott, and Nancy E. Westcott

Prepared for the
National Oceanic and Atmospheric Administration

March 1997

Illinois State Water Survey
Atmospheric Sciences Division
Champaign, Illinois

A Division of the Illinois Department of Natural Resources

INVESTIGATIONS OF PURPOSEFUL AND INADVERTENT WEATHER AND CLIMATE MODIFICATION AND THE IMPLICATIONS OF ALTERED ATMOSPHERIC CONDITIONS

By

Stanley A. Changnon, Robert R. Czys,
Steven E. Hollinger, Floyd A. Huff, Robert W. Scott,
and Nancy E. Westcott

FINAL REPORT
to the Board of Trustees of the University of Illinois
pursuant to
National Oceanic and Atmospheric Administration
Award No. NA47RA 0225

Illinois State Water Survey
Champaign, IL

February 1997

CONTENTS

Page

A. Introduction 1

B. Numerical Simulations of Seeding Effects on Illinois Clouds 8

C. Research on Mitigating Ice Accumulations from Freezing' Rain 23

D. Preliminary Study of Physical Conditions Associated with Large Responses to Seeding 53

E. Integration of 1989 PACE Cloud Data with Laboratory Results to Improve Understanding about the Origin of Ice in Illinois Cloud 74

F. Dry Periods in Illinois 105

G. Inadvertent Weather and Climate Modification 106

Temporal Variability of Thunderstorms and Hail 106
Urban Effects on Lightning Activity 106
Changes in Cirrus Cloud Cover Due to Contrails and Effects on Climate 112
Urban and Lake Influences on Precipitation in the Chicago Region . . 112

H. Effects of Altered Weather Conditions on the Corn Crop 149

I. Impacts and Responses to Weather and Climate Conditions 278

Relationship of Weather and Climate to Government Policies 278
Impacts of Climate Change on the Chicago Area 278
Detection of Climate Change in Illinois 278
Shifts in Precipitation and Streamflow 279

Appendix 281

Project Publications 281
An Analysis of Possible Contrail Influence on Diurnal Temperature Range (David J. Travis) 287

SECTION A

INTRODUCTION

Stanley A. Changnon

The scientific research described herein has been conducted within the context of the Precipitation-Cloud Changes and Impacts Project (PreCCIP) of the Illinois State Water Survey from June 1994 to February 1997. PreCCIP, which ends its six-year research endeavors in February 1997, was originally entitled Precipitation Augmentation for Crops Experiment (PACE). PreCCIP and PACE represent a continuing program that has had a 15-year history of research relating to atmospheric modification.

The overall goal of PreCCIP has been to understand and measure a) the modification of atmospheric processes, resulting from inadvertent human activities or purposeful cloud seeding, and b) the impacts of altered weather and climate conditions on the hydrologic cycle, agricultural activities, and on the social and institutional structure of Illinois and the Midwest. Findings from the PreCCIP research concerning atmospheric processes and the effects of changed conditions have served as key inputs into a myriad of individual and institutional decisions affecting Illinois. They include major questions about 1) the application of cloud seeding to try to alter precipitation; 2) the magnitude and factors causing inadvertent climate change at the local and regional scales; 3) the types and importance of physical effects and socioeconomic impacts caused by altered weather, and 4) the monitoring, control, and regulation of activities leading to either purposeful or inadvertent modification of weather and climate. PreCCIP has thus embraced a wide range of scientific research including studies of physical processes in the

atmosphere, research to define how additional summer rain alters a corn crop and shifts farm income, and how altered weather conditions affect local, state, and federal governmental activities.

The research conducted since 1994 was defined on the basis of five major considerations. First were the findings from pre-1994 research. The findings from the 1981-1993 research have been summarized in a step-by-step approach to develop an understanding of atmospheric processes and their modification. The recent research was also based upon findings of the results of the 1986 and 1989 cloud modification experiments. The third factor affecting the design of the 1994-1997 research has been the status of our understanding of our research on effects of altered weather on various physical and socioeconomic systems. Our staff capabilities and facilities available to the project were a fourth factor influencing the research. The needs for scientific information relating to altered weather and climate in Illinois and the Midwest were a fifth factor in our research.

The 1994-1997 research of PreCCIP focused on three broad topical areas. Each of these has been embraced throughout the past seven years of the 13-year project. The first is a continuing study of cloud and precipitation processes. This has been an essential part of understanding how to purposefully modify precipitation in Illinois and the Midwest. Our studies of cloud and rain modification were based on the results of the 1986 and 1989 seeding trials in Illinois. Generally negative results concerning the dynamic seeding approach, coupled with limitations for nocturnal seeding at cloud top levels, have led us to conclude that a shift to assess different modification hypotheses and seeding approach was desirable.

The second programmatic area of PreCCIP has concerned studies of inadvertent

modification of weather and climate conditions in Illinois and the Midwest. Much of the desired research has been accomplished over the past seven years and research pursued since 1994 has been designed to increase our knowledge about urban and lake influences on precipitation and storms.

The third area of endeavor relates to studies of the effects of altered weather and climate conditions. This research has embraced studies of the impacts of altered conditions on water resources, agriculture, transportation, the economy, and government activities.

Rationale for Modification Research

The following section addresses a series of interrelated issues about a) the rationale and focus of the broad-based and diverse atmospheric modification research program, and b) the relevance of the program to Illinois, the Midwest, the nation, and NOAA's Atmospheric Modification Program (AMP).

The multi-year approach and diversity of research endeavors in PreCCIP resulted from critical state policies which establish the dimensions of the Illinois research program relating to atmospheric modification. These factors must be taken into consideration to understand the focus and dimensions of this research program in Illinois.

The concerns and interests over atmospheric modification in Illinois have been established by several conditions including: 1) the humid continental climate of the Midwest; 2) the concern over reliable sources of quality water including Lake Michigan, and 3) the mix of Corn Belt agriculture, heavy industry, diverse commerce, and huge urban areas where most Illinois citizens reside. The physical factors (climate and water supplies) and socioeconomic

factors interact to create broad dimensions framing the state's interest in atmospheric modification, a topic that has been identified in the Illinois Water Plan as one of the state's eleven key water issues (Changnon and Semonin, 1982).

Key questions Illinois identified 18 years ago (Changnon 1979) relating to atmospheric modification include:

- Can we modify clouds and/or precipitation (rain or hail) to enhance agricultural production or water supplies? Do we know enough to conduct operational cloud seeding projects?
- How should we control purposeful attempts to modify the weather? What is prudent to attempt and when?
- What is the areal extent, magnitude, and causes of inadvertent weather modification and resulting shifts in climate at the local, urban, and regional scales?
- What is the significance of modified clouds and precipitation, as measured in our natural systems (water, soils, etc.) and socioeconomically?
- What, if anything, should be controlled or regulated to address undesirable modification of weather? Inadvertent weather modification has created localized climate modification. Are weather-sensitive facilities or activities to be designed or done differently to cope with these changes? (For example, ISWS research detected heavier short-duration rainfall rates now occur over Chicago due to localized atmospheric influences, and these altered rain frequencies are now state-mandated as design rainfall values for Chicago.)

- What does study of local/regional-scale weather (and climate) modification teach us that helps the state derive policies relating to global climate change and related national environmental issues? (Illinois has a Global Climate Change Task Force which assesses these issues and recommends policy to the Governor.) .

The mission and nature of the Illinois State Water Survey (ISWS) means that it serves as the state's action arm for providing the scientific answers to the weather and climate questions listed above. The Survey's mission in atmospheric and hydrospheric research is to conduct the research and to provide the answers to such an array of questions.

The relevance of atmospheric modification to regional interests and national issues is a key because the constituency of PreCCIP should and has extended well beyond the boundaries of Illinois. The clouds and precipitation of Illinois are typical of those found throughout the central United States, and atmospheric modification techniques developed in Illinois will extend well beyond the state's borders. Findings about how the weather is modified in Illinois, and the impacts of modified conditions, are applicable to all other parts of the industrialized Corn Belt. Thus, the findings from Illinois have a) regional relevance, and b) national significance because of the state's and region's importance to the nation's economy.

The "nature" of Illinois' informational needs and the responsive research of the ISWS, as identified above, create a set of conditions which explain and indeed have shaped the dimensions of the ISWS's modification research in the past.

First, the scientific research necessary to address the issues can not be limited to the study of just weather modification "processes." The research has, of necessity, embraced various time and space scales of the atmosphere, as well as effects of changed weather conditions. For

example, the successful application of long-term cloud seeding to change rainfall over an area, if pursued for many seasons, creates a "modified climate." There is a continuum from weather modification into climate change at the local and regional scales. Hence, our research has logically embraced them both, but *not* at the larger scales (continental or larger) and which constitute changes in all atmospheric conditions.

Second, to understand weather modification requires an understanding of atmospheric modification. Integral to understanding purposeful and inadvertent weather modification is the *understanding of how natural modification occurs.* That is, the process by which water bodies and surface physiography alter the atmosphere and create local weather-climate anomalies must be addressed. One cannot define how St. Louis or Chicago alter the atmosphere and change clouds and precipitation without understanding and isolating the local-regional atmospheric effects of the Mississippi River Valley and the hills west of St. Louis, or the effects of Lake Michigan on the weather at Chicago. Study of atmospheric modification created by surface conditions also held many lessons useful for the conduct of purposeful modification.

Third, atmospheric modification research relevant to the Midwest and Illinois, is quite different from that in other parts of the nation where drastically different climates, water resources, and economic forces exist. Scientists in the arid areas of the west are driven to explore purposeful precipitation modification to enhance water supplies. The Illinois-based questions for cloud seeding designed to produce more water were: a) can we enhance precipitation in extended dry periods (and droughts), and b) could we enhance crops in drier growing seasons? Our research based on impacts of altered weather has already shown that the costs of developing a hail suppression capability, coupled with operational costs of a suppression

project, make hail suppression a non-viable economic alternative to hail insurance (Changnon and Morgan, 1976).

The analysis of effects of added water on Illinois corn and soybeans crops has provided results which indicate important needs for modification research. For example, it will be very difficult to make economically viable increases in summer rainfall unless a) we use forecasts of summer weather conditions and use the modification of rain based on dry season outlooks; and b) have a capability to enhance rainfall at night when nearly 50% of all summer rain occurs (and when current aircraft-based cloud-top seeding approaches cannot effectively function).

The fourth condition which has explained and shaped the dimensions of the Illinois program (PreCCIP), is the fact that ISWS research dealing with 1) purposeful weather modification; 2) inadvertent weather-climate modification; 3) modification by natural features; and 4) the impacts of modification by any process has been under way for 26 years. Research has moved ahead on many fronts, which are already undergirded, in most instances, by extensive scientific knowledge.

SECTION B

NUMERICAL SIMULATIONS OF SEEDING EFFECTS ON ILLINOIS CLOUDS

Robert R. Czys

Summary: The numerical simulations reported on here were conducted in an effort to better understand primary results about apparent seeding effects in the 1989, and to a certain extent those from the 1986 exploratory cloud seeding field programs. The 1989 field experiment yielded two contradictory results: 1) effects on individual (feeder) clouds indicated that if seeding had any effect at all it was negative on cloud growth, and 2) effects on the multi-celled system (i.e. the accumulation of feeder clouds) as a whole may have resulted in significant rainfall enhancements at least on a few occasions. Another purpose of the simulations was to begin to gather information that would be useful in determining if hygroscopic (i.e. salt) seeding would be more effective than AgI at producing a rain enhancement. Two different cases from the 1989 field program were chosen for simulation: 1) a June case characterizing could cloud bases and a weak coalescence process, and 2) a July case representing warm cloud bases and a moderately strong coalescence process.

The simulations resulted in several important findings. Seeding effects were found to be very sensitive to the time at which the seeding material was delivered to the cloud The June case was found to be not affected to the extent that the July case was, but early salt flare seeding in the June case produced a notable difference. Three distinct results in rainfall were apparent in the July case and these were partly due to timing. Both the salt (100 g km^{-1}) and salt flare at 93 min. produce the least rainfall along with salt at 108 min. A second group was formed by the

secondary ice cases and the AgI at 120 case. The secondary ice produced effects similar to AgI, and the rainfall amounts resulted in decreases from the standard run at about 10 kT km^{-1}. The last group produced little effect on rainfall. This group is the late AgI and salt flares at 105 and 108. This shows that timing of seeding is quite important.

These simulations were performed as part of a subcontract with the Institute of Atmospheric Sciences at the South Dakota School of Mines and Technology and was presented at the 13th AMS Conference of planned and Inadvertent Weather Modification, held January 28 - February 2, 1996, Atlanta Georgia.

1. Introduction

Cloud seeding experiments are conducted in Illinois by the Illinois State Water Survey as part of the Precipitation Augmentation for Crops Experiment (PACE). This ongoing experiment conducted by the Illinois State Water Survey since 1978 is trying to address two fundamental questions relating to precipitation enhancement in Illinois: Can it be accomplished? and is it worth doing? (Czys *et al. 1995)*. The 1989 field project for PACE produced a number of good experimental units. The seeding operations used silver iodide for seeding and sand as a placebo. This was a randomized seeding experiment. The primary study area was located within a 100 mile radius of Champaign-Urbana.

The seeding hypothesis of PACE was designed around a dynamic seeding hypothesis. They expected a net increase in buoyancy by a release of a latent heat of freezing when a conversion of liquid water to ice particles occurs. Seeding effects were hypothesized to be communicated downward and result in an increased moisture convergence below cloud base.

They anticipated that this may result in a stronger development of clouds and may produce cloud mergers.

The numerical simulations reported on in this paper were conducted on two particular case study days, June 23 and July 23, 1989. These two days were chosen because they represent two quite different types of air masses and somewhat different dynamics. The July case was a more stable case. Numerical simulations have been run on both clouds for a standard or unseeded case. See Appendix for depiction of results. Then various seeding experiments were performed on the standard cases. Both silver iodide and salt seeding were simulated. The silver iodide involves simulating droppable flares through the cloud tops when the cloud tops reach the -10' C level consistent with what was done in the operational program. The salt experiments, while not done operationally in 1989, are anticipated for the future. We have therefore simulated the release of 100 kilograms of salt per kilometer into the updraft below cloud base as well as simulated the burning of 500 grams per kilometer of salt-type flares. The salt flares were below cloud base also.

2. Cloud model

The cloud model is described in Orville and Kopp (1977) and Lin *et al*. (1983). The model is two-dimensional time dependent with an extent of 20 kilometers in the horizontal and the vertical. The model is composed of a finite difference grid with a grid spacing of 200 meters in both the horizontal and the vertical. Non-linear differential equations are solved for the fundamental variables of potential temperature, total water and vorticity. Pressure is eliminated from the horizontal and vertical equations of motion resulting in a vorticity equation. The

evolution of the vorticity permits a stream function to be defined from which the horizontal and vertical wind is calculated. Also, an equation for a form of entropy is used which permits us to deduce saturated conditions. This leads to additional non-linear differential equations for the cloud water, water vapor, rain, cloud ice, graupel and snow fields.

a. AgI seeding

Hsie *et al*. (1980) goes into detail concerning AgI seeding simulations. A conservation equation is used for the seeding agent. The AgI is advected throughout the grid and interacts with the supercooled liquid water and rain. As the AgI interacts, the seeding agent field is "used up" at appropriate rates and the AgI disappears from the grid. Once AgI interacts with liquid and forms ice, that AgI is not available again.

b. Salt seeding

Operational salt seeding can be divided into two categories; first, the older technology of using fine salt particles at rates of 100 kg km^{-1} below cloud base; and second, the new technology of salt flares, which produce a smaller salt particle enhancing the number of large cloud droplets. The first technology produces drizzle drops very quickly from the large salt particles. The salt flares enhance the coalescence process by increasing the number of large droplets in the cloud leading to earlier or faster production of rain. Both of these salt seeding technologies are simulated in the cloud model.

The first technology is simulated by activating the seeding agent field in the model (Hsie *et al*, 1980) and converting the salt and cloud water into rain. Thus, at grid points with both salt and cloud water, rain is produced at the rate of 50 g rain for each g of salt with the water taken from the total water (cloud water plus water vapor) budget. Effectively, this reduces the cloud

water (transforms cloud water to rain). The salt has a half life of 15 seconds to reduce numerical noise so rather than instantly transforming all of the salt to rain in one time step a few time steps are required. Seeding rates of 100 kg km^{-1} are simulated in these runs.

For the salt flare simulations, autoconversion is turned-on where the seeding agent is located. The seeding agent then decays at 1150 the rate of rain water production from autoconversion. Seeding rates are greatly reduced for this technology with rates of 500 g km^{-1} used in these simulations.

c. Secondary Ice

In the July case some experiments were run with secondary ice turned on. (Aleksic *et al.* 1989). This process is the Hallett-Mossip generation of ice particles from graupel-large cloud drop collisions. A standard, AgI, and salt case are run with secondary ice turned on.

3. Experiments

The soundings used are shown in Figure 1. The June 23, 1989 sounding was taken at the Willard Airport at Champaign at 1:00 P.M. local time. The July sounding was taken at 12 Z at Peoria. One can see the July sounding is somewhat more stable than the June sounding. There is more surface water in the July sounding, but, there is somewhat less water vapor above the surface to 700 mb. The standard June simulation is done with 5×10^{-5} convergence whereas in the July case no convergence is imposed.

With the standard case established for the June case, a silver iodide case is initiated at a simulated time of 48 minutes when the cloud top reached the -10°C level. Salt cases are initiated at 45 minutes with a 100 kg km^{-1} case and a salt flare case. Another salt flare case is initiated at 42 minutes. The salt cases are initiated at a somewhat earlier period of time because the clouds

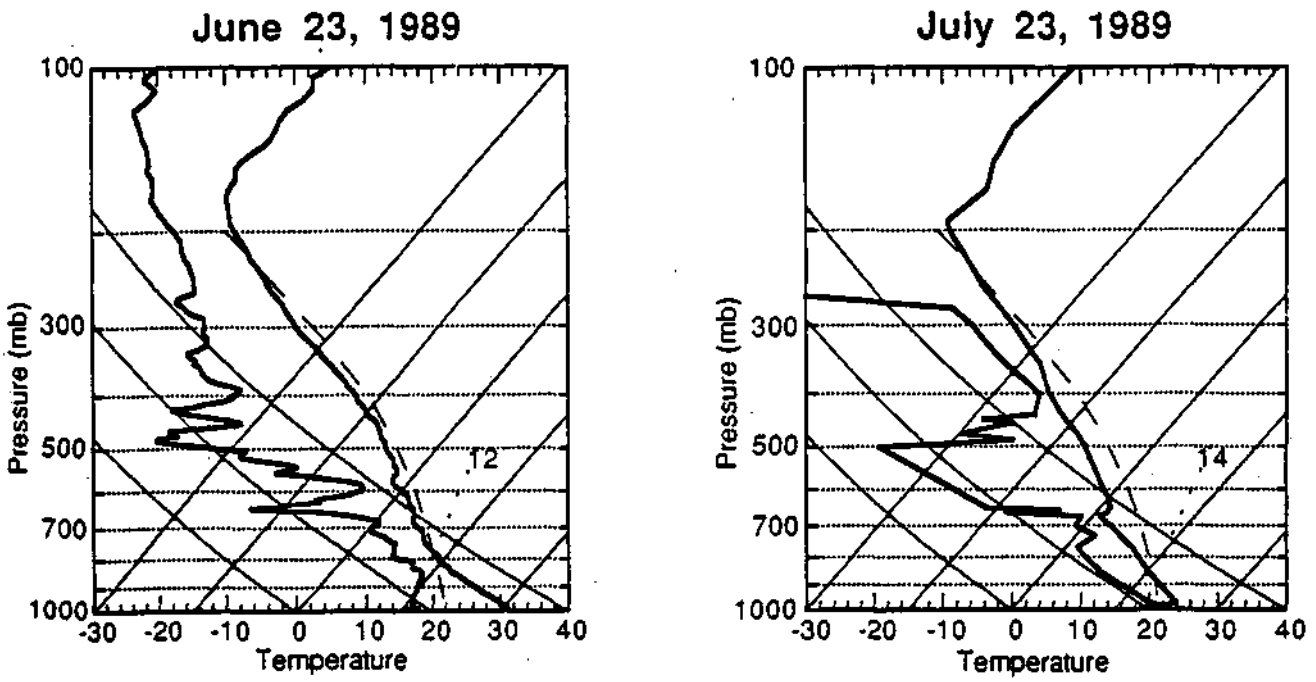

Figure 1. Soundings used to initiate cloud model for the two cases reported on here. The diagrams are Skew T-log P format The 12 and 14 demark a 12 and 14 g kg^{-1} mixing ratio line and the dashed line is a representative wet adiabate.

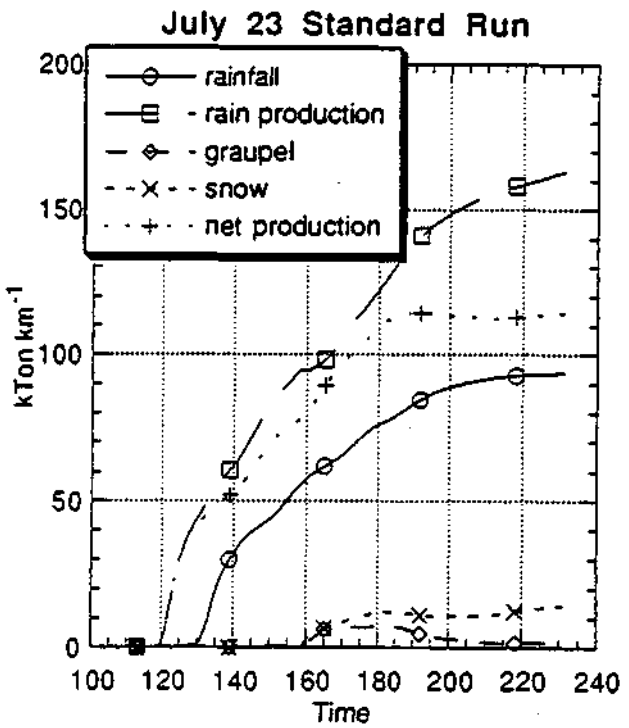

Figure 2. July 23 Standard Run showing amounts of precipitation versus time (min.). Production for liquid and ice is the amount produced during simulation that is not converted to another form. The amounts are in kiloTons (kT) per kilometer and are integrated over entire grid.

have developed a significant amount of cloud water and with salt seeding it is not necessary to reach the -10°C level before seeding can be effective.

With the July standard case established a number of experiments are performed with both salt and silver iodide. The silver iodide seeding is initiated at 120 minutes of simulated time. The 100 kg salt seeding case is done at 93 minutes and at 108 minutes. In the later salt seeding case, secondary ice production is simulated. A natural case is then run with secondary ice. Another silver iodide case is run with seeding done at 147 minutes and three salt flare cases are run at 93, 105 and 108 minutes with no secondary ice.

4. Results

a. July Case

The rainfall amount on the ground for the standard run is 93 to 94 kTons km^{-1} shown in Fig. 2 as a solid line. Total net production, the total of the rain, graupel and snow production less evaporative effects, begins its production at 120 min. and continues to about 190 min. (Fig. 2). Rain is still forming from melting snow and graupel. The standard run produces very little precipitation in the form of either graupel or snow, with peak amounts at 10 - 15 kT km^{-1}. The graupel melts into rain from 180 to 220 min., while the snow remains suspended or new snow replaces old at a steady rate.

Figure 3 is a comparison of the rainfall for all the seeding runs. Rainfall from the standard run is subtracted from the seeded run, so if there is a positive difference on the graph this is an indication of an increase and all of the cases show early increases in the rainfall with the later results showing a reduction of up to 30 kT km^{-1} on the ground. The 100 kg km^{-1} salt

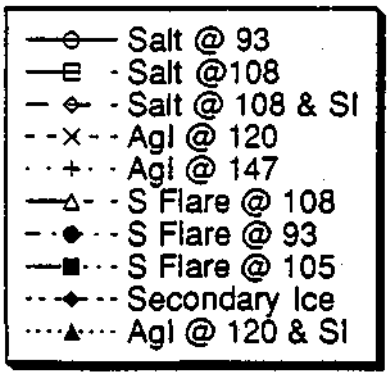

Figure 3a. Symbols used in difference graphs for July cases. Each line in the graphs have a distinct symbol and pattern (solid, dashed, dotted, etc.) so one can be distinguished from another.

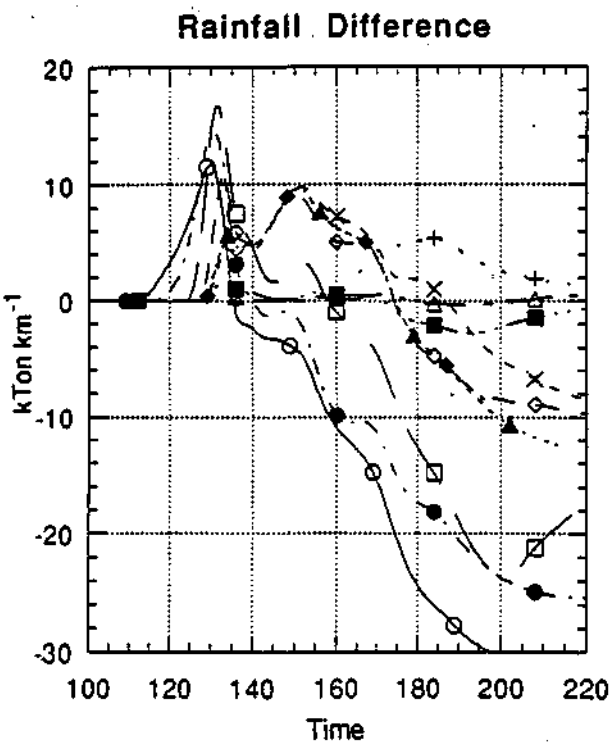

Figure 3. Rainfall differences for seeded cases relative to standard run. The standard case is subtracted from seeded run. See the symbol chart in Fig. 3a for key to cases.

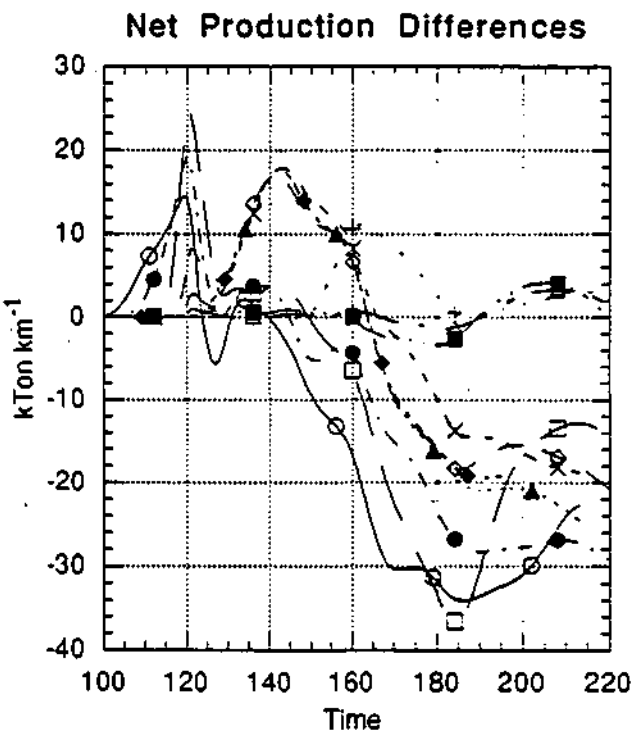

Figure 4. Net production of all precipitation differences. The production of rain, graupel and snow are totaled for each simulation and the standard run is subtracted to give a difference. See Fig. 3 a for key to symbols.

seeding case that was done at 93 min. resulted in the largest decrease in rainfall toward the end of the simulation amounting to 30 $kTkm^{-1}$. This particular case also shows the earliest rainfall on the ground peaking at about 130 min. The standard run by comparison in Fig. 2 does not produce any rainfall on the ground prior to approximately 130 min. Thus we see that the early salt seeding produces rain earlier and tends to load the updraft and produces rain on the ground earlier which apparently resulted in a reduction in the overall dynamics of the cloud.

One can see from Figure 4 that the early salt case results in a net reduction in overall precipitation production after 140 min. The salt cases did not add to the hail production or snow production which is quite low in the standard case to begin with. Analysis of the hail production and snow production shows that the salt cases actually do result in reductions in hail and snow in the time frame after 160 min. which also suggests that the early seeding results in reduced dynamics in the later stages of the cloud and thus reduces the overall precipitation. The salt case seeding at 108 min. has less impact on the rainfall but still amounts to about a 20 km^{-1} decrease overall.

The silver iodide cases on the other hand tend to produce a much different seeding effect. The silver iodide is released at 120 min. and the differences (Fig. 4) show after 130 min. The increases can be seen to continue throughout the period of time from 130 to nearly 160 min. Included with the AgI case are the secondary ice cases that follow along the production and rainfall curves. One of these cases is also the standard case with the secondary ice production turned on. All of these cases tend to result in about a 10 kT per km reduction in overall rainfall.

The salt flare and late AgI are more successful. The late seeding with silver iodide case produced a positive result of about 1 or 2 kT per km. The salt flare at 108 and 105 min. produce

little effect on rainfall (Fig. 3) although the net production shows a slight increase. The early (93 min.) salt flare is comparable to the other salt cases with decreases of 25 kT km^{-1} in rainfall.

b. June Case

Total rainfall shown in Figure 5 for the June case amounts to about 130 kT per km by the end of the run at 120 min. There is a slight amount of hail in-cloud which shows that this case is more active than the July case. The ice processes are far more active in this particular case than they are in the July case. Graupel production reaches nearly 40 kT per km at about 60 minutes and snow production reaches 30 k-T per km. The greater instability in tills case combined with the convergence results in a much faster developing cloud. We see that the cloud development is actually over by 120 minutes, whereas in the July case growth is only getting started by 120 minutes.

Silver iodide seeding is performed at 48 minutes, as shown in Figure 6, and rainfall is reaching the ground by 60 minutes. It continues to exceed the standard case up to 70 minutes with a peak increase of nearly 5 kT per km on the ground. After lagging behind the standard case a bit, the total increase is about 4 kT per km. The flare salt seeded cases result in a very slight increase in rainfall. The salt case at 45 minutes with 100 g km^{-1} results in a slight but negligible decrease in rainfall, whereas the flare cases result in about ½ kT per km increase. The hail fall difference is not shown but is very small.

The net precipitation production differences shown in Fig. 7 demonstrate that all of the seeding cases result in some increases at some time during the simulation. The silver iodide case is much more effective at producing increases in precipitation inside the cloud. Particularly in

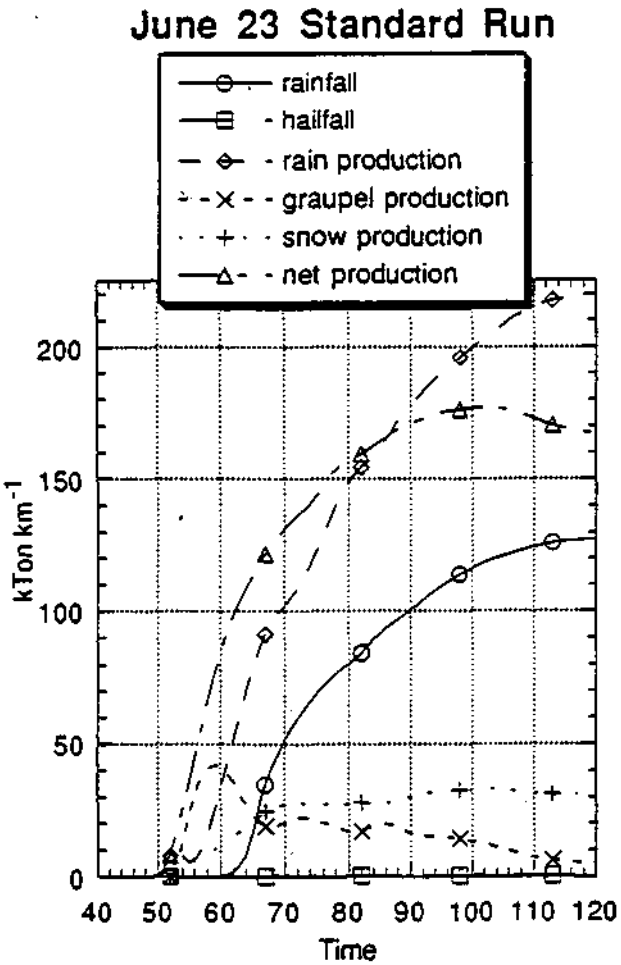

Figure 5. Standard run results for June 23 cases. See fig. 2 for further explanation.

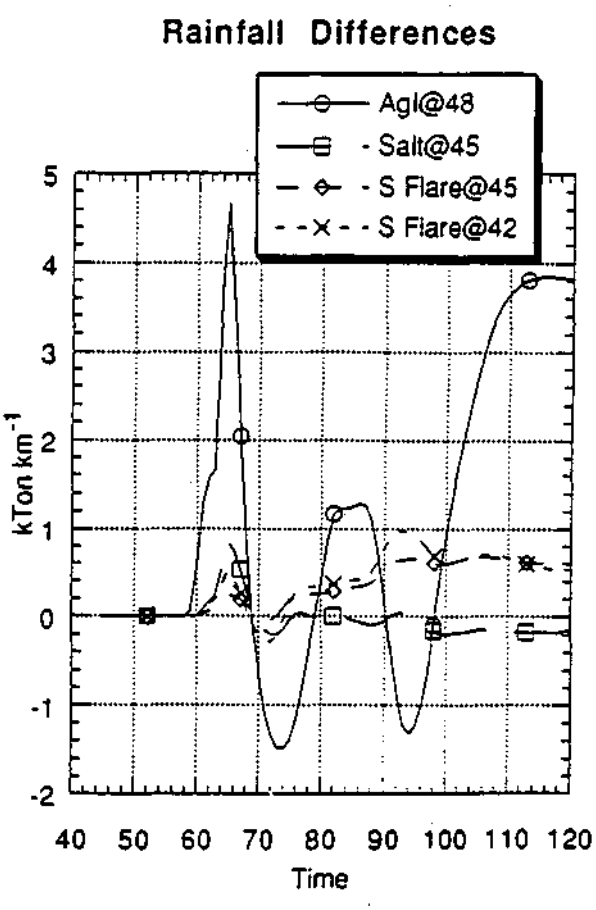

Figure 6. Rainfall differences for June case. Much like Fig. 3 except symbols are embedded in graph.

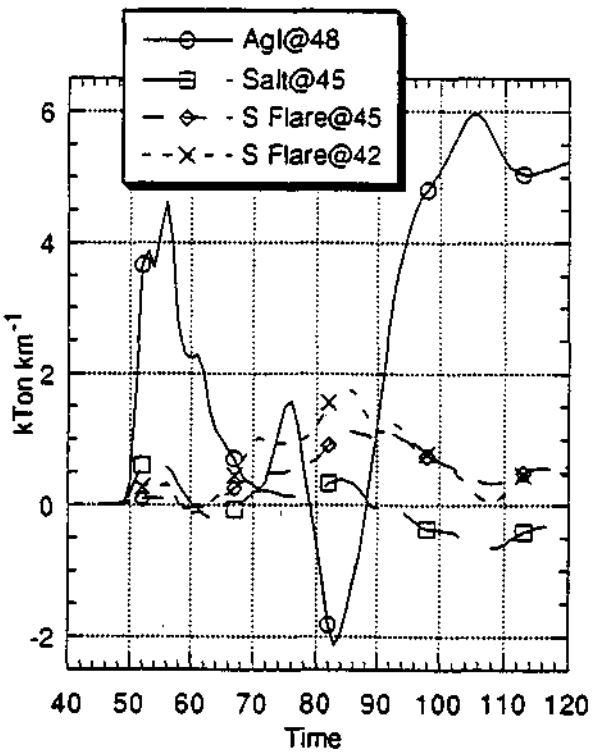

Figure 7. Net production for June case. Like Fig. 4 except symbol key is embedded in graph.

the few minutes following seeding, and then again toward the end of the cloud's life time. The salt cases are much slower to have an effect but maximum effects are apparent approximately 40 minutes after seeding. While not shown here, the silver iodide primarily initiates an ice phase increase in the early stages after seeding which then eventually melts and forms rain in the later stages of the simulation. The salt cases do have minor increases in the ice phase, but the rain production is increased too. Thus, it is very difficult to conclude that any one phase produced the salt increases. Of course, the salt increases are very modest compared to the silver iodide.

5. Conclusions

Clearly the timing of seeding is critical in both of these cases. The June case is not affected to the extent that the July case is by seeding, but the early salt flare in the June case did produce a distinct difference, as seen in Fig. 7. Three distinct results in rainfall seem apparent in the July case from consideration of the rainfall effects shown in Fig. 3. Part of this difference is due to timing. Both the salt (100 g km^{-1}) and salt flare at 93 min. produce the least rainfall along with salt at 108. A second group is formed by the secondary ice cases and the AgI at 120 case. The secondary ice produces effects similar to AgI and the rainfall amounts result in decreases from the standard run at about 10 kT km^{-1}. The last group produces little effect on the rainfall. This group is the late AgI and salt flares at 105 and 108. This shows that timing is quite important. The type of seeding material is also of importance and the choice of material affects the timing choices.

7. References

Aleksic, N.M., R.D. Farley and H.D. Orville, 1989: A numerical cloud study of the Hallett-

Mossip ice multiplication process in strong convection. *Atmos Res.*, **23**, 1-30.

Czys, R.R., S.A. Changnon, N.E. Westcott, R.W. Scott and M.S. Petersen, 1995: Responses of warm-based, midwestern cumulus congestus to dynamic seeding trails. *J App. Meteor.*, **34**,1194-1214.

Hsie, E.Y., R.D. Farley and H.D. Orville, 1980: Numerical simulation of ice-phase convective cloud seeding. *J. App. Meteor.*, **19**, 950-977.

Orville, H.D. and F.J. Kopp, 1977: Numerical simulation of the history of a hailstorm. *J. Atmos. Sci.*, **34**, 1596-1618.

Lin, Y.L., R.D. Farley and H.D. Orville, 1983: Bulk parameterization of the snow field in a cloud model. *J. Climate and Applied Meteorology*, **22**, 1065-1092.

8. APPENDIX

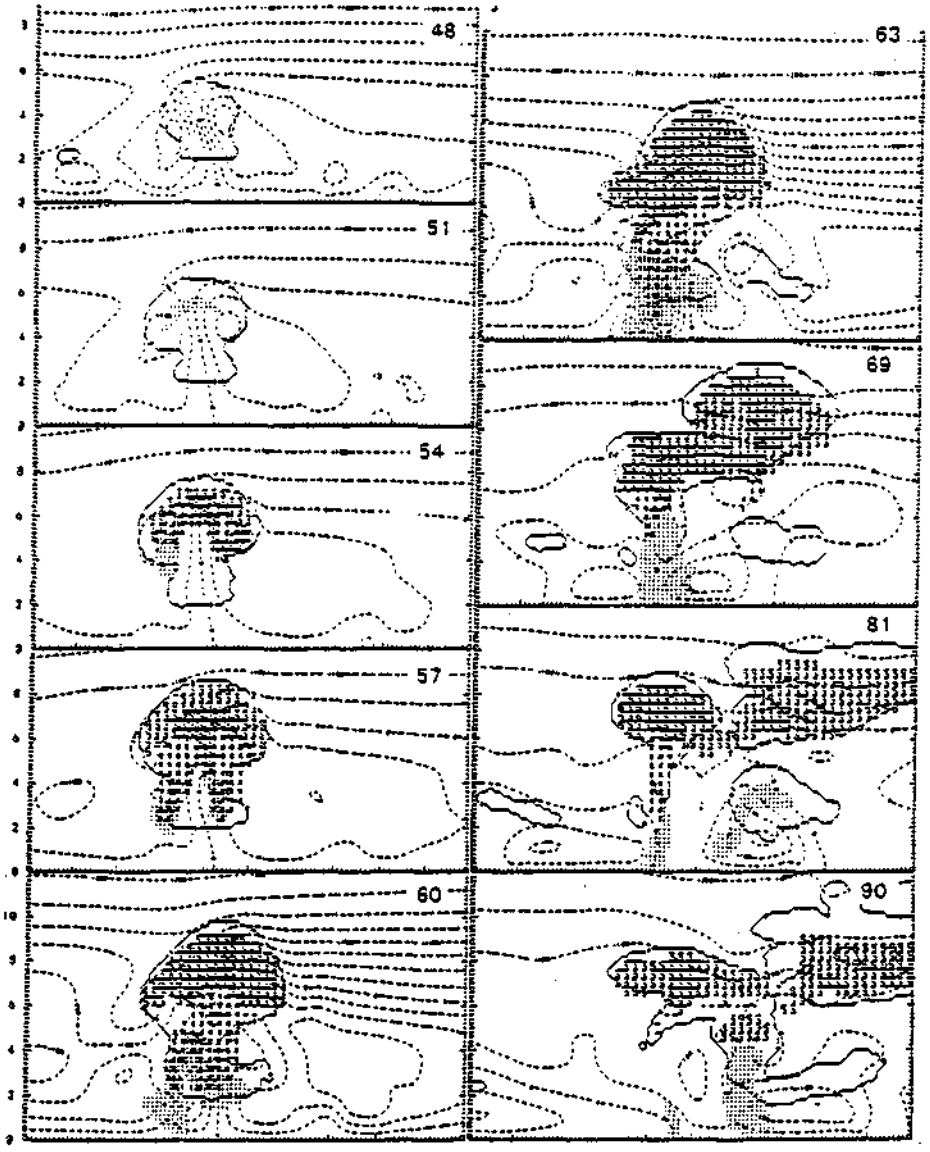

Figure 1 a.

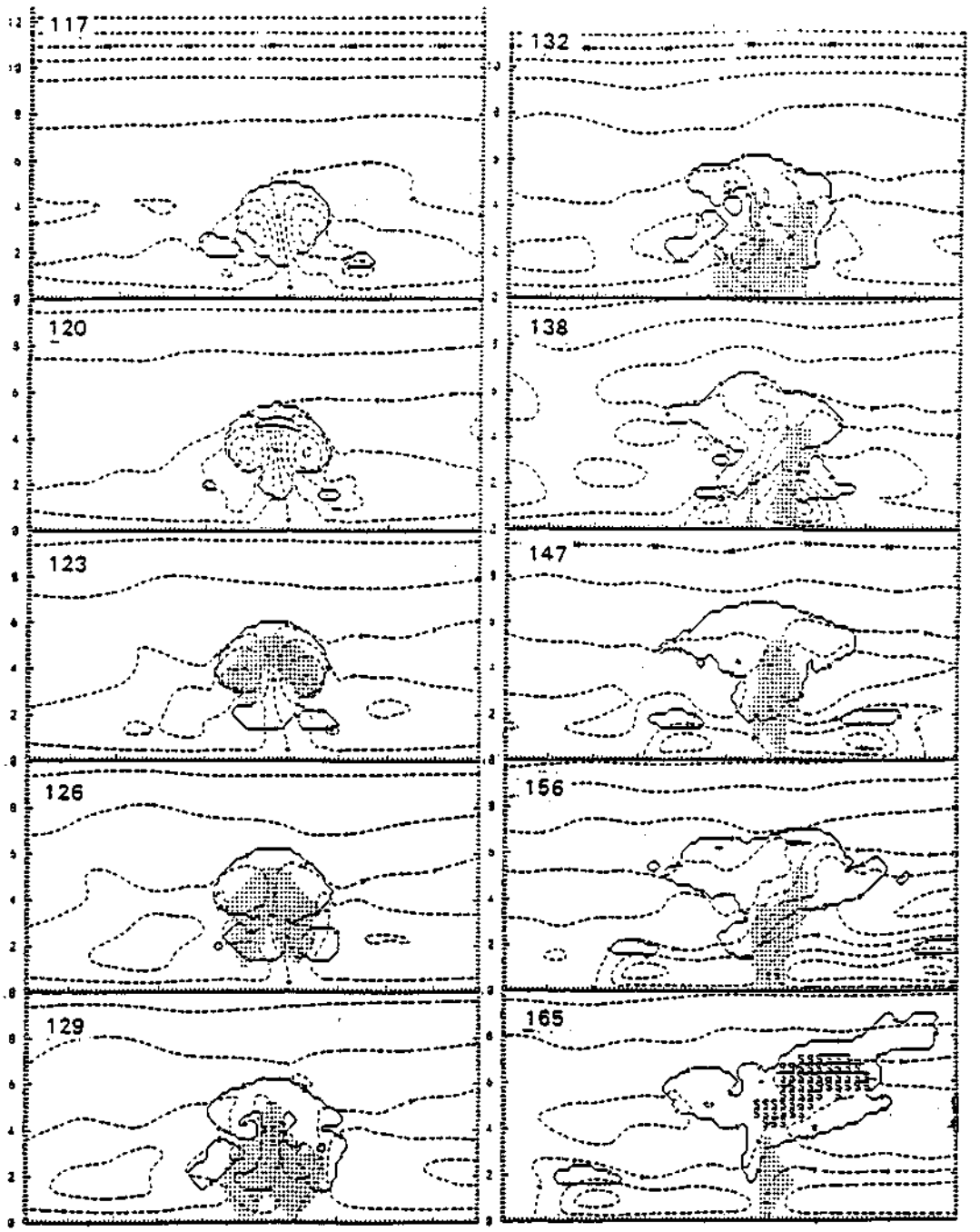

Figure lb. June (Fig. la) and My (Fig. lb) standard runs. Cloud outline is shown by solid line, dashed lines are stream lines, dots are rain, * is graupel and S is snow. Simulated time is in upper right corner.

SECTION C
RESEARCH ON MITIGATING ICE ACCUMULATIONS FROM FREEZING RAIN

Robert R. Czys

Summary: This section summarizes progress made in the development of cloud seeding to convert freezing rain to ice pellets, and thereby mitigate ice accumulations in freezing rain storms. Sections 1 through 5 focus on the analysis of conditions that lead to freezing rain and the development of a forecast methodology that can be used to recognize opportunities for mitigating ice accumulations. A single parameter is derived from well-established knowledge that most incidents of freezing rain and ice pellets are associated with an elevated warm layer and a subcloud layer of below-freezing air, and that any cloud-ice must completely melt for freezing rain to occur; otherwise ice pellets would result. The parameter was obtained from the ratio of the time available for melting to the time required for complete melting. The mesoscale and thermodynamic conditions that existed with the 1990 St. Valentine's Day ice stormthat affected much of the Midwest is used to demonstrate the methodology. Section 6 briefly discusses how cloud seeding could be used to intervene in the process of freezing rain to mitigate ice accumulations.

1. Introduction

To use cloud seeding to mitigate heavy ice accumulations in freezing rain storms, it is necessary to identify when and where freezing rain will occur. However, distinguishing between regions that will receive freezing rain from those that will receive ice pellets[1] presents a difficult

[1]The term freezing rain is used here to mean rain that falls as supercooled raindrops and that freeze on impact with the ground or other objects exposed at the earth's surface. By ice pellets we use the definition given in the *Glossary of Meteorology* which states "a type of precipitation consisting of transparent or translucent pellets of ice, 5 mm or less in diameter."

challenge in short range forecasting. This challenge exists even though the physical processes by which most instances of freezing rain and ice pellets occur have been recognized for a long period of time (see for example Brooks, 1920). Penn (1957) pointed out in a U.S. Weather Bureau forecasting guide that freezing rain and ice pellets are accompanied by a shallow wedge of sub-freezing[2] air positioned adjacent to the earth's surface that underlies an elevated layer of above-freezing air, and that the extent to which ice particles melt in the elevated warm layer would determine whether freezing rain or ice pellets would reach the earth's surface.

If an ice particle completely melts during its fall through the mid-level warm layer of cloud, raindrops fall out of cloud base into air that is subfreezing where, owing to a lack of ice nuclei (Flethcher 1962, Bigg 1953, 1955, and Vali 1994), they supercool and reach the earth as freezing rain. If the ice particles only partially melt during their fall through the elevated warm layer, the presence of the ice in the liquid-ice hydrometeor allows freezing to proceed in the cold air beneath cloud base so that ice pellets reach the earth.

The importance of a melting zone in the production of freezing rain and ice pellets has been noted in numerous other studies that focused on winter precipitation type (see for example, Young 1978, or Stewart and King 1987). The zone was clearly evident in composite temperature and dew point profiles constructed by Bocchieri (1980) from 127 freezing rain radiosondes (RAOBs) for 48 stations. Bocchieri's research also showed instances of freezing drizzle when the sounding was everywhere colder than 0°C. These have since been attributed to a coalescence process strictly involving supercooled drops (Huffman and Norman 1988).

[2]Air temperatures colder than or equal to 0°C are referred to as "subfreezing" or "freezing" although stictly speaking, 0°C is the temperature at which ice melts.

Model calculations by Stewart and McFarquhar (1987) of ice particles melting in an elevated warm layer clearly showed a progression of precipitation type from freezing rain, to ice pellets, to snow as the melting diminished the warm layer. The presence of an elevated warm layer and degree of ice particle melting are reasons why thickness, the depth of the warm layer and height of the freezing level above the surface, have provided useful guidance in distinguishing between where freezing rain and ice pellets will occur (Booth 1973, Boyden 1964, Burnash and Hug 1970, Glahn and Bocchieri 1975, Koolwine 1975, Lumb 1963 and 1961, Mahaffy 1961, Murray 1952, Pandolfo 1957, Wagner 1957, Younkin 1967).

Bocchieri (1980) used the technique of Regression Estimation of Events Probability (REEP) (Miller, 1964) to relate RAOB parameters to diagnose winter precipitation type. Bocchieri's set of linear regression equations had short-range predictive value to the extent that they could be used with either near real-time or model output data. The probabilistic method did well at discriminating between rain and snow, but did not perform so well at distinguishing between freezing ruin and ice pellets.

2. Formulation

Figure 1 shows the conceptual model that was used to formulate the non-dimensional parameter. Shown is a vertical cross-section of a cloud whose top temperature is colder than 0°C. The bold line indicates environment temperatures. The figure is meant to illustrate how temperature varies in the vertical direction only with respect to cloud. The cloud straddles a mid-level warm layer, or melting zone, and temperatures beneath cloud base are colder than freezing. The critical factor that can decide between the production of freezing rain and ice pellets is whether an ice

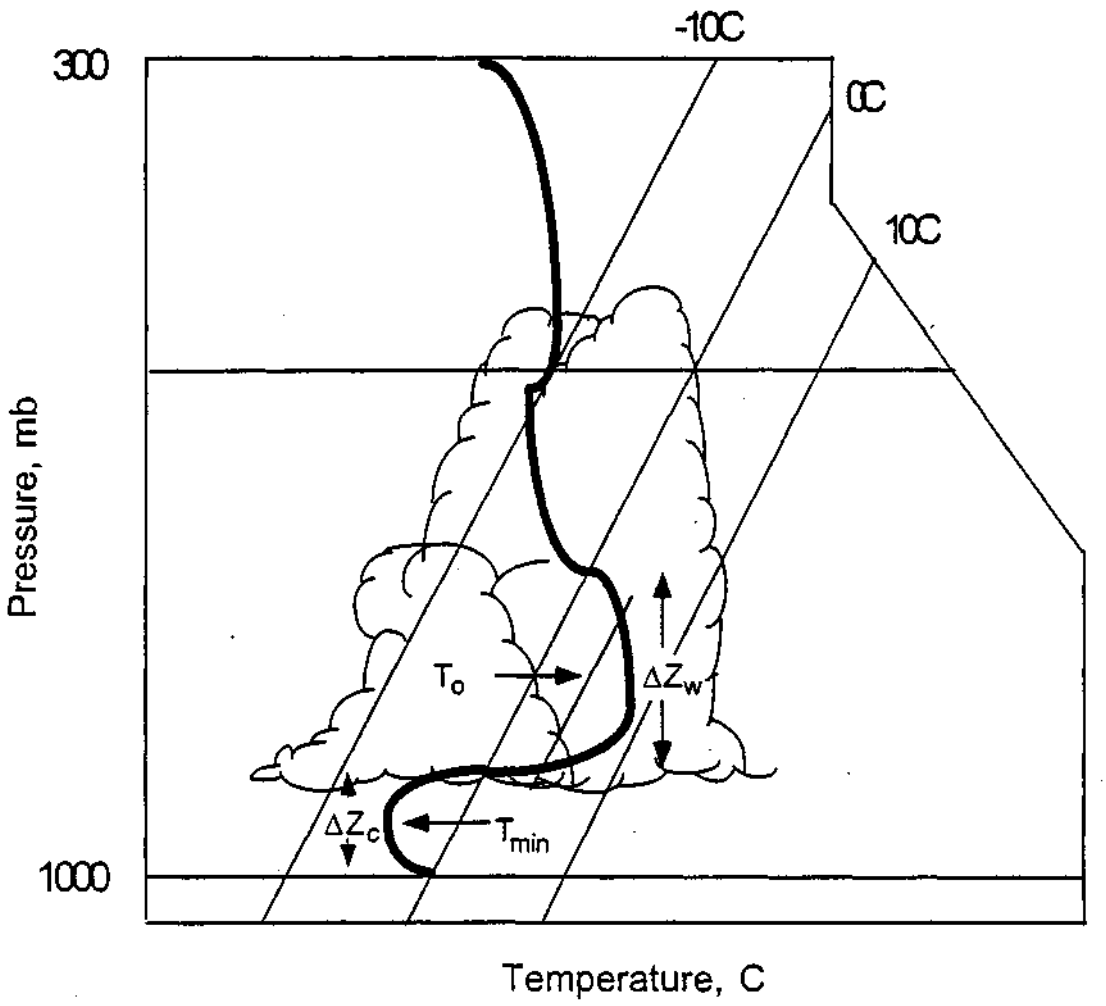

Figure 1. Conceptual model showing relationship between vertical cloud cross section and temperature structure conducive to the development of freezing rain and ice pellets depending on the characteristics (T_o and ΔZ_w) of the elevated warm layer.

particle will completely melt in the elevated warm layer before entering the subfreezing air beneath cloud.

An indication of whether complete melting will occur can be obtained from the ratio, τ, between the residence time, t_{res}, of a particle in the melting zone with a radius, a, and the time, t_{melt}, required for complete melting. If the ice particle size distribution is characterized by a maximum particle radius, a_c, then the combination of layer depth, layer mean temperature, and resident time will define a value of $\tau \geq 1$ indicating that conditions are sufficient for complete melting of the largest and all smaller particles to favor freezing rain. Locations where the physical conditions of the warm layer define $\tau < 1$, suggest only partial melting of the largest particles. Hence, for $\tau < 1$, the extent to which ice pellets reach the earth depends on the concentration of particles smaller than a_c, and the likelihood that smaller drops will survive evaporation and collection after falling out of the cloud.

The resident time of a particle in the melting zone can be estimated from the ratio of the vertical distance the particles must fall (i.e. depth of the warm layer, ΔZ_w) and the velocity at which they fall through the warm layer

$$t_{res} = \frac{\Delta Z_w}{U(a) - \bar{V}} \qquad (1)$$

where $U(a)$ is particle terminal velocity and $\bar{V}$ represents the mean vertical air motion. For simplicity, $\bar{V} = 0$ has been assumed although melting and particle loading would dictate otherwise (see for example Szeto et al. 1988). Also assumed is that a and $U(a)$ remain constant as a particle falls and melts, and that it does not change size by collection and/or condensation-evaporation mechanisms.

By neglecting these aspects, Eq. 1 would be too low an estimate if the vertical air motion was upward and particle sizes decreased by evaporation, and would be too high if the particle increased size and/or the vertical air motion was downward.

The time required for a particle to completely melt can be estimated from a balance between the rate of energy required to transform the solid to liquid, and the rate that the environment can supply the needed energy. Following the discussion in Pruppacher and Klett (1978) of the work of Mason (1956), Macklin (1963), Drake and Mason (1966) and Bailey and Macklin (1968), a spherical ice particle of radius, *a,* is considered that falls at terminal velocity in an environment of constant relative humidity and temperature. If the ice particle is relatively large then through most of the period of melting, it can be modeled as an ice core of radius *r* surrounded by a liquid water layer of thickness (*a - r),* assumed to be uniform and symmetrical throughout the period of melting. This implies that the time required for an aggregate to collapse to a liquid/ice drop is relatively short compared to the total time for melting. It is further assumed that the particle does not shed the liquid layer, nor does it change size by collection or evaporative processes although the effect of evaporative cooling on the temperature at the particle/environment interface will be taken into account.

Now, the energy balance between the rate of latent heat of melting and the rate at which heat can be transferred through the water layer and disposed of in the environment can be written as

$$4\pi\rho_i L_{sl} r^2 \frac{dr}{dt} = \frac{4\pi a\, r k_w [T_o - T_a(r)]}{a - r} \qquad (2)$$

where p_i is the density of ice, L_{sl} the latent heat of melting, k_w is the thermal conductivity of water, T_o is the temperature at the ice/water interface assumed to be 273°K, and $T_a(r)$ is the temperature at the particle/environment interface which is a function of the size of the ice core. Integration of Eq. 2 results in

$$t_{melt} = \frac{L_{sl}\,\rho_i}{k_w\,a} \int_a^0 \frac{r(a-r)\,dr}{T_o - T_a(r)} \tag{3}$$

The temperature at the particle/environment interface, $T_a(r)$ in Eq. 3 can be found iteratively from

$$\frac{4\pi k_w\, a\, r\,[T_o - T_a(r)]}{(a-r)} = -4\pi a k_a [T_\infty - T_a(r)]\bar{f}_h - 4\pi a L_{lv} D_v (\rho_{v,\infty} - \rho_{v,a})\bar{f}_v \tag{4}$$

where k_a is the thermal conductivity of air, $\bar{f}_h$ and $\bar{f}_v$ are ventilation coefficients for heat and vapor, D_v, the diffusivity of vapor, L_{lv} the latent heat of vaporization, and is the difference between the vapor density of the environment and the saturation vapor density at the particle's surface.

The ratio of Eq. 1 and 3 results in the non-dimensional discriminator parameter

$$\tau \equiv \frac{t_{res}}{t_{melt}} = \frac{\Delta Z_w\, k_w\, a}{(U(a) - \bar{V})\, L_{sl}\, \rho_i \int_a^0 \frac{r(a-r)\,dr}{T_o - T_a(r)}} \tag{5}$$

Particle fall velocity, $U(a)$, can be estimated from

$$U(a) = c_1 - c_2 \exp(-c_3 a) \tag{6}$$

where c_1 = 965 cm s^{-1}, c_2 = 1030 cm s^{-1}, and c_3 = 12 cm^{-1} (Best 1950; Atlas et al. 1973). An empirical relationship for liquid raindrops has been used since this should better approximate the speed of a partially melted particle in free fall.

3. An example ZR-IP diagnosis

A ZR-IP diagnosis is presented using the 1990 St. Valentine's Day ice storm as an example. This ice storm was selected because certain aspects of it were poorly forecast, and also because it has received a great deal of research attention. It occurred during four independent atmospheric field projects located from the Rocky mountains to the eastern Great Lakes (Martner et al. 1992, Rasmussen et al. 1995, Rauber et al. 1994). A variety of severe weather was produced, in addition to freezing rain and ice pellets, including heavy snowfall, thunderstorms, hail, and tornadoes. Thirty-five states were effected resulting in an estimated $120 million in property damage.

Surface weather conditions in Illinois were characterized by a cold front that passed through east-central Illinois (see Fig. 2) 12 UTC on 14 Febraury 1990. After passage, the front assumed an orientation parallel to the southwesterly upper-level, 500-mb flow, resulting in a stationary overrunning precipitation pattern. The accumulation of ice at the surface was estimated to be between 0.15 and 0.65 cm, and occurred from three rain episodes between the hours of 2200 UTC, 14 February and 1300 UTC, 15 February, 1990. The total amount of precipitation measured at the cooperative station in Champaign, Illinois was 3.3 cm (melted equivalent). Air temperatures at shelter level were only a few tenths of a degree colder than 0°C during the entire course of the event: beginning at about -1°C at 23 UTC on 14 February 1990, and steadily increasing to a few tenths of a degree colder than 0°C when the rain ended at about 12 UTC 15 February 1990.

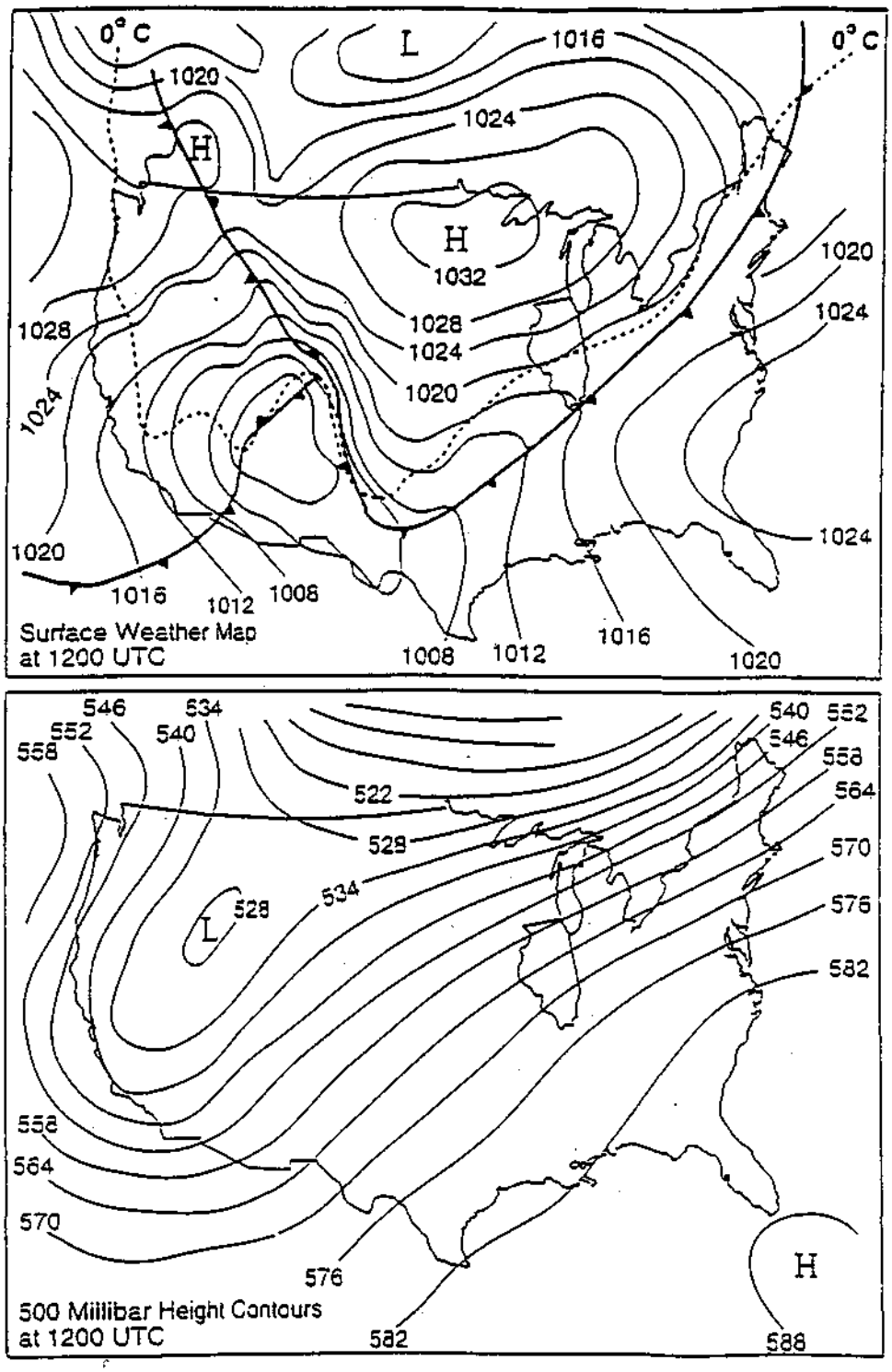

Figure 2. Synoptic scale conditions for 12 UTC 14 February 1990. Upper panel shows surface isobaric pattern (solid lines, values in millibars). Dashed line shows position of surface 0°C isotherm. Bottom panel shows 500 millibar heights.

A NCAR/CLASS sounding taken during the evening of 14 February 1990, as part of the field operations of the University of Illinois Winter Precipitation Program (UNIWIPP), is shown in Fig. 3 (Ramamurthy et al. 1991). The sounding shows the well recognized cold-air layer near ground level from 990 to 925 mb, with an elevated warm air layer above from 925 to 710 mb. In the cold-air layer, temperatures reached a minimum of about -4°C (at ~930 mb), while temperatures aloft reached a maximum of +8°C (at ~840 mb). Cloud bases were estimated to be approximately 1 km (940 mb), and cloud tops were as high as 9 km.

In practice, a value for critical particle radius, a_c, needs to be determined at each location in space that t is calculated. To gain a rough indication of what the critical ice particle radius may have been, we followed a procedure that used reflectivity data from the NWS radar summary along with established relationships between reflectivity and characteristics of the particle size distribution. The reflectivity relationship used was

$$Z(\text{dBZ}) = f(\lambda, N_o, a_{min}, \text{and } a_{max}) \qquad (7)$$

where, λ is the slope, N_o is the intercept, and a_{min} and a_{max} are the minimum and maximum particle radii, respectively, of the size distribution. In this case $a_{\max}$ is equivalent to a_c. A specific form of Eq. 7 has been found by Czys and Tang (1995) who integrated the defining equations for Z (see for example Pruppacher and Klett 1978) over the finite drop size range a_{min} to a_{max}. The integration was accomplished by assuming an exponential particle size distribution defined by

$$N(a) = N_0 e^{-\lambda a} \qquad (8)$$

where N_o is the intercept, λ the slope and a particle radius (Marshall and Palmer 1948). For the present problem, a Marshall and Palmer value of $N_o = 0.08$ cm^{-4} was used. Although observation

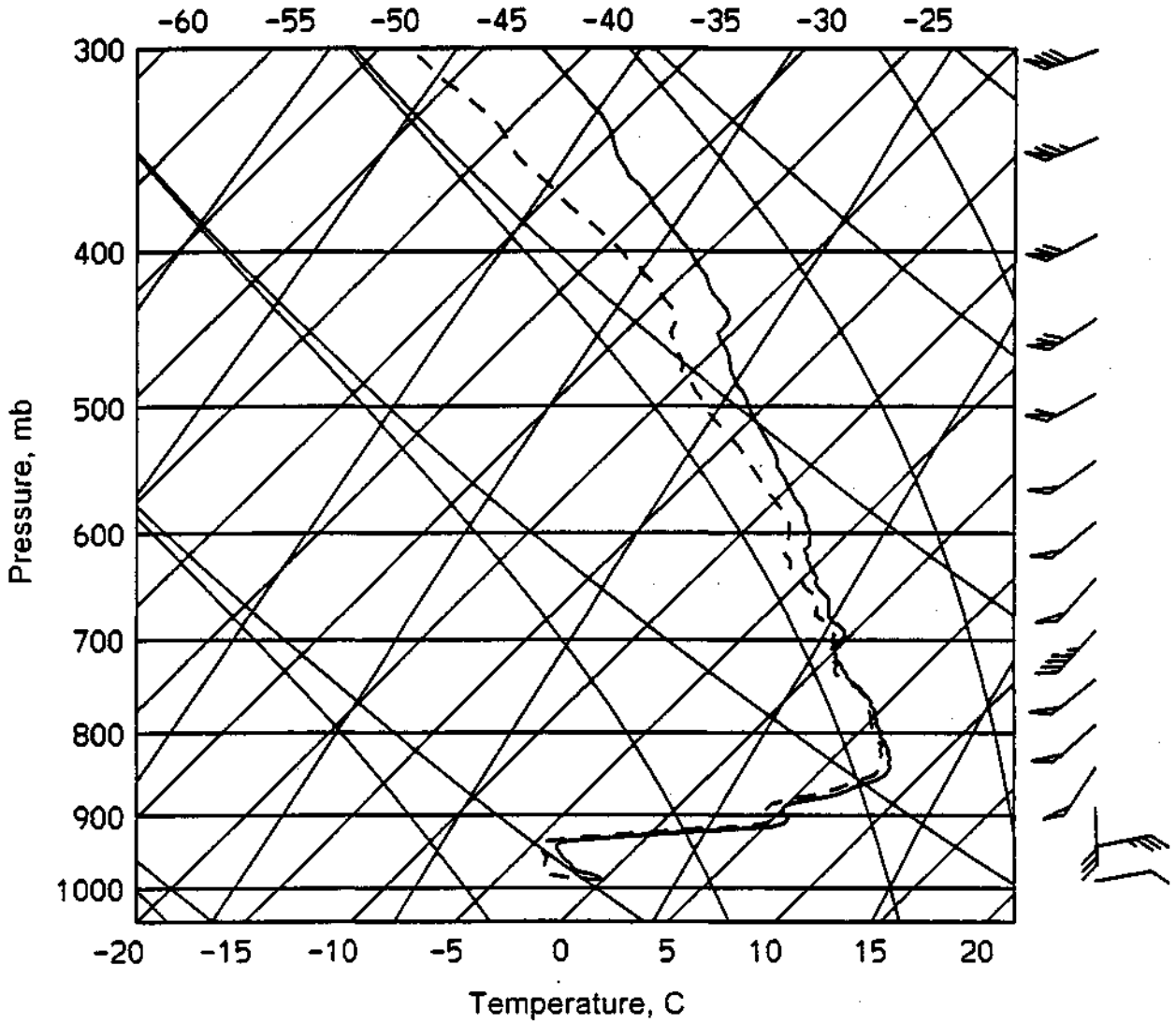

Figure 3. Thermodynamic diagram showing temperature (solid line) and dew point (dashed line) for 1200 12 UTC 14 February 1990. Diagram shows a well defined elevated warm layer extending from 925 mb to 710 mb.

has not always supported use of Marshall-Palmer values, especially for mixed-phased regions and/or the condition of significant ice particle melting, if provided a value needed in the absence of a better choice allowing the next step of the calculations to be taken.

The slope of the particle size distribution was obtained from the rainfall rate relationship

$$\lambda = 41\ \mathcal{R}^{-0.21} \qquad (9)$$

given by Gunn and Marshall (1958) where $\mathcal{R}$ is the rainfall rate (mm hr^{-1}). Observed rainfall rates from rain gage data were used with Eq. 9. Now that we have numbers for N_o and λ, and if we assume that $a_{min} = 0$, a_c can be computed directly from Eq. 7, the calculations resulted in a critical radius of 400 μm.

Values of τ were calculated from Eq. 5 using 00 UTC 15 February 1990 radiosonde data and are plotted in Fig. 4. The data for each sounding were interrogated using a simple computer program that first determined if a melting layer existed, and if it did, it computed melting layer depth and mean temperature (where the mean temperature of the melting layer was also used for T_v in Eq. 4). When no melting layer existed, ΔZ_w was set to 0 effectively setting τ to 0. The field of τ shown in Fig. 4 was then used with a surface isotherm analysis for the same time (see Fig. 5) to arrive at a final diagnosis. Surface temperature was used to rule-out the possibility of making a diagnosis of freezing rain where surface temperatures wanner than 0°C would simply result in rain.

The final diagnosis is shown in Fig. 6. In general, the diagnosis indicates two elongated regions extending southwest to northeast with the northern most region diagnosed to have ice pellets and the southern region to have freezing rain. The southern boundary of the region of freezing rain exactly corresponds to the location of the 0°C isotherm shown in Fig. 5. The northern boundary of the region for ice pellets corresponds to the northern = 0 line in Fig. 4. The boundary separating the

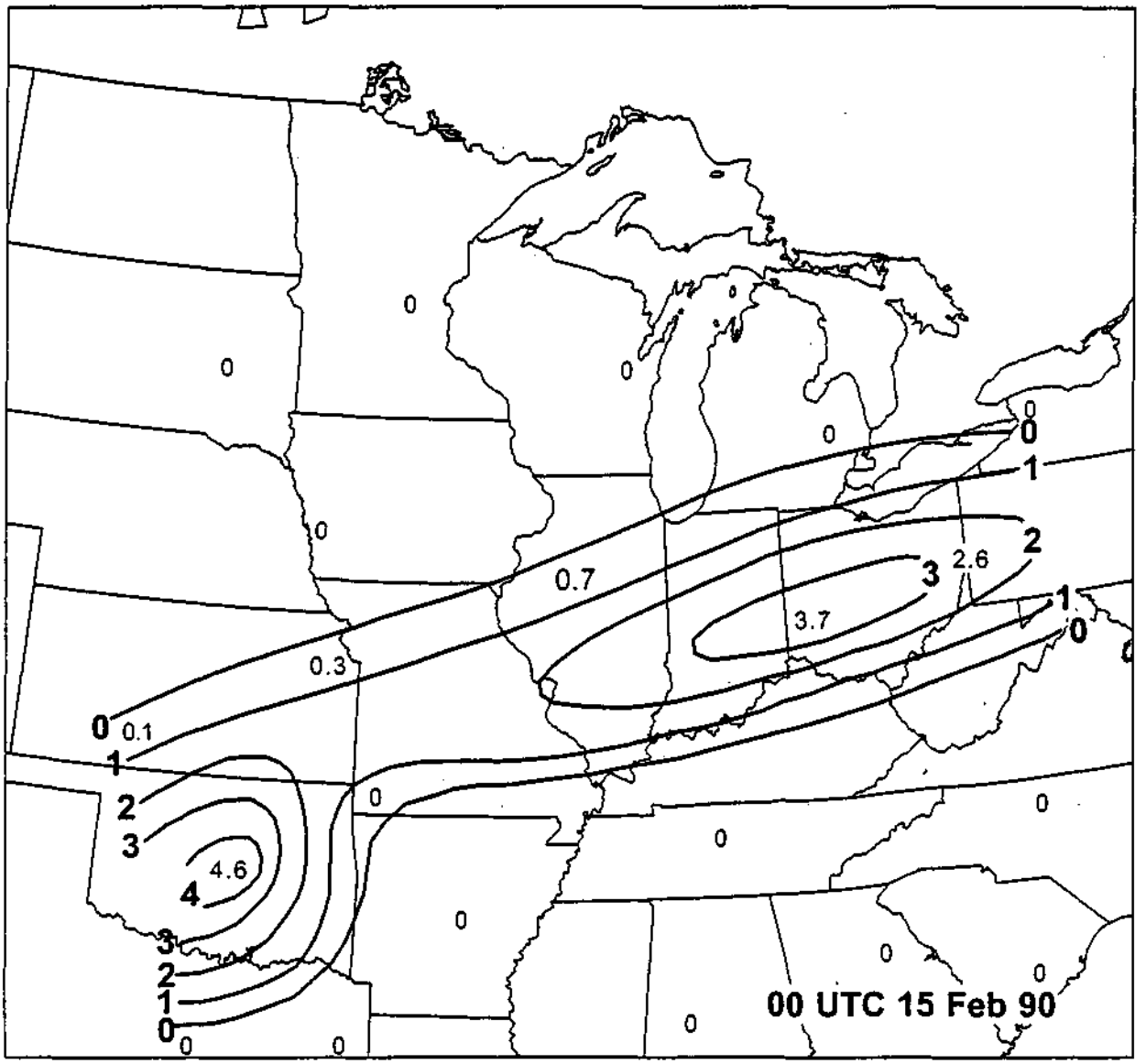

Figure 4. Diagram showing contours (solid lines) of τ for 00 UTC 15 February 1990. Individual values of t used to draw the contours are shown at each radiosonde site that had available data.

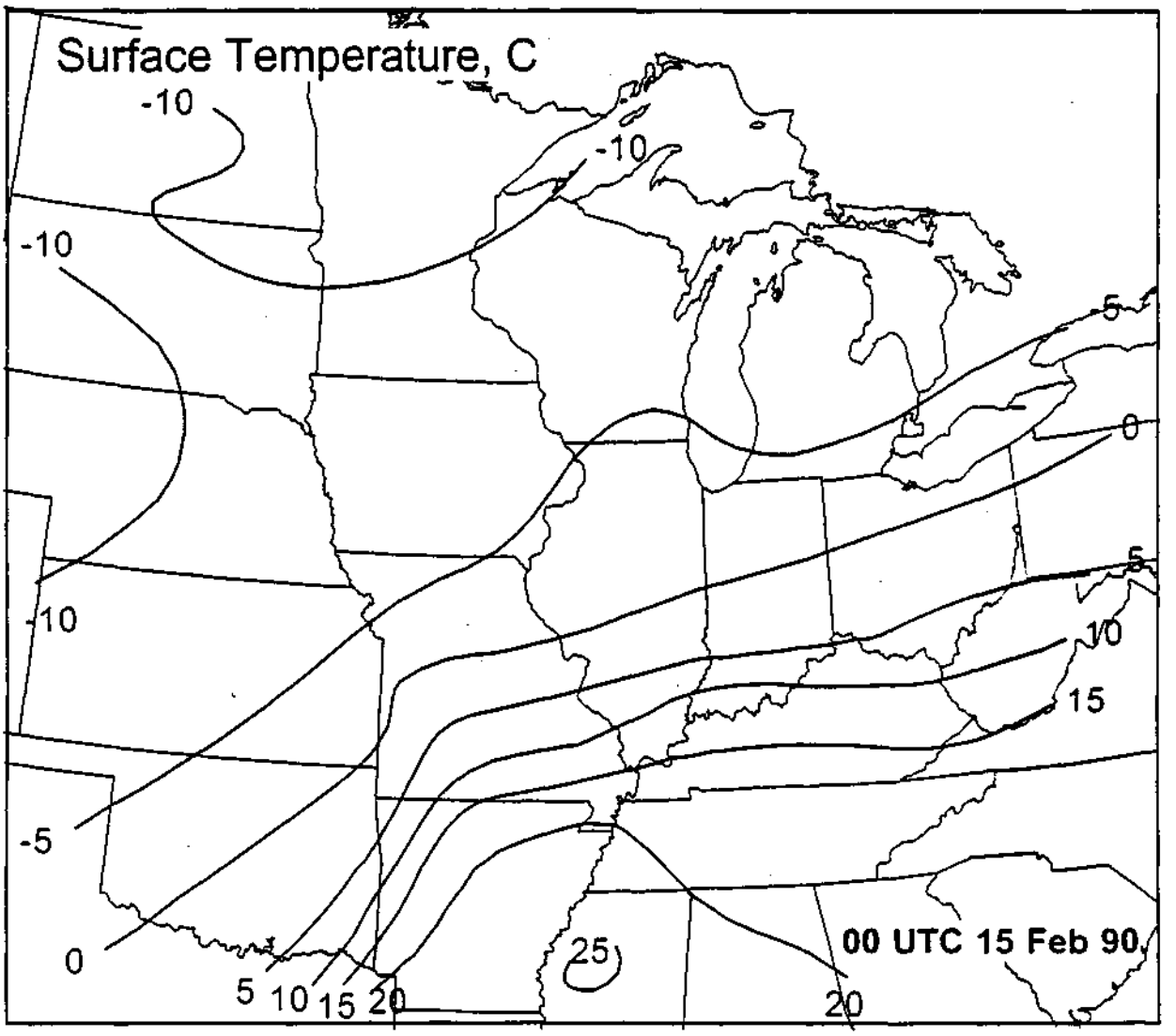

Figure 5. Surface isotherm pattern at 00 UTC 15 February 1990.

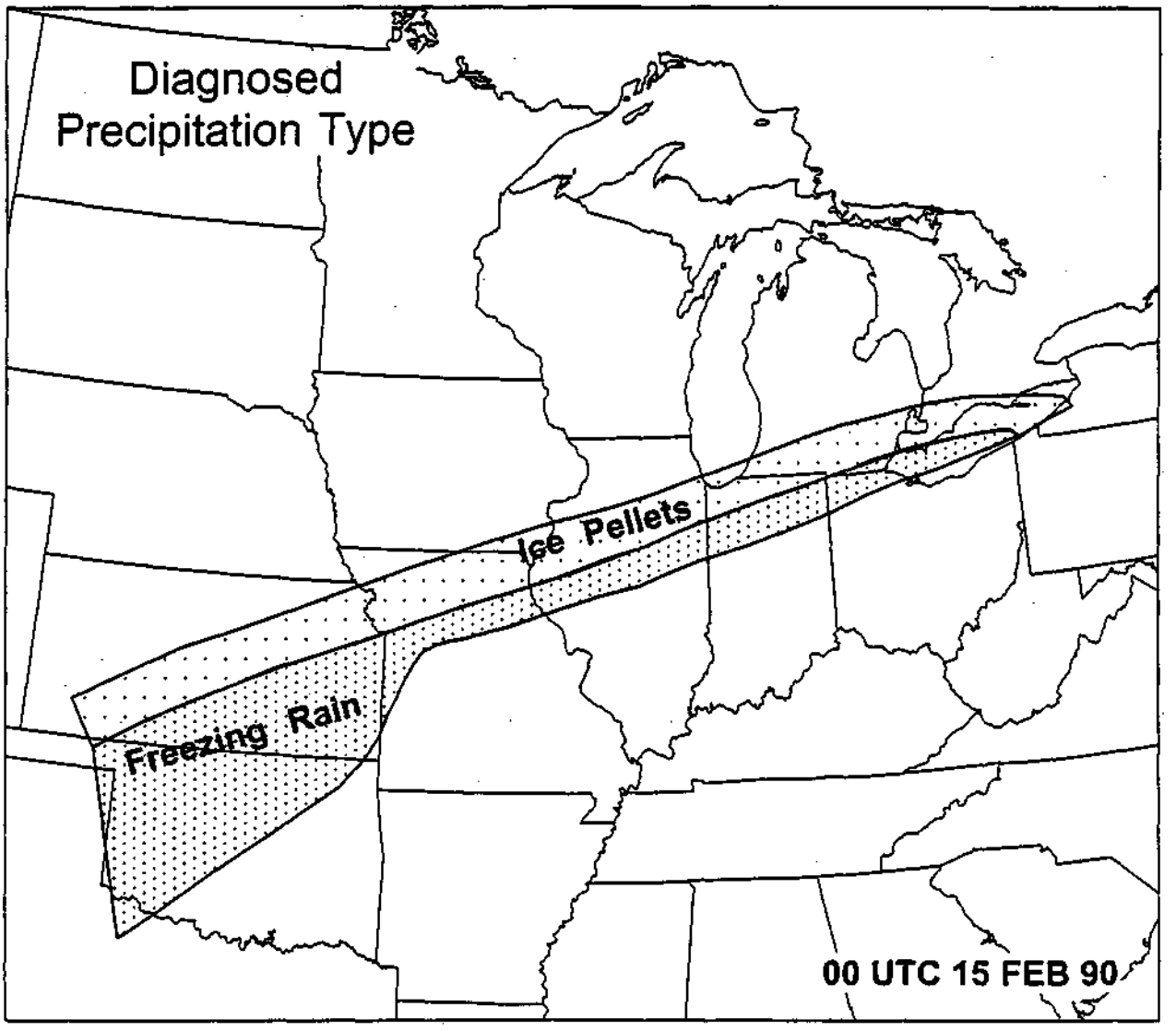

Figure 6 Pattern for freezing rain arid ice pellets diagnosed at 00 UTC 15 February 1990 using the information in Figure 4 and 5.

regions of freezing rain and ice pellets corresponds to the $t = 1$ line in the region with surface temperatures colder than 0°C.

4. Preliminary evaluation

The observed distribution of precipitation type at 00 UTC 15 February 1990 is shown in Fig. 7. The diagnosed and observed regions for freezing rain and ice pellets are in remarkably good agreement considering that a number of marginal assumptions were made, and in spite of the coarse spatial resolution of the radiosonde data.

The diagnosed field shows an area of freezing rain that almost exactly coincides with that observed except for a large region of false alarm in central Oklahoma and south central Kansas. This region of false alarm occurred because it was an area without precipitation and no attempt was made in the diagnosis to filter according to the presence or absence of precipitation. This can be easily done in practice. The diagnosis of ice pellets coincides with the region of observed except that it is not as narrow. This difference probably occurred because of the coarse spatial resolution of the sounding data. When conditions for freezing rain and ice pellets were diagnosed for the observation times of 12 UTC 14 February 1990 and 12 UTC 15 February 1990, corresponding to the beginning and end of the St. Valentine's event, similar good agreement was found and the same types of qualitative errors were uncovered.

The methodology was further evaluated in a cursory forecast experiment conducted during the winter of 1995-96 with the cooperation of the NWSFOs at St. Louis, MO and Indianapolis, IN. At total of seventeen freezing rain and ice pellets episodes were identified within the geographic domain represented in, Fig. 7. As found in the analysis of the St. Valentine's Day ice storm, qualitatively the methodology tended to accurately identify areas where freezing rain and ice pellets

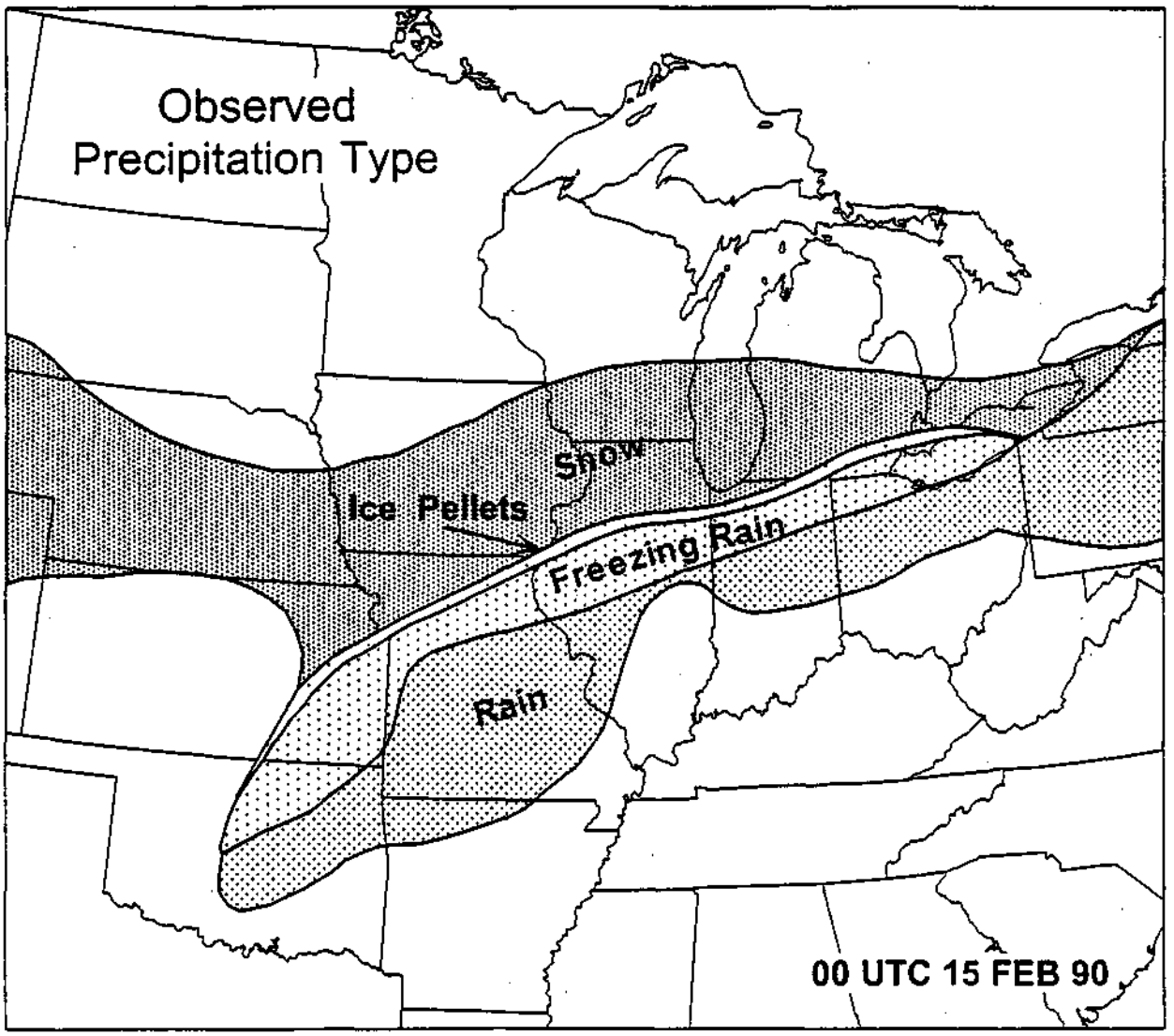

Figure 7. Patterns of snow, ice pellets, freezing rain and rain observed at 00 UTC 15 February 1990.

did occur. Also in keeping with the St. Valentine's example, false alarms resulted by not taking into consideration the areal distribution of precipitation. Another source of false alarm uncovered in the experiment was occasions when an elevated warm layer developed as a result of strong nocturnal cooling in the boundary layer in the absence of precipitation. A tendency for the diagnosis to have a less detailed spatial fit than observed was also noted in the experiment.

A preliminary evaluation leads to consideration of a few improvements. First, the simplified theoretical treatment for the heat balance equation governing melting given in Eq. 2 could better specify the effect that the ice-liquid mixture has on consumption of energy from the environment. Future research needs to be conducted so that the type of ice entering the top of the melting layer can be better taken into account. The present theory assumes that the ice is initially spherical when in reality it may start out as aggregates, or possibly large individual crystals that may or may not exhibit some degree of riming. It can be suspected that an aggregate would take longer to melt than another form of ice because of the delay induced by the time required for melting to collapse the aggregate into a spherical liquid with an ice core, as assumed in development of Eq. 2.

GOES-8 satellite data could be used to improve the diagnosis by helping to delineate between the presence and absence of clouds and to estimate cloud-top temperature to determine the extent to which ice may be involved in the formation and evolution of precipitation. Further improvement can be made if values of the critical radius were determined over a higher spatial resolution and regular grid spacing using, for example, composite WSR88D reflectivity data with rain rate data. This would require future research to determine the best location within the echo structure to extract reflectivity for use and development of specific rain rate relationships for freezing rain and ice pellets.

5. Demonstration of methodology

Figure 8 was created to allow Eq. 5 to be applied simply. It shows isopleths of $\tau = 1$ computed over a range of critical ice particle radii, warm layer depths, and mean warm layer temperatures. In the seventeen cases identified in the winter 1995-96 forecast experiment, depths and mean temperatures as large as about 5000 m and 10°C, respectively, were found. The $\tau = 1$ isopleth for $a_c = 400$ μm has been highlighted because this radius proved to be adequate for the variety of freezing rain and ice pellets situations encountered in the forecast experiment.

A diagnosis can be made from Fig. 8 by first determining values for warm layer depth and mean layer temperature from radiosonde or another source of sounding data. For example, suppose that a warm layer depth of 2500 m and a mean layer temperature of +4°C were indicated. This combination indicates freezing rain because it intersects well above the T = 1 line for a_c - 400 μm. Next, a judgment has to be made about the adequacy of assuming a value of 400 μm for the critical ice particle radius. This judgment could be based on a quantitative assessment using rain rate and reflectivity data, as was illustrated in section 3, or it could be qualitative based on inspection of WSR88D reflectivity data. Of course, the further away a point plots from the $\tau = 1$ line for a_c = 400 urn radius, the less uncertainty about the diagnosis. As one cautionary note, those using Fig. 8 need to keep in mind that it will fail to identify instances of freezing drizzle when the sounding is everywhere colder than 0°C. However, experience from the 1995-96 forecast experiment suggests that this is a highly localized phenomena.

Figure 8 also gives a semblance of the sensitivity of Eq. 5 to the selection of critical radius. It clearly shows that a modest variation in critical radius will result in selecting one form of precipitation type over the other. Thus, it is interesting that a value of 400 μm seemed to apply so well to the seventeen cases examined during the 1995-96 forecast experiment. This suggests the

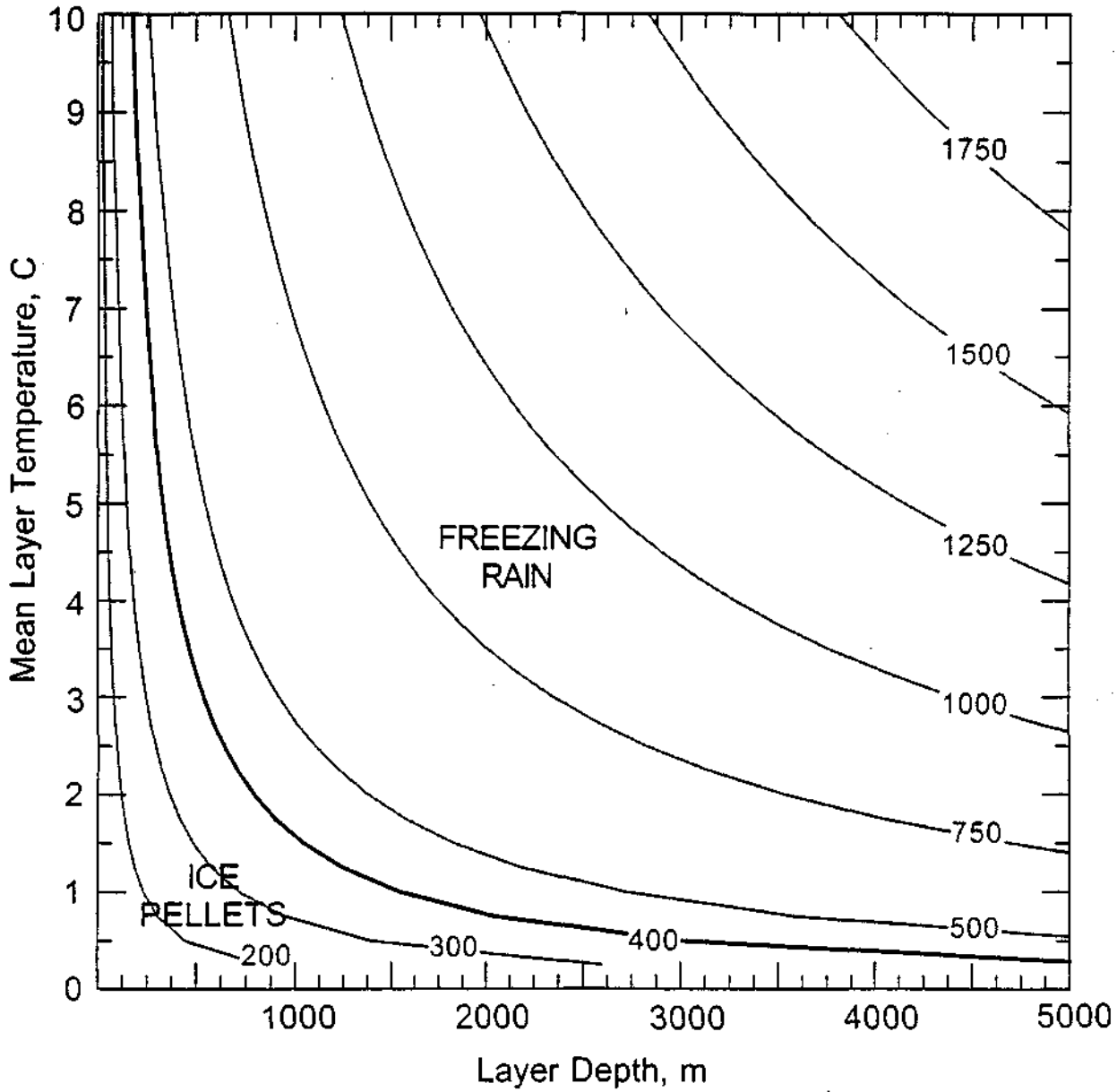

Figure 8. Isonomograph that can be used to diagnosis for freezing rain and ice pellets if the depth of the elevated warm layer and its mean temperature are known.

hypothesis that the natural variability of particle size distribution in and around the bright band associated with freezing rain and ice pellets is not as large as the sensitivity shown in Fig. 8. This accentuates the need for future additional microphysical observations through the bright band associated with freezing rain and ice pellets, to compare these observations with the bright band of other mesoscale structures, and to find a means to readily estimate critical ice particle radius using remote observations.

6. Implications for cloud seeding

In this section, we consider how the above forecasting technique might be utilized in a cloud seeding operation to mitigate ice accumulations in a freezing rain episode. In this consideration, we use the conditions that existed with a 1995 freezing rain episode that effected an area east of Indianapolis, Indiana. This episode was selected for demonstration because high quality Doppler radar data were available from the Indianapolis WSR88D site and the mesoscale radar rainfall pattern provided a good example for illustration.

Figure 9 shows surface conditions for 19 December 1995 at 12Z. The surface map shows a very broad region of precipitation that was associated with a low pressure system that was moving through the Ohio River valley. Similar to the case of the 1990 St. Valentine's Day Ice Storm, the broad band of precipitation, extending from southwest Missouri into southern Illinois and into all of Indiana and Ohio, was associated with overrunning of warm moist gulf air. Because surface temperatures in the southern part of the precipitation pattern were well above 0°C, liquid precipitation reached the earth's surface. As shown by the bold solid lines in Figure 9, freezing surface temperatures prevailed in the north two thirds of the state of Indiana such that a narrow band of freezing rain was reported that included Indianapolis. The path of the low pressure system just

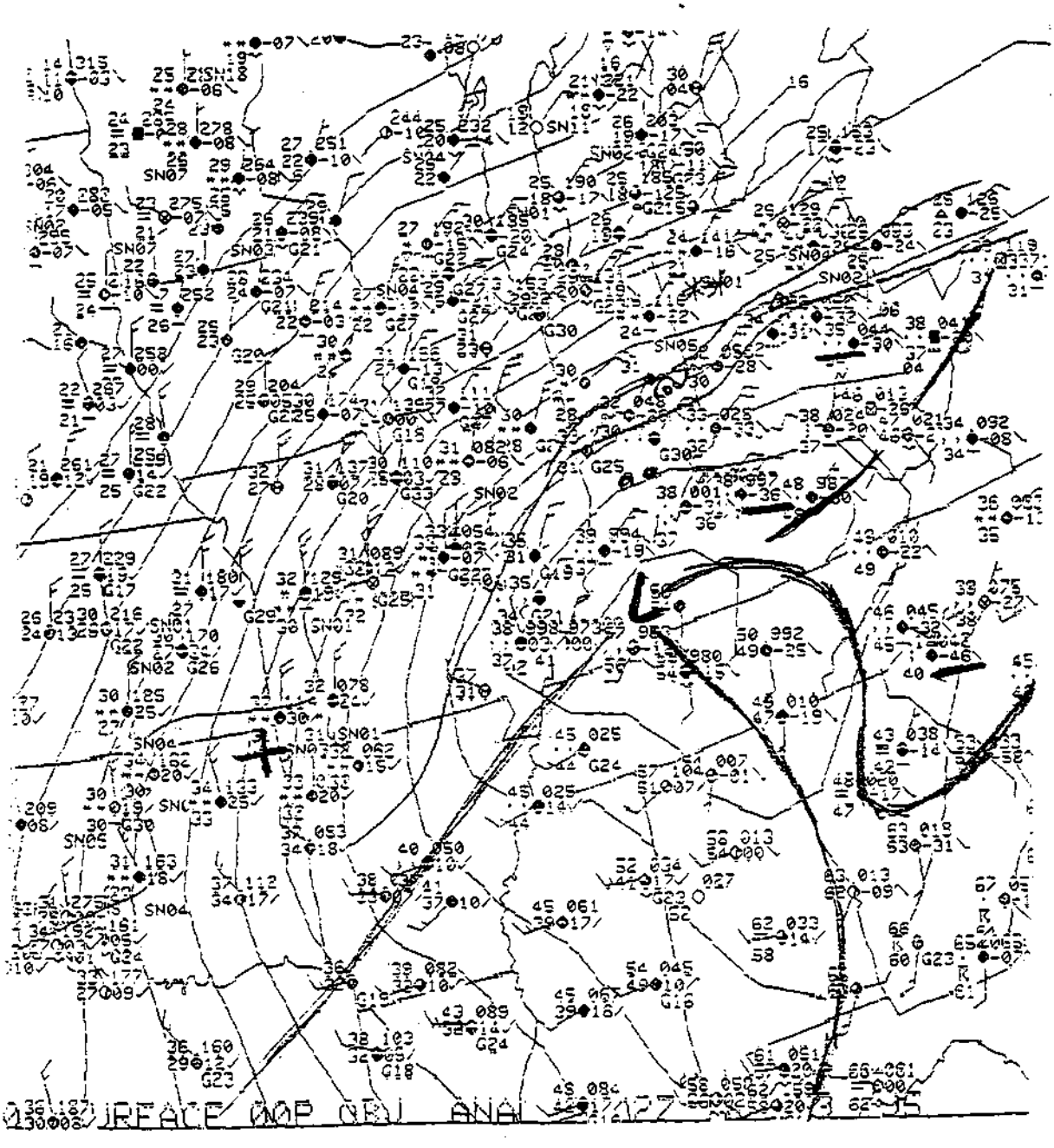

Figure 9. Surface weather conditions for 12 UTC 19 December 1995. Areas of rain, freezing rain, and snow are shown with location of surface fronts.

south of the Ohio river valley allowed the overrunning to persist, and thereby result in heavy ice accumulations from moderate freezing rainfall that continued over many hours.

Figure 10 shows a zoom-in of the Indianapolis, IN WSR88D reflectivity pattern recorded at 13 Z on 19 December 1995. In this presentation black denotes areas of no echo, light gray denotes light precipitation echoes and medium gray denotes moderate to strong echo. Based on this shading convention, the reflectivity pattern in the upper part of the figure shows an echo with a west-to-east arc of moderate to heavy precipitation that cuts through Tipton and Madison Counties, and then turns south to be located just south of Muncie/Yorktown and then southwest of Lynn, IN. This area of greatest reflectivity is generally to the north of the surface 0°C isotherm. It can be inferred from soundings for Dayton, Ohio and Quincy, Illinois that the echoes were embedded in an elevated warm layer. The methodology discussed in the previous sections was applied to these conditions, and the τ-analysis along with the surface temperature analysis picked out the northern arc-like echo region as being favorable for freezing rain.

The bold circles in Fig. 10 indicate echo regions that might be targeted for seeding. These regions were selected for several reasons. First, they represent population centers where the effects of freezing rain would be most severe. Second, the size of the areas are easily manageable in aircraft maneuvers.

One delivery technique that was considered and could be effective at converting the rain to ice pellets was the use wing-tip AgI generators. The seeding material would be released in the rain just above cloud base where cloud temperatures would be just warmer than 0°C to avoid dangerous aircraft icing. This would require that the seeding material act as immersion nuclei for that which would immediately come into contact with the raindrops and perhaps contact nuclei for that which

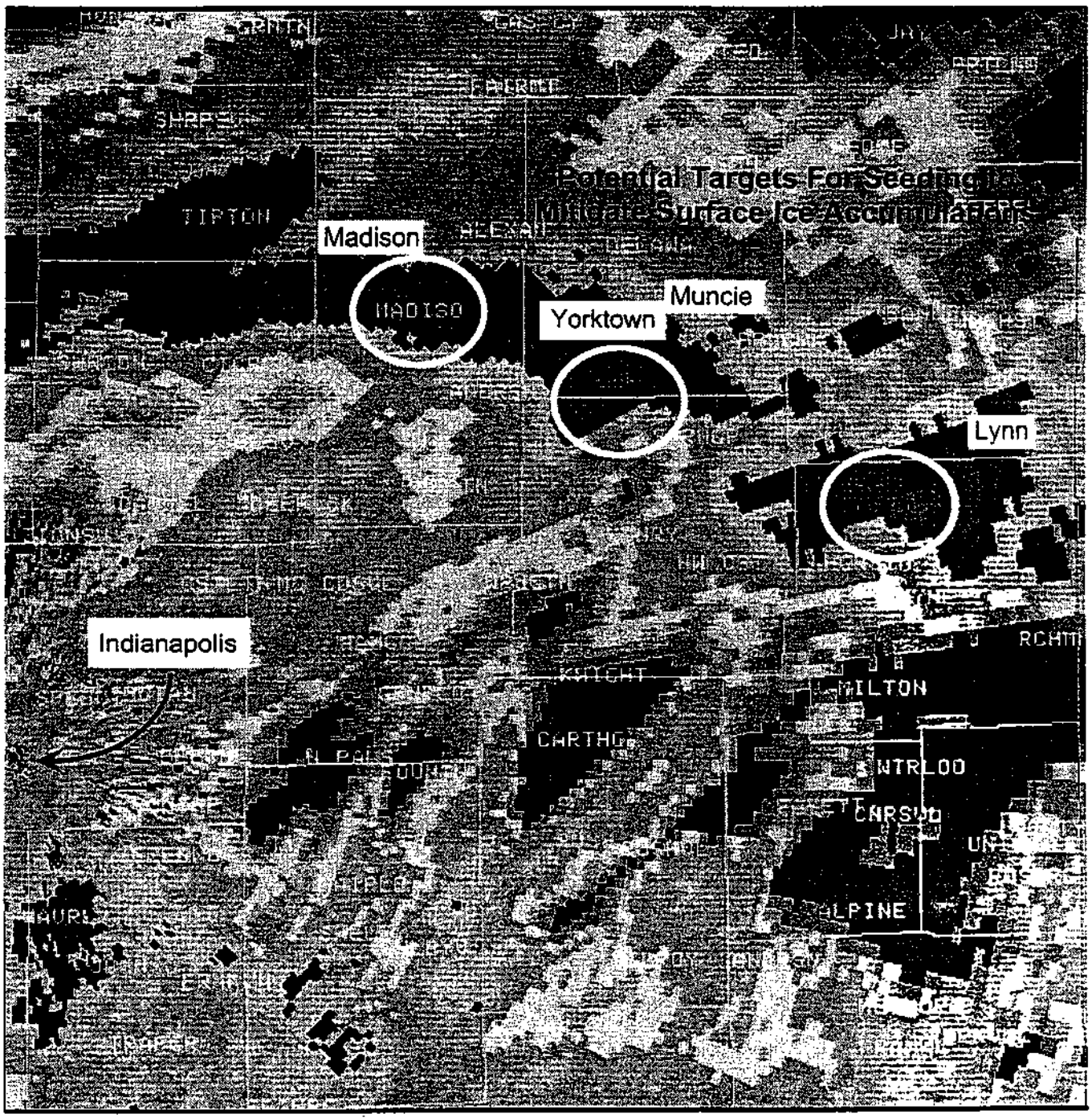

Figure 10. WSR88D reflectivity pattern east of Indianapolis, Indiana at 13 UTC on 19 December 1995. Darker shades of gray indicate higher reflectivities. Solid white circles show potential targets for seeding to mitigate surface ice accumulations.

might come into contact with the rain drops below cloud base. Seeding above cloud base in the warm air also has the necessary advantage of avoiding dangerous aircraft icing conditions.

In an exploratory field program, evaluation of the effectiveness of the strategy could be accomplished by aircraft surveillance of the ground. Locations just downwind of where the seeding material was target should show little or no evidence of glaze ice, while regions surrounding the downwind trajectory would show heavy accumulations. As compared to evaluations of precipitation enhancement or hail suppression programs where response variables (rain fall, hail fall, in-cloud conditions, radar reflectivity, etc.) show a degree of variability that greatly reduces noise ratios. A major advantage in testing the use of seeding to mitigate ice accumulations would be in evaluation. This would only have to rely on direct visual evidence, say by surveying the target/control region immediately following an operation, which either confirm or deny that ice accumulations were less in the seed plume than they were in surrounding no seed areas.

7. Conclusions

A non-dimensional parameter was presented that can be used to assist in the diagnosis of conditions favorable for the occurrence of freezing rain and ice pellets. The parameter was derived from consideration of the time required for ice particles to melt in an elevated layer of above-freezing air to an estimate of the residence time of the ice particles in the warm layer. The parameter was applied to the mesoscale thermodynamic conditions that existed with the 1990 St. Valentine's Day ice storm that affected much of the Midwest. This application showed agreement between diagnosed and observed locations for freezing rain and ice pellets. The method could provide the corner stone for the development of an exploratory cloud seeding field program to determine the feasibility of seeding to mitigate ice accumulations. The method could be used to determine when

and where freezing rain was expected. Being so altered, radar reflectivity patterns could be assess and research aircraft capability to deliver seeding material could be directed to locations for operations. Initially these locations could be selected to favor rural areas so that the general public would not be subjected to any unanticipated effects. The effectiveness of seeding could be simply accomplished by comparing surface glaze ice accumulations, perhaps by air photography, that would provide direct visual evidence that seeded regions either did or did not, exhibit accumulations of ice.

Acknowledgments. The authors wish to thank the Meteorologists In Charge, Science and Operations Officers and meteorologists at the St. Louis, MO, Indianapolis, IN, Chicago, IL, Lincoln, IL, Davenport, IA, and Milwaukee, WI NWSFOs, for their helpful comments and insights as this work developed. The authors appreciate the help of Dr. Richard McNulty of the NWS Training Center in providing information on current NWS training methods for winter precipitation type and for supplying some of the reference material. This research was conducted as part of the Precipitation, Cloud Changes and Impacts Project (PreCCIP) under NOAA cooperative agreement COM- NA27RA0173.

6. References

Atlas, D., R.C. Srivastava, and R.S. Sekhon, 1973: Doppler radar characteristics of precipitation at vertical incidence. *Rev. Geophys. Space Phys.*, **11**, 1-35.

Bailey, I.H. and W.C. Macklin, 1968: Heat transfer from artificial hailstones. *Quart. J. Roy. Meteor. Soc.*, **94**, 93.

Best, A.C., 1950: Empirical formulae for the terminal velocity of water drops falling through the atmosphere. *Quart. J. Roy. Meteor. Soc.*, **76**, 302-311.

Bigg, E.K., 1953: The formation of atmospheric ice crystals by the freezing of droplets. *Quart. J. Roy. Meteor. Soc.,* **79**, 510-519.

Bigg, E.K., 1955: Ice-crystal counts and the freezing of water drops. *Quart. J. Roy. Meteor. Soc.*, **81**, 478-479.

Bocchieri, J.R., 1980: The objective use of upper air soundings to specify precipitation type. *Mon. Wea. Rev.,* **108,** 596-603.

Booth, B.J. 1973: A simplified snow predictor. *Meteor. Mag.,* **102,** 332-340.

Boyden, C.J., 1964: A comparison of snow predictors. *Meteor. Mag.*, **93**, 353-366.

Brooks, C.F., 1920: The nature of sleet and how it is formed. *Mon. Wea. Rev.*, **48**, 69-73.

Burnash R.J. and F.E. Hug, 1970: Predicting precipitation types. ESSA Tech. Memo. WBTM WR-49, 7 pp. [NTIS PB 190-962].

Czys, R.R., and K.C. Tang, 1995: An exact analytical solution for raindrop collision rate. *J. Atmos. Sci.,* **52**, 3289-3292.

Drake, J.C. and B.J. Mason, 1966: The melting of small ice spheres and cones. *Quart. J. Roy. Meteor. Soc.,* **92**, 500.

Fletcher, N.H., 1962: *Physics of Rain Clouds.* Cambridge University Press, 390 pp.

Glahn, H.R., and J.R. Bocchieri, 1975: Objective estimation of the conditional probability of frozen precipitation. *Mon. Wea. Rev.,* **103,** 3-15.

Gunn K.L.S. and J.S. Marshall, 1958: The distribution with size of aggregate snowflakes. *J. Meteor.,* **15**, 452-461.

Huffman, G.J., and G.A. Norman, 1988: The supercooled warm rain process and the specification of freezing precipitation. *Mon. Wea. Rev.,* **116,** 2172-2182.

Koolwine, T., 1975: Freezing Rain. MS thesis, Dept. of Physics, University of Toronto, Ontario, Canada, 92 pp.

Lumb, F.E., 1963: Downward penetration of snow in relationship to the intensity of snow. *Meteor. Mag.,* **92**, 1-14.

Lumb, F.E., 1961: The problem of forecasting the downward penetration of snow. *Meteor. Mag.*, **90**, 310-319.

MacKlin, W.C., 1963: Heat transfer from hailstones. *Quart. J. Roy. Meteor. Soc.,* **89**, 360.

Mahaffy, F.J., 1961: The ice storm of 25-26 February 1961 at Montreal. *Weatherwise*, No. 6, 241-244.

Marshall, J.S., and W.McK. Palmer, 1948: The distribution of raindrops with size. *J. Meteor.*, **5**, 165-166.

Martner, B.E., R.M. Rauber, R.M. Rasmussen, E.T. Prater, and M.K. Ramamurthy, 1992: Impacts of a destructive and well-observed cross-country winter storm. *Bull. Amer. Meteor. Soc.,* **73**, 169-172.

Mason, B.J., 1956: On the melting of hailstones. *Quart. J. Roy. Meteor. Soc.,* **82**, 209.

Miller, R.G., 1964: Regression estimation of events probabilities. Tech. Rep. No. 1, Contract CWB-10704, The Travelers Research Center, Inc., Hartford, CT, 153 pp. [NTIS AD60237].

Murray, R. 1952: Rain and snow in relation to the 1000-700 mb and 1000-500 mb thickness and the freezing level. *Meteor. Mag., 81,* 5-8.

Pandolfo, J.P., 1957: An objective method for forecasting precipitation type during the winter months at New York City. *Bull. Amer. Meteor. Soc.,* **38**, 571-574.

Penn, S., 1957: The prediction of snow vs. rain. *Forecasting Guide No. 2,* U.S. Weather Bureau, 29 pp. [Available from the ISWS Library, Champaign IL or the NOAA Library, Rockville, MD].

Pruppacher, H.R., and J.D. Klett, 1978: *Microphysics of Clouds and Precipitation.* Reidel, 714 pp.

Ramamurthy, M.K., R.M. Rauber, B.P. Collins, M.T. Shields, P.C. Kennedy, and W.L. Clark, 1991: UNIWIPP: A University of Illinois field experiment to investigate the structure of mesoscale precipitation in winter storms. *Bull. Amer. Meteor. Soc.,* **72**, 764-776.

Rasmussen R.M., B.C. Bernstein, M. Murakami, G. Stossmeister, and J. Reisner, 1995: The 1990 Valentine's Day arctic outbreak. Part I: Mesoscale and microscale structure and evolution of a Colorado front range shallow upslope cloud. *J. Appl. Meteor.,* **34**, 1481-1511.

Rauber, R.M., M.K. Ramamurthy, and A. Tokay, 1994: Synoptic and mesoscale structure of a severe freezing rain event: The St. Valentine's Day ice storm. *Wea. Forecasting,* **9**, 183-208.

Stewart, R.E., and G.M. McFarquhar, 1987: On the width and motion of a rain/snow boundary. *Water Resources Research,* **23**, 343-350.

Stewart, R.E. and P. King 1987: Rain/snow boundaries over southern Ontario. *Mon. Weather Rev.,* **115**, 1270-1279.

Szeto, K.K., C.A. Lin, and R.E. Stewart, 1988: Mesoscale circulations forced by the melting of snow in the atmosphere, Part I: Basic simulations and dynamics. *J. Atmos. Sci.,* **45**, 1629-1641.

Vali, G., 1994: Freezing rate due to heterogeneous nucleation. *J. Atmos. Sci.,* **52**, 1843-1856.

Wagner, J.A., 1957: Mean temperature from 1000 mb to 500 mb as a predictor of precipitation type. *Bull. Amer. Meteor. Soc.,* **38**, 584-590.

Young, W.R., 1978: Freezing Precipitation in the Southeastern United States. MS thesis, Texas A&M University, 123 pp.

Younkin, W.H., 1967: A snow index. ESSA Tech. Memo. WBTM NMC-40, 7 pp. [NTIS PB 175-641].

SECTION D

PRELIMINARY STUDY OF PHYSICAL CONDITIONS ASSOCIATED WITH LARGE RESPONSES TO SEEDING

Robert R. Czys

Summary: This analysis was conducted as a first-look to determine if any physical evidence existed to support the finding in the 1989 PACE analysis that AgI-treated experimental units produced more (radar estimated) rainfall than the sand treated units. The analysis was based on data for 6 AgI-treated units and 6 sand-treated units and was sorted into three broad categories; analysis of 1) Synoptic Variables, 2) Radar Variables, and 3) Aircraft Variables. The analysis was restricted to subsets of each data category selected according to variables considered to be important for dynamic responses to seeding, the premise under which the 1989 PACE field experiment was designed. The primary research focus was on two AgI-treated experimental units that apparently had a very large positive reaction to seeding as indicated by radar-estimated rainfall. Statistical comparisons were made to reveal any special features of the experimental units that might help explain why these two units had a preferably larger positive reaction to seeding than the other AgI-treated units.

When the two experimental units with apparent large rainfall enhancements were compared to the other four experimental units treated with AgI, none of the analysis categories (Synoptic, Radar, or Aircraft) indicated any consistent pattern of physical evidence that supported the greater rainfall enhancement. However, this finding does not rule-out the possibility of a rainfall enhancement because the hypothesis and variable selection of this preliminary analysis may not have been consistent with what occurred in nature.

1. Introduction

The 1989 PACE field program produced two primary findings: 1) that individual echo cores probably did not behave as expected from the dynamic seeding hypothesis, and 2) experimental unit and radar-estimated rainfall indicated that the multicelled cloud systems as a whole may have experienced a rainfall enhancement. An interesting feature of the radar-rainfall estimates was that two of the six AgI experimental units exhibited much larger rainfall amounts than the other four units even though their initial rainfall amounts were about the same as the other four units. One interpretation of this behavior in the data, is that the two with the larger radar-estimated rainfall experienced a much larger enhancement then the other four units. To the extent that this interpretation is correct, this suggests that there may have been a number of physical aspects of these two units that were more conducive to producing a rainfall enhancement. Thus, it may be possible to improve on seedability criteria by identifying these physical conditions. Hence, a preliminary analysis, guided by the dynamic seeding hypothesis, which was the design hypothesis for the 1989 PACE field program, was conducted to identify these physical conditions. The next sections describe the methods that were employed and present a few of the preliminary findings and conclusions.

2. Methods

Three parallel analysis were conducted: one that focused on variables that characterized synoptic conditions, one that characterized prerequisite echo core conditions, and one that focused on cloud conditions and targeting of the seeding material. Appendix A lists the variables and their

definition for each of the Synoptic, Radar, and Aircraft components of the analysis.

Variables in the synoptic category, such as tccl, L, and pb were selected based on the hypothesis that clouds with more active coalescence process would tend to more readily produce supercooled drizzle and raindrops, and therefore, might be expected to exhibit a larger response to seeding than clouds characterized by weak coalescence processes. Synoptic variables, such as CAPE, vshr, and Ri were selected to address the prevalent cloud dynamics under the hypothesis that "days" with too strong or too weak attendant dynamics might have background conditions that would overwhelm any potential reaction to seeding.

The variables in the radar category were selected to represent conditions that might be best suited for AgI seeding at echo formation (those variables beginning with the letters "FE" indicating a property at first echo), and those conditions at the time of treatment (those variables beginning with the letters "CP" indicating a property at the treatment "cloud pass").

The variables that compose the aircraft category were selected to represent several difference aspects of initial in-cloud conditions needed for a positive response to seeding according to the Dynamic Seeding Hypothesis. Mean_FWC, Mean_Dia, Mean_Conc, and Dmax_W were chosen to represent the distribution of supercooled cloud droplets under the assumption that certain character of the cloud droplet population might be more amenable to the production of ice crystals.

This would result in a negative dynamic response because the droplets would tend to grow at the expense of the evaporation of cloud droplets. SWCc, the solid water content, was included as an indicator of cloud age with more mature cloud parcels being less desirable for seeding than fresh parcels because they more mature ones would possess high ice content that seeding would have little effect on. Variables Buoy_Enh and PBuoy were included to provide indication of the clouds'

potential for buoyancy enhancement in relation to its buoyancy. Clouds that are very negatively or positively buoyant would require very large buoyancy enhancements for an effect to be evident, while neutrally buoyant would require a large enhancement for a signal to be noticed. Finally, the aircraft component of the analysis included such parameters as the number of flares delivered, and the percent that were released in an updraft to provide a measure as to whether or not the seeding material was properly targeted.

Mean values for each variable were sorted into a number of different sub-categories to allow for meaningful comparison of the cases. Means were computed for all the sand- and AgI- treated experimental units. Then, the means for the AgI-treated units were computed for Experimental Units 05 and 18 against those for units 11, 19, 22, 25. Means for each individual AgI unit (05, 11, 18, 19, 22, 25) were also compared. Of the six total Experimental AgI Units, units 05 and 18 were separated from 11, 19, 22, 25 because EU 05 and 18 exhibited very large (radar-estimated) rainfall enhancements. Hence, we hypothesized that if the enhancements occurred by more than chance, we might expect the physical conditions associated with EU's 05 and 18, or seeding conditions, to differ in ways that may lead to insights, in general, about the adequacy of the seeding hypothesis.

For each category of variable, comparisons were made to determine if there was something special or different about the two experimental units that showed a large positive rainfall enhancement (i.e. 05 and 18) and the other experimental units in the data set. The Wilcoxon Sum Rank Test was used to test for statistical significance in differences between the means. This non-parametric test was selected because it provides an indication of whether the direction and magnitude of the difference between two distributions is statistically significant, while a simple sign test would be used to determine if only the direction is statistically different. The sum rank test was also

developed because it works well with small samples. Because the selection of a p-value to indicate significance can be somewhat arbitrary, shading as been used in each p-Value table to indicate three levels of significance. Dark shading to indicates a level between 0.00 and 0.05, medium shading indicates values between 0.06 and 0.10, and light shading indicates values between 0.11 and 0.15. Of course, the more shading present in an array, the larger the number of differences between comparisons that were found to be significant.

To complete the statistical analysis, results are provided in two more tables for each category. One summarizes the standard deviations associated with the computation of each mean. This table provides some information in regard to the variance associated with each variable, the higher the variance in relation to the mean the less likely that differences exist. Lastly, a listing of sample size is provided for each variable category.

3. Findings

a. Examination of synoptic variables

Table 1.A lists means for the synoptic variables chosen for investigation. The analysis of synoptic variables was based on a total of 54 statistical tests (6 variables by 9 test categories). Therefore, by the rule of multiplicity, we expect that at least 10% of the tests would show a statistical difference (i.e. 5 or 6 tests would show a significant level of 0.15 or less). In the analysis, 30 of the tests had p-values of 0.15 or less, 27 had 0.10 or less, and 22 had p-values of 0.05 or less. Hence, a substantial portion of the tests revealed significant differences.

The first group of three variables (tccl, L and pb) were selected because they address the issue of whether or not the mesoscale conditions were conducive to the production of supercooled drizzle

and raindrops at the seeding level. The dynamic seeding hypothesis indicates that supercooled drops in this size range is important to achieve latent heat releases that would be sufficient large to impact cloud buoyancy and thus enhance vertical cloud growth. For this discussion, we focus on the variable, L, because this is a direct measure of coalescence activity, with increased coalescence activity being indicated as L becomes more negative.

The p-value results for L listed in Table 1.B show an extremely high level of significance when Experimental Units (EUs) 05 and 18 (the two units with suspected very large rain enhancement) are compared to the other AgI treated units (EUs 11, 19, 22, and 25) and when compared to all AgI EUs. However, examination of the means for L for EU 05 and 18 show a large (18) and a small (05) value. That fact that the individual values of L are not consistent with each other does not support the hypothesis that the units suspected of having a large response to seeding may have somehow been related to an appropriately active coalescence process and the presence of suitable concentrations of supercooled drizzle and raindrops for desired buoyancy enhancement.

The last three synoptic variables were selected for their relevance to cloud environment dynamics. Too strong or too weak dynamics and potential seeding might be overwhelmed by governing kinematics. Examination of Table 1.B suggests that CAPE and wind shear (vshr) may have been significantly different for the two units (05 and 18) that have suspected (radar estimated) rainfall enhancements from seeding. However, as was the case for coalescence activity, means for CAPE and vshr are quite different when examined individually (i.e. EU 05 compared to EU 18). Therefore, this inconsistency does not support the hypothesis that the environmental dynamics for EU 05 and 18 somehow favored a rainfall enhancement over the other AgI experimental units.

b. Examination of radar variables

A total of 81 statistical tests were made on the radar variables (9 variables by 9 sub-categorize). Therefore, at least 10% of the tests, or 8 or 9 could be expected to show a statistically significant difference. Table 2.B shows that 15 tests had significance, several more than expected.

In contrast to the analysis of synoptic variables, only one of the radar variables (FECPT, or the time from first echo to treatment) had a significance level of less than 0.15 when the mean for EU 05 and 18 was compared to the mean for EUs 11, 19, 22, and 25. Furthermore, the p-value is greater than 0.10. Had a criteria of less than 0.10 been established, this comparison would have been judged not to be significant. The weak significance in this one variable, combined with the lack of significance for the other variables, suggests that there was nothing remarkably different in the echo core characteristics of the two EUs that were suspected as being rainfall enhancements compared to the other AgI-treated EUs.

c. Examination of aircraft variables

A total of 135 tests were performed on the aircraft variables (15 variables by 9 sub-categories). If 10% of the tests can be expected to produce a statistically significant difference by chance, then 13 to 14 tests listed in Table 3.B should have p-values of 0.15 or less. Examination of Table 3.B shows that only 5 of the tests had p-values of less than 0.15. This is approximately a third of the total expected. Furthermore, the p-values are all between 0.10 and 0.15, which can be interpreted as having weak significance. Hence, the analysis of aircraft variables does not contain any evidence that might support the hypothesis that the physical in-cloud conditions, or targeting of the seeding material was different for

the two experimental units that have suspected large rainfall enhancements due to seeding.

4. Summary and Conclusions

Three broad categories of variables (synoptic, radar, and aircraft) were analyzed to determine if any physical evidence could be found to help explain why two of the AgI-treated experimental units (05 and 18) showed exceptionally large rainfall enhancements, in comparison to the other four AgI-treated units (i.e. EUs 11, 19, 22, and 25). Neither the synoptic, radar, or aircraft categories produced a consistent picture of physical evidence that would support the greater rainfall enhancements, at least for the variables selected according to cloud responses expected under the dynamic seeding hypothesis. However, the results of this analysis can not be used to reject the impression that the network and experimental rainfall of the AgI-treated units was enhanced. The analysis was cursory and selection of different variables based on a difference hypothesis about the response of the clouds to seeding may lead to different results and conclusions.

5. References

Siegel, S., 1956: *Nonparametric Statistics for the Behavioral Sciences*. McGraw-Hill Book Company, Inc., 312 pp.

Tabel 1.A. SYNOPTIC MEANS

	Sand All	AgI All	AgI 05,18	AgI 11,19 22,25	AgI 05	AgI 11	AgI 18	AgI 19	AgI 22	AgI 25
tccl	16.3	16.4	15.3	16.9	18.0	15.8	13.8	17.9	16.2	18.7
L	-0.6	1.9	6.3	0.1	1.7	1.4	9.0	3.4	-1.4	-3.9
pb	4.1	5.6	7.5	4.9	6.4	5.0	8.2	7.4	3.6	3.6
CAPE	482.2	773.0	877.0	732.1	1339.0	636.0	613.0	1278.0	475.0	588.0
vshr	12.8	9.8	14.2	8.1	25.0	11.7	8.0	7.0	7.0	6.2
Ri	62.1	88.8	68.1	96.9	53.5	54.2	76.5	181.9	68.0	94.8

Tabel 1.B. SYNOPTIC P-VALUES

	05,18 & 11,19 22,25	05,18 & AgI All	11,19 22,25 & AgI All	05 & AgI All	11 & AgI All	18 & AgI All	19 & AgI All	22 & AgI All	25 & AgI All
tccl	0.07	0.17	0.46	0.02	0.05	0.00	0.09	0.90	0.00
L	0.00	0.00	0.11	0.56	0.67	0.00	0.05	0.01	0.00
pb	0.00	0.00	0.11	0.56	0.67	0.00	0.05	0.01	0.04
CAPE	0.08	0.19	0.48	0.00	0.28	0.67	0.01	0.30	0.21
vshr	0.00	0.01	0.18	0.00	0.01	0.28	0.13	0.08	0.00
Ri	0.27	0.41	0.66	0.00	0.01	0.28	0.00	0.39	0.08

Table 1.C. SYNOPTIC STANDARD DEVIATION

	Sand All	AgI All	AgI 05,18	AgI 11,19 22,25	AgI 05	AgI 11	AgI 18	AgI 19	AgI 22	AgI 25
tccl	2.1	1.6	2.0	1.1	0.0	0.0	0.0	0.0	0.0	0.0
L	4.6	4.0	3.5	2.5	0.0	0.0	0.0	0.0	0.0	0.0
pb	2.1	1.8	0.9	1.6	0.0	0.0	0.0	0.0	0.0	0.0
CAPE	214.0	336.0	349.2	321.5	0.0	0.0	0.0	0.0	0.0	0.0
vshr	12.6	5.4	8.2	2.1	0.0	0.0	0.0	0.0	0.0	0.0
Ri	30.5	45.2	11.1	50.6	0.0	0.0	0.0	0.0	0.0	0.0

Table l.D. SYNOPTIC SAMPLE SIZE

	Sand All	AgI All	AgI 05,18	AgI 11,19 22,25	AgI 05	AgI 11	AgI 18	AgI 19	AgI 22	AgI 25
tccl	32.0	39.0	11.0	28.0	4.0	7.0	7.0	7.0	10.0	4.0
L	32.0	39.0	11.0	28.0	4.0	7.0	7.0	7.0	10.0	4.0
pb	32.0	39.0	11.0	28.0	4.0	7.0	7.0	7.0	10.0	4.0
CAPE	32.0	39.0	11.0	28.0	4.0	7.0	7.0	7.0	10.0	4.0
vshr	32.0	39.0	11.0	28.0	4.0	7.0	7.0	7.0	10.0	4.0
Ri	32.0	39.0	11.0	28.0	4.0	7.0	7.0	7.0	10.0	4.0

Table 2.A. RADAR MEANS

	Sand All	AgI All	AgI 05,18	AgI 11,19 22,25	AgI 05	AgI 11	AgI 18	AgI 19	AgI 22	AgI 25
CPA56	23.1	13.6	8.2	15.7	18.0	3.9	2.6	6.3	31.2	14.2
CPZ56	31.6	21.0	16.2	22.9	29.7	15.8	8.4	9.6	37.1	22.9
FEHtp10	6.3	5.4	5.5	5.4	5.0	5.9	5.7	4.3	5.8	5.2
FEdpth10	2.3	1.9	1.7	2.0	2.8	2.9	1.1	1.4	1.7	2.0
FEA10	12.2	5.6	5.6	5.6	10.8	5.4	2.7	2.9	7.9	5.2
FEVol10	36.0	12.8	11.8	13.2	25.5	14.0	4.0	7.1	16.6	13.8
FEMxZ	29.5	22.1	19.8	23.0	31.6	24.0	13.1	11.7	26.9	31.8
FEHMxZ	4.8	4.3	4.5	4.2	3.0	4.6	5.3	3.4	4.8	3.8
FECPt	8.8	6.0	3.7	6.9	5.7	6.6	2.3	2.0	6.1	14.5

Table 2.B. RADAR P-VALUES

	05,18 & 11,19 22,25	05,18 & AgI All	11,19 22,25 & AgI All	05 & AgI All	11 & AgI All	18 & AgI All	19 & AgI All	22 & AgI All	25 & AgI All
CPA56	0.44	0.56	0.75	0.18	0.18	0.08	0.17	0.01	0.69
CPZ56	0.32	0.45	0.68	0.23	0.50	0.06	0.09	0.01	0.83
FEHtp10	0.84	0.88	0.93	0.31	0.93	0.34	0.98	0.92	0.54
FEdpth10	0.70	0.77	0.87	0.26	0.16	0.23	0.44	0.72	0.82
FEA10	0.81	0.86	0.92	0.02	0.89	0.13	0.12	0.40	0.85
FEVol10	0.65	0.73	0.85	0.04	0.59	0.06	0.25	0.46	0.83
FEMxZ	0.43	0.55	0.75	0.09	0.81	0.05	0.10	0.32	0.18
FEHMxZ	0.62	0.71	0.84	0.09	0.94	0.08	0.66	0.74	0.46
FECPt	0.13	0.25	0.53	0.82	0.50	0.17	0.16	0.81	0.05

Table 2.C. RADAR STANDARD DEVIATION

	Sand All	AgI All	AgI 05,18	AgI 11,19 22,25	AgI 05	AgI 11	AgI 18	AgI 19	AgI 22	AgI 25
CPA56	18.9	18.7	9.9	20.8	9.4	5.4	4.1	11.6	11.6	12.9
CPZ56	16.4	16.3	13.7	16.9	4.6	12.5	10.8	11.8	11.8	14.3
FEHtp10	1.7	2.2	2.0	2.2	0.7	1.1	2.4	3.8	3.8	0.8
FEdpth10	1.5	1.5	1.5	1.6	1.3	1.6	1.2	1.5	1.5	1.4
FEA10	10.2	5.1	4.5	5.4	2.6	3.7	2.0	3.0	3.0	2.8
FEVol10	44.0	11.3	11.4	11.3	7.4	10.7	2.2	7.2	7.2	9.7
FEMxZ	11.7	12.6	10.5	13.3	5.4	11.3	5.7	10.7	10.7	11.7
FEHMxZ	1.7	2.0	2.1	2.0	0.7	0.9	2.2	3.1	3.1	1.5
FECPt	10.9	6.1	5.1	6.2	6.2	4.0	3.7	5.9	5.9	7.1

Table 2.D. RADAR SAMPLE SIZE

	Sand All	AgI All	AgI 05,18	AgI 11,19 22,25	AgI 05	AgI 11	AgI 18	AgI 19	AgI 22	AgI 25
CPA56	32.0	39.0	11.0	28.0	4.0	7.0	7.0	7.0	10.0	4.0
CPZ56	32.0	39.0	11.0	28.0	4.0	7.0	7.0	7.0	10.0	4.0
FEHtp10	32.0	39.0	11.0	28.0	4.0	7.0	7.0	7.0	10.0	4.0
FEdpth10	32.0	39.0	11.0	28.0	4.0	7.0	7.0	7.0	10.0	4.0
FEA10	32.0	39.0	11.0	28.0	4.0	7.0	7.0	7.0	10.0	4.0
FEVol10	32.0	39.0	11.0	28.0	4.0	7.0	7.0	7.0	10.0	4.0
FEMxZ	32.0	39.0	11.0	28.0	4.0	7.0	7.0	7.0	10.0	4.0
FEHMxZ	32.0	39.0	11.0	28.0	4.0	7.0	7.0	7.0	10.0	4.0
FECPt	32.0	39.0	11.0	28.0	4.0	7.0	7.0	7.0	10.0	4.0

Table 3.A. AIRCRAFT MEANS

	Sand All	AgI All	AgI 05,18	AgI 11,19 22,25	AgI 05	AgI 11	AgI 18	AgI 19	AgI 22	AgI 25
UP_Dia	1900.0	1050.8	995.0	1065.2	-99.0	620.1	-99.0	1415.9	1026.9	1316.6
Mean_VW	6.6	3.9	3.8	3.9	-99.0	2.1	-99.0	6.6	3.4	3.5
U#_flrs	4.5	2.7	2.1	2.9	-99.0	2.0	-99.0	3.3	3.2	2.8
Buoy_Enh	0.5	0.5	0.4	0.5	-99.0	0.5	-99.0	0.5	0.5	0.5
PBuoy	-0.7	-1.0	-0.2	-1.2	-99.0	-1.8	-99.0	-2.1	-1.2	0.8
SWC_frac	0.2	0.2	0.2	0.2	-99.0	0.1	-99.0	0.0	0.1	0.6
Cld_Dia	3801.1	3213.2	2898.5	3336.9	3364.4	2735.4	2632.2	3049.5	3562.8	4327.6
%_Updraft	59.9	37.5	34.8	38.2	-99.0	27.0	-99.0	49.2	31.8	53.4
%_in_Up	84.2	52.6	37.1	56.6	-99.0	36.4	-99.0	63.8	49.3	95.8
Mean_FWC	1.1	1.3	0.9	1.4	-99.0	1.9	-99.0	1.7	1.4	0.6
Mean_Dia	18.1	17.5	18.7	17.2	-99.0	18.2	-99.0	16.9	16.4	18.0
Mean_Conc	204.1	257.1	247.5	259.3	-99.0	367.6	-99.0	321.3	235.2	106.2
Dmax_W	1.8	1.4	1.3	1.4	-99.0	1.8	-99.0	0.3	2.3	0.9
LWCc	0.5	0.6	1.6	0.4	-99.0	-99.0	-99.0	-99.0	-99.0	-99.0
SWCc	1.1	0.5	0.3	0.6	-99.0	0.4	-99.0	-99.0	-99.0	0.4

Table 3.B. AIRCRAFT P-VALUES

	05,18 11,19 22,25	05,18 & AgI All	11,19 22,25 & AgI All	05 & AgI All	11 & AgI All	18 & AgI All	19 & AgI All	22 & AgI All	25 & AgI All
UP_Dia	0.59	0.66	0.86	NaN	0.28	0.66	0.36	0.94	0.34
Mean_VW	0.90	0.92	0.97	NaN	0.17	0.92	0.15	0.99	0.94
U#_flrs	0.25	0.35	0.70	NaN	0.60	0.35	0.56	0.68	0.60
Buoy_Enh	0.10	0.17	0.59	NaN	0.66	0.17	0.56	0.40	0.14
PBuoy	0.44	0.52	0.80	NaN	0.36	0.52	0.11	0.84	0.01
SWC_frac	0.44	0.52	0.80	NaN	0.79	0.52	0.08	0.80	0.12
Cld_Dia	0.47	0.59	0.77	0.74	0.52	0.34	0.93	0.64	0.24
%_Updraft	0.72	0.77	0.90	NaN	0.29	0.77	0.25	0.56	0.23
%_in_Up	0.22	0.31	0.67	NaN	0.31	0.31	0.46	0.79	0.03
Mean_FWC	0.45	0.53	0.81	NaN	0.25	0.53	0.35	0.92	0.14
Mean_Dia	0.32	0.41	0.75	NaN	0.46	0.41	0.71	0.75	0.84
Mean_Conc	0.75	0.80	0.92	NaN	0.24	0.80	0.54	0.91	0.14
Dmax_W	0.93	0.94	0.98	NaN	0.35	0.94	0.11	0.25	0.56
LWCc	0.64	0.69	0.88	NaN	0.69	0.69	NaN	0.72	NaN
SWCc	0.43	0.55	0.76	NaN	0.88	0.55	0.19	0.19	0.81

Table 3.C. AIRCRAFT STANDARD DEVIATION

	Sand All	AgI All	AgI 05,18	AgI 11,19 22,25	AgI 05	AgI 11	AgI 18	AgI 19	AgI 22	AgI 25
UP_Dia	1223.9	915.0	1070.3	869.6	-99.0	649.8	-99.0	1047.4	1047.4	570.6
Mean_VW	3.7	3.4	3.4	3.3	-99.0	2.5	-99.0	4.6	4.6	0.9
U#_flrs	3.1	2.9	3.4	2.7	-99.0	2.3	-99.0	2.7	2.7	1.1
Buoy_Enh	0.0	0.1	0.1	0.0	-99.0	0.0	-99.0	0.0	0.0	0.0
PBuoy	3.7	1.6	2.2	1.4	-99.0	0.5	-99.0	1.3	1.3	0.3
SWC_frac	0.3	0.3	0.2	0.3	-99.0	0.1	-99.0	0.0	0.0	0.3
Cld_Dia	2469.2	1372.2	1276.6	1388.6	1042.2	865.9	1321.0	956.1	956.1	1710.3
%_Updraft	19.9	26.2	28.0	25.7	-99.0	25.7	-99.0	24.7	24.7	24.9
%_in_Up	22.4	37.5	35.7	36.9	-99.0	38.2	-99.0	37.3	37.3	7.2
Mean_FWC	0.5	0.9	0.4	1.0	-99.0	0.6	-99.0	1.0	1.0	0.1
Mean_Dia	3.2	4.2	6.4	3.5	-99.0	0.8	-99.0	3.9	3.9	1.2
Mean_Conc	92.7	159.0	122.6	166.1	-99.0	114.4	-99.0	203.0	203.0	14.0
Dmax_W	1.5	1.7	1.6	1.8	-99.0	1.2	-99.0	0.2	0.2	0.9
LWCc	0.6	0.9	1.6	0.5	-99.0	-99.0	-99.0	-99.0	-99.0	-99.0
SWCc	2.3	0.4	0.1	0.4	-99.0	0.1	-99.0	-99.0	-99.0	0.2

Table 3.D. AIRCRAFT SAMPLE SIZE

	Sand All	AgI All	AgI 05,18	AgI 11,19 22,25	AgI 05	AgI 11	AgI 18	AgI 19	AgI 22	AgI 25
UP_Dia	32.0	39.0	11.0	28.0	4.0	7.0	7.0	7.0	10.0	4.0
Mean_VW	32.0	39.0	11.0	28.0	4.0	7.0	7.0	7.0	10.0	4.0
U#_flrs	32.0	39.0	11.0	28.0	4.0	7.0	7.0	7.0	10.0	4.0
Buoy_Enh	32.0	39.0	11.0	28.0	4.0	7.0	7.0	7.0	10.0	4.0
PBuoy	32.0	39.0	11.0	28.0	4.0	7.0	7.0	7.0	10.0	4.0
SWC_frac	32.0	39.0	11.0	28.0	4.0	7.0	7.0	7.0	10.0	4.0
Cld_Dia	32.0	39.0	11.0	28.0	4.0	7.0	7.0	7.0	10.0	4.0
%_Updraft	32.0	39.0	11.0	28.0	4.0	7.0	7.0	7.0	10.0	4.0
%_in_Up	32.0	39.0	11.0	28.0	4.0	7.0	7.0	7.0	10.0	4.0
Mean_FWC	32.0	39.0	11.0	28.0	4.0	7.0	7.0	7.0	10.0	4.0
Mean_Dia	32.0	39.0	11.0	28.0	4.0	7.0	7.0	7.0	10.0	4.0
Mean_Conc	32.0	39.0	11.0	28.0	4.0	7.0	7.0	7.0	10.0	4.0
Dmax_W	32.0	39.0	11.0	28.0	4.0	7.0	7.0	7.0	10.0	4.0
LWCc	32.0	39.0	11.0	28.0	4.0	7.0	7.0	7.0	10.0	4.0
SWCc	32.0	39.0	11.0	28.0	4.0	7.0	7.0	7.0	10.0	4.0

APPENDIX A

Abbreviations and definitions of the variables that were analyzed in this study.

Abbreviation		Definition
Synoptic:		
tccl		Temperature of the Convective Condensation Level, °C
L		Coalescence activity
pb		Potential buoyancy, °C
CAPE		Convective Available Potential Energy, m2 s^{-2}
vshr		Vertical shear of the horizontal wind, m s^{-1}
Ri		Richardson Number
Radar:		
CPA56		Area at flight level at treatment, km^2
CPZ56		Max. reflectivity at flight level at treatment, dBZ
FEHtp	10	First Echo top height defined by the 10 dBZ contour, km
FEdpth	10	First Echo depth defined by the 10 dBZ contour, km
FEA	10	First Echo max. area defined by the 10 dBZ contour, km^2
FEVol	10	First Echo volume defined by the 10 dBZ contour, km^3
FEMxZ		First Echo maximum reflectivity, dBZ
FEHMxZ		Height of maximum reflectivity of First Echo, km
FECPt		Time from First Echo to Treatment, min
Aircraft:		
UP_Dia		Updraft diameter, m
Mean_VW		Mean updraft velocity, m s^{-1}
U#_flrs		Total number of flares released
Buoy_Enh		Buoyancy enhancement, °C
PBuoy		Potential buoyancy, °C
SWC_frac		Fraction of total condensate that was ice
Cld_Dia		Cloud diameter, m
%_Updraft		Percent of cloud penetration that was updraft
%_in_Up		Percent of total flares delivered to updraft
Mean_FWC		Mean FSSP liquid water content for penetration, g m^{-3}
Mean_Dia		Mean FSSP cloud droplet diameter, µm
Mean_Conc		Mean FSSP cloud droplet concentration, cm^{-3}
Dmax_W		Maximum diameter of supercooled drizzle and rain drops, mm
LWCc		2D liquid water content, g m^{-3}
SWCc		2D solid water content, g m^{-3}

SECTION E

INTEGRATION OF 1989 PACE CLOUD PHYSICS DATA WITH LABORATORY RESULTS TO IMPROVE UNDERSTANDING ABOUT THE ORIGIN OF ICE IN ILLINOIS CLOUDS

Robert R. Czys

Summary: The following research was conducted, as part of our proposed efforts, to improve understanding of natural cloud and precipitation processes in order to improve the scientific knowledge about summertime precipitation enhancement in Illinois. The following section reports on how results from laboratory experiments, largely supported by the National Science Foundation, were integrated with cloud physics data collected as part of the 1989 PACE field program. This led to discovery of a new mechanism for the production of graupel embryos in Dlinois clouds. This section begins with a description of laboratory experiments performed by creating a light shower of supercooled rain in a vertical wind tunnel to investigate interactions between small precipitation-size drops at temperatures colder than 0°C. We then report on one trial in which the subject drop froze and subsequently interacted with a supercooled drop in the tunnel rain shower to form a dumbbell shaped ice particle. Examination of two-dimensional optical array probe data obtained at the -10°C level in warm-based Midwestern rain clouds revealed a number of dumbbell shaped images that could not be accounted for by particle collocation in the sample area of the 2D laser beam. Theoretical analysis indicated that the number of liquid-frozen interactions (LFIs) between precipitation-size particles can be sufficient to account for observed concentrations of dumbbell shaped ice.

The mechanism that was observed in the wind tunnel experiments would be a powerful mechanism for the production of graupel embryos in clouds. The findings suggest that failure to include dumbbell shapes in the schemes of image classification software risks underestimating concentrations of in situ ice, while overlooking a mechanism that contributes to the evolution of ice in clouds.

1. Introduction

In the evolution of precipitation under mixed phased conditions, ice particle-water drop interactions are most commonly considered to be those involving droplets on the order of sizes smaller than about 100 μm diameter, i.e. supercooled cloud droplets. Laboratory and field studies that have focused on the small end of the size spectra are too numerous to review, but they have generally emphasized either riming growth or splinter production for ice multiplication. Somewhat neglected in considerations of the evolution of precipitation, especially in deep warm-based convective rain clouds characterized by and active coalescence process, are interactions that may involve precipitation-size drops at temperatures colder than 0°C. Berry and Reinhardt (1974) referred to this interaction size regime as "self-collection." They found that it was crucial to the rapid increase of the predominate radius and the emerging shape of the total spectra at temperatures warmer than 0°C.

Berry and Reinhardt and many previous numerical simulations have not concentrated on the profound effect self-collection may have on the conversion of supercooled water-to-ice, or they have relegated the matter to bulk computations. As a cloudy parcel of air containing the full range of drop

sizes is transported above the melting level, the particles initially supercool and continue to interact just as they did below the melting level. Shortly thereafter, some of the rain drops begin to freeze which has been born out in many previous field studies. The importance of the role of supercooled drizzle and rain drops in the generation of ice and the evolution of precipitation was probably first brought to light from observations in Project Whitetop (Koeing 1963, Braham 1964) and excellent overall reviews on the origin of ice in clouds have been made by Mossop 1985 and Beard 1992. What is not well know is the outcome of interactions solely involving supercooled drizzle and rain drops nor what happens when a frozen raindrop interacts with a neighboring supercooled drizzle or raindrop.

This work presents *the first* laboratory evidence, along with supporting observational evidence, of the production of a new ice particle form that may serve as an efficient graupel embryo.

2. Experimental

a. Setup

The UCLA vertical wind tunnel was used in this study to produce collisions between small, supercooled precipitation-size drops. A description of the general features and arrangement of the wind tunnel has been given by Beard and Pruppacher (1969). Figure 1 shows a schematic diagram of the experiment setup and the relative configuration of the major system components as we used it.

Water drops for experimentation where produced in the upper tunnel's working section from a simple drop fountaining system (see Fig. 2). The fountain consisted of a curved vertically oriented

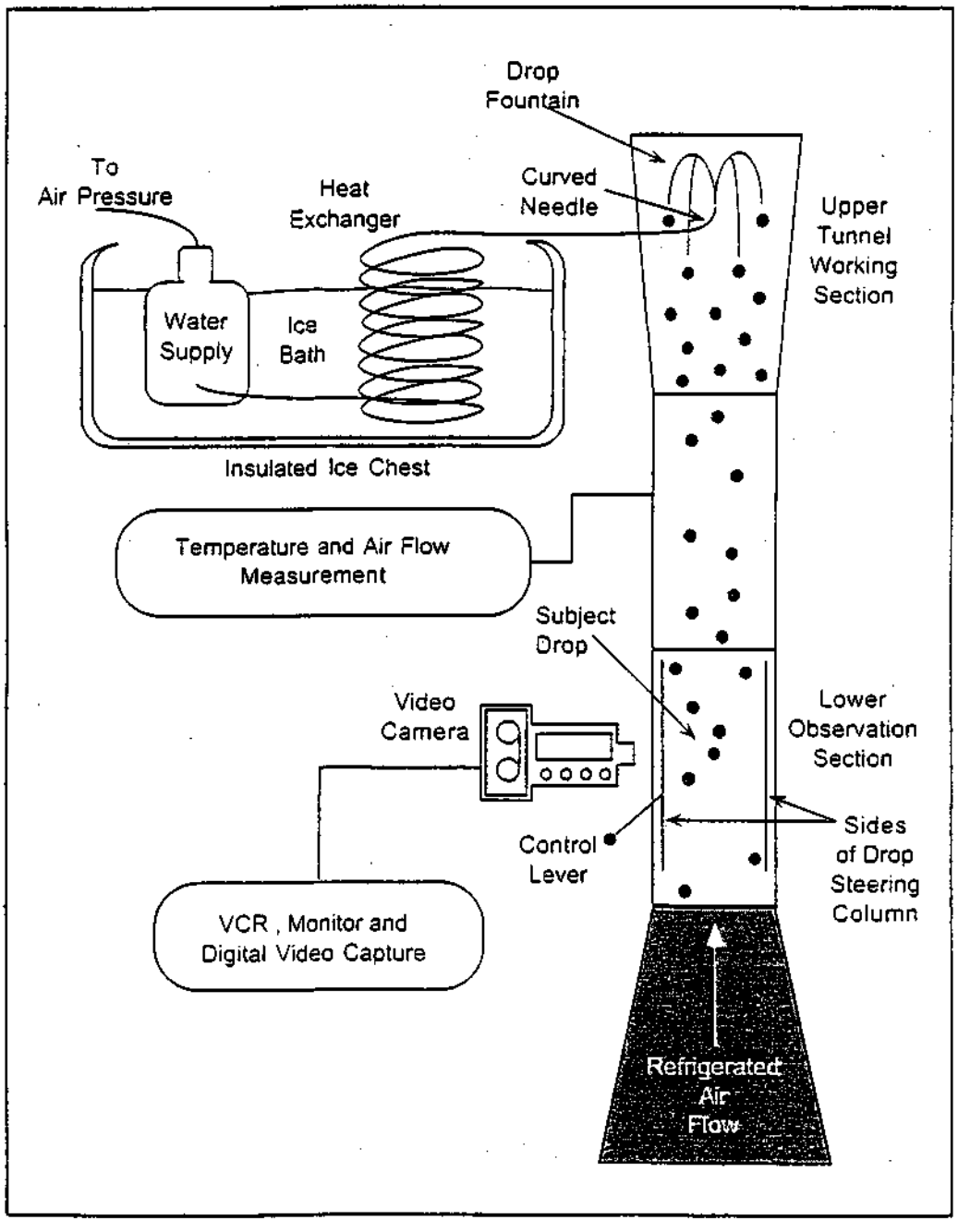

Figure 1. Schematic diagram showing experiment set up to study interactions between supercooled drops in a vertical wind tunnel.

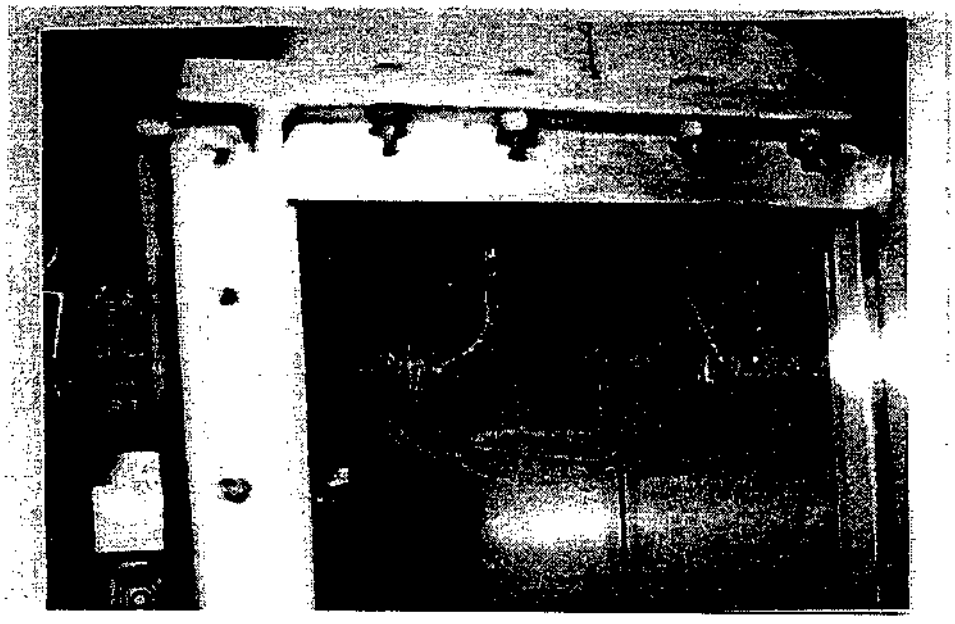

Figure 2. Photograph showing curved needle that was used to generate a spray of small precipitation-size drops for experimentation.

hypodermic needle that was fed by a 5 liter polyethylene bottle and heat exchanger coil. The supply bottle, filled with distilled deionized water, was slightly pressurized to cause water to continuously issue from the needle tip. The liquid jet emanating from the needle would break-up into a spray of water drops. The spray naturally produced a distribution of drops sizes in the range from about 500 to 1000 μm radius. The smallest drops where carried upward by the tunnel air flow out of the upper tunnel working section. Larger drops fell downward against the air flow in effect producing a light shower of supercooled rain.

Drops from the fountain were introduced at a temperature very near 0°C. This was accomplished by submerging the water supply bottle and heat exchanger coil in an ice bath, as illustrated in Fig. 1. A thermocouple was fastened to the tip of the hypodermic needle to obtain an estimate of the temperature of the water drop as they entered the tunnel. At times during a trial, it was not unusual for the measured temperature at the needle tip to be several degrees colder than 0°C because of additional cooling caused by the cold tunnel air flow. The continuous flow of water and positive temperature gradient from needle tip to tunnel wall prevented the nucleation of ice in the needle. Another thermocouple, located between the upper and lower tunnel sections, was used to measure tunnel air temperature. All temperature measurements, as well as tunnel air velocity, were recorded continuously during each trial using a PC-based data acquisition system.

b. Procedural

A trial began when the fountain needle was inserted into the upper tunnel working section. Next, using a flow-controller-insert (see Figs. 1 and 3) the system operator would "catch" a drop in the shower and "float" it at a quasi-fixed position relative to the view of a macro video camera. Study

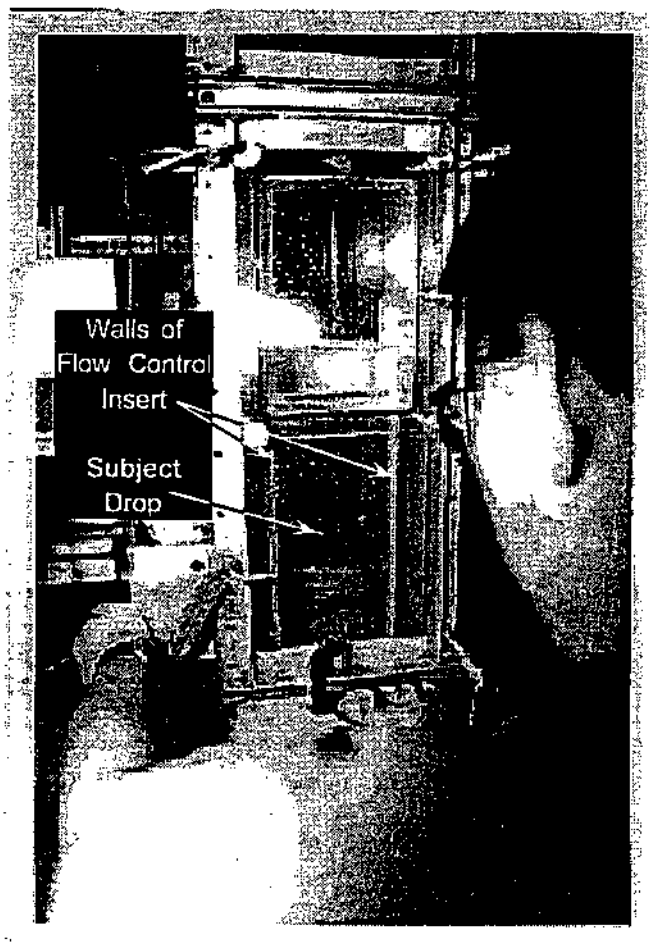

Figure 3. Photograph showing tunnel operating "floating" a subject drop in the presence of a very light shower of drizzle drops.

drops were typically about 500 μm radius as indicated by the tunnel air velocity which was sufficient to float the drop.

Interactions between a subject drop and a drop in the supercooled rain shower were random events. Figure 4 shows a cumulative percentage of the number of interactions that subject drops experienced during the experimentation. In this work, 99 different subject drops were floated. Thirty percent of them experienced no interaction, while another 38 percent experienced at least on interaction. Of the remaining 32 percent multiple interactions are characterized by a series of glancing bounces where it was possible to recover the original subject drop that ended with a coalescence where the resultant drop was usually driven out of view or a bounce from a less glancing hit which would impart a lateral velocity that drove the drops into the tunnel wall.

Examination of the video images of bouncing events shows no evidence, over the very short period of time from the interaction to when the drops collide with the tunnel wall, that the mechanical shock of the collision caused ice to nucleate in either of the resultant drops. However, the few frames of video available for each bounce event are probably too few to draw a definitive conclusion about mechanical ice nucleation in the experiment. Although it was difficult to keep the interaction within view, occasionally the operator was successful at anticipating an interaction, and thus was ready to make appropriate velocity corrections that would maintain the result within the viewing area. These one or two occasions did not show evidence of mechanical ice nucleation in the experiment.

A trial was terminated for several reasons; when the build-up of water obscured vision into the tunnel and/or caused air flow instabilities so large that it made it impossible to float and control a

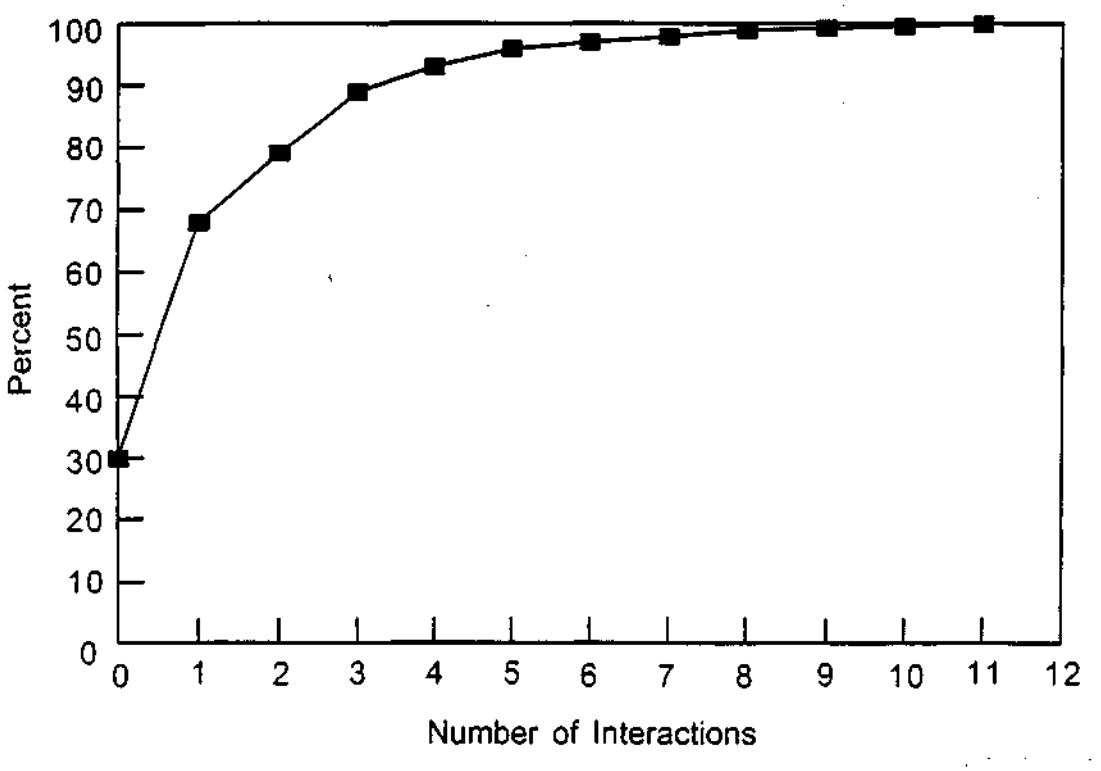

Figure 4. Cumulative percentage of the number of interactions that subject drops experienced during the experimentation. In this work 99 different subject drops were floated. Thirty percent of them experienced no interaction, while another 38% experienced at least one interaction.

subject drop. Trials usually lasted about 5 to 20 minutes after the fountain needle was inserted into the upper section of the tunnel. At termination, the fountain needle was removed, the refrigeration system was shut-down and the access ports of the tunnel opened to allow room temperature air to circulate through the tunnel to remove the water and ice build-up.

c. Control Trials

Trials in which no interaction occurred served as control data to demonstrate that the subject drop could be reliably supercooled. These trials showed that it was readily possible to float a supercooled subject drops for times extending out to 8 minutes after which time the subject drop was abandoned either because: 1) it was necessary to catch another subject that might more likely interact with drops in the rain, 2) the subject became so small from evaporation it could not be tracked by the system operator, or 3) vision into the tunnel became so obstructed by the collection of drops on the inner walls that the system operator could no longer follow a drop.

On the few occasions when the subject drop did spontaneously freeze it always occurred immediately upon being caught. Freezing always required a reduction of tunnel velocity to compensate for a decrease in terminal velocity associated with the difference in drag force between a liquid and solid particle. Frozen subject drops also exhibited an initial erratic circular drift followed by a very regular orbiting motion around a quasi-stationary point in space once outer solidification of the particle was completed. This behavior is very consistent with reports from previous wind tunnel studies of frozen drops such as those of Pitter and Pruppacher (1973).

3. Wind Tunnel Results

The wind tunnel investigations resulted in an important finding that occurred during one of the trials when the subject drop spontaneously froze. Upon freezing, we observed and the video record clearly shows that the solidifying particle progressed vertically owing to the decrease in terminal velocity and the delayed response of the operator. As the freezing subject drop progressed vertically, it happened to interact, in a glancing collision, with one of the larger supercooled drops in the rain shower. Upon interacting with a supercooled drop, a "dumbbell-shaped" ice particle was created. During the time of freezing and interaction, the system operator was fortunately able to make sufficient adjustments to the tunnel air velocity to stabilize the position of the newly formed particle in the view of the observers and the video camera.

Figure 5 shows an extreme close-up of a dumbbell-shaped ice particle that was observed. The figure was produced by capturing a single frame from the video imagery recorded several seconds after the particle motion was stabilized in the tunnel air flow. As indicated in the figure, some of the other larger circular images are out-of-focus water drops that had accumulated on the interior glass walls of the lower observation section. As was seen during the event and recorded on video, the ice particle displayed a dumbbell-shape that obviously spun around its vertical axis. This behavior contrasts with orbital motion that was always seen for single subject drops and is very consistent with the gyroscope-like spinning motion reported by Pitter and Pruppacher (1973) for frozen drops that had developed a surface protuberance of some sort.

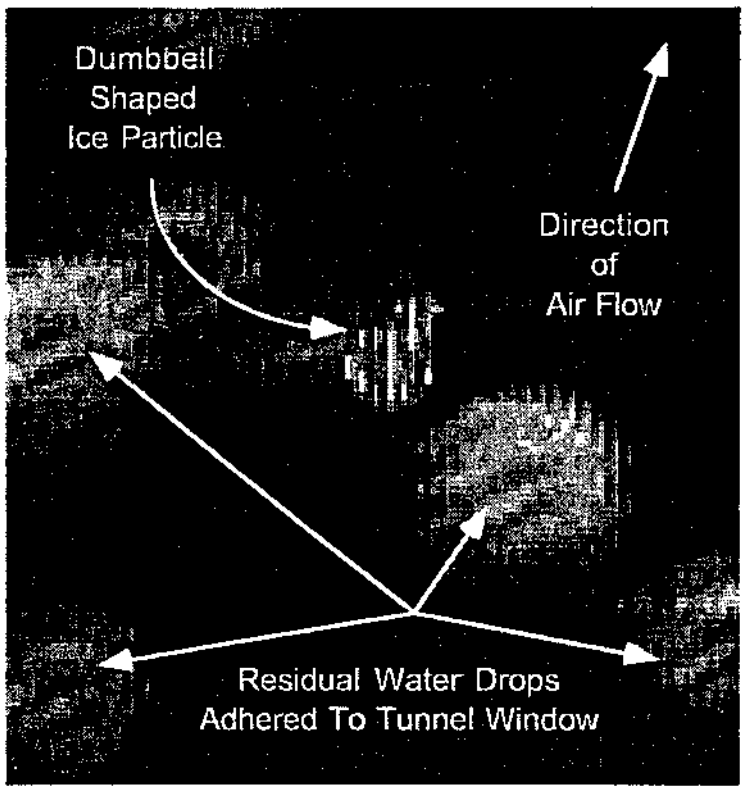

Figure 5. An extreme close-up of a dumbbell-shaped ice particle that occurred during one of the experimental trials. The particle was created when a frozen subject drop interacted one of the supercooled drops in the shower.

4. Discussion

The production of a dumbbell-shaped ice particle in this laboratory experiment helps explain the presence of similar objects that have been identified in microphysical observations of mixed phased clouds at temperatures colder than 0°C. Alkezweeny (1969) was the first to report the presence of dumbbell shaped ice particles in particle replicator data obtained at the -10°C level in Arizona convective clouds. Figure 6 shows an example of one of the dumbbell shaped ice particles found by Alkezweeny. Couplet sizes in the figure are 120 and 60 μm diameter. Alkezweeny also showed evidence for a larger couplet sizes of 200 and 140 μm diameter. Alkezweeny attributed the presence of these particles to freezing caused by "dynamic" ice nucleation caused from when two supercooled precipitation-size drops collide.

Alkezweeny's report prompted us to examine 2DC and 2DP-OAP image records obtained during the 1989 field program of the Precipitation Augmentation for Crop Experiment (PACE). The background and objects of PACE have been summarized by Changnon et al. (1991), and some of the in situ cloud measurements have been summarized in Czys et al. (1995) and Czys (1991).

Aircraft measurements were taken around the -10°C level (~20 kft over Illinois in summer) through warm-based cumuli congestus growing in association with multicelled rain systems. A total of 71 penetrations of individual clouds were made during the course of 25 flight missions. The level of initial penetration averaged about 2500 ft below cloud top and cloud top was never more than 5000 ft above the initial level of penetration. This criteria was followed to insure that the measurements would be mostly representative of the result of microphysical processes in moist adiabatic ascent.

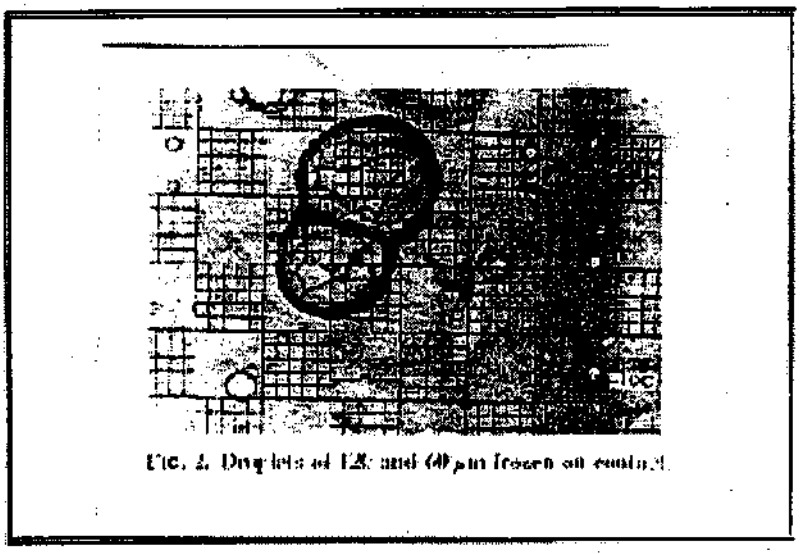

Figure 6 An example of one of the dumbbell shaped ice particles found by Alkezweeny (1969).

Examination of the 2D records for images that may have been caused by the particle observed in our experiments (and reported by Alkezweeny) was accomplished using computer software specifically developed to assist with 2D image classification in PACE. This software has been described by Czys and Petersen 1992. Examination revealed 96 dumbbell-shaped images; 21 found in the 2DP records and 75 in the 2DC records. Figure 7 shows an example from image buffers from two different cloud penetrations one made on June 1, 1989 (2DC) and another on June 23, 1989 (2DP). The "double" or dumbbell-shaped image in both image records has been surrounded by a bold circle.

The image classification software also allowed us to estimate and record the maximum dimension of each particle in the doublet. Fig. 8 displays the size relationship between the small and large particles for each double image identified in the 2D image records in Illinois. Values of constant Weber number are indicated by solid lines in Fig. 8. The Weber number is an implicit indication of impact pressure (see Czys 1989). The couplet particle sizes reported by Alkezweeny (1969) have been plotted as solid squares in Fig. 8 for comparison. As can be seen, couplet sizes determined from the 1989 PACE 2D data are in very good agreement with the couplet sizes reported by Alkezweeny.

However, there are several questions that must be considered before these images can be accepted as being present because of an interaction between frozen and unfrozen precipitation-size drops:

1. Is particle collocation in the 2D laser beam responsible for the images?
2. Are collision rates between small precipitation size drops sufficiently high to account for

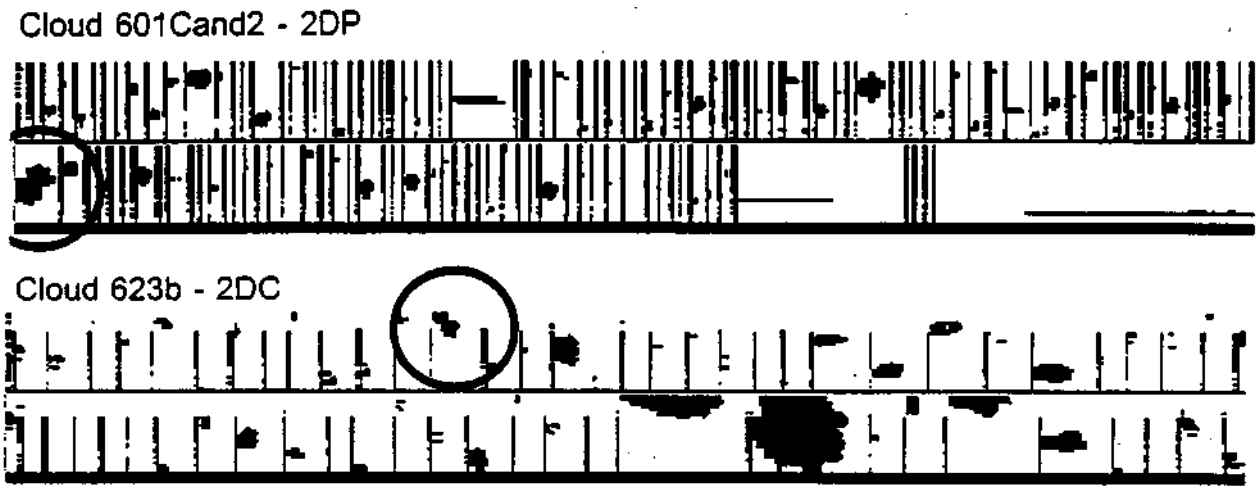

Figure 7. Example image buffers from two different cloud penetrations one made on June 1, 1989 (2DC) and the other made on June 23, 1989 (2DP). The "double" or dumbbell-shaped image in both image records has been surrounded by a bold circle.

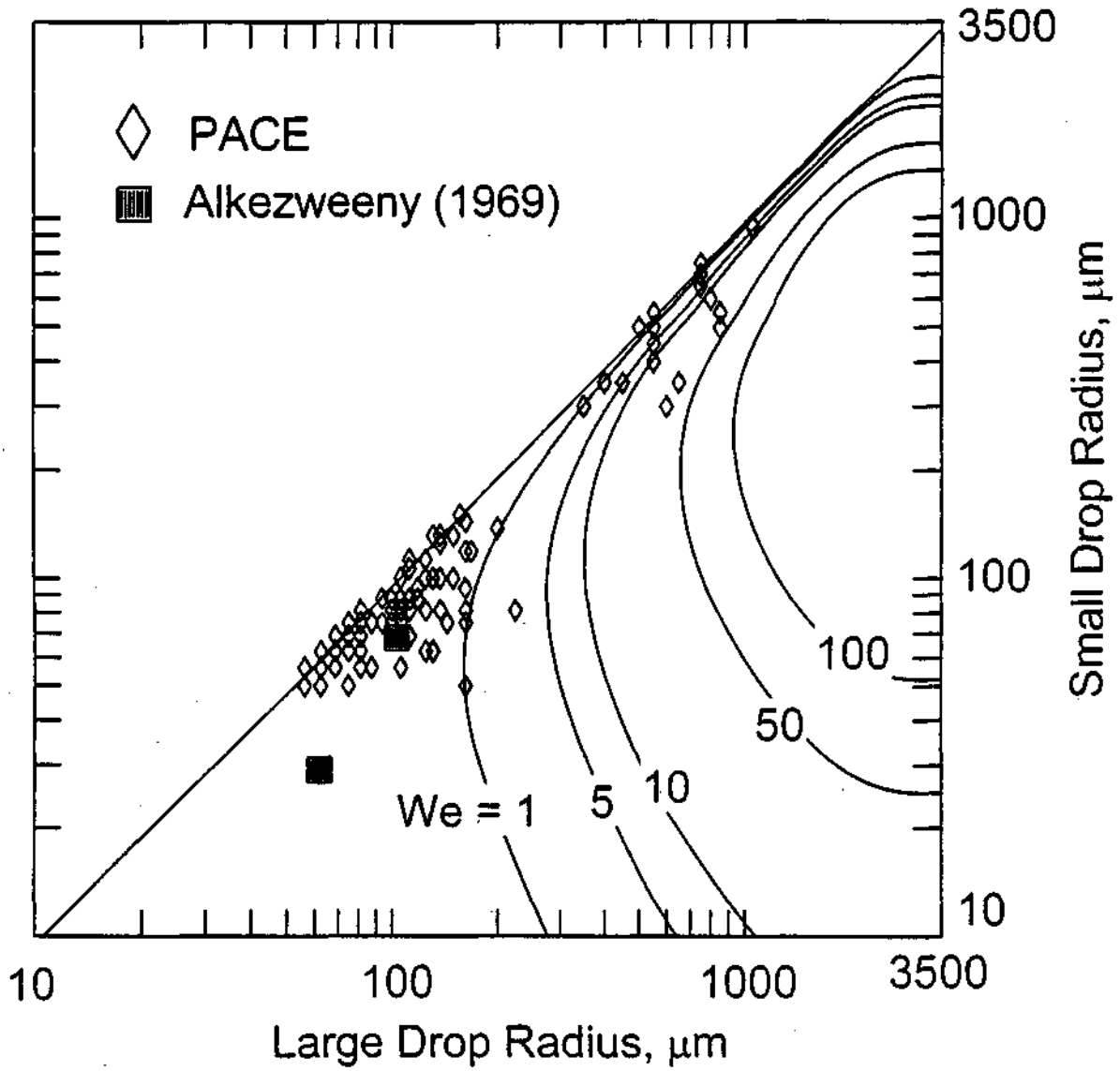

Figure 8. Size relationship between the small and large particle for each double image identified in the 2D image records plotted as diamonds. Values of constant Weber number are indicated by solid lines. Couplet particle sizes reported by Alkezweeny (1969) have been plotted as solid squares

observed concentrations of the image couplets?

3. Is the interaction time sufficiently long to allow the liquid drop to solidify rather than allow the drop to spread over the colliding ice particle?

a. Particle Collocation

The question of particle collocation can be addressed in a way theoretically similar to that by Baumgardner et al. (1985) for the problem of coincidence in FSSP data. The probability that two particles will be collocated in the sample volume of the laser beam can be estimate, assuming that the particles are homogeneously distributed in space, using a probability density function of the form

$$P_t = \int_0^{\tau_1} \beta e^{-\beta t} dt = 1 - e^{-\beta \tau_1} \qquad (1)$$

where β is the mean expected inter-arrival rate of the particles, and τl is the average transit time of the particle through the laser beam. The mean inter-arrival rate can be found from

$$\beta = N_o W L_D v \qquad (2)$$

N_o is the "actual concentration," W is beam width, L_D is depth of field, and v is true air speed. According to specifications we have for the 2DC probe used in the 1989 PACE field program, a value of 0.432 cm^2 was used for the sample area ($W \times L_D$). True air speed was approximately 100 m s^{-1}, and a value of N_o = 0.001 cm^{-3} was computed based on data provided by our image classification software (Czys and Petersen 1992). A value for the average transit period, τ_1, was obtained from the ratio of the beam width to the true air speed, or $\tau_1 = 8.0 \times 10^{-6}$ s. Substitution of these values in the right-hand side of Eq. 1 yields

$$P_t = 3.456 \times 10^{-5} \quad (3)$$

This value can be interpreted as meaning that there was approximately one chance in 30,000 images to find two collocated precipitation-size particles.

Approximately 120,000 images were examined for dumbbell-images in the 1989 PACE 2D data (not including streakers, streamers, or other artifacts, but including zero-area and one-diode images). Hence, only about four image frames can be expected to depict the shadow of two collocated particles. Hence, the number of images records with dumbbell shaped images is many times more than can be accounted for by "coincidence".

b. Sufficiency of Collision Rates

The collision rate between a frozen drizzle or rain drop and a supercooled precipitation-size drop must be sufficiently high so that only a small production probability (or at least some reasonably small value) can account for observed concentrations of the particle.

Determination of the production probability was address in two parts. First we estimated the concentration of dumbbell shaped particles from the PACE 2D image records, and then compare that concentration to that which might be expected to occur based on estimates of concentrations of frozen drops, supercooled drizzle and rain drops and the collision frequency between them to arrive at the probability from:

$$P_{DSP} = (N_{DSP,\,Expected} / N_{DSP,\,Observed}). \quad (4)$$

1) ESTIMATED CONCENTRATION OF DUMBBELL SHAPES

The concentration of dumbbell shaped images (N_{DSP}) was estimated from data we had available for the 2DC image records. Here, we simply made an estimate of the average, maximum and minimum sample volume based on knowledge of the 2DC sample area (A_{Sample}) multiplied by a representative range of cloud diameters (L), and then adjusted for probe activity during the penetration ($P_{Activity}$). Typically, we found anywhere from 0 to very occasionally 3 images of dumbbell shaped images in the image records of any particular penetration and hence used values of n_{DSP} of 1 and 3 to obtain an estimate of the range of concentrations from

$$N_{DSP,\,Observed} = n_{DSP} / (A_{Sample}\, L\, P_{Activity}) \qquad (5)$$

where we used a value of 0.432 cm^2 for A_{Sample} according to specifications available for the 2DC optical array probe used in the 1989 Precipitation Augmentation for Crops Experiment (PACE) field program. Of the 71 cloud penetrations that were examined in detail as part of the PACE analysis (Czys et al. 1995), we determined that the diameter of an individual cumulus congestus ranged from a minimum of 1600 m to a maximum of 5400 m and averaged 3500 m, using FSSP cloud particle concentrations to define when the airplane entered and exited cloud. Hence, Eq. 5 resulted in a concentration that ranges from a low of 2 m^{-3} (assuming that 1 particle was encountered during a penetration with a probe activity of 50%) to a high of 43 m^{-3} (assuming that 3 particles were encountered during a penetration with a probe activity of 100%) with an average that ranges from 3 to 19 m^{-3}.

2) ESTIMATED PRODUCTION OF DUMBBELL SHAPES

The expected concentration of dumbbell shaped particles in a cloudy parcel of air was calculated from the product between the probability P_{DSP}) that any particular supercooled-frozen drop interaction will result in a dumbbell shaped particle and the rate at which liquid-frozen drop interactions (LFI's) occur per unit volume, or

$$N_{DSP,\,Expected} = p_{DSP} \times \iint_{a_L a_F} k(a_L, a_F) N(a_L) N(a_F) \mathrm{E}(a_L, a_F)\, da_L\, da_F \qquad (6)$$

In Eq. 6, $k(a_L , a_F)$ is simply the collision kernel defined as the volume swept-out per unit volume per unit time, or

$$k(a_L, a_F) = \pi (a_L, a_F)^2 \left[V(a_L)\right] - \left[V(a_F)\right] \qquad (7)$$

where a_L and a_F represent the radius of the liquid and frozen particles, respectively. The size distributions of liquid and frozen particles are represented by $N(a_L)$ and $N(a_F)$. Finally, $E(a_L,a_F)$ is the collision efficiency for liquid and frozen precipitation-size particles.

In Eq. 6, we assumed that the population of supercooled drizzle and raindrops could be represented by a Marshall-Palmer (1948) type distribution or

$$N(a_L) = N_{o,a_L}\, e^{-\Lambda_L a_L} \qquad (8)$$

where N_{o,a_L} is the slope and Λ_L is the intercept of the distribution even though this may not always

be true. For terminal velocity of the liquid drops an exponential was used of the form

$$V(a_L)=a-b\exp(-2ca_L) \tag{9}$$

that was proposed by Best (1950) who used values of a = 965 cm s^{-1}, b = 1030 cm s^{-1}, and c = 6 cm^{-1} that where suggested by Atlas et al. (1973).

We further assumed that the distribution of supercooled drizzle and raindrops had an intercept of N_{o,a_L} = 0.08 cm^{-4} that was obtained from Marshall and Palmer's observations lacking any better approach to arriving at a value for the intercept. The slope of the size distribution was found from the reflectivity factor Z

$$Z\left(mm^6 m^{-3}\right)=\frac{720N_{a_L,o}}{\Lambda_L{}^7}\times 10^{12} \tag{10}$$

where Λ_L has units of cm^{-1}. For a reflectivity of 40 dBZ (which is. representative of 10 cm reflectivity data we have for the -10°C level of warm-based convective rain clouds in Illinois), Eq. 9 produces a value of Λ_L = 24.8 cm-1.

Because the PACE data on dumbbell shaped images was obtained in developing cumuli and the penetrations performed (see Czys et al. 1995 for a detailed description of the flight maneuvers) in a manner so that the observations are representative of the result of microphysical processes in moist adiabatic ascent, we imaged a cloudy parcel of air that had just risen above the 0°C level where it

initially contained drizzle and raindrops that supercooled. Shortly thereafter, a few of the supercooled drops began to freeze, but not so many that they represented a continuous size distribution. Hence, the frozen rain drop population could not be adequately described by an exponential of the form of Eq. 8, but rather by a discrete concentration of frozen drops, N_{aF}, of a specific size, a_F. These assumption led to a very low initial concentration of frozen drops, and hence a very conservative estimate of the expected concentration of dumbbell shaped particles.

Table 1 summarizes the results of one illustrative set of calculations for a range of frozen drop concentrations, liquid-frozen drop interactions (LFI's), assuming a value of a_F = 250 μm. The number of LFI's expected after 500 s is also listed to represent the number of interactions that might occur in the time a parcel of cloudy air would take to travel from the 0 to -10°C level, assuming that the depth of the layer was 2000 m and the updraft velocity was 4 m s^{-1}. The list of production probabilities (P_{DSP}) was computed to be that required to explain an observed dumbbell shaped concentration of 5 m^{-3} at the -10°C level. It should be further noted that the calculation assumes that the initial concentration of frozen drops is static through the parcel's rise to the 0°C level which would also push the estimate toward a lower bound. Inspection of Table 1 suggests that realistic P_{DSP}'s could account for the concentration of dumbbell shaped particles observed in the image records of the PACE data set once frozen drop concentrations exceed a value of 1 m^{-3}.

Table 1. Summary of Interaction Rates (LFI's) and Production Probabilities For a_F = 250 μm Assuming An Observed Concentration of Dumbbell Shaped Particles of 5 m^{-3}.

$N(a_F)$ m^{-3}	LFI $m^{-3}\ s^{-1}$	LFI m^{-3} 500 s^{-1}	P_{DSP} %
0.1	0.0021	1.1	451
1	0.0216	11	45
2	0.0443	22	23
5	0.1108	55	9
10	0.2216	111	4.5
100	2.226	1108	0.45

Inspection of values in Table 1 suggests that realistic P_{DSP}'s could account for the concentration of dumbbell shaped particles observed in the image records of the PACE data set for frozen drop concentrations of a small as 1 to 2 m^{-3}. This suggests that the concentration of supercooled drizzle and raindrops, initial concentration of the very first frozen raindrops is can explain concentrations of dumbbell shaped ice particles noted in our PACE 2D image data.

c. Preservation of Initial Drop Identity

In this section, we wish to determine whether the supercooled drop in the liquid-frozen interaction has enough time to form an outer ice shell, in comparison to the amount of time the two particle spend in interaction so that the liquid and solid drops retain much of their original identity to form a dumbbell shape rather than spreading and coating the frozen particle. Although either the larger or the smaller drop in the interaction may be the frozen particle, we chose for the large drop

of radius a_F to be frozen. Figure 9 illustrates the interaction geometry for two instants in the interaction, the initial time of contact, t_o, and the instant, $t_o + \Delta t$, that the two particles would begin to separate if they were not physically connected.

The interaction time, ti, can be simply computed by taking the ratio of the perimeter turned, s, during the interaction to the relative velocity, AV, where

$$s = \frac{\theta}{360} 2\pi a_F,$$

$$\Delta V = V_L - V_F, \text{ and}$$

$$t_i = \frac{s}{\Delta V} \qquad (11)$$

In our wind tunnel experiments a_L = 1000 μm, a_F = 700 μm, V_L = 6 m s^{-1} and V_F = 5 m s^{-1}. Hence, the interaction time from Eq. 11 is 7.85 ms for θ = 45°, meaning there is about that much time for the liquid drop to solidify in a way that would preserve its original identity, and thus allow the new mass to result in a dumbbell shaped particle.

The nucleation of ice in the supercooled drop was treated as a two stage process. The first, very short stage, was the formation of an ice shell around the outside of the drop. In this stage latent heat is released in an amount sufficient to raise the particle temperature to near 0°C. In the second longer stage, solidification of the drop is completed at a rate dictated by the rate at which the latent heat of fusion can be disposed of in the environment.

We now can compute how long it will take for an ice shell to travel around the entire periphery and this can be estimated as the time required for the ice to propagate around the length of a cord of

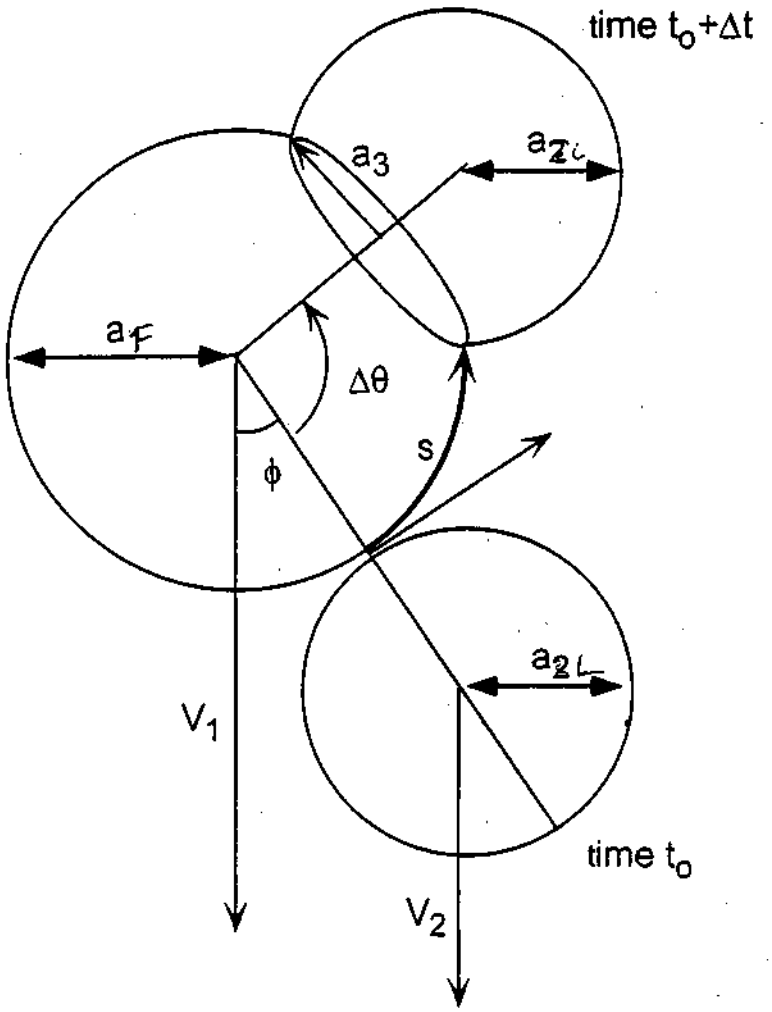

Figure 9. Interaction geometry at two instants during a collision, the initial time of contact, t_o, and the instant, $t_o + \Delta t$, that the two particles would begin to separate if they were not physically connected.

the drop. Hence, the time can simply be computed from the ratio of the chord length to the so called free growth rate (G_m) of ice in supercooled water or

$$t_F = \frac{2\pi a_L}{G_m} \qquad (12)$$

The parameter, G_m is referred to as the "so called" free growth rate because it has been determined from experiments with ice growth in narrow tubes and capillaries where the proximity of walls had an influence on heat exchanges that can influence growth rate.

Hallett (1964), Pruppacher (1967a, b), Ryan and Macklin (1968) and Gokhale and Lewinter (1971) represent a few who have obtained relationships between the amount of supercooling, ΔT_∞, and G_m. In general, these studies have indicated that the growth rate varies nearly as the square of the supercooling. For this application, we chose the relationship provided by Pruppacher (1967a, b)of

$$G_m = 0.035(\Delta T_\infty)^{2.22} \qquad (13)$$

because 1) it applies to a range of supercooling that are appropriate for our experiment and consistent with observational evidence, and 2) the coefficients are about in the middle-range of those reported by others. For this calculation, we used a supercooling of $\Delta T_\infty = 5°C$ which results in a free growth rate of 1.25 cm s^{-1}. Hence, from Eq. 12 a time for complete propagation of the ice around the perimeter of the chord is about 350 ms. If we take the ratio of the interaction time to the net solidification time we find that the time available is only 2.2% of that necessary for completion of the ice shell. This corresponds to about 10 μm of propagation. Hence, we conclude that either

insufficient time exists for the process, something is excluded in the consideration, or that the time although short is sufficient for the shell to cup the liquid drop so that the original identity of the drops is preserved.

5. Conclusions

Laboratory experiments were performed by creating a light shower of supercooled rain in a vertical wind tunnel to investigate interactions between small precipitation-size particles at temperatures colder than 0°C. In one of the trials, a subject drop froze and subsequently interacted with a supercooled drop in the tunnel rain shower. The net result of this interaction was the production of a dumbbell shaped ice particle. This laboratory result, combined with a previous field observation of the same shape, motivated us to examine the 2D optical array probe data from 1989 for the presence of images that may have been cast by dumbbell shaped ice particles in clouds. This examination revealed a large number of dumbbell shaped images. It was concluded that the dumbbell shaped images were present in the 2D data from a mechanism like that which was observed in the wind tunnel experiments. This was concluded because theoretical evidence indicated that the number of dumbbell shapes in the 2D data set far exceeded that which can be expected from particle collocation in the sample area of the 2D laser beam, and the number of liquid-frozen interactions (LIT) between precipitation-size particles was sufficient to account for observed concentrations of dumbbell shaped ice particles in clouds. However, our calculation of the time required to solidify the liquid drop in the LFI does not support the laboratory observation. This may reflect poor knowledge of the "free" growth rate for ice in supercooled water and suggests an area

where laboratory work is needed.

The mechanism that was observed in the wind tunnel experiments would be a powerful mechanism for the production of graupel embryos in clouds. The findings of this research also suggest that failure to include dumbbell shapes in the schemes of image classification software will not only run a risk of underestimating concentrations of in situ ice, but risks overlooking an active mechanism that contributes to the evolution of ice in clouds.

6. References

Alkezweeny, A.J., 1969: Freezing of supercooled water droplets due to collision. *J. Appl. Meteor*, **8**, 994-995.

Atlas, D., R.C. Srivastava, and R.S. Sekhon, 1973: Doppler radar characteristics of precipitation at vertical incidence. *Rev. Geophys. Space Phys.*, **11**, 1-35.

Baumgardner, D., W. Strapp, J.E. Dye, 1985: Evaluation of the Forward Scattering Spectrometer Probe. Part II: Corrections for Coincidence and dead-time losses. *J. Atmos. Ocean. Technol.*, **2**, 626-632.

Beard, K.V., 1992: Ice initiation in warm-base convective clouds: An assessment of microphysical mechanisms. *Atmos Res., 28*, 125-152.

Beard, K.V., and H.R. Pruppacher, 1969: A determination of the terminal velocity and drag of small water drops by means of a wind tunnel. *J. Atmos. Sci.*, **26**, 1066-1072.

Berry, E.X, and R.L. Reinhardt, 1974: An analysis of cloud drop growth by collection: Part I-IV. *J. Atmos. Sci.*, **31**, 1814-1831, 2118-2135.

Best, A.C., 1950: Empirical formulae for the terminal velocity of water drops falling through the atmosphere. *Quart. J. Roy. Meteor. Soc.,* **76**, 302-311.

Braham, R.R., Jr., 1964: What is the role of ice in summer rain-showers? *J. Atmos. Sci.,* **21**, 640-645.

Changnon, S.A., R.R. Czys, R.W. Scott, and N.E. Westcott, 1991: The Illinois precipitation modification program. *Bull. Amer. Meteor. Soc.,* **72**, 587-604.

Czys, R.R., 1991: A preliminary appraisal of the microphysical nature and seedability of warm-based midwestern clouds at -10°C. *J. Wea. Mod.,* **23**, 1-17.

Czys, R.R., 1989: Ice initiation by collisional forcing in warm-based cumuli. *J. Appl. Met.,* **28**, 1098-1104.

Czys, R.R., and K.C. Tang, 1995: An exact analytical solution for raindrop collision rate. *J. Atmos. Sci.,* **52**, 3289-3292.

Czys, R. R. and M. S. Petersen, 1992: A roughness detection technique for objectively classifying drops and graupel in 2D image records. *Jour. Atmos and Ocean Tech.,* **9**, 242-257.

Czys, R.R., S.A. Changnon, N.E. Westcott, R.W. Scott, and M.S. Petersen, 1995: Responses of warm-based, Midwestern cumulus congestus to dynamic seeding trials. *J. Appl. Meteor.,* **34**, 1194-1214.

Gokhale, N.R. and O. Lewinter, 1971: Microcinematographic studies of contact nucleation. *J. Appl. Meteor.,* **10**, 469-473.

Hallett, J., 1964: Experimental studies of the crystallization of supercooled water. *J. Atmos. Sci.,* **21**, 671-682.

Koenig, L.R., 1963: The glaciating behavior of small cumulonimbus clouds. *J. Atmos. Sci.*, **20**, 29-47.

Marshall, J.S., and W.McK. Palmer, 1948: The distribution of raindrops with size. *J Meteor.*, ***5***, 165-166.

Mossop, S.C., 1985: The origin and concentration of ice crystals in clouds. *Bull. Amer. Meteor. Soc.*, **66**, 264-273.

Pitter, R.L. and H.R. Pruppacher, 1973: A wind tunnel investigation of freezing of small water drops falling at terminal velocity in air. *Quart. J. Roy. Meteor. Soc.*, **99**, 540-550.

Pruppacher, H.R., 1967a: Some Relations between the structure of the ice-solution interface and the free growth rate of ice crystals in supercooled aqueous solutions. *J. Colloid and Interface Sci.*, **25**, 285-294.

Pruppacher, H.R., 1967b: On the growth of ice in aqueous solutions contained in capillaries. Z. *Naturforschg*, **22a**, 895-901.

Rogers, R.R., 1989: Raindrop collision rates. *J. Atmos. Sci.*, **46**, 2469-2472.

Ryan, B.F., and W.C. Macklin, 1968: The growth of ice in supercooled aqueous solutions. J. *Crys. Growth*, **2**, 337-340.

SECTION F

DRY PERIODS IN ILLINOIS

**Stanley A. Changnon, Floyd A. Huff, Kenneth E. Kunkel,
Robert W. Scott, and Nancy E. Westcott**

A three-year effort investigated all atmospheric aspects of dry periods in Illinois. They represent the conditions when rainfall enhancement would be beneficial. Dry periods occurred in 35 percent of all growing seasons since 1901. The dry periods also simulate the estimated future average climate of Illinois under a greenhouse-induced climate change. Additional water, from irrigation or cloud seeding, would be extremely beneficial during these periods.

This project involved a detailed hydrometeorological and climatological analyses of the 34 years with dry periods since 1900. Other studies examined the synoptic weather conditions that caused rain during dry periods. Another area of investigation assessed the properties of storm cells and clouds in dry periods. The role of surface conditions and their possible feedback on the atmosphere was studied to better understand how dry surface conditions affect atmospheric conditions either to promote or enhance dry atmospheric conditions.

The findings have been described and are printed in a major report, *Dry Periods in Illinois: A Climatological and Meteorological Analysis*. This 144-page report was published in 1996.

SECTION G

INADVERTENT WEATHER AND CLIMATE MODDFICATION

Temporal Variability of Thunderstorms and Hail **(Changnon, Westcott)**

The increasing incidence of damaging storms in Illinois and much of the United States has brought on the need to objectively examine the temporal variations in severe local storms, as input to assess potential shifts in climate. To this end, historical (1901-1996) data on hail events and thunderstorm occurrences were acquired for many weather stations in and around Illinois. We pursued extensive editing of these data to ensure quality records needed to permit studies of temporal variability. The results provide information useful to agricultural interests, insurance industry, and the general public about the changing incidence of these damaging weather events. The hail findings have been summarized in a report (Changnon, 1995), and thunderstorm data are still under assessment.

Urban Effects on Lightning Activity (Westcott)

A number of past studies have shown that during spring and summer months, rain storms which pass over Lake Michigan often will diminish in strength or dissipate. Augustine et al. (1994) using calibrated satellite data found estimated summertime rainfall values to be 18% lower than what upwind values would project. Factors which have been suggested that may explain the overtake decrease in convective activity include: the formation of a strong low-level inversion as warm air advects over the air cooled by conduction which limits vertical energy transfers (Strong, 1972); the presence of a lake breeze which could decouple the storm from the low-level inflow air (Lyons, 1966; Lyons and Wilson, 1968), the orientation of the storm (Stout and Wilk, 1962; Chandik and Lyons, 1971), the size of the storm and the character of the outflow air in contrast to the underlying

stable air (Lyons, 1966).

Westcott (1995) indicated that for moderate-sized storms (501 to 5000 cloud-to-ground [abbr., CG] flashes), the frequency of CG flashes is often enhanced over and downwind of many major midwestern urban areas. Over major urban areas adjacent to one of the Great Lakes (e.g. Chicago, Detroit and Toledo), however, thunderstorm activity often is reduced, particularly in the region located downwind of the cities, usually to the east and over one of the lakes (Chicago, Detroit, Milwaukee and Toledo). While explicit documentation of the underlying physical processes involved in the urban-related influences on convective activity has not been fully accomplished, pervious studies suggest that cities are characterized by factors that could enhance convection: They are a source of heat that can destabilize air flowing over the city, a source of cloud condensation nuclei that can alter precipitation formation processes, and a source of frictional lift that can promote convection (Oke, 1979; Landsberg, 1981; Changnon et al., 1981).

A six-year (1989-1994) sample of summer thunderstorm activity as deduced from CG lightning flash data obtained from GeoMet Data Services is used to examine the influence of urban areas on thunderstorm activity. The frequency of CG lightning flashes are described herein for three areas along the western shore of Lake Michigan region. This analysis further examines the impact Lake Michigan might have on CG frequency in urban areas adjacent to Lake Michigan and in the downwind area over Lake Michigan, so that the impact of urban influences might be better understood for coastal sites.

Three areas were selected for study: Chicago, Milwaukee, and a more rural area north of Milwaukee that encompasses Sheboygan, Wisconsin, with metropolitan populations of about 8,000,000, 1,500,000 and 50,000, respectively. Sheboygan was selected as a "control" area because

of its position along the west coast of Lake Michigan, its location approximately midway between Green Bay and Milwaukee, and because of its relatively low population density. The urban area coverage for Chicago and Milwaukee is about 2,298 km^2 and 736 km^2, respectively. For the Sheboygan area, a 1072 km^2 area adjacent to the coast was selected. An upwind (west) area and a downwind (east) area were selected for each city, with these areas having about the same diameter as the city they border. Only those storms moving slowly < 3 ms^{-1} or from the west (202.5 to 337.5°) were included in the study.

Results. Examining both the median CG flash density and the median number of storms for Sheboygan, it was noted that the largest values in the selected storm categories were found in the upwind area. A dramatic decrease in CG activity can be noted from the upwind to the urban to the downwind overtake area for Sheboygan (Table 1). The CG activity upwind of Sheboygan was significantly different from the urban and downwind over-lake area according to the two-sided Wilcoxon non-parameteric rank sum test (Westcott, 1996). The lake appeared to diminish the overall lightning activity both downwind of Sheboygan, and over Sheboygan.

For Chicago and Milwaukee (Table 1), the median over-lake values were consistently smaller than for the upwind area, but the differences were small, particularly compared to the difference in urban v.s. downwind values for the Sheboygan area. In addition, the urban values often were closer to the upwind value than to the over-lake value, and in fact sometimes were larger than the upwind area for both cities. This suggests that the influence of the urban area observed in other large midwestern cities may modulate the lake-caused diminishment of CG activity such as observed over and downwind of the Sheboygan area.

This study further suggests that the previous results indicating that cities neighboring one of the Great Lakes may be affected by the Great Lakes is likely the case. The large urban and downwind increases observed by Westcott (1995) for the 1989-1992 period, for a number of non-lake midwestern cities were much less apparent for the Chicago and Milwaukee areas. More recent analyses including years 1993 and 1994 are consistent with this finding. For the June-August 1989-1994 period, and for moderate sized afternoon storms, St. Louis, Kansas City, Dallas-Fort Worth, Minneapolis-St. Paul had increases of 16, 54, 129, and 69% over the respective urban areas, and increases of 101, 120, 148, and 50 %, respectively, downwind of the urban area. This is in contrast to the small decrease in activity over (13%) and downwind (10%) of Chicago, and to the small increase over Milwaukee (24%) and the small decrease downwind (2%) of Milwaukee (Table 1). Thus, Lake Michigan likely modulates the urban-related enhancement of convection over Chicago and Milwaukee.

Conclusions. An examination of cloud-to-ground lightning flash frequency, indicates that the urban areas of Chicago and Milwaukee may have had the effect of modulating an expected over-lake decrease in the number of CG flashes and in the number of lightning storms, and likewise that the lake may have modulated expected urban-related increases in CG flash density. Because of the combined influence of the urban and lake effects, the exact magnitude the these factors is difficult to ascertain.

Table 1. Percent Change in CG lightning flashes / 16 km^2 between the upwind, urban and downwind areas for June to August of 1989 to 1994 for Sheboygan, Chicago and Milwaukee). Shaded Values indicate differences significant at .05.

a) Sheboygan	Urban - Upwind / Upwind	Downwind - Upwind / Upwind
ALL Storms	-41.6	-32.1
1200-2100 CDT	-29.2	- 6.3
501-5000 CG	-38.4	-58.4
1200-2100 CDT and 501-5000 CG	-24.0	-60.4
b) Chicago	**Urban - Upwind / Upwind**	**Downwind - Upwind / Upwind**
ALL Storms	- 1.0	- 4.3
1200-2100 CDT	-12.0	- 5.3
501-5000 CG	- 8.0	- 4.3
1200-2100 CDT and 501-5000 CG	-13.0	-10.1
c) Milwaukee	**Urban - Upwind / Upwind**	**Downwind-Upwind/ Upwind**
All Storms	- 5.6	-17.3
1200-2100 CDT	- 0.4	- 8.9
501- 5000 CG	12.2	- 4.8
1200-2100 CDT and 501-5000 CG	24.5	- 2.4

References

Augustine, J.W., W.L. Woodley, R.W. Scott, and S.A. Changnon, 1994: Using Geosynchronous satellite imagery to estimate summer season rainfall over the Great Lakes. *J. Great Lakes Res.*, 20, 683-700.

Chandik J.F., and W.A. Lyons, 1971: Thunderstorms and the lake breeze front. *Preprint, 7th Conf. on Severe Local Storms,* AMS, Boston, 218-225.

Changnon, S.A., R.G. Semonin, A.H. Auer, R.R. Braham, Jr., and J.M. Hales: 1981: *METROMEX: A Review and Summary*, Meteor. Mono., No. 18, Amer. Meteor. Soc., 181 pp.

Landsberg, 1981: *The Urban Climate.* International Geophys. Series 28, Academic Press, 275 pp.

Lyons, W.A., 1966: Some effects of Lake Michigan upon squall lines and summer convection. *Proc, 9th Conf. on Great Lakes Res.*, International Assoc. of Great Lakes Research, Ann Arbor, 259-273.

Lyons, W.A., and J.W. Wilson, 1968: The control of summertime cumuli and thunderstorms by Lake Michigan during non-lake breeze conditions. *Satellite and Mesoscale Research Project (SMRP) Research Paper 74,* Univ. of Chicago, 32 pp.

Oke, T.R., 1979: *Review of Urban Climatology, 1973-1976.* WMOTN 169, 100 pp.

Stout G., and K. Wilk, 1962: The influence of Lake Michigan on squall line rainfall. *Proc, 6th Conf. on Great Lakes Res.*, U. Mich., Great Lakes Res. Division, 111-115.

Strong, A.E., 1972: The influence of the Great Lake anticyclone on the atmospheric circulation. *J. Appl. Meteor.*, **11**, 598-612.

Westcott, N.E., 1995: Summertime cloud-to-ground lightning activity around major midwestern urban areas. *J. Appl. Meteor.*, **34**, 1633-1642.

Westcott, N.E., 1996: Land-lake differences in thunderstorm activity in the vicinity of cities near Lake Michigan. *Preprint, 13th AMS Conf. on Planned and Inadvertent Wea. Modification*, Atlanta, Georgia, Amer. Meteor. Soc., Jan. 28 - Feb. 2, 1996, 106-109.

***Changes in Cirrus Cloud Cover Due to Contrails and Effects on Climate* (Travis, Changnon)**

Survey scientists have worked with scientists at the University of Wisconsin at Whitewater to assess the effects of jet contrails on Midwestern cloud cover and the surface climate conditions. Contrails were found to be a primary cause for Midwestern increase in high (cirrus) clouds since 1960. Current findings reveal contrail clouds differ from natural cirrus, and thus affect the surface climate in different ways. The final report on this research is in the Appendix.

***Urban and Lake Influences on Precipitation in the Chicago Region* (Huff and Changnon)**

Water Survey scientists have been investigating precipitation conditions in the Chicago region for 45 years. These investigations have related primarily to how urban influences and lake influences on the atmosphere act and interact, to influence clouds and precipitation.

An early investigation utilizing precipitation data from a gage installation four miles east of Chicago in Lake Michigan defined a sizable lake vs land difference, 21 percent less precipitation in the lake (Changnon, 1961). This lower lake precipitation was assessed as largely due to lake influences acting to decrease rainfall, although urban and lake influences acting to enhance convection and summer rainfall over the city were also considered as a possibility.

An ensuing study also based on historical data identified anomalously heavy precipitation, largely in the warm season, at a weather station in northwestern Indiana, labeled the "LaPorte Anomaly," and located 25 miles east of the metropolitan area (Changnon, 1968). This study identified increases of 30 percent in precipitation and 25 percent in thunderstorms, and their development over time were aligned with the growth of the Chicago metropolitan area. These findings indicated more definitely that the metropolitan area was having sizable influences on

convective processes leading to heavier summer rainfall.

The debate over the LaPorte anomaly (Holzman and Thorn, 1970; Changnon, 1970, 1971) led to further research of other geographical data for the region. Hidore (1971) established that streamflow from the basin draining that corner of Indiana also had anomalous increases matching the temporal increases in precipitation. Thus, by 1970 there was mounting evidence of urban and lake influences on warm season precipitation at Chicago and environs.

Other climatological studies of the 1960s assessed the influence of Lake Michigan on precipitation and storms (Changnon, 1968). Notable lake effects to lessen squall line rainfall and thunderstorm activity had been documented using weather radar and raingage data (Stout and Wilk, 1962; Changnon and Huff, 1966). In certain storm conditions, the relatively cool lake acted to stabilize warm season convection and to decrease rainfall and storm activity over and beyond the lake (Changnon, 1968).

Further climatological studies of Chicago's precipitation and local influences on it continued during the 1970s. Huff and Changnon (1973) found 15 to 20 percent increases in thunderstorms and hail east of Chicago (over northwest Indiana). Changnon and Detwiller (1976) found a temporal increase in the annual maximum rainfalls at Chicago of 17 percent over the 1871-1970 period, and a climatological study showed the increased rainfall in northwestern Indiana was still present (Changnon, 1980b).

A major field program focusing on the Chicago area was launched in 1976 to further study urban and lake influences on Chicago and surrounding areas (Changnon and Semonin, 1978). The Chicago Area Program involved a large dense network of 320 recording raingages enveloping the city and rural areas northwest and south of the city and in northwestern Indiana and southwestern

Michigan, covering 4,000 mi^2. This three-year project involving the study of radar, raingage, and satellite data, was able to further demonstrate that the Chicago area, under certain synoptic conditions, acted to enhance summer convective precipitation systems (Changnon et al., 1979). There was also clear evidence of a counter influence due to the stabilizing lake influences on convective precipitation over the lake (Changnon, 1980b). The average enhancement of summer rainfall over Chicago identified from this field study was 15 percent (Changnon, 1984). Further studies found enhanced heavy rainfall in cases of 2 inches or more rain (Huff, 1977).

A hydrometeorological study of the precipitation data for Chicago identified, using long-term historical raingage data, that the heavy rainfall frequency values in the city area were substantially higher than those in the surrounding rural areas (Huff and Vogel, 1976).As in St. Louis, this finding revealed that urban influences to enhance convective activity in rainfall appeared most active when naturally-occurring heavy rainfall existed (Changnon, 1980a). This outcome has had considerable impact on an age-old problem in Chicago, urban flooding (Changnon, 1980).

By 1980, considerable evidence of urban and lake influences on Chicago's precipitation had been accumulated from the various climatological and field studies (Changnon, 1980). Findings indicated that the localized increase in summer rainfall over the metropolitan area of Chicago was on the order of 10 to 15 percent. Data from northwestern Indiana (LaPorte and Valparaiso) indicated that precipitation in that area had been increased 25 to 30 percent as a result of Chicago's influence on the atmosphere. Third, the urban-enhancement of summer precipitation was substantial in some but not all convective rain events, and most evident in those capable of producing heavier precipitation (Changnon et al., 1979). The urban-enhanced precipitation systems appeared often to dissipate relatively soon after moving out over southern Lake Michigan.

The establishment of a national network of cloud-to-ground lightning detectors in the 1980s provided data allowing a study of the potential influence of Chicago (and other midwestern cities) on the incidence of lightning. This offered a chance to check and verify the earlier results which showed the enhancement of thunderstorm activity over northwestern Indiana. Study of five years of cloud-to-ground lightning data for the Chicago area revealed an enhancement over the city but none east (over Lake Michigan) as was found in many other cities (Westcott, 1995).

The Chicago Area Program of 1976-1980 provided only five years of summer rainfall data from a dense raingage network to pursue this type of investigation. Much of the information about Chicago's precipitation and localized influences had been gained from climatic type studies of historical data (Huff and Changnon, 1972). The installation of a dense recording raingage network in Chicago during 1989 has now provided data covering the 1990-1994 period, allowing a new assessment of the city's precipitation pattern and whether prior findings were verified by these data. This document presents the results of this latest study of Chicago area rainfall, and contrasts the findings with those of the previous climatological and raingage network studies.

Data. The precipitation data used in this study were obtained from the 5-year operation (1990-1994) of a dense raingage network in the Chicago urban area, and from raingages operated in the Chicago region by the NWS. This raingage network consists of 25 recording raingages spaced approximately 10-km apart on an area of 2500 sq km (Peppier and Huff, 1992). The network is part of an on-going assessment of precipitation related to the monitoring of water withdrawals from Lake Michigan.

Results from the 1990-1994 network operations have been compared with those from two earlier operations of raingage networks in the Chicago area. During 1976-1980, the Water Survey

operated a dense network of recording raingages in the Chicago region in conjunction with an extensive hydrometeorological research project (Huff et al., 1981). Other results were obtained from studies of data from a Chicago network of raingages operated in the urban area from 1949 to 1979 (Huff and Vogel, 1976). This earlier network consisted of 15 recording raingages operated for varying time periods by several government agencies, including the National Weather Service, the Chicago Metropolitan Sanitary District, and the Chicago Department of Engineering. This is referred to as the "old network" throughout the following text.

During 1976-1980, a large dense network of recording raingages was operated in and around Chicago metropolitan arena in conjunction with an extensive hydrometeorological research project of the Illinois State Water Survey (Changnon et al., 1980; Huff et al., 1980; Huff et al., 1981). During 1976-1978, this network consisted of 317 raingages at approximate 5-km intervals over an area of approximately 7,700 sq km (3,000 sq mi). The network was reduced to 71 raingages in 1979-1980 on approximately 1,640 sq km (640 sq mi) incorporating the Chicago metropolitan area.

Annual Precipitation. Figure 1 shows the isohyetal pattern of total precipitation for the 1990-1994 sampling period. The dashed isohyets show the normal 5-year totals, based on 1961-90 data of stations of the National Weather Service. An area of relatively heavy precipitation (>200 inches) extends northward from the extreme southern part of the network through the central urban area. An area of relatively light precipitation is indicated to the west. A decrease in precipitation is also indicated on the extreme eastern section near Lake Michigan. This may be related to the lake effects which can act to suppress convection. Comparison of the 1990-1994 totals with the normal values (dashed lines) reveals that all network gages had 5-year totals ranging from 4 to 25 inches above normal.

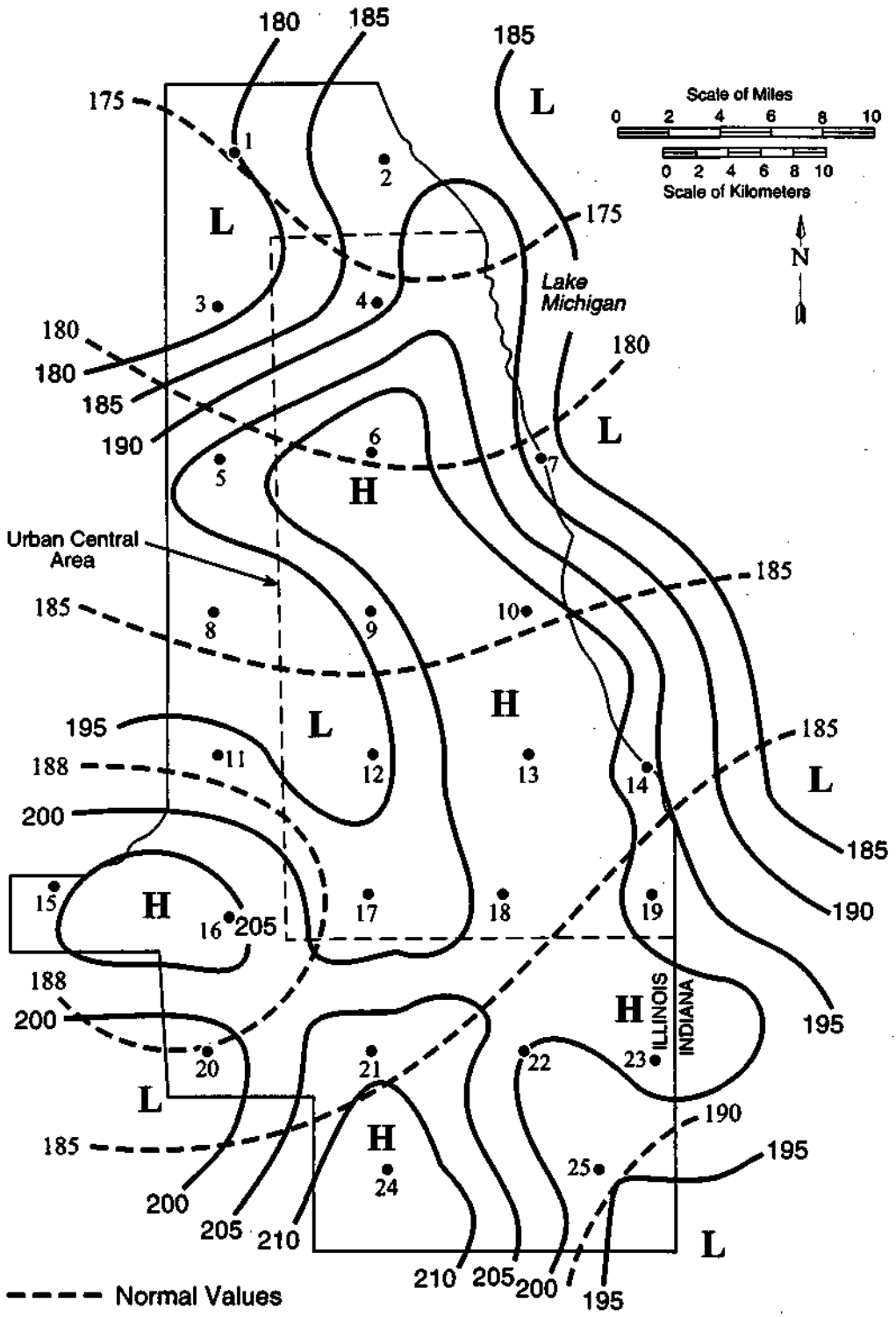

Figure 1. Annual precipitation totals (inches), 1990-1994

Within the area of the previous (old) raingage network, the 1990-1994 isohyetal pattern is very similar to that obtained for the 1949-1979 period. Data from the new network show the heavy precipitation area extending farther southward, as was hypothesized in the climatic data studies. Earlier studies concluded that the high center located in the north-central part of the old network (central urban area) and the southern high area were related to urban effects. The new network analyses lend support to the earlier findings with respect to locations of regions of relatively heavy and relatively light precipitation (highs and lows).

An initial estimate of the urban effect in the central and southern highs of 1990-1994 was made by eliminating the raingage observations in the center of each high and comparing the adjusted map with actual map. Gages 6, 10, and 13 were eliminated from the central high and gages 21, 23, and 24 from the southern high region. Differences obtained between the two maps were assumed to have been related to urban effects. The differences indicated the urban-induced increase in annual precipitation was 7 percent in the central high and 3 percent in the southern high centers.

Figure 2a shows the isohyetal pattern obtained when the values of the five heaviest storms, based on network mean precipitation during 1990-1994, were combined. Previous studies indicated the urban effect on precipitation is greatest in relatively heavy storm systems (Changnon et al., 1977; Huff and Vogel, 1976). Figure 2a has some of the pattern characteristics of Figure 1. Following the procedure described in the above annual analyses, gages at the center of each high were deleted and the isohyetal pattern redrawn. Results indicated a 6 percent increase in precipitation related to the urban effect in the north central high. This is nearly the same as found in the total precipitation analysis, and indicates the Chicago urban effect was not more pronounced in these heavier storms. A similar analysis was not done with the southern high, because it occurred at the southern boundary

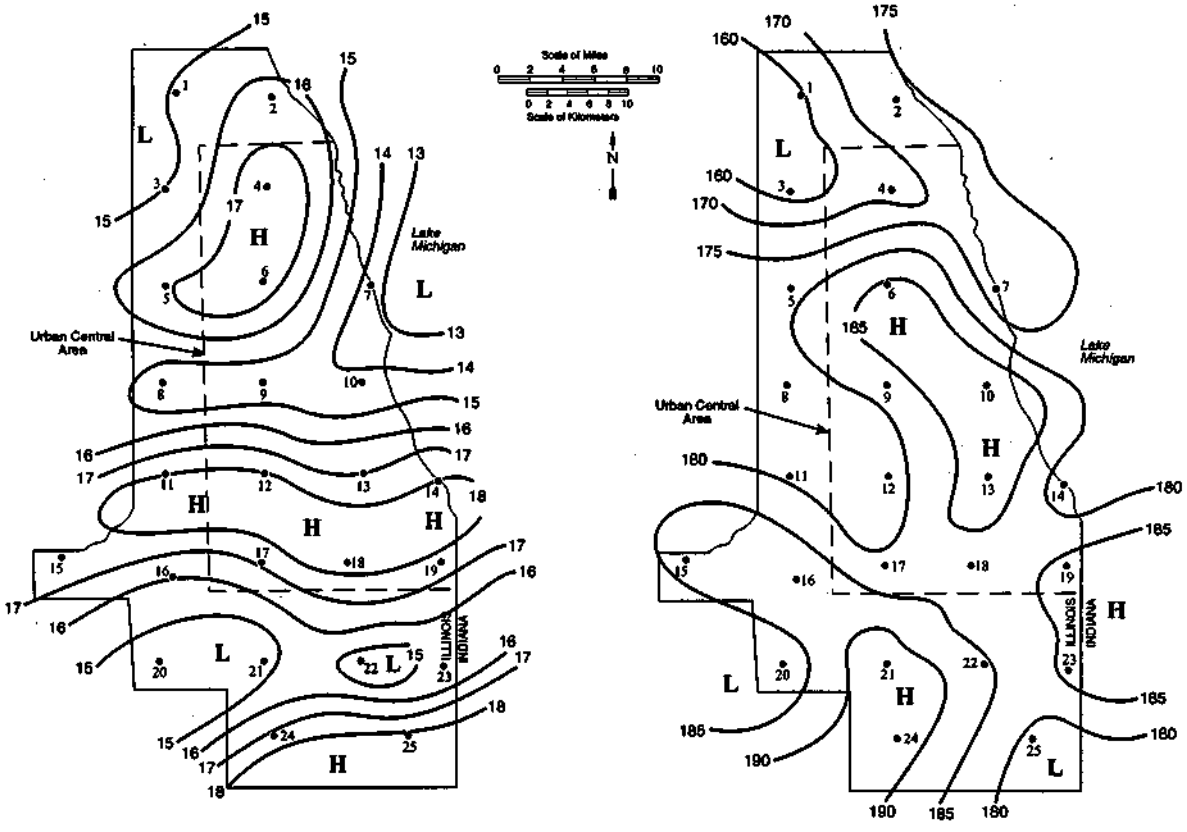

a. Total precipitation (inches) in 5 heaviest storms occurring during 1990-1994, based on network means

b. Annual rainfall totals (inches), 1990-1994, eliminating 5 heaviest storms

Figure 2.

of the network, which left no gages to the south for interpolation purposes.

Figure 2b shows the annual precipitation pattern after eliminating the five heaviest storms, providing a measure of the pattern without these unusually heavy storms. Comparison with Figure 1 shows a very similar distribution of high and low centers—in fact, the patterns are nearly an exact match. This implies that the five-heavy storm group had no major influence on the spatial pattern characteristics, and therefore, did not dictate the pattern characteristics as found in the METROMEX research at St. Louis (Changnon et al., 1977).

Figure 3 shows the pattern obtained with storms of light to moderate intensity, defined as those in which the network mean was less than one inch. Analysis indicated the central network high represents an urban-induced increase of about 7 percent. The southern high in these lighter rains was again in a position where a comparative analysis with control gages could not be performed satisfactorily. The central high increase was approximately the same as that found with the total precipitation and heavy storm patterns of Figures 1 and 2a.

Spring Precipitation. The isohyetal pattern of total spring precipitation (1990-1994) is shown in Figure 4. The spring pattern has a region of relatively heavy rainfall on a nearly north-south orientation through the middle of the present network and the central urban area. Except for an area of relatively light precipitation extending across the southern extremity of the old network, the isohyetal pattern is very similar to the annual pattern displayed in Figure 1.

Analyses were made of the five heaviest spring rainstorms in 1990-1994. Figure 5 shows the isohyetal pattern of these heaviest rainstorms, and it is nearly identical to the total rainfall pattern in Figure 4. These five storms accounted for approximately 22 percent of the 5-year spring total.

An estimate of the potential urban-induced factor in both the central and southern rainfall

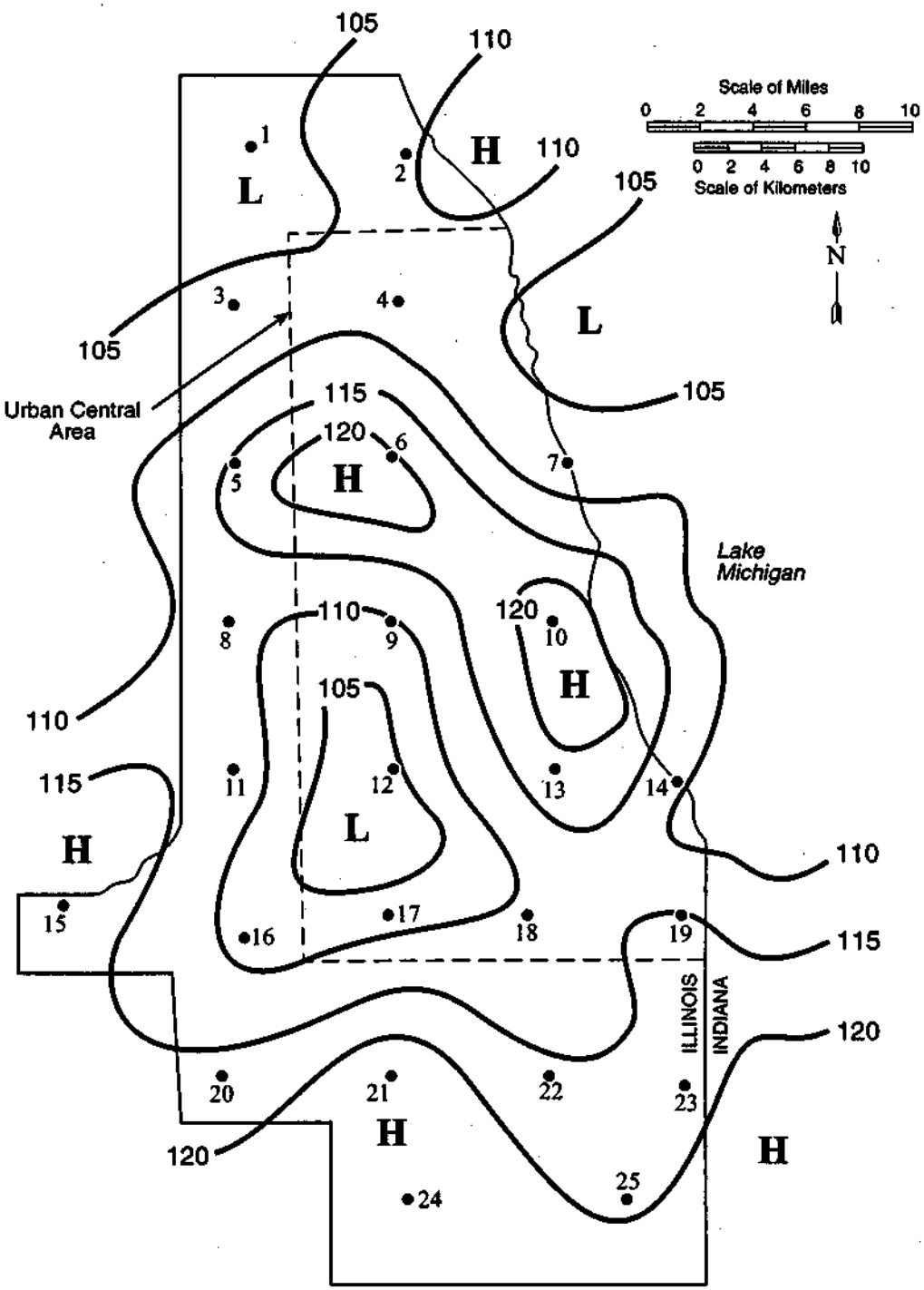

Figure 3. Total annual precipitation during 1990-1994 occurring in storms having network means <1.00 inch

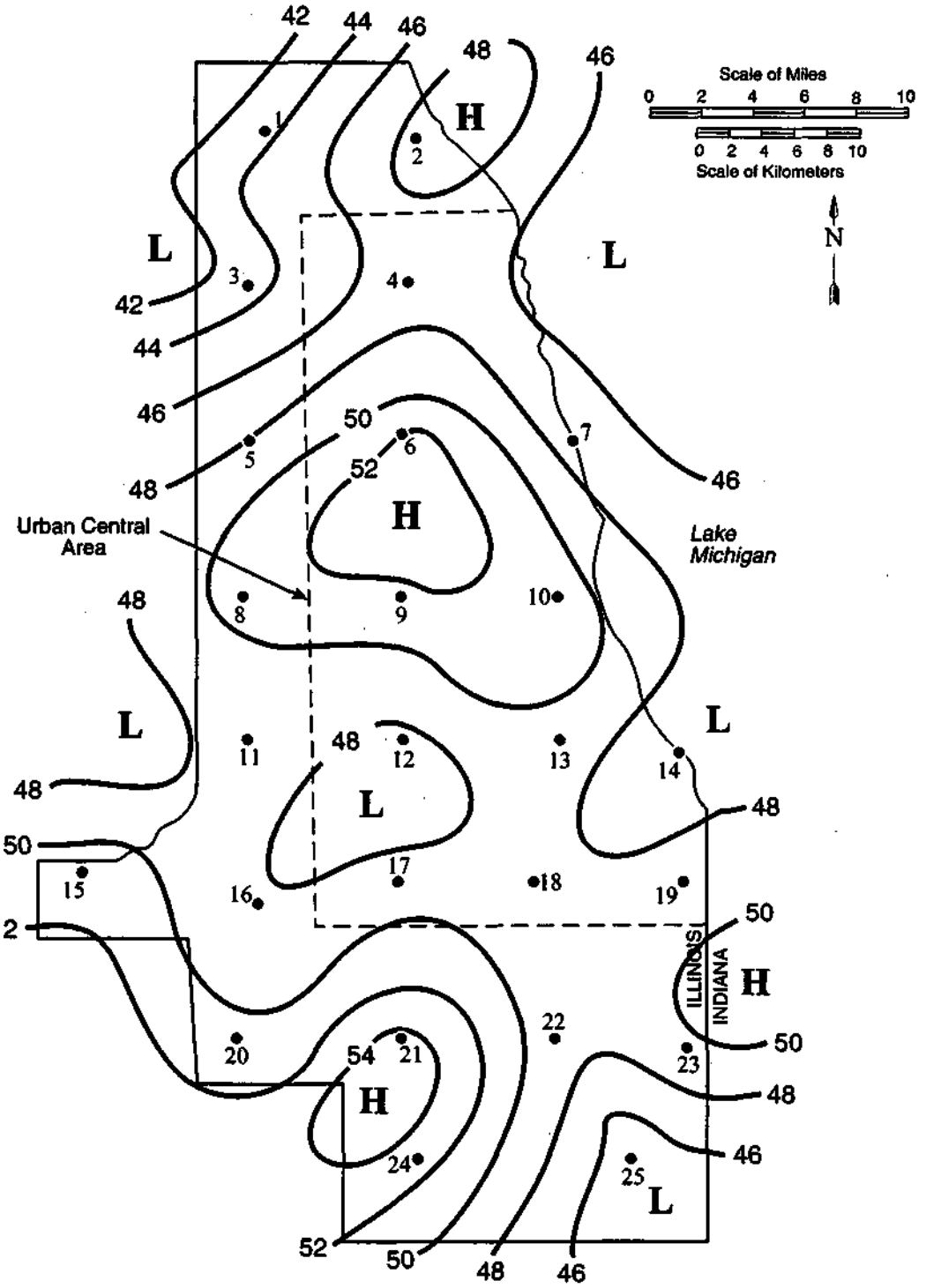

Figure 4. Spring (March-May) total rainfall (inches), 1990-1994

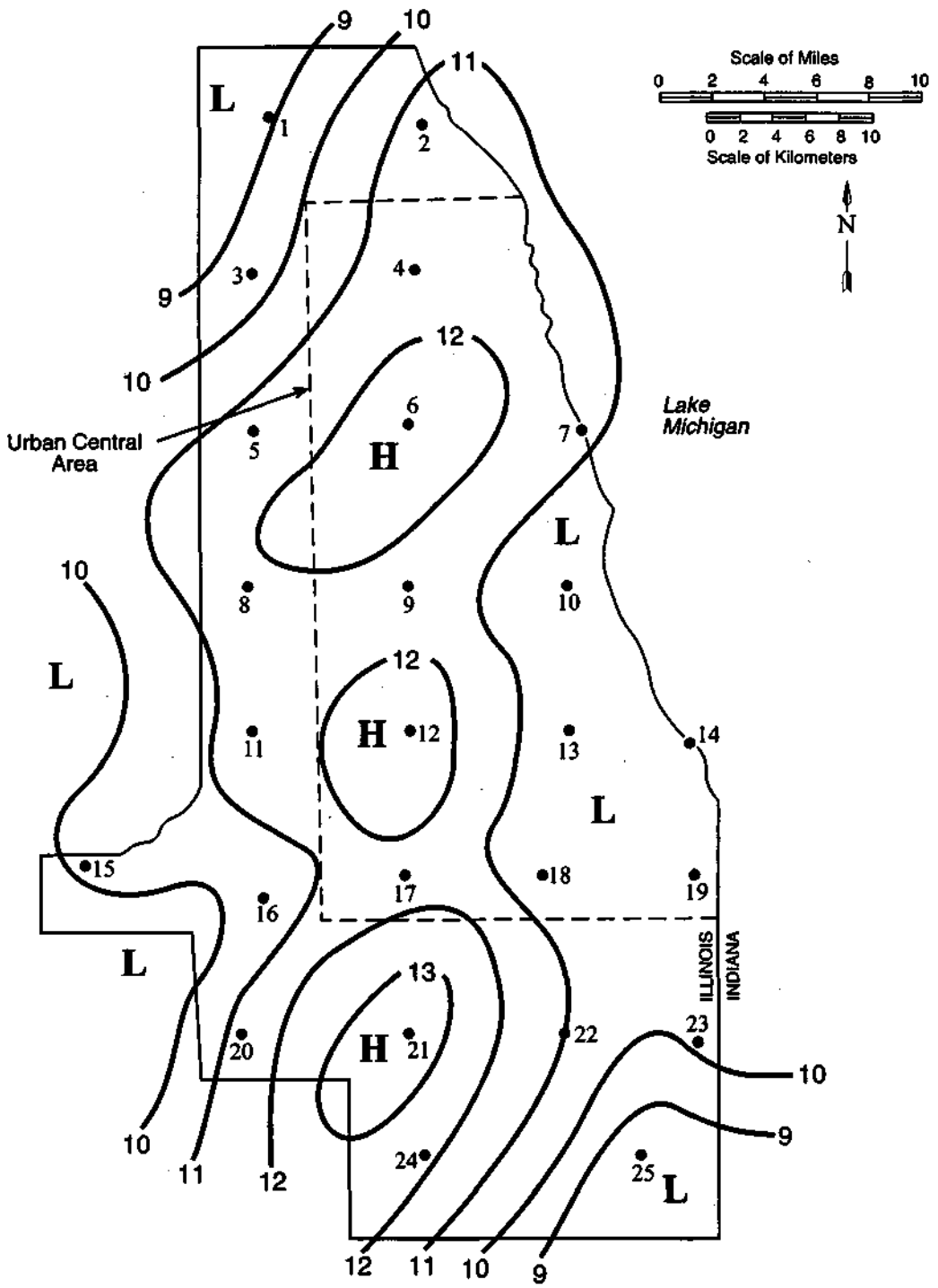

Figure 5. Total rainfall (inches) of the five heaviest spring storms: May 12-13, 1990; April 14-15, 1991; May 24-25, 1991; April 1, 1993; and May 4, 1990

highs in Figure 4 was undertaken using the method described in the annual analyses. The core stations used for the central high were numbered 6, 8, 9, and 10, and the southern high were stations 20, 22, 23, and 24. The results indicated an increase of 7 percent in the core of the central high. The localized increase indicated for the southern high was 3 percent.

Summer Precipitation. The isohyetal map of total summer rainfall for the 5-year sampling period is shown in Figure 6. The pattern is strikingly similar to the urban distribution obtained in an earlier study of heavy rainstorms over the Chicago urban area that utilized all available information (Huff and Angel, 1989). They concluded that the north-central high with an urban-induced effect. Heavy rainstorms in the Chicago area were defined as those producing storm rainfall amounts exceeding the 2-year frequency for a storm period of given duration. Comparison of the 1990-1994 totals with the normal rainfall values (dashed lines on figure 6) reveal the 5-year values were slightly above normal.

The effects of storms of various intensities on the total rainfall pattern were investigated. Figure 7 shows the pattern resulting from combining the five heaviest summer storms, and it has a spatial distribution of highs and lows similar to those in Figure 6. Thus, these 5 storms (7% of total summer storms in 1990-1994) strongly influenced the total summer pattern, and the five storms accounted for 22 percent of the total summer rainfall.

Figure 8 shows the isohyetal pattern of summer rainfall after subtracting the values of the 10 heaviest storms in 1990-1994. The general features of the total summer rainfall (Figure 6) are present—the north-central high is maintained in its approximate position, and the highs in the southern part of the network remain relatively stable with respect to location and intensity. For example, following previous procedures, the ratios of average rainfall in the north-central high to

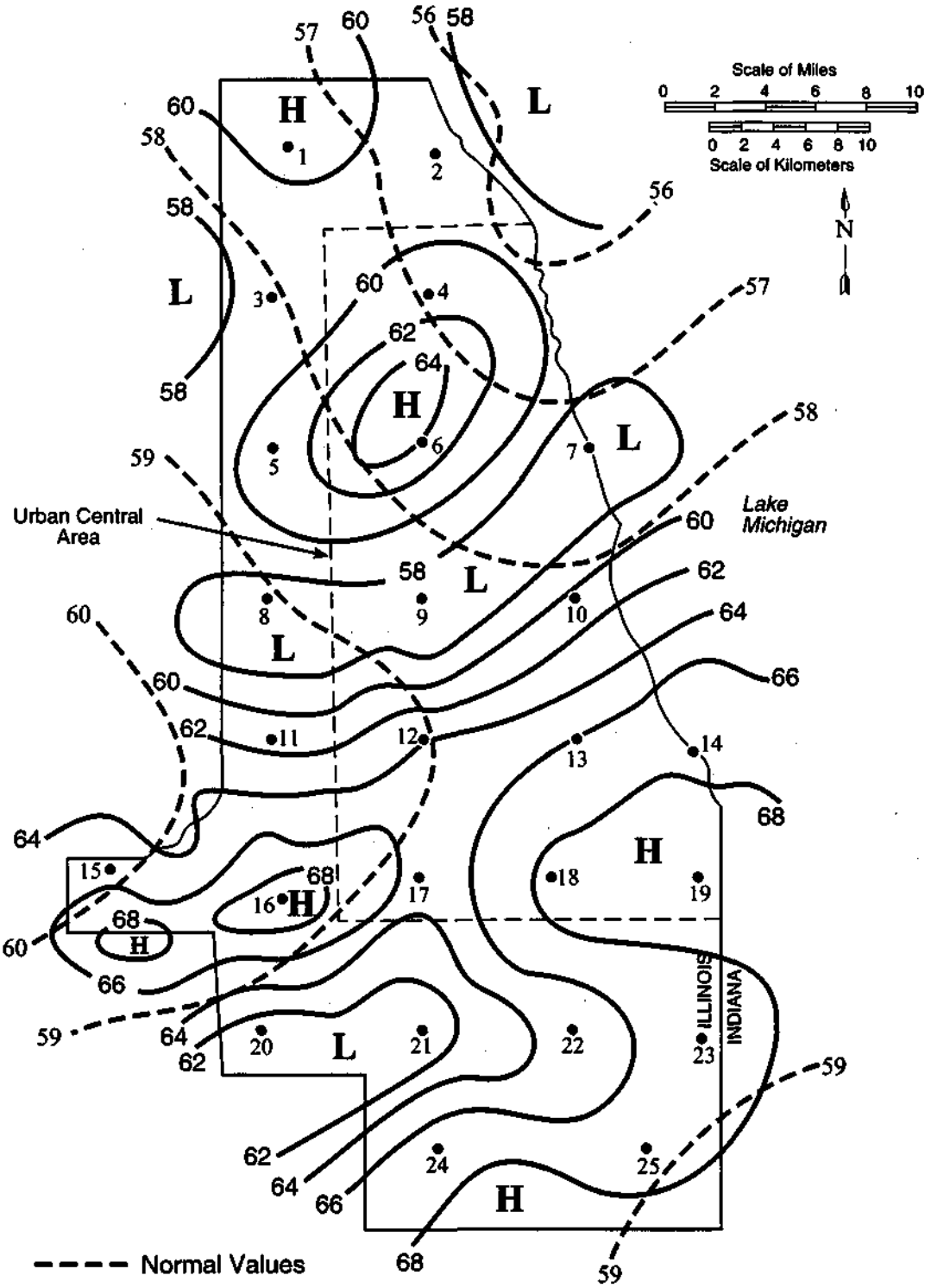

Figure 6. Total summer rainfall (inches), 1990-1994

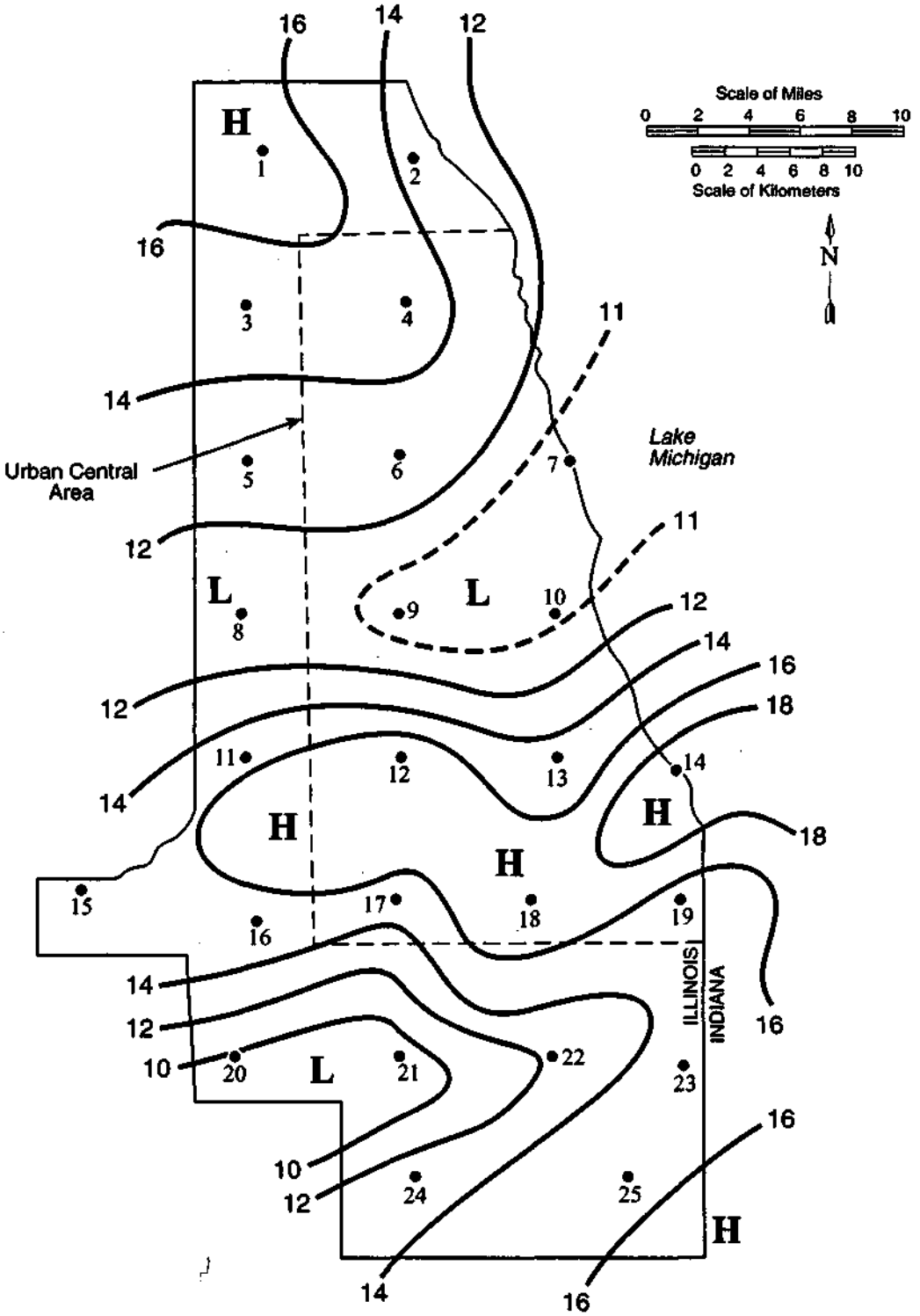

Figure 7. Total rainfall (inches) for 5 heaviest summer storm periods, 1990-1994

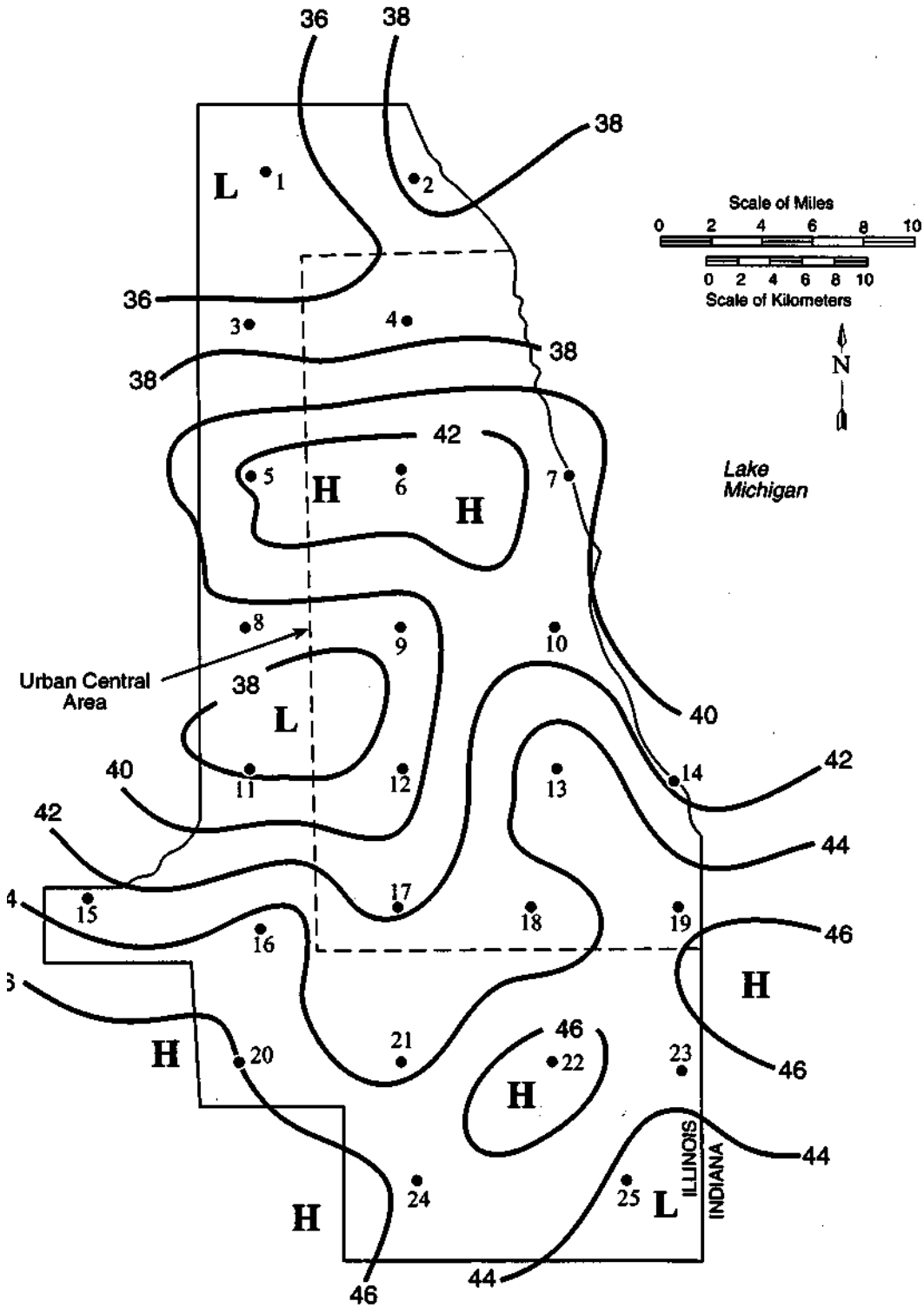

Figure 8. Total summer rainfall (inches) based on omitting 10 heaviest storms, 1990-1994

1) the average of gages 3 and 4, and 2) the average of gages 8, 9, and 10, were calculated for the total rainfall after omitting the 10 heaviest storms (Fig. 8). Results showed ratios of 1.17 and 1.09, respectively. Using similar values for the total 5-summer rainfall (Fig. 6), ratios of 1.08 and 1.04 were obtained. Thus, ratios were larger when the 10 heaviest storms were omitted. This indicates that in this 5-year period, the urban effect in summer rains was slightly greater in the light to moderate storms, but present in both classes—the heavy and light-to-moderate rains.

The total 5-summer rainfall pattern indicated that the north-central high in Chicago incorporated gages 4, 5, and 6 (Fig. 6). For comparison purposes, their 3-gage mean was compared with rainfall experienced at gage 3 (to the northwest) and at gage 7 (to the southeast). A second comparison was made with gages 8, 9, and 10 located south of the north-central center, and a third comparison was made by combining data from all these five control gages. In the computations, the ratios of mean rainfall in the north-central high to the mean rainfall in each of the comparison combinations were calculated. The same evaluation procedure was followed after eliminating the 5 and 10 heaviest storms from the sample, and for the lighter storms (less than 1-inch means). The comparative ratios are summarized in Table 1.

The results suggest a possible increase of 8% to 10% in the north-central high associated with an urban effect when all summer rainstorms are combined (total 5-summer rainfall). When the five heaviest summer storms were subtracted from the total 5-summer rainfall, the ratios were similar to the summer total. When the 10 heaviest storms were eliminated, the net effect of the resulting rainfall was an increase in the ratios, when compared with the first two categories. Table 1 also shows the ratios for those storms in which the network mean was less than one inch (storms of light to moderate intensity). The ratios agree with those for total summer rainfall.

These results suggest that an urban effect, if present, was operating in all levels of summer storm intensity. The summer urban effect values are similar to those found in the other earlier studies of the Chicago rainfall distribution (Changnon, 1980a, 1980b).

Table 1. Estimates of urban effects in north-central high.

Rainfall groups	Ratio, high mean to combination control means		
	Gages 3-7	Gages 8, 9, 10	All five Gages
total rain of all storms	1.10	1.08	1.09
all (less 5 heaviest storms)	1.09	1.06	1.07
all (less 10 heaviest storms)	1.20	1.09	1.14
storm with means < 1 inch	1.20	1.08	1.09

The above analytical procedure was used with to the southern high (Fig. 6) for total summer rainfall. Gages 16, 18, and 19 were selected to represent the high center. The average of these values was compared with the average of control gages 11, 12, and 13, located to the north of the high, and with gages 21, 22, and 23 lying south of the high center. Results indicated a potential urban-related increase of 7% and 6%, respectively, from the two combinations. These are slightly lower than those indicated for the north-central high (Table 1), but the differences are well within the limits of potential sampling errors.

An analysis was made to determine whether the summer monthly rainfall patterns varied substantially from the total summer pattern. Figure 9a shows the June pattern of the total 1990-1994 rainfall, and in the southern part of the network, the June pattern is very similar to the seasonal pattern displayed in Figure 6. However, the north-central high is not present in the June map—rather

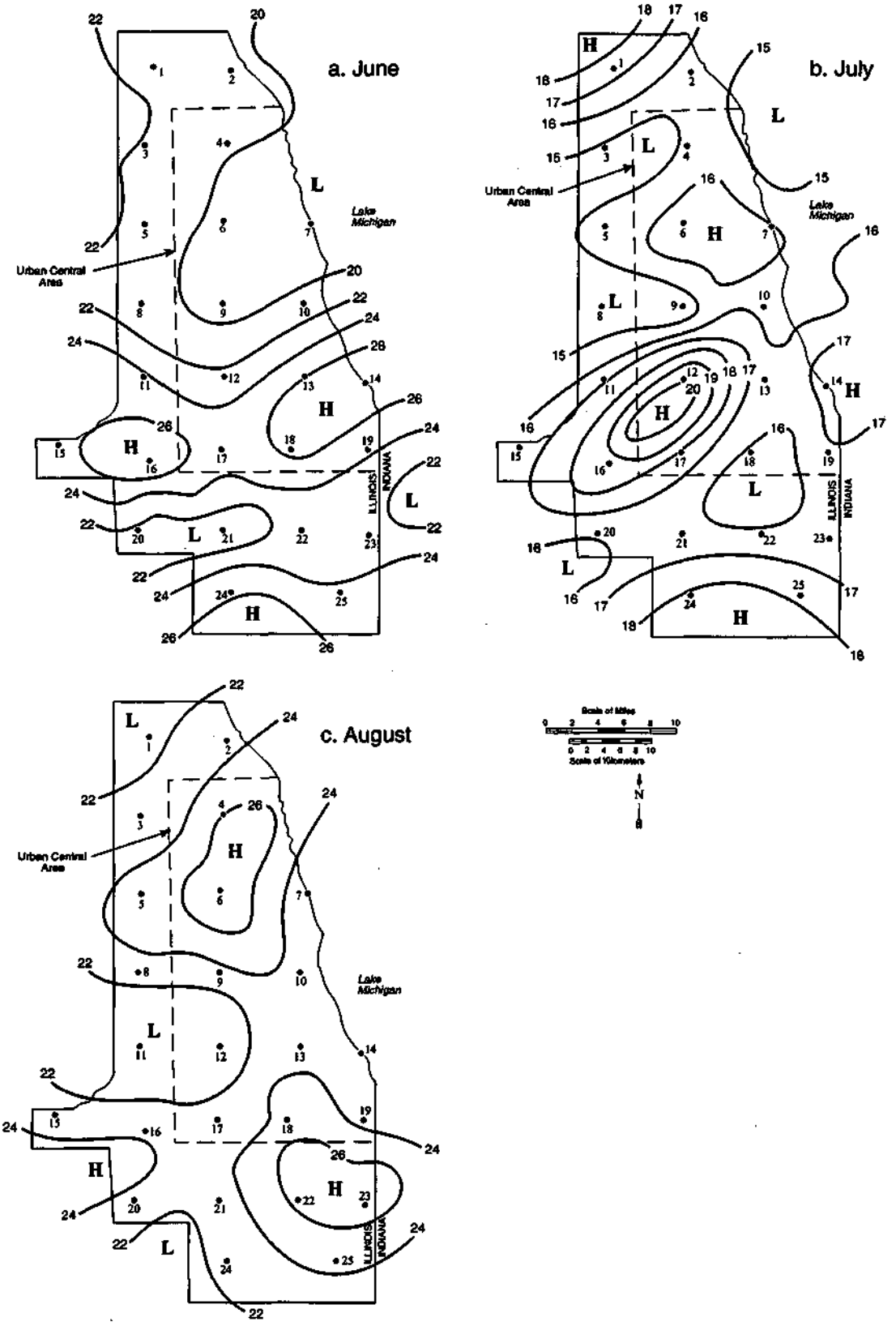

Figure 9. Total rainfall (inches), 1990-1994: a) June; b) July; and c) August

an area of relatively low rainfall is indicated.

The June pattern is heavily influenced by one of the heaviest storms ever recorded in the history of Chicago. On June 28, 1993, 12-hour amounts exceeding 6 inches were recorded in the southwest part of the network (Huff, 1995). This storm was oriented along a line closely approximating the high extending across the southern part of the network (Fig. 9a). Although this storm had an influence on the spatial characteristics of total June rainfall, the June pattern determined after eliminating the 1993 storm, reveals the high rainfall zone across the southern part of the network remains in place, as do the other major features of the total rainfall pattern in Figure 9a.

Figure 9b shows the July rainfall pattern for the 5-year sampling period. It has the north-central high and a high in south-central Chicago. The relatively intense high in the southwest is related to an unusually heavy storm on July 19-20, 1990, an event that produced 4.4 inches at one gage in the center of the high. Gage 12 also had a tendency to record above-average amounts. In the five years, the monthly rainfall at gage 12 ranked 1, 3, 4, 8, and 8 among the 25 network stations. Whether this is due to localized gage catch influences or merely a sampling vagary could not be determined. The August mean pattern (Fig. 9c) also shows a north-central high, but the southern high in July is not present.

In general, the three summer monthly patterns showed good agreement with the summer pattern. This indicates that all three summer months are subject to the same local forcing mechanisms with respect to the spatial distribution of rainfall in the Chicago area.

Values from the dense raingage network operated for the five summers 1976-1980 were compared with the summer values from the 1990-1994 network. Figure 10 shows the network

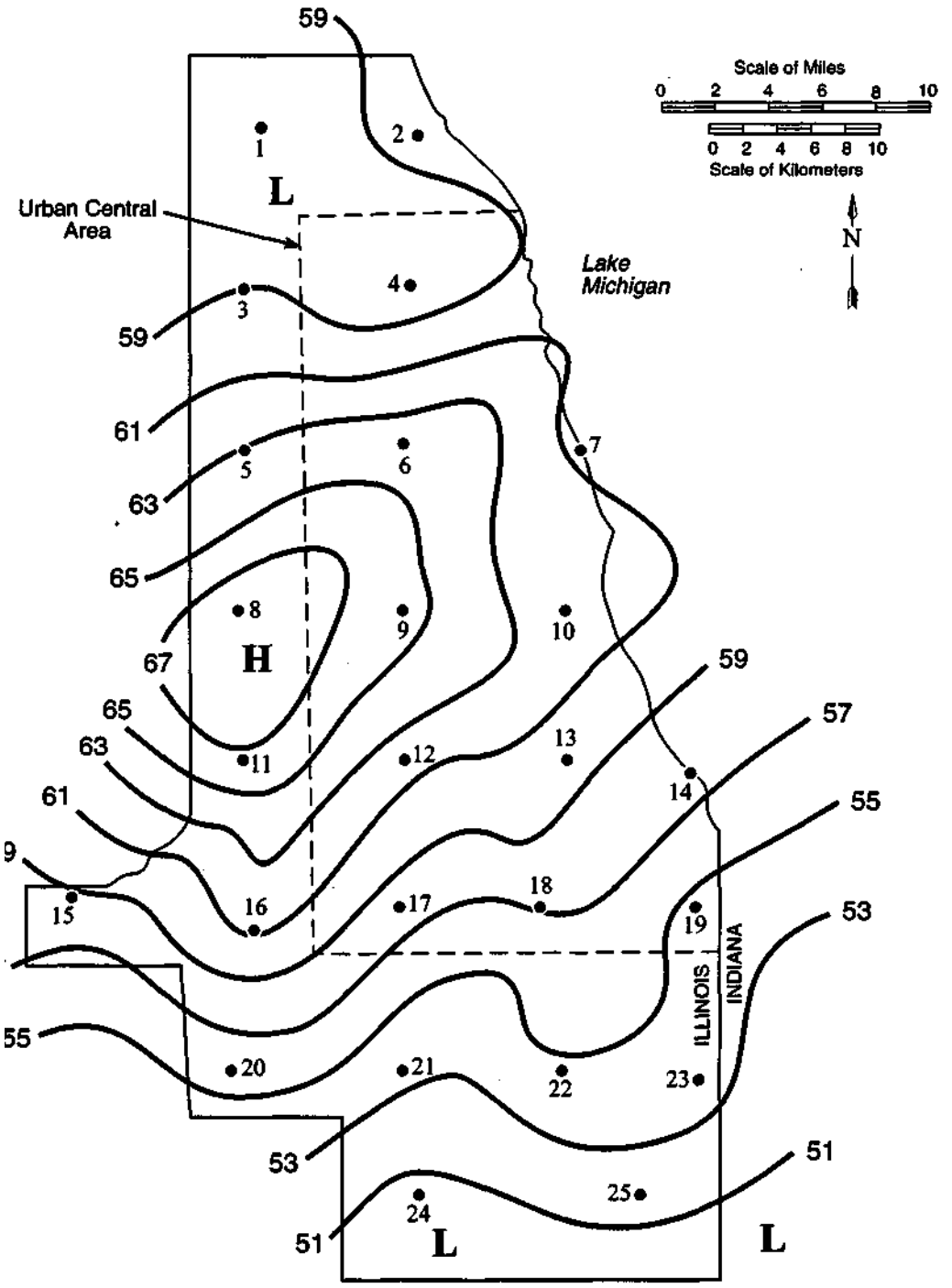

Figure 10. CHAP Network total summer rainfall (inches), 1976-1980

pattern of 1976-1980 total summer rainfall in the Chicago metropolitan area. Comparison of the 1976-1980 pattern and the new network pattern for 1990-1994 (Fig. 6) indicates a major difference in the location of the heaviest rainfall amounts. The earlier 5-year period had a single high rainfall center in the western part of the city, whereas the new 1990-1994 data (and old network data for 1949-1979) indicated two centers. These two centers were located over the north-central and southern parts of the metropolitan area. These differences are likely due to sampling vagaries during the 5-year periods.

The pattern of total summer rainfall, based on combining the 1976-1980 and the 1990-1994 values, appears in Figure 11. This shows a pattern similar to the 1990-1994 pattern (Figure 6), and similar also to the heavy rainstorm patterns for Chicago derived by Huff and Vogel (1976). Total summer rainfall in the 1990-1994 period produced a network mean of 63.26 inches, whereas the network mean calculated from the 1976-1980 data was 59.10 inches. The heavier rainfall in 1990-1994 tended to produce some bias in favor of these data when the two sets were combined.

Figure 12 shows the old network pattern based on those 24-hour storms in which the 2-year frequency values of storm rainfall were exceeded. The general similarity between Figure 12 and Figure 6 (heavy rainfall events vs. total summer rainfall) is apparent.

Rainfall data of the National Weather Service were used to construct a 1990-1994 rainfall map for the urban, suburban, and surrounding rural areas in northeastern Illinois and northwestern Indiana. This was done to ascertain whether the urban-induced high centered in the La Porte-Valparaiso region of northwestern Indiana as, identified in earlier Water Survey studies (Changnon, 1968; Changnon and Huff, 1977), was present in 1990-1994.

The isohyetal pattern (Figure 13) obtained from this climatic analysis shows a high of >66

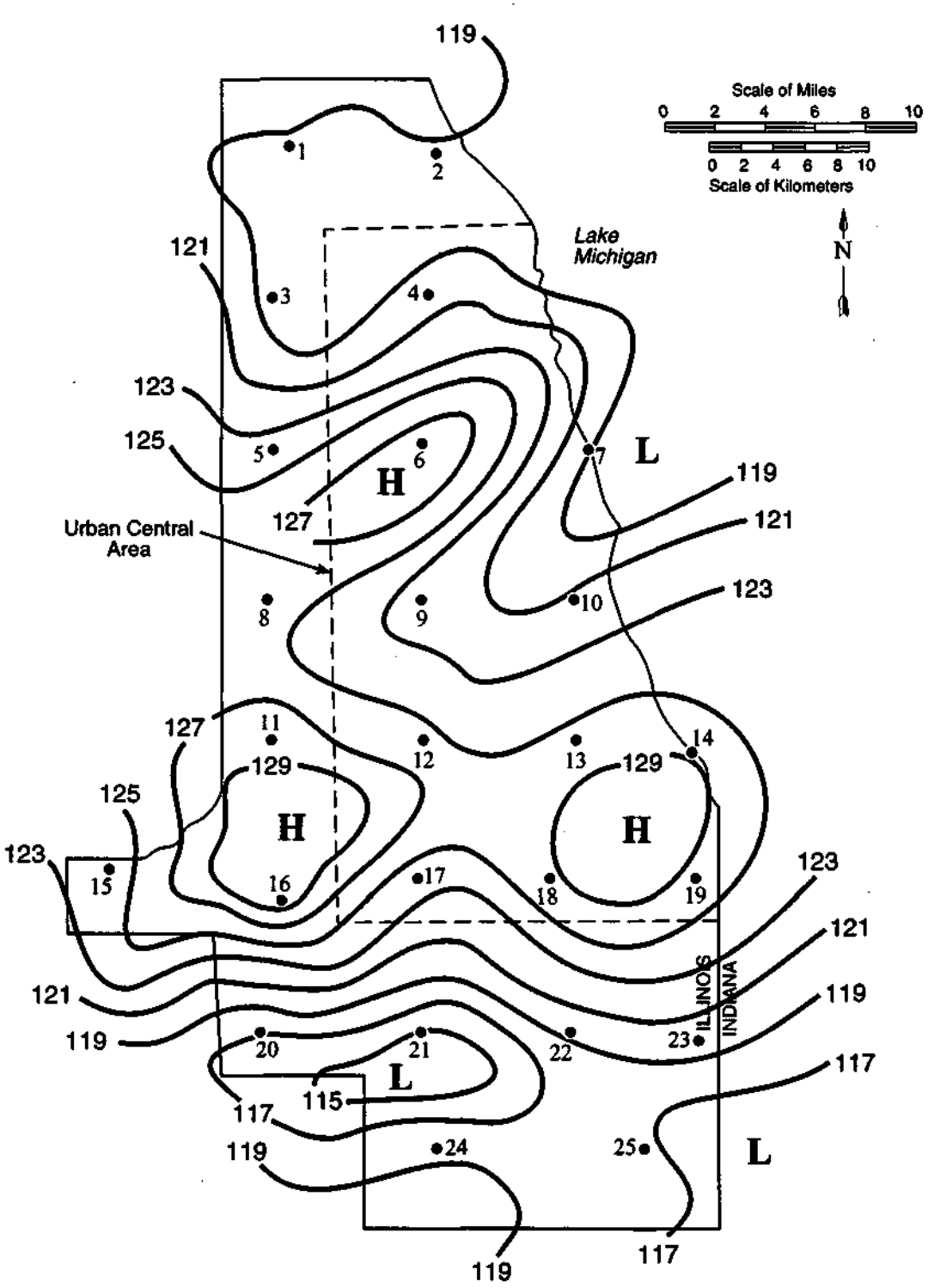

Figure 11. Total rainfall (inches) during summers of 1976-1980 and 1990-1994

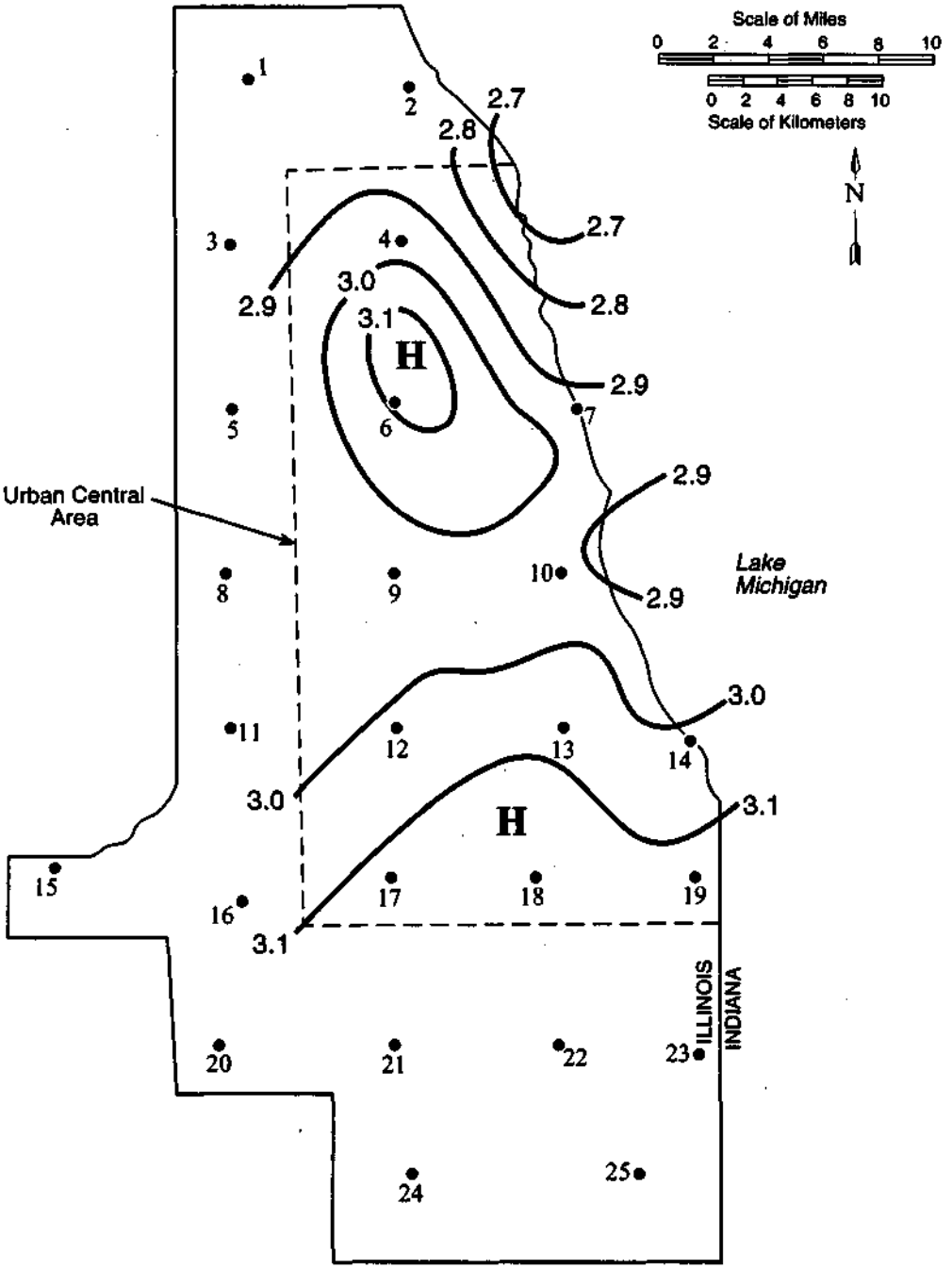

Figure 12. 2-yr, 24-hr frequency of point rainfall (inches), after Huff-Vogel, 1976

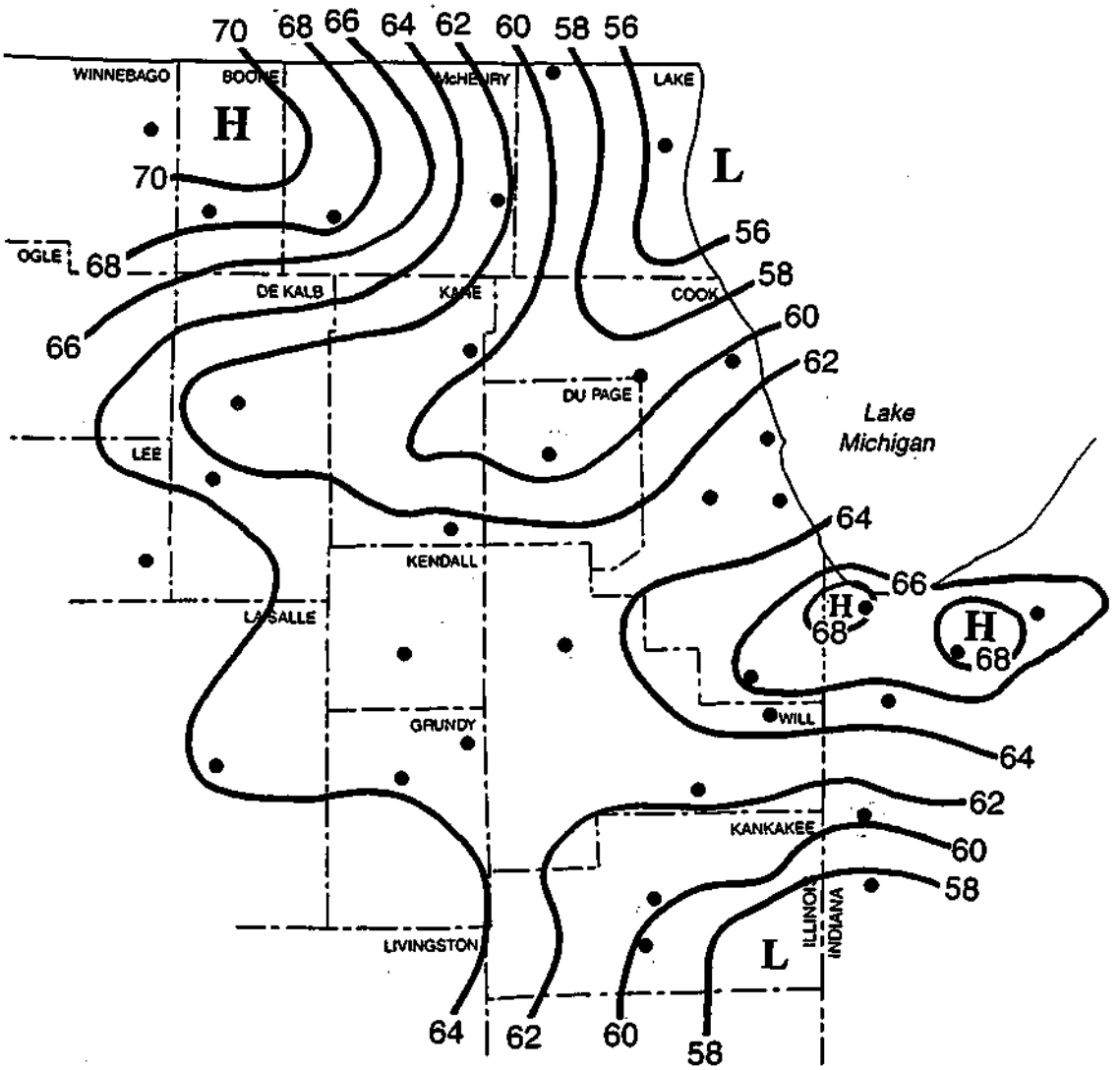

Figure 13. Total summer rainfall for 1990-1994
based on NWS Climatic Network

inches in the southern high in part of the south Chicago urban area and extending into northwestern Indiana. The Indiana high of >68 inches is centered in the La Porte-Valparaiso area, the same general area of high rainfall found in the earlier studies. Thus, this urban-related high has persisted. Comparison of Figure 13 and the summer network pattern (Figure 6) indicates the high in the south urban pattern is part of a region of relatively heavy rainfall extending eastward.

Two methods of comparison were used to evaluate the magnitude of the LaPorte-Valparaiso high in 1990-1994. Rainfall totals in the center of the high were compared with the urban-area average rainfall, as calculated from the 25-gage network data. This indicated an urban-induced increase of 8 percent in the LaPorte-Valparaiso region, with a maximum of 9 percent at Valparaiso. Secondly, the high in Indiana was compared with the average of four climatic stations located in NW, W, and SW of the urban area, and well beyond any potential urban influences. This comparison showed an average difference of 9 percent and a maximum of 10 percent. Thus, this comparison with the climatic stations indicated urban-induced increases similar to those found for the north-central high in the intra-network comparisons. The urban-induced increases of 9 to 10 percent are somewhat smaller than the 15 percent found in previous regional rainfall studies, but the differences are within ranges to be expected due to the time and space variability in summer (convective) rainfall.

Diurnal Distribution of Warm Season Rainfall. An investigation was made of the characteristics of the diurnal distribution of warm season rainfall (May-September) in the metropolitan area using data from the 1990-1994 Chicago network. The primary purpose was to determine whether a nocturnal peak occurred in the distribution, similar to that found in the St. Louis area during the 1971-1975 METROMEX program (Changnon et al,, 1977). It was found that the

St. Louis anomaly was related to urban enhancement factors.

In making the Chicago data analysis, hourly rainfall totals for each clock hour were used from the urban network of 25 recording raingages. The initial study was concentrated on the period from 1800 to 0600 CST for the months of May through September. Convective rainfall dominates during this period, and one when the urban effects have been found to be most pronounced. Huff and Vogel (1976) used data from the earlier Chicago urban network for 1949-1979 to identify an apparent urban-induced increase in heavy rainstorms across the north-central part of the city (discussed previously). However, their study incorporated all hours of the day, and no attempt was made to evaluate potential differences between day and night rainfall distributions.

In the first analysis, June-August totals for the 1800-0600 period were determined for the 1990-1993 sampling period. (Data for 1994 were not yet available at the time of this study.) The isohyetal pattern of total rainfall for the 12-hour nocturnal period showed a high extending across north-central Chicago. The location corresponded closely with the 1949-1979 pattern and with the summer patterns— Figure 6 included all data for the entire 24-hours of the day. A second nocturnal high was located across the extreme southern part of the city, and this high also corresponds closely to the other urban patterns.

In a second analysis, hourly data from all 25 raingages were combined to ascertain the time distribution of nocturnal rainfall in the network. The hourly data were combined into 3-hour moving averages for 1800-0600 CST to modulate the effect of natural rainfall variability. The St. Louis area maximum had occurred at 2100-2400 CST (Changnon and Huff, 1986). However, the Chicago network did not indicate an urban maximum at this time. The Chicago data analysis showed that July was the only month to exhibit such a nocturnal maximum, with a peak indicated in the time

distribution for the three hours ending at 0200. No indication of a late evening or early morning maximum was found in the June and August distributions. It is possible that a nocturnal anomaly is present east of the city, similar to the St. Louis anomaly. This would place it over Lake Michigan, and therefore not detectable by the raingage network. If so, the lake effects could dampen the urban-induced effect, and it would be less pronounced than the St. Louis anomaly (Changnon, 1980b).

In the third analysis, the 3-hour period in which the maximum rainfall occurred in each event (storm) during the 1800-0600 period was determined for each of the 25 raingages. The maxima for each station in the sampling period were then combined to obtain network values for each 3-hour period. This was done for both June-August and May-September. The frequency of maxima was then determined for each 3-hour period during 1800-0600. Results indicated a secondary peak in the frequency of occurrence for the three hours ending at 0200 CST. However, this peak was evident in the records of other stations in northern and north-central Illinois (Huff, 1971). Therefore, it is apparently a natural, broad-scale climatic phenomenon rather than an urban-induced effect.

This limited study did not reveal any strong evidence of an urban-induced high in the nocturnal distribution, such as found at St. Louis.

Fall Precipitation. The isohyetal pattern of total fall precipitation for the 1990-1994 period is shown in Figure 14. The fall pattern is quite similar to the annual distribution in Figure 6, with respect to placement of highs and lows. The north-central high in the annual pattern is displaced a few miles southeastward in the fall distribution, but the southern high is located close to the position of the annual high. Lows are indicated in the northern part of the network. The precipitation in the five heaviest fall storms only partly resembles the total precipitation pattern.

Figure 15 shows the isohyetal map constructed by combining all fall storms having network

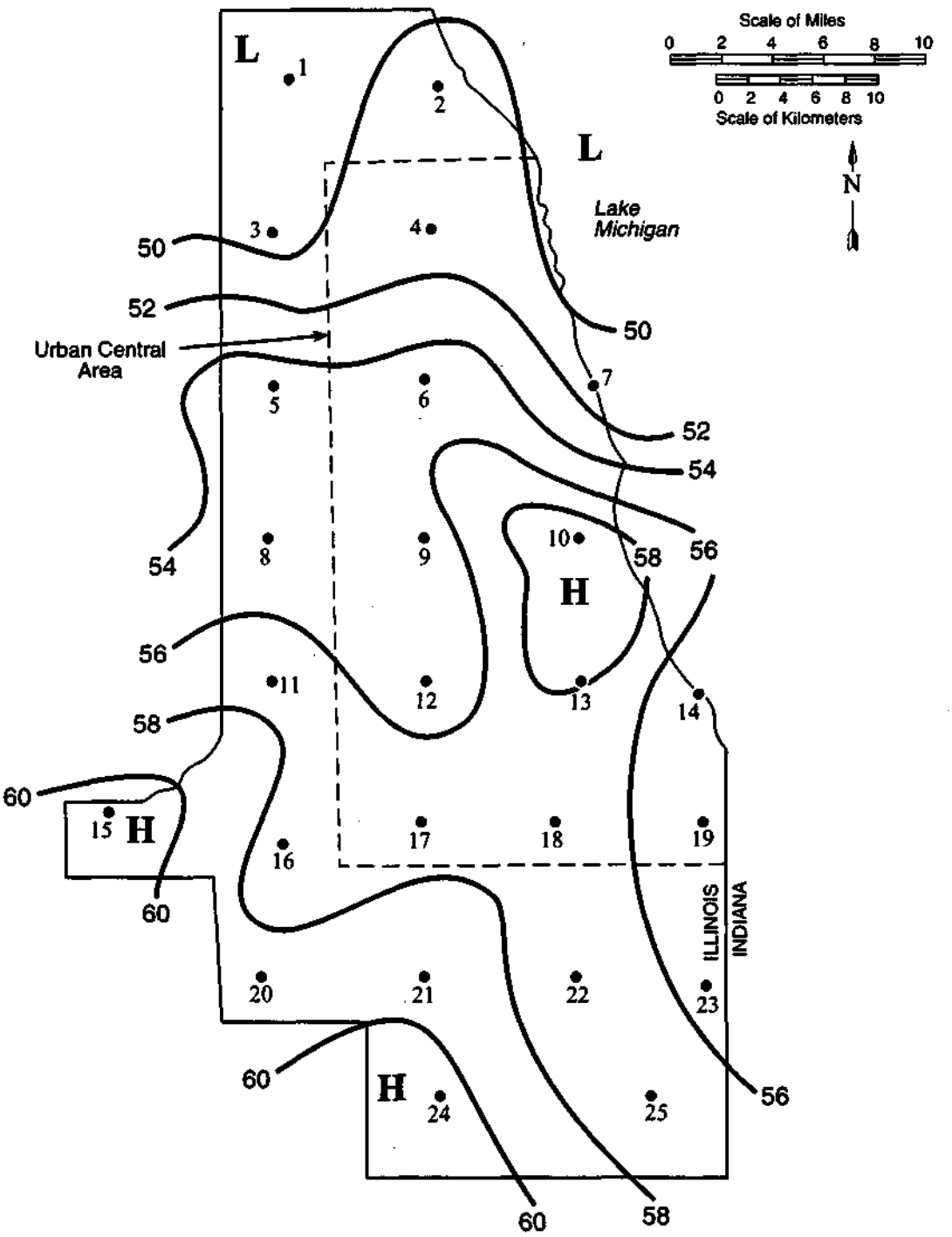

Figure 14. Total fall rainfall (inches), 1990-1994

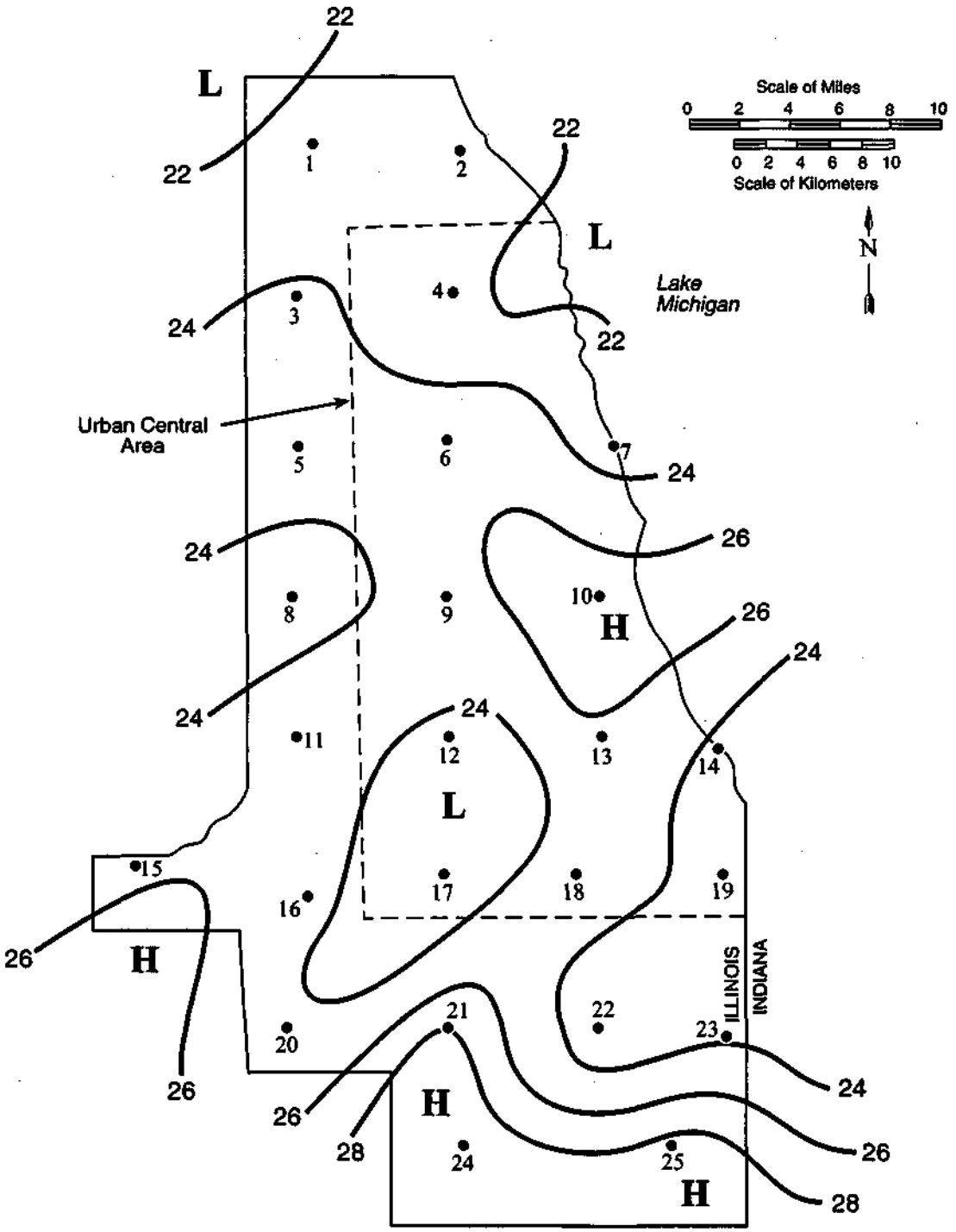

Figure 15. Total fall precipitation in storms having network means <1.00 inch

means of one inch or less. This network pattern is quite similar to Figure 14. As found in the spring and summer analyses, there is strong evidence that the urban effect at Chicago is produced in the light as well as heavier rainfall events.

An analysis of the potential urban effect was made following comparative methods described previously. Results indicated an urban-induced increase of 9 percent in the central high, which is slightly higher than obtained in the annual, spring, and summer analyses. An increase of 3 percent was obtained for the southern high, similar to annual and spring values.

Winter Precipitation. The total precipitation pattern for the five consecutive winters, 1989-90 through 1993-94, is shown in Figure 16. The major features found in the spring and summer rainfall patterns are also indicated on the winter map. An area of relatively heavy precipitation is indicated across the central part of Chicago. An area of relatively lighter precipitation is located across the south central part of the network, and this separates the central high from another high across the southern part of the network. Another small area of relatively heavy precipitation is present in the northern part of the network, similar to that in the spring. The winter and spring patterns are very similar. The light and heavy winter precipitation patterns both had features similar to the winter total (Fig. 16).

The magnitudes of the central and southern highs in winter were obtained following the procedures previously used for annual, spring, and summer dates. Gages 6, 9, and 10 were selected to represent the core of the central high in winter. Similarly, values for gages 21, 22, and 23 were used for the southern high. Results indicated an increase of approximately 8 percent from possible urban effects in the central high, and 5 percent was obtained for the southern high.

Summary. The annual and seasonal precipitation analyses suggest that localized weather

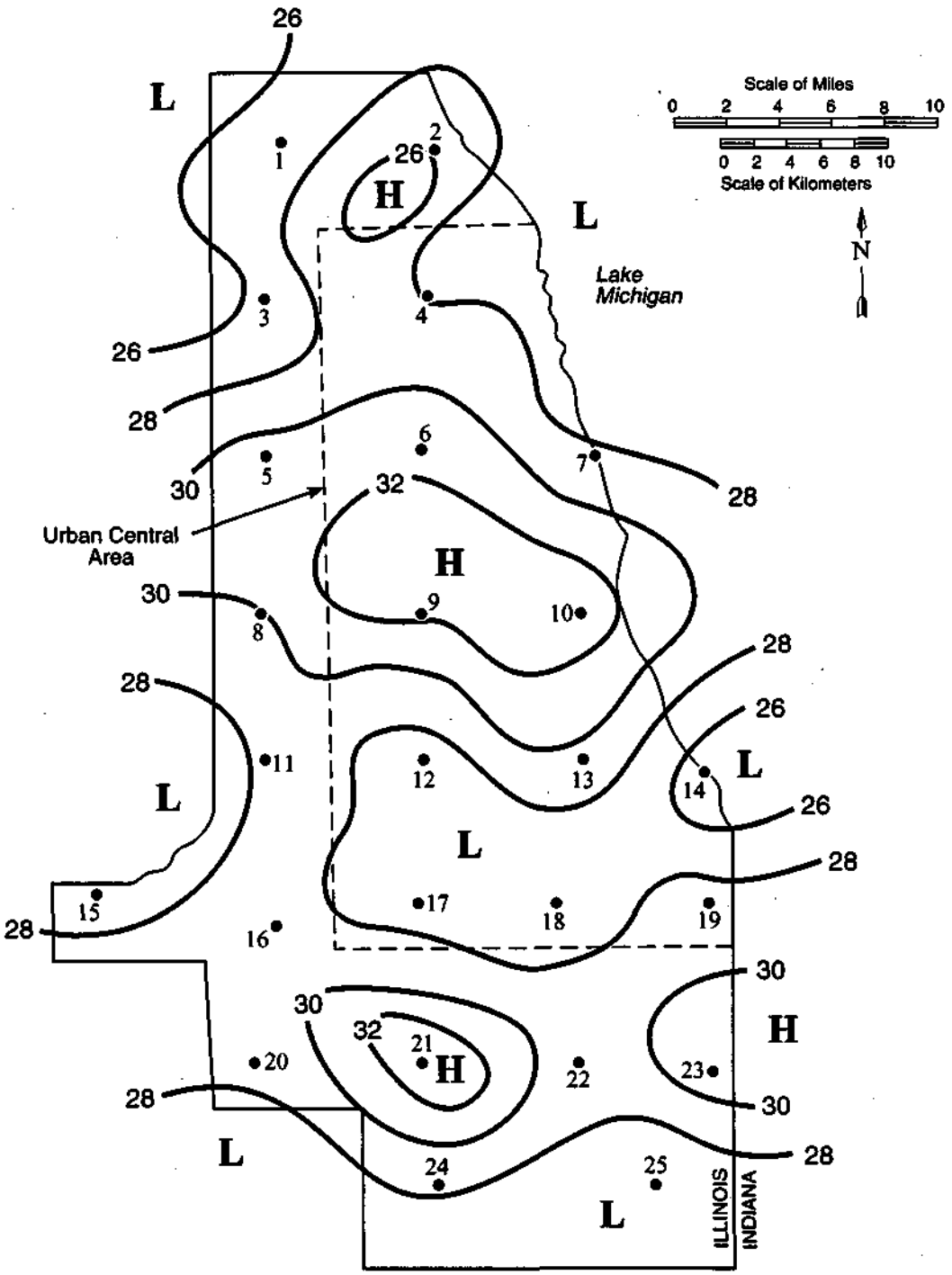

Figure 16. Total winter precipitation (inches), 1990-1994

mechanisms are occurring in Chicago and to some degree in most storms and in all seasons during 1990-1994. Furthermore, there was excellent spatial correlation in the location of the major centers of relatively heavy and light precipitation (highs and lows) with those from prior studies—persistent highs of precipitation existed over the central and southern parts of Chicago.

Analyses of annual data indicated a potential urban-induced increase of 8 percent in the central high, and 4 percent in the southern high. Previous rainfall frequency studies (Huff and Vogel, 1976; Huff and Angel, 1989) also found these highs.

The present study lends support to most earlier findings, and provides further evidence of an urban-induced precipitation increase in the Chicago metropolitan region. Table 2 shows the annual and seasonal percentage increases in average precipitation for the central and southern precipitation high centers in Chicago.

The inadvertent urban effect on precipitation indicated in the central and southern highs found at Chicago indicated near identical changes for the central high of 7, 9, and 8 percent, respectively, for spring, summer, and winter. This suggests that the effect does not vary significantly between seasons. The southern high values were 3, 6, and 5 percent, respectively, for these three seasons.

Table 2. Estimated localized increases (percentages) in average precipitation, 1990-1994.

	Central High	Southern High
Spring	7	3
Summer	9	6
Fall	8	3
Winter	8	5
Annual	8	4

The Chicago urban effect is smaller than that found at St. Louis and some other cities (Huff and Changnon, 1973; Changnon et al., 1977). One possibility is that the new Chicago network is too confined to the Chicago area to measure accurately non-urban precipitation outside the urban-effect area. That is, most of the 1990-1994 network may be subject to some urban effects. In this case, comparing the high rainfall centers with rainfall in the immediate surrounding areas would produce differences smaller than actually exist between the urban-effect and surrounding no-effect regions. In contrast, designating reliable no-effect areas (controls) was not a problem in the 5200-km^2 METROMEX network at St. Louis, where larger urban effects were found.

Another possibility for a lesser urban effect is the presence of Lake Michigan at the eastern boundary of the Chicago urban area. At St. Louis, the METROMEX project established that the urban effect maximized 25-35 km northeast of the urban center, but was also significant east and southeast of the city. Location of the maximum effect downwind of the urban centers has been found in other large cities, such as Cleveland, Baltimore, and New Orleans (Huff and Changnon, 1973). The downwind effects on precipitation could not be evaluated east and northeast of Chicago because of the lake (no routine precipitation measurements were available over the lake).

However, Changnon (1968), using historical climatic data, found evidence that an inadvertent change was induced by Chicago's urban-industrial complex extending eastward from south Chicago into extreme northwestern Indiana. An urban-induced increase of approximately 15 percent in summer rainfall for 1990-1994 was identified in the vicinity of LaPorte, Indiana, 40-60 km east of the south Chicago urban area. This percentage increase compares favorably with those found at several other large cities.

Analyses of the urban-induced high for the 1990-1994 period inside the city indicated

increases of 8 to 10 percent. These are similar to that found for the north-central Chicago high in the 1976-1980 study, and suggests that sampling variability may be responsible for differences found between the present study and previous investigations.

References

Changnon, S.A., 1961: Precipitation contrasts between Chicago urban area and offshore station in southern Lake Michigan. *Bull. Amer. Meteor. Soc.,* **42**, 1-10.

Changnon, S.A., 1968: The LaPorte anomaly—fact or fiction? *Bull. Amer. Meteor. Soc.,* **49**, 4-11.

Changnon, S.A., 1970: Reply. *Bull. Amer. Meteor. Soc.,* **51**, 337-342.

Changnon, S.A., 1971: Lessons from LaPorte. *Proceedings, International Conference on Weather Modification,* AMS, Boston, 193-198.

Changnon, S.A., 1980a: Summer floods at Chicago and possible relationship to urban-increased heavy rainfall. *Water Resources Bulletin,* **16**, 323-325.

Changnon, S.A., 1980b: Evidence of urban and lake influences on precipitation in the Chicago area. *Journal of Applied Meteorology,* **16**, 1137-1159.

Changnon, S.A., 1980: More on the LaPorte anomaly. *Bull. Amer. Meteor. Soc.,* **61**, 702-711.

Changnon, S.A., 1984: Urban and lake influences on summer rainfall in the Chicago area. *Physical Geography,* **4**, 23-29.

Changnon, S.A., and F.A. Huff, 1966: Measurement of precipitation over Lake Michigan. *J. Great Lakes Research,* **15**, 235-248.

Changnon, S.A., and J. Detwiller, 1976: Possible urban effects on maximum daily rainfall at Paris, St. Louis, and Chicago. *J. Appl. Meteoro.,* **15**, 517-519.

Changnon, S.A., and F.A. Huff, 1977: LaPorte again: A new anomaly? *Bull. Amer. Meteor. Soc.*, **58**, 1069-1072.

Changnon, S.A., and R. Semonin, 1978: Chicago area program: A major new atmospheric effort. *Bull. Amer. Meteor. Soc.*, **59**, 153-160.

Changnon, S.A., F.A. Huff, P.T. Schickedanz, and J.L. Vogel, 1977: *METROMEX—Volume 1—Weather Anomalies and Impacts,* Bull. 62, Illinois State Water Survey, 259 pp.

Changnon, S.A., F.A. Huff, J.L. Vogel, D.A. Brunkow, and D.W. Skaggs, 1980: *Rainfall Prediction-Measurement Systems and Rainfall Design Information for Urban Areas.* Circular 146, Illinois State Water Survey, 63 pp.

Changnon, S.A., J.L. Vogel, F.A. Huff, and D.A. Brunkow, 1980: *Hydrometeorologic Studies Addressing Water Resources Problems.* Final Report, Div. Problem-Focused Research Applications, Directorate for Applied Science and Research Applications, National Science Foundation, 135 pp.

Changnon, S.A., D. Gatz, A. Jameson, G. Dzurisin, R. Scott, and R. Grosh, 1979: *Studies of Urban and Lake Influences on Precipitation in the Chicago Area.* Contract Report 220, IL State Water Survey, 190 pp.

Hidore, J.J., 1971: The effect of accidental weather modification on the flow of the Kankakee River. *Bull. Amer. Meteor. Soc.*, **52**, 99-103.

Holzman, B., and H. Thorn, 1970: The LaPorte precipitation anomaly. *Bull. Amer. Meteor. Soc.*, **51**, 335-337.

Huff, F.A., 1977: Effects of the urban environment on heavy rainfall distribution. *Water Resour. Bull., AWRA,* **13**, 807-817.

Huff, F.A., 1995: Characteristics and contributing causes of an abnormal frequency of flood-producing rainstorms at Chicago. *Water Resources Bulletin,* **31:4,** 703-713.

Huff, F.A., and J.R. Angel, 1989: Frequency Distribution and Hydroclimatic Characteristics of Heavy Rainstorms in Illinois. *Bull. 70,* Illinois State Water Survey, 177 pp.

Huff, F.A., and J.L. Vogel, and S.A. Changnon, 1981: Real-time monitoring -predictions system and urban hydrologic operations. *J. Water Resour. Planning and Management* and Urban, Proc. Amer. Soc. of Civil Eng., 107:WR2, 49-435.

Huff, F.A., and J.L. Vogel, 1976: *Hydrometeorology of Heavy Rainstorms in Chicago and Northeastern Illinois, Part 1 - Historical Studies,* Report of Investigation 82, Illinois State Water Survey, 63 pp.

Huff, F.A., and S.A. Changnon, 1973: Precipitation modification by major urban areas. *Bull. Amer. Meteor. Soc.*, **54**, 1220-1232.

Stout, G.E., and K. Wilk, 1962: Influence of Lake Michigan on squall line rainfall. *J. Great Lakes Res.*, **7**, 111-115.

Westcott, N., 1995: Summertime cloud-to-ground lightning activity around major midwestern urban areas. *J. Appl. Meteor.*, **34,** 1633-1642.

SECTION H

EFFECTS OF ATLERED WEATHER CONDITIONS ON THE CORN CROP

INTRODUCTION

Temperature and rainfall are the two weather variables that are most often used to describe growing seasons. For example, the terms hot and dry, cool and wet, or cool and dry immediately provide a picture of the weather in any given summer. Such terms generally apply to the entire growing season. However, even in normal summers there are often short periods that can be described by these terms. How these short periods of abnormal weather affect final corn *(Zea mays* L.) yield are not fully understood, but they often play a very important role in determining final yields. Understanding how temperature and rainfall during each growth stage affects the development of the different corn yield components (number of kernel rows per ear, number of kernels per row, kernel masss, number of fully or paretically developed ears per unit land area) may provide an indication of the best time for weather modification activities which will result in the greatest yield increases, and therefore the greatest return on the weather modification investment.

Corn Yield Response to Temperature

Various studies have shown that temperature can greatly affect corn yields when the corn plant is pollinating (Herrero and Johnson, 1980) and during the two weeks following pollination when the kernels are developing (Jones et al., 1981, 1984, 1985). Lehenbauer (1914) demonstrated the effect of temperature on corn leaf elongation. Since that time many studies have demonstrated the relationship between temperature and the rate of corn development.

However, most of the research on the temperature effects on corn have focused on corn development and not corn growth[1] and final yield. The growing degree day concept (Cross and Zuber, 1972) and later work by Coelho and Dale (1980) have demonstrated that the rate of corn development is highly correlated to temperature. However, there are no studies that relate corn growth and final yield to the temperature experienced by the plant during its early growth stages.

The economic benefit of increased rainfall due to weather modification in the Midwest can be realized only if the additional rainfall can be produced when it is needed the most. Previous work by Hollinger and Changnon (1993) showed that if an additional 25 percent of water could be obtained from each storm from June through August, corn yields would be increased even in the wet years.

Results from the 1987 through 1991 weather modification impacts experiment (Hollinger and Changnon, 1993) showed that early growing season air temperature had a significant negative correlation with final corn yield (r= -0.83). In the experiment, the year-to-year yield variability was negatively correlated with both the maximum and minimum air temperatures during the period from planting to tassel initiation, with yields decreasing with increasing temperature.

Watts (1972a, 1972b) and Warrington and Kanemasu (1983a, 1983b) studied the effects of temperature on leaf initiation and expansion during the seedling stage of growth. However, they did not continue leaf area measurements after treatments were removed, nor did they look at

[1]Corn development is defined as the rate of leaf initiation and elongation, stem elongation, and tassel and ear initiation and development. Corn growth is defined as the accumulation of dry matter in the various plant compartments. While corn growth and development are highly correlated, the number of leaves and ears are determined by the genetic makeup of the plant. The final size of the leaves, stems, and ears is greatly affected by the environment in which the corn plant grows.

the effects of these early temperature treatments on yield. Other studies concerned with early season temperature have dealt with the effects of no-till or minimum tillage on soil temperature and yield (Fortin and Pierce, 1990; Fortin et al., 1994). These studies generally show decreased soil temperature under reduced tillage methods and correspondingly, reduced corn yields. The reduced yields with cooler early season soil temperatures appear to be counter to the results observed by Hollinger and Changnon (1993). The apparent contradiction is due to the fact that one would expect soil temperatures to increase with increased air temperatures. Therefore, reduced yields would be expected with increased soil temperatures.

Two hypotheses can be proposed regarding the effect of early season temperature on yield. The first is that increased soil temperature results in decreased corn yields. The second is that increased air temperature results in decreased corn yields.

Corn Yield Response to Rainfall

During the summers of 1987 through 1991, experiments in rain shelters (Banwart, 1987, 1988) were conducted to evaluate the impact of increased rainfall on corn (Zea mays L.) yields in east-central Illinois (Hollinger and Changnon, 1993). The increases in rainfall were designed to simulate the effects of enhanced rainfall due to cloud seeding in typical dry, average and wet summers. Results of that study showed that increased rainfall resulted in larger grain yields. However, the increase in yields due to more rain during the typical dry, average, and wet summers were small compared to the variability of corn yields among the five years.

It has been long accepted that the two to four weeks around corn pollination is the most critical period for rainfall in determining corn grain yield. Most studies have related the rainfall

response of corn to the calendar (Runge, 1968; Huff and Changnon, 1972). This approach was used because planting dates in individual years were unknown on a regional basis of the yield data. A major problem with this approach is that the corn crop is never planted at exactly the same time each year, and the temperature regime under which it is grown can either lengthen or shorten a given growth stage. Thus, the response of corn yield to a calendar period, while informative, does not allow for fine tuning of either weather modification for rainfall enhancement, or water application through irrigation.

The 1987 through 1991 weather modification impacts experiment was not designed to determine which growth stages of corn would benefit most from additional rainfall. Most of the other studies conducted to determine the timing of additional rainfall that would benefit the corn crop have been conducted using observed weather and crop reporting district yields. These studies most often use monthly precipitation totals to relate final corn yields to rainfall. Changnon and Neill (1968) reported that the three critical weeks for rainfall for corn yield were the weeks of 20 June to 5 July, 6 July to 12 July, and 3 August to 9 August. These periods most often relate to the growth periods just before tasseling and pollination when the potential number of kernels per row on each ear is being determined, and early grain fill. In a more recent study (Dixon et al., 1994), weather variables during different corn growth stages were correlated with corn yields at the Crop Reporting District level. They found that the soil moisture was significantly correlated with corn yields during the period of ear development and grain fill. However, they found no significant correlation with moisture and final corn yield when rainfall was used as the moisture variable.

These past studies have not indicated which growth stages are most sensitive to rainfall

shortages in determining corn yields in Dlinois. Theory, based on how a corn plant develops and determines yield (Table H.1.1.1), would indicate that the size of the corn plant should be affected by the rainfall from planting to silking. The number of rows on each ear should be affected by the rainfall from planting to the end of row set (approximately the 10 leaf stage of corn development). The number of kernels per row, and the final number of kernels on the ear should be affected by the rainfall from planting to the end of the lag phase, approximately 2 weeks after silking. Finally the mass of each kernel should show some relationship between rainfall from planting to maturity, and more specifically during the period from the end of lag phase to maturity. Stresses that occur before and during the development of any yield component should show an effect on that yield component. Stresses after a yield component is determined should not demonstrate any correlation between the yield component or the stress that occurs after the yield component is determined. For example, the potential number of rows per ear is determined at approximately the 10-leaf stage. Therefore, there should be no correlation between the number of rows on fully developed ears and drought stresses after the 10-leaf stage.

Objectives

The objectives of the research in this study were to determine 1) how early season temperature affects corn canopy development and final corn yield, 2) the growth stages during which final corn yield is most sensitive to water shortages, 3) how the different yield components responded to rainfall shortages during different growth stages, and 4) to define which growth stages are most likely to have rainfall shortages and/or temperature stresses based on early, normal, and late dates of planting in the North Central Region of the United States. Results from

these objectives were then used to develop a weather modification decision aid tool based on growth stage, rainfall shortage, and previous growing conditions.

Table H-1.1.1 Growth stages of corn including general lengths of growth periods, description of plant growth stages, above ground growth processes occurring during each growth stage, and expected stress response and effect on yield components.

Growth Stage	Length of Period Days	Plant Description	Growth Processes	Stress Response
Planting to Tassel Initiation	21-30	Planting to 5-leaves fully emerged	Germination, emergence, leaf initiation and growth	Reduced plant vigor
Tassel Initiation to Ear Initiation	6-8	5-leaves fully emerged to 7 leaves fully emerged	Start of tassel growth, stem elongation, continued leaf growth and emergence, and conversion of top axillary bud from vegetative to reproductive	Reduced plant vigor and size
Ear Initiation to End of Row Set	10-14	7 leaves fully emerged to 10 leaves fully emerged	Stem elongation, tassel growth, leaf growth and emergence, and number of rows on ear determined	Reduced number of rows, and final plant size
End of Row Set to Silk	14-20	10 leaves fully emerged to silk	Stem growth, leaf growth and emergence, tassel growth and emergence, cob growth, kernel primordia initiation, and silk development	Reduced final plant size, reduced number of kernel primordia per row, and ear size
Silk to End of Lag Phase	12-14	Pollination to blister stage	Embryo and endosperm development	Kernel abortion
End of Lag Phase to Maturity	38 - 50	Blister stage to black layer	Grain fill and leaf senescence	Reduced kernel size

METHODS

The objectives of this research were achieved by conducting two field experiments and extensive analysis of the ensuing data. The first experiment was designed to study the effects of soil and air temperatures on early corn growth and development, and on final yield. The second experiment was designed to study the effects on final yield, and on corn yield components, of no

rainfall, and rainfall equal to 50 and 100 percent of evapotranspiration during different corn growth stages. The results of the two field experiments were combined with climate data to address the fourth research objective.

Weather Monitoring.

Air temperature, relative humidity, solar radiation, and wind speed and direction were all monitored at the Illinois Climate Network automated weather station located at the Illinois State Water Survey Research Center 1 km west of the experimental rain shelter and plot area. Rainfall was monitored at the plot area. However, in neither of these experiments was the total rain at the plots that important. All the natural rain was kept off the rain shelter plots after the corn was planted, and the soil temperature treated plots were irrigated so that water stress would not impact the plots. The only reason for keeping track of the rainfall was for completeness of the weather record.

Soil and Air Temperature Effects

This experiment was conducted at the University of Illinois Agronomy South Farm at Urbana-Champaign during the summers of 1992 and 1993 to evaluate the response of corn growth and developmental characteristics under different soil and air temperatures during the period from planting to the 5-leaf stage. Air temperature treatments were established by planting the corn on two different dates. Soil temperature at the going point of corn was controlled while the growing point was below the soil surface (planting to 5-leaf stage).

The experiment was set up in a randomized complete block split-plot design. Dates of planting were assigned to main plots and treatments to sub-plots. Individual experimental units

were 2 rows 76 cm apart by 6 m long. Ten plants were randomly selected within each replication and non-destructive measurements taken on the same plants throughout the season.

Agronomic Methods. Pioneer Hybrid 3379, a typical full season hybrid for central Illinois, was planted on 11 May and 4 June 1992, and on 8 May and 7 June 1993. The early planting dates each year were near what is considered to be the optimum date of planting for corn in Illinois, and the late date close to the last recommended date of planting. The month separation between planting dates was selected to ensure a different air temperature treatment, and to facilitate data collection.

Corn was hand planted at a population of 68,325 seed ha^{-1}. After emergence, the plants were thinned to a spacing of one plant every 20 cm. The plots were fertilized each year with 224 kg ha^{-1} nitrogen, 56 kg ha^{-1} phosphorus, and 168 kg ha^{-1} potassium. Weeds were controlled using herbicides, and hand weeding. Because the corn crop was hand planted and preparation of the soil required physical contact between the workers hands and the soil, no root worm treatment was applied to the plots before planting. Root worm control was affected using Lorsban 4E at a rate of 7 liter per hectare (1/ha) after a severe outbreak of root worms was observed in early July in 1992, and immediately after planting in 1993.

During periods when rain was less than potential evapotranspiration, the plots were irrigated to ensure that drought stress did not impact the experiment.

Soil Temperature Control. The soil temperature treatments consisted of maintaining the temperature of the soil surrounding the corn growing point at 5°C above and below ambient temperature. Therefore, the experiment had three treatments: ambient (control); warm (5°C above ambient); and cool (5°C below ambient). The temperature was controlled until the 5-leaf

stage, after which the growing point was assumed to be above the soil surface. Soil temperatures were maintained using a hydronic system. Ambient soil temperatures were monitored and the soil temperature in the treatment plots were maintained at the desired temperature differential. Soil temperature was monitored by thermocouple arrays placed in the ambient and temperature treated rows. A datalogger sampled each sensor array once every ten seconds; calculated separate average values for all ambient, warm and cool arrays; and sent appropriate control signals to the heating and cooling systems.

The heating system consisted of a 208 liter drum with a 4500 watt, 240 volt heating element installed in the lower portion of the tank. Water was circulated by a pump through the tank at a rate of 113 1 m^{-1} through a 2.54 cm ID PVC pipe distribution network and then through 6.1 meter long 1.27 cm ID copper pipes buried next to the planted rows. Water return flow was routed through a second 2.54 cm ID PVC pipe system back to the 208 liter tank. The cooling system consisted of a 208 liter drum and 240 volt 3 phase 63.24 MJ chiller. The water circulation system was identical to that used for the heating system. A separate water loop circulated cold water through the chiller to remove waste heat removed from the circulating water supply. The copper pipe was buried in the planted rows with the bottom of the copper pipe 1 cm above and 1 cm to the side of the corn seed. The top of the copper pipe was 2 cm below the surface of the soil.

A thermocouple was installed every 1.5 meters along the copper pipe on the same side and at a depth of 2.54 cm in the ambient, heated, and cooled planting rows. These 5 thermocouples were connected in parallel to form an array whose output signal represented the average temperature along each copper pipe. The thermocouple arrays were constructed of 30

gauge, type T thermocouple wire with each junction water sealed with a coating of silicone glue and heat shrink tubing. The five junction leads were connected in parallel to a single wire that ran to a multiplexer. The junction of the five thermocouple leads was sealed with silicone glue and heat shrink tubing. The individual thermocouples were installed in the rows adjacent to copper pipe by using a 5 cm length of 0.635 cm diameter rigid plastic tubing to act as a support to hold the thermocouple probe at a distance from the copper pipe equal to the space between the seed and the copper pipe.

The copper pipes in the heated and cooled rows were connected to their respective circulation system. The copper pipes in the ambient rows were not connected to any circulation system. Thus all measured rows had identical physical obstructions to the individual plant's growth. The datalogger, a Campbell Scientific CR10, was connected to two multiplexers that facilitated the sampling of all 48 thermocouple arrays. After the arrays were measured by the datalogger, their values were averaged by cool, ambient, and warm group. The resulting numbers were used to maintain appropriate water temperatures in the respective circulating systems.

Control signals from the data logger were routed to optioisolated relays that controlled all equipment with the system. The two water pumps could be separately turned on and off manually to facilitate maintenance of the system. The heating element was switched under automatic software control by two control lines through two optoisolated relays. The chiller was automatically controlled by the data logger software through a single control line and optoisolated relay. Optical isolation of the chiller and heater was necessary to protect the data logger from power surges during lightning storms.

Data Collection and Analysis. From the time the first seedling leaf was fully emerged

until the fifth leaf was fully emerged, the length and width of the leaves, fully emerged and in the whorl, were measured. Once a leaf was recorded as fully emerged, and its length and width recorded, that leaf was not measured again. After the fifth leaf was fully emerged and the soil temperature treatments stopped, leaf length and width were measured once a week. Leaves in the whorl and those leaves that completed emergence between the weekly observations were measured. The day that each leaf senescenced, either from old age (leaf 8 to the top leaf) or because of stem expansion (lowest 6 to 7 leaves on the plant) was recorded. A leaf was considered senescenced when one-half of its leaf area had turned brown. In 1992, the size of the major and minor axes of the stem internodes, and the internode length were measured. In both 1992 and 1993 the height from the soil surface to the last visible collar was measured.

Leaf area (L_a) was calculated based on the leaf length (L_l), maximum width (L_w), and a correction factor (McKee, 1964) as

$$L_a = 0.75 L_l L_w. \qquad \textbf{(H.12.1)}$$

The whole plant leaf area on each sampling date was computed by summing all the individual leaf areas. Mean leaf areas were calculated for each treatment at each sampling date throughout the season.

Growing Degree Days (GDD) were calculated using the Modified Growing Degree formula (MGDD) (Cross and Zuber, 1972). From planting to the fifth leaf stage, GDD were computed using the soil temperature from each treatment. After the soil temperature treatments were shut off the GDD calculations were based on the air temperature.

The plants that had been repeatedly measured during the growing season were harvested

separately, and the following variables recorded: number of ears per plant, number of kernel rows per ear, average number of kernels in a row, weight of the whole ear, mass of the grain from each ear, the mass of 100 kernels, and plant biomass. In addition, the grain yield of all the plants in each experimental unit was included to determine the overall plot yield.

Rainfall during Different Growth Stages

Two rain shelters (Banwart, 1987, 1988; Changnon and Hollinger, 1988) were used to protect a total of 72, 3 m X 3 m plots from all natural rainfall. The rain shelters were equipped with sprinkler nozzles so water could be applied to the plots when desired. Water application dates were selected based on the climatological distribution of most likely rain dates (Table H.1.2.1). When consecutive rain days occurred in the climatological sequence, water was applied on only one of the days. The first water application was made on the first "rain" day after planting. The total amount of water applied to each plot changed throughout the growing season depending upon the growth stage, and evapo-transpiration since the last watering. Generally there were three to seven days between each water treatment. Water applied to the plots was deionized and ions added to the water to resemble normal rain chemistry in central Dlinois.

A fractional factorial experiment was set up in the two rain shelters. Two levels of water--no water, and water equal to potential evapotranspiration --were applied to each plot during the first three corn growth stages (planting to tassel initiation, tassel initiation to ear initiation, and ear initiation to end of row set). Three water treatments (no water, water equal to 50 percent and 100 percent of potential evapotranspiration were applied during the growth stages of end of row set to silking, silking to end of lag phase, and end of lag phase to maturity. The total number of

combinations of water treatments and growth stages (Table H.1.2.2) was seventy-two. Therefore, there was no replication of treatments in the experiment.

Table H-2. Climatic sequence of rain days and dry days in Champaign-Urbana used to select water application dates for the rain effects in different corn growth stages.

Day of Month	May	June	July	August	September	October
1	Dry	Dry	Dry	Dry	Dry	Dry
2	Rain	Rain	Rain	Rain	Dry	Rain
3	Rain	Dry	Dry	Rain	Rain	Dry
4	Dry	Dry	Dry	Dry	Dry	Dry
5	Dry	Dry	Dry	Dry	Dry	Dry
6	Dry	Rain	Rain	Dry	Dry	Dry
7	Rain	Dry	Rain	Rain	Rain	Dry
8	Dry	Dry	Dry	Dry	Rain	Rain
9	Dry	Rain	Dry	Dry	Dry	Rain
10	Rain	Dry	Dry	Dry	Dry	Dry
11	Rain	Dry	Dry	Dry	Dry	Dry
12	Dry	Dry	Dry	Rain	Dry	Dry
13	Dry	Dry	Rain	Rain	Dry	Dry
14	Dry	Rain	Rain	Dry	Rain	Rain
15	Dry	Rain	Dry	Dry	Dry	Dry
16	Rain	Dry	Dry	Dry	Dry	Dry
17	Dry	Dry	Dry	Dry	Dry	Dry
18	Dry	Dry	Dry	Dry	Dry	Rain
19	Dry	Rain	Rain	Rain	Rain	Rain
20	Rain	Rain	Dry	Dry	Dry	Dry
21	Dry	Dry	Dry	Dry	Dry	Dry
22	Dry	Dry	Dry	Dry	Dry	Rain
23	Rain	Rain	Dry	Dry	Rain	Dry
24	Rain	Dry	Rain	Rain	Dry	Dry
25	Dry	Dry	Dry	Dry	Dry	Dry
26	Dry	Dry	Dry	Dry	Dry	Dry
27	Dry	Rain	Dry	Rain	Dry	Rain
28	Dry	Rain	Dry	Dry	Rain	Dry
29	Rain	Dry	Rain	Dry	Rain	Dry
30	Dry	Dry	Dry	Dry	Dry	Dry
31	Dry		Dry	Dry		Dry

Table H.1.2.2. Description of the seventy-two rainfall treatments applied in the rain shelters. The growth stages are defined as planting to tassel initiation (P-TI), tassel initiation to ear initiation (TI-EI), ear initiation to end of row set (EI-ERS), end of row set to silk (ERS-S), silk to end of lag phase (S-ELP), and end of lag phase to maturity (ELP-M). Water treatments are no water (0), 50 percent (1), and 100 percent of potential evapotranspiration (2).

Treat.	Growth Stage						Treat.	Growth Stage					
No.	P-TI	TI-EI	EI-ERS	ERS-S	S-ELP	ELP-M	No.	P-TI	TI-EI	EI-ERS	ERS-S	S-ELP	ELP-M
1	0	0	0	0	0	0	37	0	1	0	0	2	0
2	0	0	0	2	2	2	38	0	1	0	0	0	2
3	0	0	0	1	2	0	39	0	1	0	0	1	1
4	0	0	0	1	0	2	40	0	1	0	1	1	0
5	0	0	0	0	1	2	41	0	1	0	1	0	1
6	0	0	0	2	1	0	42	0	1	0	1	2	2
7	0	0	0	2	0	1	43	0	1	0	2	0	0
8	0	0	0	0	2	1	44	0	1	0	2	1	2
9	0	0	0	1	1	1	45	0	1	0	2	2	1
10	1	1	1	0	0	0	46	1	0	1	0	2	0
11	1	1	1	0	2	2	47	1	0	1	0	0	2
12	1	1	1	2	2	0	48	1	0	1	0	1	1
13	1	1	1	1	0	2	49	1	0	1	1	1	0
14	1	1	1	1	1	2	50	1	0	1	1	0	1
15	1	1	1	0	1	0	51	1	0	1	1	2	2
16	1	1	1	2	0	1	52	1	0	1	2	0	0
17	1	1	1	2	2	1	53	1	0	1	2	1	2
18	1	1	1	0	1	1	54	1	0	1	2	2	1
19	0	0	1	1	0	1	55	1	0	0	0	2	0
20	0	0	1	0	1	0	56	1	0	0	0	0	2
21	0	0	1	0	2	2	57	1	0	0	0	1	1
22	0	0	1	1	0	0	58	1	0	0	1	1	0
23	0	0	1	1	2	1	59	1	0	0	1	0	1
24	0	0	1	1	1	2	60	1	0	0	1	2	2
25	0	0	1	2	2	0	61	1	0	0	2	0	0
26	0	0	1	2	0	2	62	1	0	0	2	1	2
27	0	0	1	2	1	1	63	1	0	0	2	2	1
28	1	1	0	0	0	1	64	0	1	1	0	2	0
29	1	1	0	0	1	0	65	0	1	1	0	0	2
30	1	1	0	0	2	2	66	0	1	1	0	1	1
31	1	1	0	1	0	0	67	0	1	1	1	1	0
32	1	1	0	1	2	1	68	0	1	1	1	0	1
33	1	1	0	1	1	2	69	0	1	1	1	2	2
34	1	1	0	2	2	0	70	0	1	1	2	0	0
35	1	1	0	2	0	2	71	0	1	1	2	1	2
36	1	1	0	2	1	1	72	0	1	1	2	2	1

The extremes of treatments were one plot with no water applied from planting to maturity, and one plot with water applied at the rate of 100 percent of potential evapotranspiration during each

growth stage. Potential evapotranspiration was computed using the van Bavel version of the Penman evaporation equation (Rosenberg et al., 1983). During the first three growth stages, the ET was adjusted for leaf area by a crop coefficient that ranged from 0.5 to 0.7.

The 72 different rainfall treatment combinations represented a broad range of rainfall during each of the four years over which the experiment was conducted. Each year the treatments within the rain shelters were re-randomized. Because the experiment was repeated over four years, each rainfall treatment was exposed to four different temperature and humidity regimes.

Agronomic Practices. The plots were planted in late May or early June after the rainshelters had been covered with plastic. The corn hybrid, Pioneer 3379, was planted at a density of 84,000 plants ha^{-1} and thinned to 59,280 plants ha^{-1} before tassel initiation (5-leaf stage). Before planting, the plots were fertilized with 225 kilogram per hectare (kg ha^{-1}) of nitrogen (N), 56 kg ha^{-1} of phosphorus (P), and 168 kg ha^{-1} of potassium (K). Weeds were controlled by the application of 2.25 kg-Dual ha^{-1} and 1.12 kg-Atrazine ha^{-1} applied before planting, and through hand weeding during the growing season. Corn root worms were controlled by a single pre-plant application of Force. When the soil was very dry before planting, the plots were irrigated approximately one week before planting to ensure an adequate soil moisture supply in the profile before planting the crop.

Data Collection and Analysis. Crop growth stages were taken before each water application to determine when to change treatments. After the crop had matured and dried down, plants from the center 2.5 meters (m) of the middle two rows of each plot were harvested. Crop variables recorded were total number of plants, number of ears, number of barren plants, total vegetative plant mass, cob mass, number of kernel rows per ear, number of kernels per row, and

kernel mass. Incompletely formed ears that did not have well defined rows were labeled as nubbins, and the total number of kernels on each nubbin recorded.

The experiment was designed so the data could be analyzed using analysis of variance and linear regression. Effects that can be evaluated are the main linear effects of rainfall in the first three growth stages, linear and quadratic effects in the last three growth stages, and simple interactions.

Midwest Corn Growth Stage Rainfall Probabilities

Application of the rain shelter data to the Midwest requires a knowledge of the probabilities of rainfall shortages during the different growth stages. These probabilities were computed by first determining the average day when 50 percent of the corn crop is normally planted in each Crop Reporting District (CRD) in the Midwest--the states of Illinois, Indiana, Iowa, Kansas, Kentucky, Michigan, Minnesota, Missouri, Nebraska, North Dakota, Ohio, South Dakota, and Wisconsin. The dates of planting in each of the CRDs were obtained from State Agricultural Statistical Service (SASS) publications. The beginning and ending dates of each of the six corn growth stages was computed from growing degree unit requirements for corn hybrids normally planted in each CRD, and daily temperature data for each CRD. Typical hybrid growing degree requirements from planting to silking, and from planting to maturity were obtained from Pioneer Hybrid data (Howard Brown, 1996 Personal Communication).

The beginning and ending dates of each corn growth stage was computed for each CRD normal date of planting, dates of planting 30, 20, and 10 days before the normal date, and dates of planting 10, 20, and 30 days after the normal date of planting. The beginning date of each

growth stage was computed using the modified growing degree unit method with the assumption that tassel initiation occurred when 33 percent of the growing degree units (GDU) from planting to silk had accumulated; ear initiation occurred when 44 percent of planting to silk GDU had accumulated; end of row set occurred when 58 percent of the planting to silk GDU had accumulated; silk occurred when 100 percent of the planting to silk GDU had accumulated; the end of lag phase occurred when 125 percent of the planting to silk GDU had accumulated; and maturity occurred when 200 percent of the planting to silk GDU had been accumulated. The mean maximum and minimum air temperature, and the mean total precipitation and potential evapotranspiration were computed for each growth stage for each CRD and each of the seven dates of planting using daily temperature and precipitation data for the 1961 to 1990 climate period for each CRD. The daily temperature, precipitation, and potential evapotranspiration data were obtained from the Midwest Climate Center.

The probability of rainfall totals less than 100, 75, 50, 25, and 10 percent of mean potential evapotranspiration demand was computed by fitting the rainfall totals for each CRD for each planting date to the Weibull distribution. Both the Gamma and Weibull distributions were considered for fitting the rainfall probability distribution. The Weibull was selected because of the ease with which the probability of a given amount of rainfall could be calculated, after the Weibull distribution parameters were obtained. The Gamma distribution parameters are easier to fit than the Weibull, but the computation of the probability for a given rainfall amount must be computed using an interactive procedure and is more labor intensive than the probability from the Weibull distribution. The probability computation from the Weibull is given by

$$F(x) = 1 - \exp\left[-\left(\frac{x}{\beta}\right)^{\alpha}\right] \qquad \textbf{(H.1.2.2)}$$

where β is the scale parameter and α is the shape parameter (Wilks, 1995). The Weibull parameters were computed using an iterative likelihood technique (Wong, 1977). The initial estimates for a and β were obtained using estimators based on the sample mean (Y) and standard deviation (S_y) (Conradsen et al., 1984).

$$\begin{aligned} \alpha^* &= \exp(\bar{Y} + 0.45006 S_y) \\ \beta^* &= 1.28255/S_y \end{aligned} \qquad \textbf{(H.1.2.3)}$$

Maps showing the mean maximum and minimum air temperatures, and the probability of receiving less than 100, 75, 50, 25, and 10 percent of potential evapotranspiration during each growth stage based on the seven different assumed planting dates, were created.

RESULTS

The field experiments resulted in significant yield and yield component responses to both the soil and air temperature during the planting to tassel initiation stage, and to rainfall during the planting to tasseling initiation stage.

Soil and Air Temperature Effects

Analysis of the data is presented as the effects of date of planting, and soil temperature on final yield and canopy size and structure. The canopy structure of interest is the difference between the lower canopy (all leaves from the ear leaf to the base of the stem), and the upper

canopy (all leaves from the first leaf above the ear leaf to the top of the canopy). This structure is defined because Bollero (1994) found that with the cool soil temperature treatments the lower canopy was larger than the lower canopy from the warmer treatments, and conversely, the warmer soil temperature treatments resulted in a larger upper canopy.

The soil temperatures were controlled with a high degree of accuracy during the first planting period in both experimental years, but less accurately during the second planting. Final yield and the yield components were all affected by the soil temperature treatments during both planting dates of both years.

Growing Season Weather

The weather conditions during the periods from planting to 5-leaf stage, 5-leaf stage to tasseling, and tasseling to harvest is shown in Table H.1.3.1 for the 1992 summer and Table H.1.3.2 for the 1993 summer. Solar radiation, potential evaporation, and air and soil degree days are summed over the periods. The other weather variables are the means for the different growth periods. For the first growth period (planting to 5-leaf stage), averages and totals were computed for the entire first stage except for solar radiation which was summed from emergence to the 5-leaf stage. Soil temperature was reported for the first growth stage only. Precipitation was not included because the plots were kept well watered throughout the growing season by irrigation. The three soil temperature treatments were all planted on the same day for each date of planting. However, the weather experienced by the three treatments during their different growth stages was not the same because of the different lengths of time, in days, required to complete each growth stage.

Although there were fewer soil temperature growing degree days accumulated in the cooler soil temperature treatments, the cooler soil temperatures resulted in more days required to reach the 5-leaf stage. Therefore the total solar radiation received during the period from emergence to the 5-leaf stage was greater under the cooler soil temperatures. During the period from tasseling to maturity the total solar radiation received at the surface by the warm soil temperature treated plants was greater than for the cool treated plants.

During the planting to 5-leaf stage, air temperature experienced by the warm treatment averaged 1°C less than in the cool soil temperature treatment of the first planting date, but only 0.3°C less in the second planting date in 1992 and only 0.1°C in 1993. Between planting dates, the second planting date was 2.6°C warmer than the first planting date in 1992 and 5.7°C warmer in 1993. The mean soil temperatures during the second date of planting was greater than during the first date of planting in both years (Tables H.1.3.1, & H.l.3.2).

Accuracy of Soil Temperature Treatments

The procedure used to maintain the soil temperature treatments did not require complex modeling of the soil heat capacity or conductivity, because the actual soil temperatures were being monitored and the temperature continuously modified. Time lags existed in the system, therefore, a constant 5°C temperature difference from ambient was not expected. Temperature control was most effective during the treatment period of the first date of planting in both years (Figure H.l.3.1). The large deviations of temperature control during the first dates of planting were due to equipment failures. During the 1993 season the coolers used to maintain the cool temperature treatment began to fail because of the age of the equipment. Generally, the

Table H.1.3.1. Mean wind speed, air temperature, relative humidity, dew point temperature, barometric pressure, maximum air temperature, minimum temperature, soil temperature, total solar radiation, air temperature growing degree days, soil temperature growing degree days, and potential evapotranspiration during the period from planting to the 5-leaf stage, 5-leaf stage to tasseling, and tasseling to maturity for the summer of 1992.

Date of Plant	Soil Temp. Treat.	Wind Speed (m/s)	Solar Rad. (MJ/m^2)	Max. Air Temp. (°C)	Min. Air Temp. (°C)	Mean Air Temp. (°C)	Rel. Hum. (%)	Dew Point Temp. (°C)	Potential Evap. (mm)	Baro-metric Press. (mb)	Soil Temp. (°C)	Air Deg. Days (°C)	Soil Deg. Days (°C)
						Planting to 5-Leaf Stage							
May	Cool	1.71	534.4	24.7	13.7	19.3	70.7	12.8	162.3	990.7	15.3	327.6	220.4
11	Amb	1.73	450.7	23.8	12.7	18.3	70.0	12.0	143.0	991.1	20.1	272.9	304.9
	Warm	1.76	345.8	23.5	12.6	18.0	72.1	12.1	119.4	991.2	24.0	226.9	369.6
	Cool	1.76	529.0	26.5	15.3	21.1	67.7	14.2	158.5	986.5	17.0	334.0	225.5
June 4	Amb	1.71	466.8	26.3	14.9	20.9	66.1	13.7	144.5	986.7	21.9	295.7	315.1
	Warm	1.78	414.9	26.1	15.1	20.8	66.5	13.6	132.6	986.8	27.2	270.1	394.5
						5-Leaf Stage to Tasseling							
May	Cool	1.77	940.4	26.0	16.4	21.3	79.5	17.1	208.0	987.8		518.5	
11	Amb	1.76	952.1	26.4	16.6	21.6	78.2	17.1	211.6	987.6		534.6	
	Warm	1.73	986.7	26.6	16.4	21.6	75.2	16.4	219.5	987.7		531.8	
	Cool	1.71	809.8	26.0	17.2	21.6	86.0	18.9	179.3	989.9		487.0	
June 4	Amb	1.71	813.1	26.4	17.5	21.9	86.4	19.3	180.9	989.2		500.3	
	Warm	1.65	791.2	26.3	17.2	21.7	85.8	19.0	175.8	988.9		480.8	
						Tasseling to Maturity							
May	Cool	2.08	1,593.4	22.5	11.7	17.1	76.7	12.4	337.1	992.4		682.2	
11	Amb	2.07	1,665.4	22.6	11.8	17.2	77.3	12.6	352.6	992.3		720.8	
	Warm	2.05	1,735.7	22.7	12.1	17.4	77.8	12.9	372.6	992.1		769.6	
	Cool	2.13	1,308.6	22.0	10.9	16.4	75.7	11.5	299.5	992.4		535.6	
June 4	Amb	2.13	1,367.5	22.0	11.0	16.4	75.7	11.6	286.5	992.5		560.6	
	Warm	2.13	1,441.3	22.3	11.3	16.8	75.8	11.9	303.8	992.4		605.7	

Table H.1.3.2. Mean wind speed, air temperature, relative humidity, dew point temperature, barometric pressure, maximum air temperature, minimum temperature, soil temperature, total solar radiation, air temperature growing degree days, soil temperature growing degree days, and potential evapotranspiration during the period from planting to the 5-leaf stage, 5-leaf stage to tasseling, and tasseling to maturity for the summer of 1993.

Date of Plant	Soil Temp. Treat.	Wind Speed (m/s)	Solar Rad. (MJ/m^2)	Max. Air Temp. (°C)	Min. Air Temp. (°C)	Mean Air Temp. (°C)	Rel. Hum. (%)	Dew Point Temp. (°C)	Potential Evap. (mm)	Baro-metric Press. (mb)	Soil Temp. (°C)	Air Deg. Days (°C)	Soil Deg. Days (°C)
						Planting to 5-Leaf Stage							
May 8	Cool	2.55	480.9	24.0	11.5	18.0	66.6	10.7	180.3	988.0	15.4	319.8	245.8
	Amb	2.58	467.0	23.8	11.2	17.8	67.1	10.6	166.9	987.8	19.3	294.7	354.1
	Warm	2.71	404.9	22.9	10.0	16.8	65.2	9.2	139.9	987.7	23.4	218.6	414.3
June 7	Cool	2.10	407.8	28.9	17.8	23.3	75.8	18.0	145.0	988.6	20.0	370.6	175.5
	Amb	2.17	385.5	28.9	17.6	23.2	74.1	17.5	125.3	989.1	24.0	315.5	327.5
	Warm	2.15	364.3	28.9	17.5	23.2	73.3	17.4	114.5	989.3	28.0	289.2	249.5
						5-Leaf Stage to Tasseling							
May 8	Cool	1.92	910.5	28.9	19.1	23.8	82.0	20.0	208.4	989.0		578.1	
	Amb	1.97	878.6	28.7	18.9	23.7	80.2	19.3	200.4	989.2		546.0	
	Warm	1.99	956.1	28.9	18.8	23.7	79.6	19.3	218.8	988.9		587.2	
June 7	Cool	1.57	830.1	28.4	17.8	23.0	84.4	19.6	187.3	990.1		506.7	
	Amb	1.65	850.7	28.5	18.2	23.2	84.6	19.7	192.4	989.5		513.1	
	Warm	1.74	832.8	28.8	18.7	23.6	84.7	20.1	189.0	989.1		514.2	
						Tasseling to Maturity							
May 8	Cool	1.44	1,162.3	25.9	14.5	20.2	84.0	16.9	254.7	990.6		664.5	
	Amb	1.44	1,253.7	26.2	14.8	20.4	84.3	17.3	276.1	990.5		721.7	
	Warm	1.44	1,293.5	26.2	15.0	20.5	84.1	17.3	284.7	990.5		756.6	
June 7	Cool	1.48	804.1	25.3	14.4	19.7	84.6	16.8	175.3	990.5		478.5	
	Amb	1.44	868.9	25.5	14.5	19.9	84.6	17.1	189.8	990.5		527.2	
	Warm	1.41	935.2	25.5	14.3	19.8	84.5	16.9	204.1	990.7		552.4	

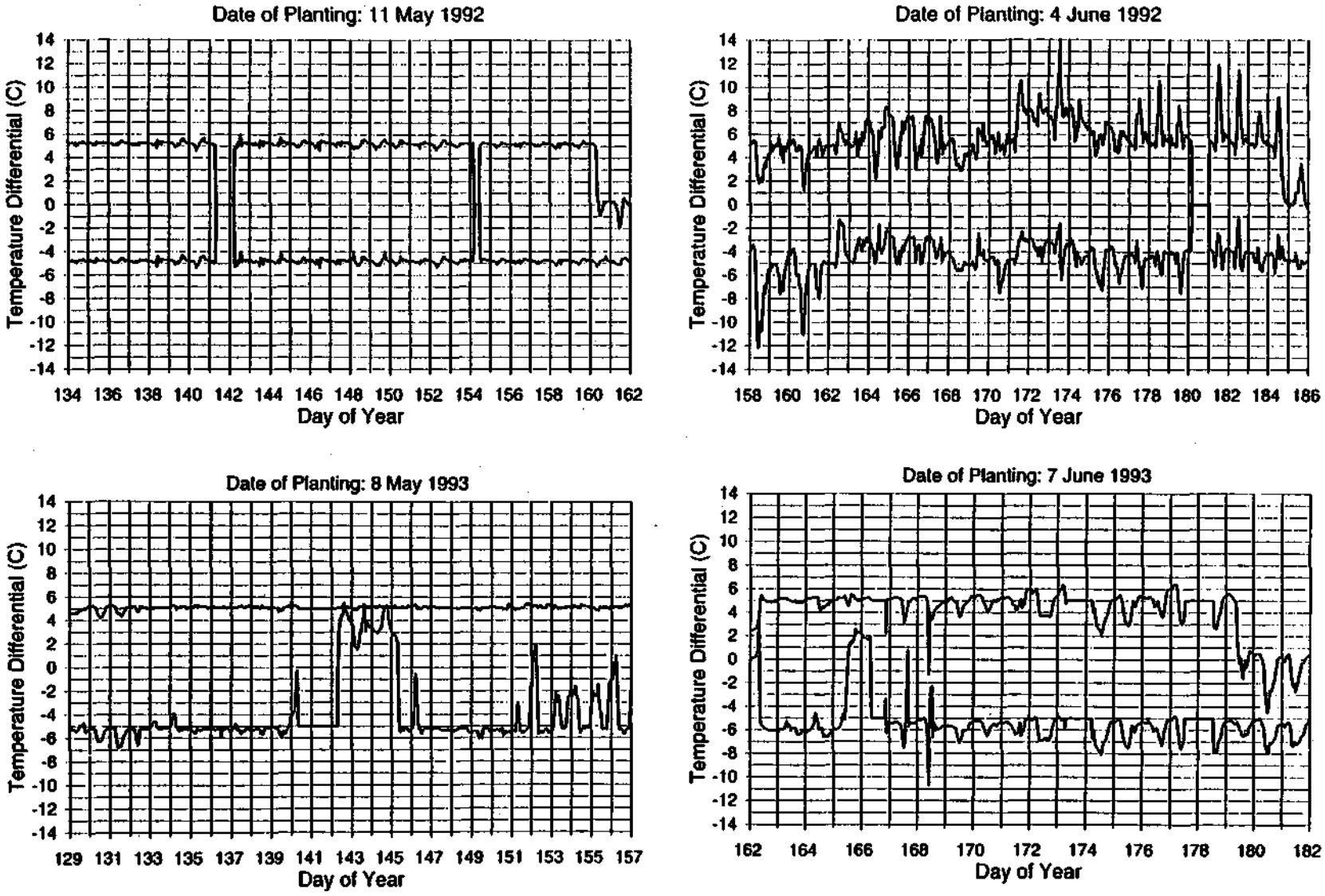

Figure H.1.3.1. Accuracy of temperature control during each of the planting date treatments. The goal was to control the cool temperature treatment 5°C below ambient (represented by the 0°C line), and the warm temperature treatment at 5°C above ambient.

temperature differentials were maintained in the correct direction. The large variation in the temperature control during the second planting date of each year requires the data to be analyzed as a function of the observed soil temperature.

Yield and Yield Components

The corn yields and the yield components that make up the corn yield responded to the date of planting and soil temperature treatments (Table H.1.3.3). Yields were largest with the warm soil temperature treatment, the first date of planting, and in 1992. Mean yields in 1992 (8.1 15 Mg ha^{-1}) were greater than in 1993 (7.632 Mg ha^{-1}), and mean yields over years for each date of planting were greater for the early date of planting (9.122 Mg ha^{-1}) than for the later date of planting (6.625 Mg ha^{-1}). The yield components which contributed most to these yield differences were the number of kernels per row and kernel mass. There were more kernels per row in the ears from the plots with warm soil treatments and date of planting. The mean leaf area in each of the treatment-planting in the early plantings. Kernel mass tended to be greater in the cool soil treatments, but was greater in the early date of planting compared to the later date of planting each year.

Neither the date of planting nor the soil temperature treatments affected total vegetative mass as evidenced by a lack of significant differences or trends in the total vegetative mass data. However, the distribution of the leaf area within the canopy was affected by both soil temperature treatments date combinations tended to show larger leaf areas in the top of the canopy (Table H.1.3.3) in the warm soil temperature treatments. Conversely, the lower canopy leaf area was larger in the cool soil temperature treatments.

Table H-3. Corn yield and yield component by date of planting and soil temperature treatment.

Yield Component	Year	Date of Planting	Treatment Cool	Ambient	Warm	Date of Planting Mean
Final Yield (kg/ha)	1992	11 May	8.821	9.338	9.882	9.347
		4 June	5.344	7.896	7.405	6.882
	1993	8 May	8.245	9.113	8.896	8.751
		7 June	5.678	6.322	7.104	6.368
Treatment Mean			7.022	8.167	8.322	7.837
Numberof Rows/ear	1992	11 May	15.18	15.20	15.05	15.14
		4 June	13.00	14.13	14.50	14.42
	1993	8 May	14.88	15.10	14.40	14.79
		7 June	15.74	14.82	15.00	15.19
Treatment Mean			14.70	14.81	14.74	14.89
Numberof kernels/row	1992	11 May	35.00	35.83	38.20	36.34
		4 June	29.05	33.28	35.53	32.55
	1993	8 May	35.18	36.65	39.08	36.97
		7 June	33.72	33.26	38.70	35.22
Treatment Mean			33.24	34.76	37.88	35.27
Kernel Mass (g/kernel)	1992	11 May	0.349	0.346	0.340	0.345
		4 June	0.343	0.311	0.315	0.323
	1993	8 May	0.302	0.311	0.321	0.311
		7 June	0.268	0.243	0.249	0.253
Treatment Mean			0.316	0.303	0.306	0.308
Leaf Area Index Top 7 leaves of the Canopy	1992	11 May	1.84	1.65	1.55	1.68
		4 June	1.66	1.90	1.82	1.79
	1993	8 May	2.09	2.00	2.33	2.14
		7 June	2.23	2.13	2.17	2.18
Treatment Mean			1.96	1.92	1.97	1.95
Leaf Area Index Total Canopy	1992	11 May	4.91	4.63	4.25	4.60
		4 June	4.61	4.79	4.67	4.69
	1993	8 May	5.05	4.97	5.05	5.02
		7 June	4.82	4.62	4.69	4.71
Treatment Mean			4.85	4.75	4.67	4.76

Final yield is a function of the size of the grain sink, and how much carbon is fixed during grain fill. With most modern corn hybrids there is generally one ear produced per plant, approximately at the middle of the stem height. With our hybrid, the ear was generally 8 leaves

below the tassel. The leaf subtending the ear or the leaf immediately below the ear is generally the largest leaf on the plant. Above and below the largest leaf, the individual leaves decrease in size. As leaves fix carbon, the sugars formed are either stored in the leaves, or transported to other plant organs. The top ear is the largest sink on the plant during its development and during grain fill. Therefore, sugars transported from the leaves above the ear tend to feed the ear (Allison and Watson, 1966), while leaves beginning at the ear leaf and below, transport sugars to the roots, and to a lesser extent, up to the ear. How much carbon is fixed by the canopy during the growing season is a function of the leaf area and solar radiation received at the earth's surface.

An estimate of the photosynthetic potential during the life of the plant can be determined by estimating the quantity of solar radiation intercepted during the life of plant. Because we periodically measured leaf size and senescence during the growing season, we can estimate the total solar radiation intercepted (I) by the plant using

$$I = I_0 - I_0 e^{-kL} \qquad \textbf{(H.1.3.1)}$$

where I_0, is the radiation at either the top of the canopy or the top of the canopy layer of interest, k is an extension coefficient assumed to be 0.72 (Monteith, 1969), and L is the leaf area index of the full canopy or the portion of the canopy layer of interest. In our case we computed the intercepted solar radiation for both the upper canopy, and the total canopy (Table H.1.3.4). In our computation, solar radiation intercepted by the top seven leaves of the canopy was initiated when the leaves began to appear in the whorl of the rapidly growing corn plant.

Table H-4. Total solar radiation (MJ m^{-2}) intercepted by the upper canopy (top seven leaves) and the total canopy throughout the life of the crop by soil temperature treatment, date of planting and year.

	Date	Soil Temperature Treatment					
	of	Upper Canopy			Full Canopy		
Year	Planting	Cool	Ambient	Warm	Cool	Ambient	Warm
92	1	1,248	1,179	1,219	2,021	2,026	2,047
	2	1,053	1,178	1,161	1,729	1,787	1,779
93	1	1,051	1,051	1,187	1,639	1,683	1,744
	2	1,046	1,068	1,096	1,504	1,533	1,560
Treatment Mean		1,100	1,119	1,166	1,723	1,757	1,783

The mean total solar radiation intercepted by the upper part of the canopy over the two planting dates in 1992 was 1,173 Megajoules per square meter (MJ m^{-2}), while in 1993 it was only 1,083 MJ m^{-2}. The mean total solar radiation intercepted by the total canopy throughout the growing season was 1,899 MJ m^{-2} in 1992 and only 1,611 MJ m^{-2} in 1993. Averaged across two years for the two planting dates, the total solar radiation intercepted by the early planted crops totaled 1,156 MJ m^{-2} in the upper canopy, and 1,860 MJ m^{-2} for the total canopy. For the late planting date, the total radiation intercepted by the upper canopy was 1,101 MJ m^{-2}, and by the total canopy 1,649 MJ m^{-2}. The intercepted radiation rankings agree with the rankings of observed yields (1992 > 1993, and early planting > late planting), but are the reverse of the observed 1992 and 1993 total leaf areas.

The lower yields tended to be associated with larger full canopy leaf areas (Table H.1.3.3). In 1993 the mean total canopy leaf areas for the two planting dates was 4.87 m^2m^{-2} and in 1992 the mean canopy leaf area was 4.65 m^2m^{-2}. In 1992 the canopy of the late planted crop was larger than the canopy of the early planted crop. In 1993, the opposite was true.

Because the leaf areas in 1993 are greater than 1992, one would expect more radiation to be intercepted in 1993. The reason they differ is in the duration of the crop growing season. In 1992, the duration from planting to the death of the last leaf was 162 days for the early planting, and 137 days for the late planting. In 1993, the durations were 129 days for the early planting, and 114 days for the late planting. The rankings of radiation intercepted agree with the yield rankings because of the interaction of leaf area and leaf area duration.

The early growth cool soil temperature treatments resulted in a larger canopy from the ear leaf to the base of the stem (lower part of the canopy). The lower canopy leaf area for the four planting dates averaged 2.89 m^2m^{-2} for the cool treatment, while the leaf area from the warm treatments averaged 2.67, and 2.83 for the ambient. The leaf area of the upper canopy did not show any consistent effects (Table H. 1.3.3) among the three soil temperature treatments.

Our hypothesis was that warmer soil temperatures would result in lower corn yields. The mean yield rank for the soil temperature treatments were cool < ambient < warm (Table H.1.3.3). Therefore, the hypothesis must be rejected, and the alternative hypothesis accepted that cooler soil temperature from planting to tassel initiation reduce yields. This conclusion is consistent with the results of Fortin and Pierce (1990) and Fortin et al. (1994).

Air Temperature Effect. Temperatures experienced by the crop during the period from planting to the 5-leaf stage varied by soil temperature treatment, date of planting, and year (Tables H.1.3.1 & H.1.3.2). The mean maximum air temperature for the two 1992 planting dates for the early growth stage was 25.2°C, and in 1993 was 26.2°C. The corresponding minimum temperatures were 14.1 °C for 1992, 14.3°C for 1993. The mean maximum air temperature averaged across years for the early panting dates was 12.0°C, and 16.4°C for the late planting

date. The average temperature for the entire crop growth period in 1992 was 19.2°C, and in 1993 was 22.1°C. In both years the average temperature for the entire growing season was cooler for the early planting date than for the late planting date.

To explore the relationship between the individual soil temperature and date of planting treatments for both years, a regression analysis was conducted using maximum and minimum air temperatures, and mean soil temperature during the period from planting to tassel initiation, intercepted radiation in the upper canopy, total intercepted radiation, and the ratio of the upper canopy intercepted radiation to the product of the maximum and minimum air temperature (Table H.1.3.5). The linear regressions show the high negative correlation between air temperature during the early growth stage and yield. The fact that there is a low correlation between soil temperature treatments and yield, indicates that the effect of soil temperature at the growing point of corn does not appear to be the controlling factor in the effects of soil temperature on final yield. An indirect effect of early season soil temperature on corn yield, is the delay in growth and development of the seedling. Bollero (1994) showed that the cool soil temperature treatment extended the period from planting to 5-leaf stage by 8 to 10 days in the early planting and 6 days in the late planting. This delay was enough to cause the aerial parts of the corn plant to experience a different air temperature during this initial growth period, with the plants grown under the cool soil temperature treatment experiencing warmer air temperature.

These data confirm the observation of Hollinger and Changnon (1993), that cooler temperatures from planting to tassel initiation (5-leaf stage) result in larger yields. It is not possible with the data collected here to determine the actual causal mechanism.

Table H.13.5. Linear regression coefficients and r^2 of yield vs. different weather variables. Air and soil temperatures are for the period from planting to 5-leaf stage. Intercepted radiation is for the entire growing season.

Variable	β_0	β	r^2
Maximum Air Temperature	22.718	-0.578	0.733
Minimum Air Temperature	14.394	-0.461	0.648
Soil Temperature	8.084	-0.000762	0.001
Intercepted Radiation			
Upper Canopy	-6.990	0.0132	0.420
Total Canopy	-1.703	0.00546	0.472
Upper Canopy Intercepted Radiation and Temperature ratio	-0.140	3.617	0.793

Growth and Development

As expected, corn development was delayed by the cool soil temperature treatments and sped up by the warm soil temperature treatments (Figure H.1.3.3). Corn leaf area development was delayed as much as 10 days by the cool soil temperature treatment compared to the warm soil temperature treatment. This development delay was maintained even after the soil temperature treatments were terminated.

Even though the warm soil temperature treated canopies developed faster than the cool soil temperature treated canopies, the warm treated canopies required more growing degree units to arrive at the same development stage as the cool treated canopies. This difference in the required growing degree unit accumulation to arrive at the same growth stage indicates a weakness in the growing degree unit concept for crop development. Attempts to remove this difference in growing degree requirements by modifying the base temperature used in the growing degree unit computation were unsuccessful.

Effects of Temperature on Leaf Area

Bollero (1994) described the effect of soil temperature, air temperature, and solar radiation on the development of the corn canopy leaf area (L) of the individual soil temperature and date of planting treatment combinations. He fit the Richard's function

$$L = A\ (1 \pm e^{(b-kt)})^{-\frac{1}{n}} \qquad \textbf{(H.1.3.2)}$$

to the leaf area (L) using accumulated growing degree days as the time factor (t). The four Richard's function coefficients can be interpreted to have biological meaning. A, the asymptote of the function, defines the maximum leaf area of the canopy, b relates the start of leaf area development to t, k represents the growth rate of the leaf area, and n defines the point at which the rate of leaf area increase begins to decrease. The four coefficients of the Richard's function obtained for each of the different treatments were then related to air temperature during different growth stages, the soil temperature treatments, and solar radiation from planting to tasseling. In the step-wise multiple regression procedure used, soil temperature at the growing point was included in all the models of the four coefficients. The coefficient "A" was related to the minimum air temperature from the 5-leaf stage to tasseling (T_{mn2}) and the average air temperature from the 5-leaf stage to tasseling (T_{a2}) in addition to the soil temperature at the growing point (T_{s1}). The relationship between A and these weather variables had an R^2 of 0.80. Coefficients b and n were related to the average air temperature from planting to tasseling (T_{al2}), and T_{s1}; while coefficient k was related to the intensity of solar radiation from planting to tassel initiation (S_1), from tassel initiation to tassel emergence (S_2), and from planting to tassel emergence (S_{12})

expressed as Megajoules per day (MJ d^{-1}), and T_{s1}. The R^2 for the b coefficient model was 0.95, for the k coefficient model 0.88, and for the n coefficient model 0.91. The four regression equations with their coefficients are (Bollero, 1994):

The coefficients of eq. H.1.3.3 were computed using all the temperature and solar radiation data and the Richard's coefficients fit to the leaf area data from each date of planting and soil temperature treatment. Therefore the coefficients in eq. H.1.3.3 are the mean of the 4 date of planting and soil temperature treatments. The leaf area of each date of planting and soil temperature treatment is modeled by first computing the four Richard's coefficients from the appropriate temperature and radiation data, then solving the Richard's equation (eq. H.1.3.2)

$$\begin{aligned} A &= 175.80 - 0.0227T_{s1} + 13.118T_{mn2} - 0.360T_{mn2}^2 - 25.430T_{a2} + 0.558T_{a2}^2 \\ b &= 22.926 + 0.557T_{s1} - 1.269T_{a12} \\ k &= 0.0332 + 0.00049T_{s1} + 0.00451S_{12} - 0.00240S_1 - 0.00348S_2 \\ n &= 19.063 + 0.0687T_{s1} - 2.640T_{a12} + 0.342T_{a12}^2 \end{aligned} \qquad \textbf{(H.1.3.3)}$$

using the observed growing degree days accumulated in the experiment. The model shows the correct general relationship of leaf area development as a function of growing degree days (Figure H.1.3.2). The model tends to be more accurate in predicting the cool soil temperature treated canopies in the early date of planting. In all treatments, the maximum leaf area is over predicted by the model. Figure H.1.3.3 demonstrates that the warm soil temperature treated canopies developed earlier and faster than the cooler soil temperature treated canopies. Figure H.1.3.3 also shows that the model predicts canopy development faster and predicts a larger canopy than observed. Before the model can be used in actual practice, algorithms that do a better job of predicting the value of A and k of the Richard's equation need to be developed.

The Richards equation model does show that, in a well watered canopy, the rate of leaf area development and final size of the canopy are dependent upon the soil and air temperature environment and solar radiation.

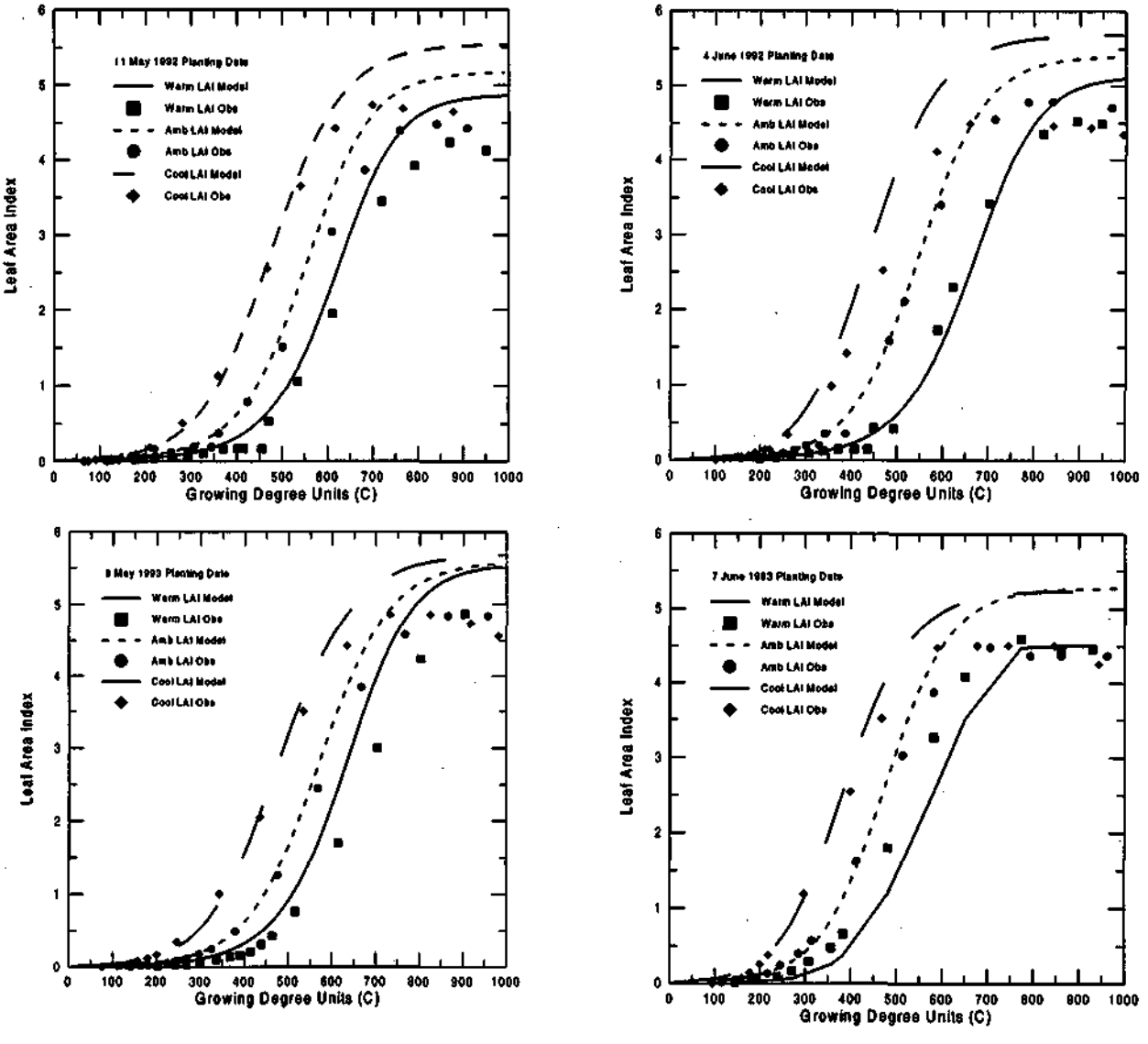

Figure H.1.3.2. Leaf area development as simulated with the Richard's equation using observed growing degree days as the "time" variable.

Rainfall during Different Growth Stages

The total water applied to the single rain shelter plot that was well watered all season (Treatment 11) ranged from 461.3 mm in 1995 to 531.9 mm in 1994 (Table H.1.3.6). Total potential evapotranspiration for the season was reduced in 1995 because the crop was planted late (June 6) and the summer was very moist with higher than normal dew point temperatures. The summer of 1994 was the driest of the four summers.

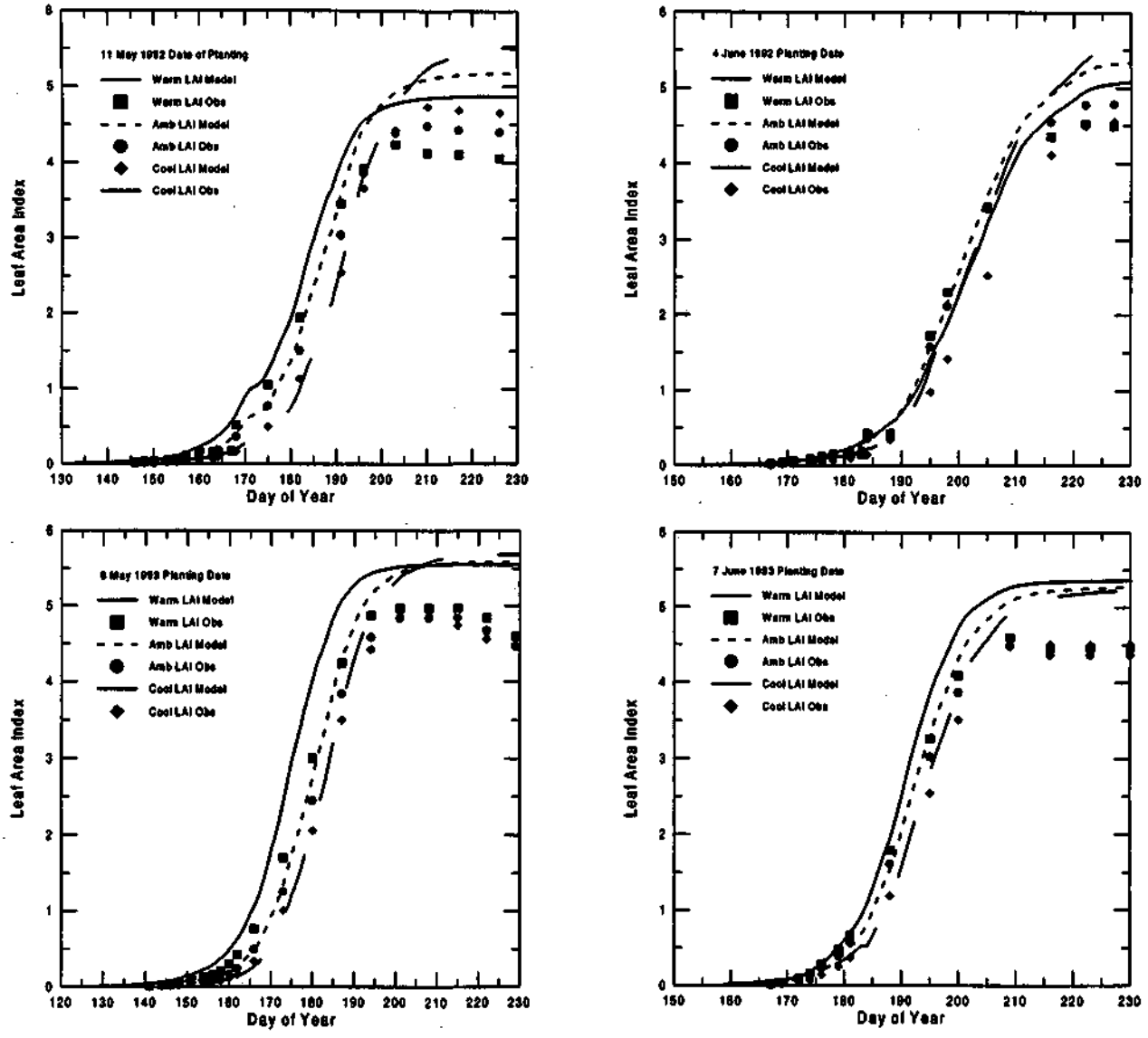

Figure H.1.3.3. Leaf area development as simulated with the Richard's equation using observed growing degree days as the "time" variable, but plotted as a function of the day of year.

The two growth stages that received the greatest amount of water were the end of row set to silk and end of lag phase to maturity stages. These two growth stages are the longest growth stages in the corn growth cycle (Table H.1.1.1). The shortest growth stage is the period from tassel initiation to ear initiation and was the growth stage that received the least water each summer. Treatment 1 received no water during the summers of 1992, 1994 and 1995. The water received during the summer of 1993 was applied to help the crop germinate. This was necessary because the plots were tilled with a rototiller a week before planting and the surface layer dried out too much for adequate germination and stand establishment. The deeper soil layers were fully recharged so that once the roots of the seedlings were established they were able to obtain adequate water to maintain growth.

Table H.1.3.6. Maximum water (mm) applied during each growth stage during the four summers of the Rainshelters experiment. Water applied during the stages of planting to tassel initiation, tassel initiation to ear initiation, and ear initiation to end of row set were reduced from potential evaporation by 0.5, 0.5 and 0.7 respectively. This reduction was to account for leaf area index less than 1.0.

	Year				
Growth Stage	1992	1993	1994	1995	Mean
Planting to Tassel Initiation	56.6	98.0	63.0	46.0	65.9
Tassel Initiation to Ear Initiation	15.0	24.6	14.0	22.4	19.0
Ear Initiation to End of Row Set	32.3	26.9	50.0	46.7	39.0
End of Row Set to Silk	109.2	106.7	95.5	92.7	101.0
Silk to End of Lag Phase	56.1	49.3	86.9	65.8	64.5
End of Lag Phase to Maturity	217.9	226.3	247.4	187.7	219.8
Total for Growing Season	487.5	531.9	556.8	461.3	509.4

The mean yield of all the treatments ranged from 6.537 Mg ha^{-1} in 1995 to 9.508 Mg ha^{-1} in 1992. Mean yields by treatment (Table H.1.3.8) in each of the four summers ranged from 1.911 Mg ha^{-1} (30 bu ac^{-1}) in 1994, to 11.876 Mg ha^{-1} (189 bu ac^{-1}) in 1992. The lowest single

plot yield was in the plot treated with no water during the 1994 growing season, while the highest yield was in treatment 13 which was watered with 100 percent of ET through the end of row set, 50 percent of ET from the end of row set to silk, and 100 percent of ET from end of lag phase to maturity in 1992. The lowest yield of the mean treatments for the four years was in the no water treatment (5.761 Mg ha^{-1} - 92 bu ac^{-1}), and the highest yield was in treatment 51, 100 percent ET from planting to tassel initiation, ear initiation to end of row set, silk to maturity, and 50 percent ET from end of row set to silk, (10.061 Mg ha^{-1} -- 160 bu ac^{-1}).

The growth stage with the greatest yield response was the period from planting to tassel initiation (Table H.1.3.9). Over the four years of the experiment yields were increased by 12 percent (increase from 8.107 Mg ha^{-1} or 129 bu ac^{-1} to 9.106 Mg ha^{-1} or 144.8 bu ac^{-1}) when water equal to 100 percent of potential evapotranspiration was applied compared to no water applied during that growth stage. This difference was significant at the 5 percent level. The only other growth stage to show a significant yield response to the water treatments was the period from end of row set to silk, where yields were increased by at least 10 percent (increase from 8.060 Mg ha^{-1} or 128 bu ac^{-1} to 8.872 Mg ha^{-1} orl41 bu ac^{-1}) by applications of water equal to 50 or 100 percent of potential evapotranspiration. The next largest response to water equal to 100 percent of potential evapotranspiration was during the period from end of lag phase to maturity, an increase from 8.347 Mg ha^{-1} (133 bu ac^{-1}) to 8.856 Mg ha^{-1} (141 bu ac^{-1}), however this increase was not statistically significant at the 5 percent level.

The yield means for the different growth stage water treatments include all 72 treatments each year. For example, the yield mean for the no water treatment during the period from planting to tassel initiation includes 36 plot yields each year, and the 100 percent potential

evapotranspiration water treatment for the same period includes 36 plot yields. The total number of plot yields included in the 4 year mean for the same treatments and growth period are 144. For the four growing seasons, the mean season total water applied on the no water treatment for the planting to tassel initiation growth stage was 228 mm with a range from 0 to 454 mm (Table H.1.3.10). For the 100 percent potential evapotranspiration during the same growth stage, the mean season total water applied was 286.4 mm with a range of 101 to 557 mm. The growth stage with the greatest difference between the no water treatment and 100 percent potential evapotranspiration water treatment was the end of lag phase to maturity period. If yields were most sensitive to rainfall during that period, the mean yield differences between the 0 and 100 percent potential evapotranspiration water treatments should be significantly different. This was not the case.

Based on Tables H.1.3.9 and H.1.3.10, a mm of rainfall during the planting to tassel initiation period would result in a yield increase of 17 kg ha^{-1} (6.9 bu ac^{-1} per inch of rain), as long as the total rainfall was less than or equal to potential evapotranspiration. The yield increase for the tassel initiation to ear initiation stage would be 15 kg ha^{-1} (6.2 bu ac^{-1} per inch of rain); for ear initiation to end of row set the yield increase would be 8 kg ha^{-1} (3.2 bu ac^{-1} per inch); for end of row set to silk, 8 kg ha^{-1} (3.2 bu ac^{-1} per inch); for silk to end of lag phase, 1 kg ha^{-1} (0.6 bu ac^{-1} per inch); and for end of lag phase to maturity, 2 kg ha^{-1} (0.8 bu ac^{-1} per inch). These yield increases also assume that the soil profile is fully recharged at planting. If the soil profile is not fully recharged at planting, then a greater response to rainfall would be expected during the different growth stages.

Table H.1.3.7. Total water (mm) applied to the 72 different treatments in the rain shelters in each of the 4 summers of the experiment.

Treat.	Year					Treat.	Year				
No.	1992	1993	1994	1995	Mean	No.	1992	1993	1994	1995	Mean
1	0.0	45.2	0.0	0.0	11.4	37	71.1	80.1	100.8	88.1	85.1
2	383.3	388.6	429.8	346.2	387.1	38	232.9	296.0	261.4	210.1	250.1
3	110.7	147.8	134.6	112.3	126.2	39	152.0	207.5	181.1	149.1	172.4
4	272.5	324.9	295.1	234.2	281.7	40	97.7	108.8	105.2	101.6	103.3
5	246.1	257.3	290.8	220.7	253.7	41	178.6	197.4	185.4	162.6	181.0
6	137.3	176.5	138.9	125.6	144.6	42	343.7	398.7	396.0	322.2	365.1
7	218.2	265.1	219.2	186.6	222.3	43	124.2	137.5	109.5	115.1	121.6
8	165.1	168.8	210.6	159.6	176.0	44	370.2	427.4	400.3	335.7	383.4
9	191.6	236.4	214.9	173.1	204.0	45	289.3	338.8	320.0	274.7	305.7
10	116.5	110.7	127.0	115.1	117.3	46	157.6	174.3	199.9	158.5	172.6
11	499.8	492.9	556.7	461.3	502.7	47	319.4	351.3	360.4	280.4	327.9
12	227.2	213.3	261.6	227.2	232.3	48	238.5	224.0	281.1	219.5	240.5
13	389.0	390.3	422.1	349.1	387.7	49	184.2	164.1	240.2	172.0	181.1
14	362.5	400.5	417.8	335.7	379.1	50	265.1	252.7	284.5	232.9	258.8
15	253.8	280.9	265.9	240.7	260.3	51	430.2	415.1	495.0	392.6	433.2
16	334.7	369.4	346.2	301.6	338.0	52	210.7	231.7	208.5	185.4	209.1
17	281.6	273.1	337.5	274.7	291.7	53	456.7	113.8	499.3	406.0	451.5
18	308.1	340.7	341.7	288.7	319.7	54	375.8	394.1	419.1	345.1	383.5
19	141.2	185.3	173.8	140.6	160.2	55	125.5	147.3	149.7	111.8	133.6
20	60.3	58.0	93.6	79.6	72.9	56	287.3	285.5	310.3	233.7	279.2
21	306.3	308.9	384.4	300.2	325.0	57	206.4	235.8	230	172.7	211.2
22	86.8	125.5	97.9	93.1	100.8	58	152.0	176.0	154.1	125.2	151.8
23	251.9	249.1	308.5	252.7	265.5	59	232.9	264.5	234.3	186.2	229.5
24	332.8	337.6	388.7	313.7	343.2	60	398.0	427.0	444.9	345.8	403.9
25	197.5	189.3	232.5	205.2	206.1	61	178.6	204.7	158.4	138.7	170.1
26	359.3	366.3	393.0	327.2	361.5	62	424.6	416.8	449.2	359.3	412.5
27	278.4	277.8	312.8	266.2	283.8	63	343.7	328.3	368.9	298.3	334.8
28	193.3	235.7	200.5	162.2	197.9	64	103.3	146.0	151.0	134.9	133.8
29	112.4	108.3	120.3	101.2	110.6	65	265.1	284.2	311.5	256.8	279.4
30	358.4	398.2	411.1	321.8	372.4	66	184.2	195.6	231.2	195.8	201.7
31	138.9	175.9	124.6	114.7	138.5	67	129.8	135.8	155.3	148.3	142.3
32	304.0	299.5	335.2	274.3	303.2	68	210.7	224.3	235.6	209.3	220.0
33	384.9	426.9	415.4	335.3	390.6	69	375.8	425.6	446.1	368.9	404.1
34	249.7	278.5	259.2	226.8	253.6	70	156.4	164.5	159.6	161.8	160.6
35	411.5	455.6	419.7	348.7	408.9	71	402.4	454.3	450.4	382.4	422.4
36	330.6	328.2	339.5	287.8	321.5	72	321.5	327.0	370.2	321.4	335.0

Table H.1.3.8. Total grain yield (Mg ha^{-1}) by treatment for the summers of 1992, 1993, 1994, and 1995.

Treat.	Year					Treat.	Year				
No.	1992	1993	1994	1995	Mean	No.	1992	1993	1994	1995	Mean
1	8.323	6.815	1.911	5.996	5.761	37	7.354	7.662	7.027	6.158	7.050
2	5.802	4.316	10.938	7.806	7.215	38	6.784	8.604	7.661	6.415	7.366
3	8.788	7.703	9.624	8.056	8.543	39	9.532	7.353	7.238	4.850	7.243
4	8.565	9.471	9.757	6.342	8.534	40	9.681	5.826	6.826	7.479	7.453
5	10.527	5.599	9.221	6.626	6.503	41	9.295	8.611	9.215	6.174	8.324
6	7.228	10.235	7.924	6.706	8.023	42	10.951	9.906	9.881	6.552	9.322
7	7.984	8.999	9.664	5.839	8.121	43	11.167	8.815	9.774	6.528	9.071
8	10.501	7.722	6.713	6.225	7.790	44	10.396	8.952	9.010	7.524	8.970
9	9.226	9.740	8.467	6.041	8.369	45	9.553	10.092	10.163	5.716	8.881
10	9.018	10.183	8.114	6.138	8.363	46	9.177	9.269	7.382	7.490	8.330
11	10.580	10.187	11.348	5.468	9.396	47	8.723	10.037	10.750	5.383	8.723
12	9.904	10.944	11.068	6.483	9.600	48	10.706	9.186	9.940	4.876	8.677
13	11.876	10.860	9.485	6.617	9.710	49	9.040	9.459	10.064	5.899	8.616
14	10.755	10.477	11.196	7.282	9.928	50	9.536	8.992	8.037	7.241	8.451
15	10.390	11.077	10.529	6.455	9.613	51	11.582	9.964	11.789	6.911	10.061
16	10.378	11.004	10.288	7.419	9.772	52	9.537	10.261	8.976	7.307	9.020
17	9.920	9.455	10.401	6.627	9.101	53	11.517	10.210	12.123	5.922	9.943
18	8.285	10.555	11.207	5.997	9.011	54	8.305	11.818	11.733	6.324	9.545
19	9.386	8.861	8.301	7.859	8.602	55	9.205	8.782	6.825	7.311	8.031
20	7.035	7.779	8.872	6.479	7.542	56	10.631	8.813	7.039	8.929	8.853
21	8.317	7.684	9.192	7.083	8.069	57	10.291	10.448	6.679	5.994	8.353
22	9.671	8.412	9.407	6.931	8.605	58	10.680	10.448	8.073	6.145	8.837
23	11.542	9.848	10.561	7.879	9.958	59	10.231	10.439	8.240	7.883	9.199
24	8.406	7.839	10.351	6.466	8.265	60	11.590	9.987	11.458	6.343	9.844
25	9.316	8.578	11.060	4.038	8.248	61	9.988	11.220	9.633	7.273	9.529
26	9.576	5.783	10.474	4.418	7.563	62	11.032	9.328	10.717	3.676	8.688
27	8.007	5.188	9.448	5.617	7.065	63	11.452	8.395	10.247	6.409	9.126
28	8.901	8.943	7.436	6.219	7.875	64	7.664	8.841	10.186	7.699	8.598
29	9.868	7.579	6.096	6.970	7.628	65	9.373	7.218	8.992	6.316	7.975
30	11.015	9.810	9.546	7.072	9.361	66	7.750	6.359	10.473	6.294	7.719
31	9.826	10.158	8.920	6.756	8.915	67	6.782	7.066	8.540	6.431	7.205
32	11.318	8.885	10.538	7.044	9.446	68	10.758	5.877	9.884	6.899	8.355
33	10.251	10.699	10.501	7.725	9.794	69	7.609	10.789	10.308	7.001	8.927
34	11.226	11.232	11.029	6.853	10.085	70	6.730	8.868	9.193	6.325	7.779
35	11.032	9.469	10.038	7.658	9.549	71	8.383	11.764	11.492	6.341	9.495
36	9.135	9.476	10.972	5.858	8.860	72	9.677	9.372	11.715	6.682	9.362

Yield Component Response

Yield components were divided into the 1) vegetative components, which included the stover (stalks, leaves and sheaths) and cob biomass; and 2) the grain yield components, which included the number of rows on fertile ears, the number of kernels per row on the fertile ears, kernel mass, and barrenness which included the number of plants in the harvested area that were totally barren and the number of ears that were not well formed. A fertile ear was considered to be one where the rows were well defined. Nubbins were ears where rows were not well defined and kernels were randomly scattered on the cob.

Table H.1.3.9. Mean yields (Mg ha^{-1}) of the different growth stage water treatments.

	Treatment	Year				
Growth Stage	% ET	1992	1993	1994	1995	Mean
Planting to Tassel Initiation	0	8.823	8.126	9.152	6.329	8.107[a]
	100	10.192	9.946	9.678	6.610	9.106[b]
Tassel Initiation to Ear Initiation	0	9.484	8.823	9.211	6.327	8.461[a]
	100	9.531	9.249	9.619	6.612	8.753[a]
Ear Initiation to End of Row Set	0	9.704	8.904	8.750	6.477	8.459[a]
	100	9.311	9.168	10.080	6.461	8.755[a]
End of Row Set to Silk	0	9.198	8.478	8.216	6.347	8.060[a]
	50	9.808	9.270	9.675	6.804	8.889[b]
	100	9.516	9.360	10.354	6.257	8.872[b]
Silk to End of Lag Phase	0	9.553	9.030	8.800	6.703	8.521[a]
	50	9.307	8.860	9.415	5.987	8.392[a]
	100	9.662	9.218	10.030	6.718	8.907[a]
End of Lag Phase to Maturity	0	9.048	9.050	8.627	6.663	8.347[a]
	50	9.589	8.948	9.482	6.415	8.618[a]
	100	9.886	9.074	10.136	6.330	8.856[a]

Means with different letters are significantly different at the 5 percent level.

Table H.1.3.10. Mean total seasonal rainfall (mm) corresponding to the different growth stage treatments.

	Seasonal Water Applied (mm)								
	0%ET			50% ET			100% ET		
Growth Stage	Mean	Min	Max	Mean	Min	Max	Mean	Min	Max
Planting to Tassel Initiation	227.6	0.0	454.3				286.4	101.2	556.7
Tassel Initiation to Ear Initiation	247.5	0.0	499.3				266.5	71.1	556.7
Ear Initiation to End of Row Set	238.8	0.0	455.5				275.1	58.0	556.7
End of Row Set to Silk	206.5	0.0	417.8	257.0	86.8	494.8	307.5	109.5	556.7
Silk to End of Lag Phase	225.5	0.0	455.5	256.6	58.0	499.3	288.8	71.1	556.7
End of Lag Phase to Maturity	147.5	0.0	280.8	256.6	135.9	419.1	366.9	210.1	556.7

The individual grain yield component response to the rainfall treatments are shown in Table H.l.3.11. Both the number of kernel rows per fertile ear and the number of kernels per row on the fertile ears showed a significant response to the water treatment during the period from planting to tassel initiation. In addition the number of kernels per row on the fertile ears show a significant response to the end of row set to silk water treatment. Kernel mass showed no significant response to water treatments in any growth stage.

Grain yield is dependent upon the size of the plant available to fix carbon during grain fill. This is referred to here as vegetative mass. The water treatments had a significant effect on vegetative mass during the period from planting to tassel initiation, from ear initiation to end of row set, from end of row set to silk, and from the end of lag phase to maturity (Table H.1.3.12). At silk the final size of the plant is determined and the vegetative mass would not be expected to change after that time. The significant effect of rainfall from the end of lag phase to maturity is not expected. The cause of this significant change could be due to the early senescence and degradation of the lower leaves so that they would not be included in the harvested vegetative mass. When the plants were harvested every effort was made to include any leaves on the ground

in the vegetative mass. Measured separate from vegetative mass was the mass of the cobs. The size of the cobs were not affected by any of the rainfall treatments.

Table H.1.3.11. Grain yield component responses to rainfall during different growth stages.

	Treatment	Year				
Growth Stage	% ET	1992	1993	1994	1995	Mean
	Number of Kernel Rows per Fertile Ear					
Planting to Tassel Initiation	0	14.1	14.2	14.3	15.0	14.4[a]
	100	14.2	14.4	14.7	15.0	14.6[b]
Tassel Initiation to Ear Initiation	0	14.1	14.1	14.4	15.1	14.4[a]
	100	14.1	14.5	14.7	14.9	14.5[a]
Ear Initiation to End of Row Set	0	14.2	14.3	14.2	15.0	14.4[a]
	100	14.1	14.3	14.9	14.9	14.6[a]
End of Row Set to Silk	0	14.1	14.3	14.5	14.9	14.5[a]
	50	14.1	14.3	14.5	15.0	14.5[a]
	100	14.1	14.3	14.5	15.0	14.5[a]
Silk to End of Lag Phase	0	14.0	14.3	14.5	15.1	14.6[a]
	50	14.2	14.3	14.5	14.8	14.4[a]
	100	14.0	14.2	14.6	15.0	14.5[a]
End of Lag Phase to Maturity	0	14.0	14.4	14.6	15.1	14.5[a]
	50	14.2	14.2	14.5	14.8	14.4[a]
	100	14.2	14.3	14.5	15.0	14.5[a]
	Number of Kernels per Row on Fertile Ears					
Planting to Tassel Initiation	0	35.2	34.6	35.4	33.2	34.6[a]
	100	37.2	37.7	36.3	32.8	36.0[b]
Tassel Initiation to Ear Initiation	0	36.7	35.8	35.7	32.3	35.1[a]
	100	35.6	36.6	36.0	33.7	35.5[a]
Ear Initiation to End of Row Set	0	36.3	35.8	35.4	32.7	35.0[a]
	100	36.0	36.5	36.3	33.3	35.6[a]
End of Row Set to Silk	0	36.5	34.9	33.2	32.6	34.3[a]
	50	35.9	36.9	36.7	34.3	35.9[b]
	100	36.2	36.8	37.7	32.1	35.7[b]
Silk to End of Lag Phase	0	36.9	35.8	35.1	32.8	35.1[a]
	50	35.8	36.2	35.3	33.5	35.2[a]
	100	35.8	36.5	37.2	32.8	35.6[a]
End of Lag Phase to Maturity	0	35.9	36.2	34.9	33.7	35.2[a]
	50	36.7	36.4	35.9	32.4	35.3[a]
	100	35.9	35.9	36.8	32.9	35.4[a]
	Kernel Mass					
Planting to Tassel Initiation	0	0.302	0.281	0.297	0.294	0.294[a]
	100	0.300	0.293	0.301	0.260	0.288[a]
Tassel Initiation to Ear Initiation	0	0.301	0.287	0.299	0.260	0.287[a]
	100	0.300	0.287	0.299	0.295	0.295[a]
Ear Initiation to End of Row Set	0	0.296	0.285	0.291	0.291	0.291[a]
	100	0.305	0.289	0.310	0.264	0.291[a]
End of Row Set to Silk	0	0.298	0.284	0.289	0.265	0.284[a]
	50	0.303	0.289	0.299	0.307	0.300[a]
	100	0.300	0.288	0.310	0.260	0.289[a]
Silk to End of Lag Phase	0	0.302	0.291	0.292	0.262	0.287[a]
	50	0.302	0.288	0.304	0.311	0.301[a]
	100	0.298	0.282	0.300	0.260	0.285[a]
End of Lag Phase to Maturity	0	0.299	0.285	0.291	0.308	0.296[a]
	50	0.298	0.288	0.295	0.263	0.286[a]
	100	0.304	0.287	0.310	0.262	0.291[a]

Means with different letters are significantly different at the 5 percent level.

Table H.l.3.12. Vegetative yield component and harvest index responses to rainfall during different growth stages.

Growth Stage	Treatment % ET	Year 1992	1993	1994	1995	Mean
		Vegetative Mass (Mg ha^{-1})				
Planting to Tassel Initiation	0	7.750	5.678	5.379	4.794	5.900[a]
	100	8.475	6.789	6.215	4.714	6.549[b]
Tassel Initiation to Ear Initiation	0	8.116	5.937	5.656	5.821	6.133[a]
	100	8.109	6.530	5.938	4.686	6.316[a]
Ear Initiation to End of Row Set	0	7.937	5.901	5.048	4.770	5.914[a]
	100	8.288	6.566	6.546	4.738	6.535[b]
End of Row Set to Silk	0	7.728	5.831	4.944	4.688	5.798[a]
	50	8.460	6.228	6.010	5.022	6.445[b]
	100	8.150	6.582	6.439	4.553	6.431[b]
Silk to End of Lag Phase	0	8.077	6.185	5.725	4.774	6.190[a]
	50	8.224	6.352	5.684	4.609	6.217[a]
	100	8.037	6.164	5.984	4.880	6.266[a]
End of Lag Phase to Maturity	0	7.855	6.019	5.182	4.869	5.981[a]
	50	8.032	6.098	5.644	4.515	6.072[a]
	100	8.451	6.584	6.567	4.879	6.620[b]
		Cob Mass (Mg ha^{-1})				
Planting to Tassel Initiation	0	1.453	1.201	1.270	1.249	1.293[a]
	100	1.628	1.411	1.328	1.040	1.352[a]
Tassel Initiation to Ear Initiation	0	1.519	1.303	1.282	1.050	1.288[a]
	100	1.563	1.309	1.316	1.239	1.357[a]
Ear Initiation to End of Row Set	0	1.563	1.262	1.211	1.046	1.271[a]
	100	1.518	1.350	1.387	1.243	1.374[a]
End of Row Set to Silk	0	1.509	1.265	1.155	1.346	1.319[a]
	50	1.566	1.302	1.321	1.074	1.316[a]
	100	1.547	1.350	1.421	1.013	1.332[a]
Silk to End of Lag Phase	0	1.543	1.292	1.236	1.069	1.285[a]
	50	1.518	1.266	1.294	1.066	1.286[a]
	100	1.562	1.360	1.368	1.298	1.397[a]
End of Lag Phase to Maturity	0	1.514	1.295	1.226	1.320	1.339[a]
	50	1.513	1.323	1.303	1.070	1.302[a]
	100	1.596	1.300	1.369	1.044	1.327[a]
		Harvest Index				
Planting to Tassel Initiation	0	0.485	0.538	0.579	0.505	0.527[a]
	100	0.500	0.549	0.563	0.535	0.538[a]
Tassel Initiation to Ear Initiation	0	0.493	0.547	0.572	0.508	0.530[a]
	100	0.494	0.541	0.571	0.533	0.535[a]
Ear Initiation to End of Row Set	0	0.502	0.553	0.581	0.518	0.538[a]
	100	0.485	0.534	0.560	0.523	0.526[a]
End of Row Set to Silk	0	0.498	0.544	0.573	0.504	0.530[a]
	50	0.493	0.549	0.571	0.529	0.535[a]
	100	0.491	0.537	0.570	0.528	0.531[a]
Silk to End of Lag Phase	0	0.497	0.545	0.556	0.536	0.534[a]
	50	0.487	0.536	0.577	0.497	0.524[a]
	100	0.497	0.550	0.580	0.528	0.539[a]
End of Lag Phase to Maturity	0	0.490	0.552	0.571	0.525	0.535[a]
	50	0.501	0.546	0.579	0.535	0.521[a]
	100	0.490	0.533	0.560	0.500	0.540[a]

Means with different letters are significantly different at the 5 percent level.

The harvest index is the ratio of the grain to the vegetative and cob mass. This number, in spite of the different water treatments, was relatively constant and the mean for the various treatments over the four summers showed no significant difference between the no water and 100 percent of potential evapotranspiration watered plots.

Plant barrenness can also have a major effect on final yield. The only period that the water treatments significantly affected complete plant barrenness was during the period from tassel initiation to ear initiation (Table H.13.13). Barrenness was reduced by more than 50 percent when water equal to 100 percent of evapotranspiration was received during this short growth period, generally around seven days in length. Although this was the only period when barrenness was significantly reduced, the other three vegetative growth stages (planting to tassel initiation, ear initiation to end of row set, and end of row set to silk) also consistently showed a reduction in barrenness when water equal to 100 percent of evapotranspiration was applied. Partial plant barrenness, as measured by the existence of an ear that was not fully fertilized, was generally not affected by water treatments in any growth stage. In the silk to end of lag phase, partial barrenness was least in the 50 percent of evapotranspiration water treatment, and the 0 and 100 percent evapotranspiration water treatments were not significantly different from each other (Table H.1.3.13).

The number of kernels per nubbin was significantly reduced when water equal to 100 percent of evapotranspiration was applied during the period from planting to tassel initiation. A reduction in the number of kernels per nubbin would at first thought result in reduced yield. However, when the entire picture is looked at the yield lost due to fewer kernels per nubbin is more than made up for by the reduction in both the number of completely and partially barren

plants. Using the yield components to compute the mass of grain in the plots which received no water from planting to tassel initiation (eq. H.1.3.4)

$$Y = \{[(64{,}583\text{-}B)RK_r]+(NK_n)\}\ K_m \qquad \text{(H.1.3.4)}$$

the yield for the no water from planting to tassel initiation is computed as 9.449 Mg ha^{-1}, and for the 100 percent of evapotranspiration is 9.744 Mg ha^{-1}. In eq. 3.4 Y is the computed yield, R is the number of rows on each fertile ear (Table H.1.3.11), K, is the number of kernels per row (Table H.1.3.11), N is the number of nubbins (Table H.1.3.13), K_n is the number of kernels per nubbin (Table H.1.3.13), K_m is the kernel mass (Table H.1.3.11), B is the number of barren plants per hectare (Table H.l.3.13) and 64,583 is the number of plants per hectare.

The results reported here differ from those reported by Claassen and Shaw (1970) where the greatest yield losses occurred during the period of silk to end of lag phase. It does however agree with Loomis and Conner (1994) who show the importance of rainfall during wheat establishment and again during spike formation, heading and anthesis.

Disagreement of these experimental results with the results of Claassen and Shaw (1970) is due to the method and timing of imposing the water stress. Claassen and Shaw imposed the water stress only during the periods of rapid vegetative growth (tassel initiation to silk), pollination and early grain fill, and rapid grain fill. Further the plants were grown in large containers that confined the root system, and limited the soil available for the roots to explore. Therefore, Claassen and Shaw effected better control of the timing of the stress application than was able to be effected in this experiment's natural soil conditions. In addition, plants grown in

such containers experience water desiccation at a more rapid rate than those grown in field conditions (Ludlow et al., 1985). As a result, the plants grown in the containers are not able to adjust to the impending stress. Plants grown in the field, on the other hand, are able to adjust stomatal conductance and photosynthetic rate to changing leaf water potential, and therefore become less sensitive to water stress as drying proceeds.

To relate these results to actual calendar dates and the expected rainfall during each growth stage, the average dates of the different corn growth stages in eastern Illinois were determined from crop reporting district data. Such an analysis is necessary in order to determine the potential benefit of weather modification to corn grown in Illinois. In this analysis, we are assuming that the optimum rainfall amount applied to the crop is equal to the 100 percent PET treatment of this experiment. With the estimate of this rainfall quantity for each growth stage, the probability of exceeding the optimum rainfall (Table H.1.3.14) during each growth stage can be computed. The probability of exceeding the optimum rainfall amounts in each growth stage were computed by fitting the gamma distribution to the 30 year normal (1961 to 1990) rainfall observed in each of the different growth periods.

Based on this analysis, rainfall would be most limiting in eastern Illinois during the growth stages from end of row set to silk, and end of lag phase to maturity, closely followed by the period of silk to end of lag phase. These growth periods represent the time when the corn canopy is rapidly growing, or is fully grown and transpiring the most and have been shown to be the most responsive to rainfall in most statistical studies of rainfall and corn yield in the midwest.

Table H.1.3.13. Crop barrenness response to rainfall during different growth stages.

Growth Stage	Treatment % ET	Year 1992	1993	1994	1995	Mean
		Number of Barren Plants ha^{-1}				
Planting to Tassel Initiation	0	336.4	185.7	487.1	1,458.5	616.2^{a}
	100	80.7	150.7	411.7	1,345.5	495.1^{a}
Tassel Initiation to Ear Initiation	0	298.7	223.4	597.4	1,905.2	756.2^{a}
	100	113.0	113.0	298.7	896.1	355.2^{b}
Ear Initiation to End of Row Set	0	261.0	150.7	672.7	1,458.5	635.1^{a}
	100	150.7	185.7	215.3	1,345.5	476.3^{a}
End of Row Set to Silk	0	113.0	223.4	1,009.1	1,512.3	718.8^{a}
	50	0.0	169.5	336.4	1,232.5	433.2^{a}
	100	505.9	113.0	0.0	1,458.5	519.4^{a}
Silk to End of Lag Phase	0	166.8	113.0	842.3	1,065.6	546.3^{a}
	50	56.5	279.9	279.9	1,961.7	645.8^{a}
	100	392.9	113.0	215.3	1,178.6	476.3^{a}
End of Lag Phase to Maturity	0	169.5	223.4	842.3	1,289.0	629.7^{a}
	50	166.8	223.4	223.4	952.6	392.9^{a}
	100	279.9	56.5	269.1	1,961.7	645.8^{a}
		Number of Nubbins ha^{-1}				
Planting to Tassel Initiation	0	6,576.7	4,932.6	2,316.9	3,813.1	4,410.5^{a}
	100	7,373.3	1,719.5	971.4	3,213.0	3,318.0^{a}
Tassel Initiation to Ear Initiation	0	7,324.8	3,476.7	1,905.2	3,178.0	3,971.9^{a}
	100	6,614.4	3,178.0	1,383.2	3,850.8	3,756.6^{a}
Ear Initiation to End of Row Set	0	6,689.8	2,578.0	2,099.0	3,250.7	3,654.3^{a}
	100	7,249.5	4,074.1	1,184.0	3,775.4	4,074.1^{a}
End of Row Set to Silk	0	5,268.9	3,420.2	2,411.1	3,813.1	3,727.0^{a}
	50	7,120.3	3,083.9	1,618.9	2,691.0	3,643.6^{a}
	100	8,522.3	3,476.7	834.2	4,036.5	4,219.5^{a}
Silk to End of Lag Phase	0	5,831.3	2,467.6	1,289.0	3,420.2	3,250.7^{a}
	50	7,623.5	4,709.2	1,905.2	4,259.8	4,625.8^{b}
	100	7,456.7	2,804.0	1,749.1	2,860.5	3,713.5^{ab}
End of Lag Phase to Maturity	0	7,680.1	2,914.3	2,354.6	1,289.0	4,049.9^{a}
	50	2,467.6	3,307.2	1,681.9	4,149.5	3,573.6^{a}
	100	8,027.9	3,756.6	888.0	3,140.4	3,966.5^{a}
		Number of Kernels per Nubbin				
Planting to Tassel Initiation	0	75.3	52.2	64.4	52.2	61.0^{a}
	100	63.7	36.5	29.2	51.3	45.2^{b}
Tassel Initiation to Ear Initiation	0	69.2	49.6	47.9	46.1	53.2^{a}
	100	69.8	39.0	45.7	57.4	53.0^{a}
Ear Initiation to End of Row Set	0	63.8	42.4	49.2	42.0	49.3^{a}
	100	75.2	46.2	44.4	61.5	56.8^{a}
End of Row Set to Silk	0	78.4	40.0	65.8	55.0	59.8^{a}
	50	59.7	46.5	45.0	56.9	52.0^{a}
	100	70.4	46.4	29.6	43.3	47.4^{a}
Silk to End of Lag Phase	0	68.4	39.4	44.2	50.0	50.5^{a}
	50	64.2	54.1	46.7	55.8	52.4^{a}
	100	75.9	39.5	49.5	60.4	56.3^{a}
End of Lag Phase to Maturity	0	69.3	45.1	56.8	43.8	53.8^{a}
	50	63.2	40.4	55.1	61.3	55.0^{a}
	100	76.0	47.3	28.5	50.2	50.5^{a}

Means with different letters are significantly different at the 5 percent level.

Increased rainfall from weather modification, either by cloud seeding or by irrigation, would be beneficial 5 out of 6 years during the grain fill period (end of lag phase to maturity), 4 out of 6 years during the period from silk to end of lag phase (period of embryo and starch growth in the kernels), and 4 out of 5 years during the period from end of row set to silk (rapid vegetative growth of com and initiation of kernel primordia on the ear). During the early vegetative growth stages, weather modification would be beneficial only 2 out of 5 years during the period from planting to tassel initiation, 1 out of 4 years during the period from tassel initiation to ear initiation, and 2 out of 6 years during the period from ear initiation to end of row set

Table H.1.3.14. Typical dates of corn growth stages in Illinois, assumed optimum rainfall and probability of exceeding the optimum rainfall based on the gamma distribution fit to the rainfall for each growth stage.

		Gamma Distribution Parameters		Optimum Rainfall	Probability of Exceeding
Growth Stage	Growth Period	Shape	Scale	(mm)	Optimum Rainfall
Planting to Tassel Initiation	13 May-13Jun	2.601	1.402	71.0	0.578
Tassel Initiation to Ear Initiation	13 Jun-20Jun	1.282	1.536	17.9	0.733
Ear Initiation to End of Row Set	20 Jun-2Jul	2.196	1.087	36.4	0.679
End of Row Set to Silk	2 Jul-19 Jul	1.789	1.479	103.8	0.191
Silk to End of Lag Phase	19 Jul-2 Aug	1.589	1.471	64.1	0.356
End of Lag Phase to Maturity	2 Aug-20 Sep	5.870	1.111	230.6	0.163

Midwest Corn Growth Stage Rainfall Probabilities

The above example of the probability of rainfall less than PET was expanded to include the entire North Central Region of the United States. Extension of the concept to the entire North Central Region assumes that all corn hybrids will exhibit similar responses to stress during the different growth stages as the hybrid used in this study. The probabilities presented here differ from other climatology studies in that the dates are not tied to calendar dates but to growth stages which begin at different times of the summer and have different time lengths.

Start of the growing season was determined by the typical date of planting in each of the Crop Reporting Districts (Figure H.1.3.4). The normal time when 50 percent of the corn crop is planted ranges from 25 April (Day 115) in Southeast Kansas to 25 May (Day 145) in Northwest North Dakota. Very little corn is grown north of the region where the normal date of planting is after 20 May (Day 140). The region in Southern Illinois where the normal date of planting is after 15 May is an interesting anomaly. This late planting in a region where a 10 May planting date would be expected is due to heavy clay pan soils which are slow to dry out with normal April and May rainfall.

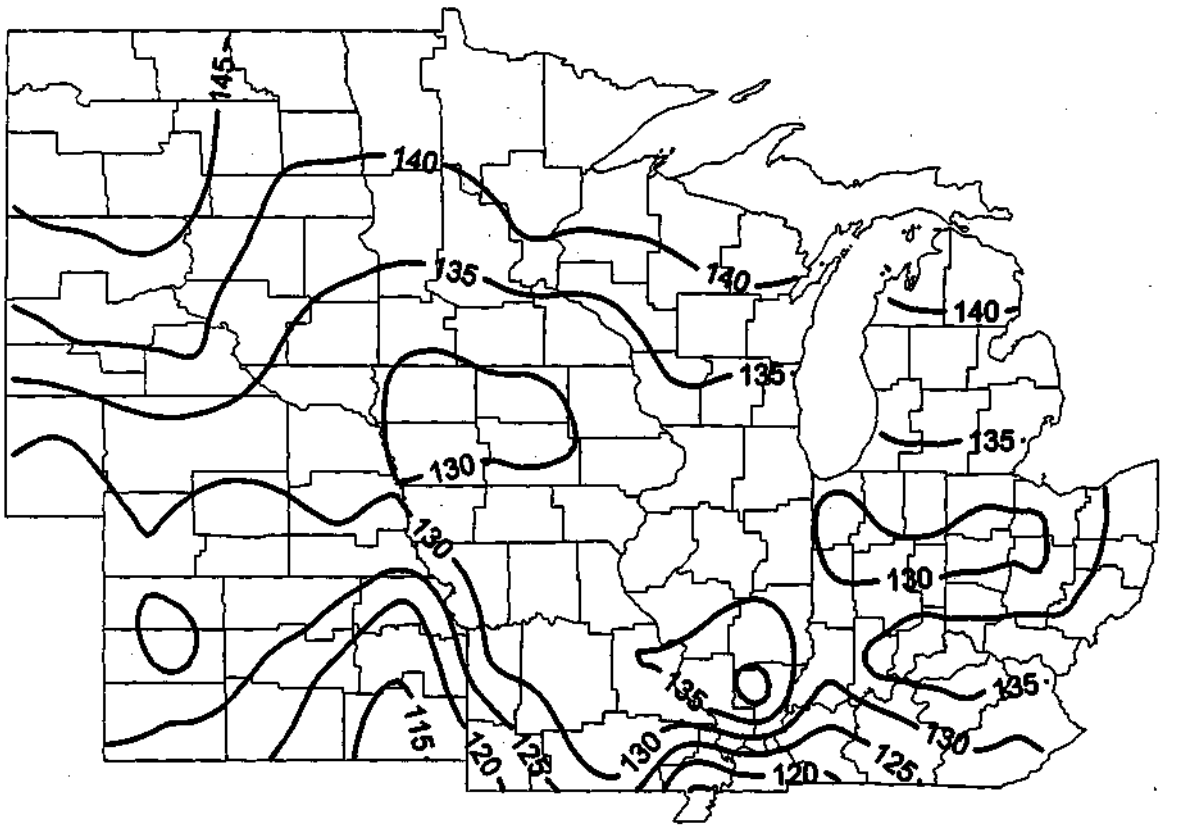

Figure H.l.3.4. Date when 50 percent of the corn crop is normally planted in each crop reporting district in the North Central Region. Day 115 equals 25 April, and day 145 equals 25 May.

The normal planting dates for the 1961 to 1990 weather data for each crop reporting district, the mean maximum and minimum temperature, precipitation, and potential evapotranspiration and probability of rainfall being less than 10, 25, 50, and 75 percent of potential evapotranspiration were computed for each corn growth stage. The mean maximum and minimum temperature, precipitation, and potential evapotranspiration and probability of rainfall being less than 10, 25, 50, and 75 percent of potential evapotranspiration were computed for planting dates 30, 20, and 10 days prior to the normal date, and 10, 20, and 30 days after the normal date.

In the figures to follow English units are used rather than metric. English units are used because the final publication of this work will be in refereed journals that require the use of English units. The figures are all grouped at the end of this section for easier reading. Because of the number of figures, they are located at the end of this section.

Maximum and Minimum Temperatures

Based on the work on Hollinger and Changnon (1993) the optimum mean minimum temperature for corn during the period from planting to tassel initiation is 56°F. When corn is planted 30 days before the normal planting date the average minimum temperature during the planting to tassel initiation growth stage is less than 50°F throughout the corn belt (Figure H.1.3.5.a). As planting is delayed after 30 days before the normal planting date, mean minimum temperatures decrease by 2 to 3°F for each 10 day delay in planting (Figures H.1.3.5.a through H.1.3.5.g). The highest minimum temperature during this growth stage occurs in Southern Illinois. The average minimum temperature in the planting to tassel initiation stage begins to

exceed 56°F whenever corn is planted at the normal time in Southern Illinois (Figure H.1.3.5.d). As planting is delayed by 10 days after the normal planting date the region of the average minimum temperatures exceeding 56°F expands from Southern Illinois to include almost all of Missouri, the southern two-thirds of Illinois, the southern one-half of Indiana, the southern one-third of Ohio, and almost all of Kentucky (Figure H.1.3.5.e). By 20 days after normal planting the area has expanded to include all of Missouri, Illinois, Indiana, Ohio, and Kentucky, the eastern three quarters of Kansas, the eastern one-third of Nebraska, the southern three quarters of Iowa, and the southern row of crop reporting districts in Michigan (Figure H.1.3.5.f). When planting is delayed by 30 days after normal planting, the area has expanded to include all of Kansas, Missouri, Iowa, Illinois, Indiana, Ohio, and Kentucky, all of Nebraska except for the Panhandle, the eastern three fourths of South Dakota, the southern one-half of Minnesota, the southern one-third of Wisconsin, and the southern one-third of Michigan (Figure H.1.3.5.g). These figures may help to explain why corn yields drop as planting is delayed after the normal planting dates.

Also as planting is delayed from 30 days before to 30 days after the normal planting date the mean minimum temperature in the growth stage from the end of lag phase to maturity decreases. The mean minimum temperature in the growth period from the end of row set to silk changes the least.

Maximum temperature greater than 90°F during the period from silk to end of lag phase can have a significant impact on yields. Corn planted 30 days before the normal date is subject to a mean maximum temperature above 90°F in the western two-thirds of Kansas and in the Southwest and South-central CRDs of Nebraska. When corn is planted from 20 days before normal to 20 days after normal, the mean maximum temperature exceeds 90°F in all of Kansas.

In Missouri the mean maximum temperature exceeds 90°F in the southern two-thirds of Missouri when corn is planted 20 days before normal; the southern one-third when plant 10 days before normal, and when planted at the normal planting time; and the southwestern one quarter when planted 10 to 20 days after normal. When corn is planted 30 days after normal the mean maximum temperature during the silk to end of lag phase exceeds 90°F only in the southern two tiers of CRD's in Kansas.

Precipitation

The temperature gradients were generally north to south with a slight east to west gradient and the warmest temperatures tended to be in the southwestern parts of the region. Precipitation, on the other hand has a strong east west gradient west of Minnesota, Iowa, and Missouri with the driest areas in the west. East of North and South Dakota, Nebraska, and Kansas rainfall gradients were less well defined during the different growth stages of the different planting dates (Figures H.1.3.7.a-g).

Rainfall in the critical growth period of planting to tassel initiation ranges from less than 3.0 in. (76.2 mm) in the Southwestern corner of the region to more than 7.0 in. (177.8 mm) in Southern Kentucky when corn is planted 30 days before normal (Figure H.1.3.7.a). Across the heart of the Cornbelt, rainfall in the earliest planted corn averages between 5.5 and 6.0 in. during this growth stage. As planting is delayed from 30 days before the normal date of planting, rainfall during this first corn growth stage decreases to an average of 3.0 to 3.5 in. in eastern Kansas, Nebraska and Minnesota, western Missouri and Wisconsin, and most of Iowa. East of this rainfall maximum the average rainfall received is between 2.5 and 3.0 in., while west of the

maximum the rainfall is between 2.0 and 2.5 in. As planting is delayed the decrease in rainfall in the eastern part of the region is greater than in the western part. The greatest decrease in rainfall is located in the extreme south. Rainfall, on the average, during this growth stage is adequate to meet the demands of the young plants. In fact the heavy rainfall normally observed during plantings before the normal date of planting is sufficient to cause localized flooding conditions in many regions of the Cornbelt.

The least rainfall was received during the period from tassel initiation to ear initiation, followed by the ear initiation to end of row set, and the silk to end of lag phase stage. These growth stages were also the shortest of the six growth stages. During the period from tassel initiation to ear initiation, rainfall across the region is generally less than 1.5 inches (38.1 mm). When planting is delayed to later than 20 days after normal, total rainfall during this growth stage is reduced to less than 1.0 inch (25.4 mm). Based on the rain shelter experimental data the number of barren plants would increase as planting is delayed more than 20 days after the normal planting date.

Rainfall during the period from ear initiation to end of row set is generally less than 2.0 inches (50.8 mm) for all planting dates. As planting is delayed from the earliest (30 days before normal) to the latest (30 days after normal) rainfall across the region decreases. The most rain during this growth stage is received in Northeast Kansas, Southwest and South Central Iowa, and Northwest Missouri (Figure H.1.3.7.a) when the crop is planted 30 days before normal.

Rainfall during rapid vegetative growth (end of row set to silk) is generally around 3.0 inches for all the planting dates except for 20 and 30 days before normal planting where the rainfall in the central part of the region is 3.0 to 3.5 inches Delays in planting do not greatly

impact the amount of rain received during this growth stage.

During the period from silk to end of lag phase, rainfall is generally greater than 1.5 inches east of North and South Dakota, Nebraska, and Kansas. During the first three planting dates (10, 20, and 30 days before normal) rainfall in the heart of the Cornbelt is between 2.0 and 2.5 inches (63.5 mm). As planting is delayed to the normal date of planting, and to 10, 20, and 30 days after normal planting rainfall in Iowa, Illinois, and Indiana drops to 1.5 to 2.0 inches. If planting is delayed to 30 days after normal planting, rainfall in the Northwest and Northeast CRDs of Illinois increases to greater than 2 inches (Figure H.1.3.7.g).

During grain fill (end of lag phase to maturity) rainfall ranges from less than 2.5 inches in the extreme west to greater than 7.0 inches in southern Wisconsin when corn is planted 30 days earlier than normal. When corn is planted 30 days later than normal rainfall across the region ranges from less than 0.5 in. in the northwest to 7.0 inches in Missouri. Except for the significant decrease in rainfall in the northwest portion of the region, the maximum rainfall is not sensitive to different planting dates. However, the position of the maximum rainfall in the region migrates from southern Wisconsin when corn is planted 30 days before normal to Missouri when corn is planted 30 days after normal. The path of the migration is initially to west-northwest, then it turns to a southwesterly direction and finally migrates directly south.

Potential Evapotranspiration

Plant water demand is measured by evapotranspiration. Evapotranspiration is dependent upon the condition of the atmosphere surrounding the plant and the soil moisture. If the soil on which a crop is growing is well watered, the atmospheric demand for water (Potential

Evapotranspiration) is normally met. However, if the soil is dry then the plant is not able to transpire as much water as the atmosphere demands and actual evapotranspiration is less than potential evapotranspiration. When potential evapotranspiration demand cannot be meet crops will experience a water stress. For a crop to experience no water stress throughout its growth, the soil profile must be fully recharged at planting and rainfall equal to or greater than potential evapotranspiration must be received. Potential evapotranspiration can be computed from solar radiation, air temperature, relative humidity, and wind speed. Daily potential evapotranspiration has been computed by the Midwest Climate Center and was used to develop the potential evapotranspiration demand for each corn growth stage for the seven different planting dates.

During the period from planting to tassel initiation potential evapotranspiration total range from 4.5 in. (114.3 mm) across the region when the crop is planted 30 days before normal (Figure H.1.3.8.a) to approximately 2.5 in. (63.5 mm) across the region when the crop is planted 30 days after the normal planting date (Figure H.1.3.8.g). The decrease in potential evapotranspiration is due to the shortening of this growth stage as planting is delayed and the temperatures experienced become warmer. During this period the mean normal rainfall is equal to or greater than the potential evapotranspiration in all planting dates (Figures H.1.3.8.a-g).

The least total potential evapotranspiration occurs in the shortest growth periods of tassel initiation to ear initiation, ear initiation to end of row set, and silk to end of lag phase. Total potential evapotranspiration in the tassel initiation to ear initiation growth period ranges from approximately 1.0 in. (25.4 mm) when the crop is planted 30 days before the normal planting date, to less than 0.5 in. when the crop is planted 20 to 30 days after the normal planting date. During the period from ear initiation to end of row set, total potential evapotranspiration ranges

from approximately 1.5 inches when planted 30 days before normal to between 1.0 and 1.5 inches when planted 30 days after normal. From silk to the end of lag phase, total potential evapotranspiration ranges from 3.0 to 3.5 inches in all the planting dates from 30 days before to 20 days after the normal planting date. When the crop is planted 30 days after normal, the total potential evapotranspiration during the silk to end of lag phase ranges from 3.5 inches in the west to 2.5 inches in the east to less than 2.0 inches in the northern parts of Wisconsin, Michigan, and the northeastern part of Minnesota.

The rainfall normally received is greater than the total potential evapotranspiration during the period from tassel initiation to ear initiation regardless of the planting date. During the period from ear initiation to end of row set, normal rainfall exceeds the normal potential evapotranspiration if the crop is planted before the normal date of planting. If the crop is planted at the normal time or later, normal rainfall does not meet the total potential evapotranspiration demand. Potential evapotranspiration always exceeds normal rainfall during the silk to end of lag phase, regardless of the date of planting. In the western part of the region rainfall is generally 2.0 inches less than potential evapotranspiration, and in the eastern parts, rainfall is generally 1.0 inch less than potential evapotranspiration.

Total potential evapotranspiration ranges from approximately 5.5 to 7.0 inches during the end of row set to silk period regardless of the planting date. Lower total potential evapotranspiration values are found in the east and the higher values in the southwest. Normal rainfall is always less than the total potential evapotranspiration for all planting dates. Generally, total potential evapotranspiration exceeds rainfall by 2.0 to 5.0 inches.

During grain fill, end of lag phase to maturity, there is a strong gradient of potential

evapotranspiration from southern Wisconsin, central Minnesota and Michigan to the most northern part of the region. This gradient shows increasing evapotranspiration in a southerly direction. The greatest total potential evapotranspiration (approximately 11.0 inches) occurs in southwest Kansas. In the eastern part of the region, total potential evapotranspiration is approximately 7.0 to 8.0 inches for planting dates that occur from 30 days before to 10 days after normal. For planting dates 20 to 30 days after normal total potential evapotranspiration ranges from 4.0 to 6.0 inches across Ohio. As with the end of row set to silk and silk to end of lag phase growth periods, normal rainfall is less than total potential evapotranspiration in all seven of the planting dates analyzed. The rainfall shortage in the west is approximately 7.0 inches and in the east is approximately 1.0 inch.

The shortage of rainfall relative to potential evapotranspiration during the last three growth stages (end of row set to maturity) is a further demonstration of why these later growth stages tend to have a greater impact on final yield than the earlier growth stages. The probabilities of rainfall being less than or equal to normal potential evapotranspiration further show the increased likelihood of rainfall shortages during the late vegetative stage and throughout the reproductive stage.

Rainfall Deficit Probabilities

The probability of rainfall being less than or equal to 75 percent of the normal potential evapotranspiration are shown in Figures H.1.3.9.a-g, for each of the seven dates of planting analyzed. Similar maps are shown for the probability of rainfall less than or equal to 50 percent of potential evapotranspiration in Figures H.1.3.10.a-g, for rainfall less than or equal to 25

percent of potential evapotranspiration in Figures H.1.3.1 l.a-g, and for rainfall less than or equal to 10 percent of potential evapotranspiration in Figures H.1.3.12.a-g. The probabilities were computed using the Weibull distribution and rainfall data from each crop reporting district.

The rainfall shortage probabilities are arbitrarily defined as extreme drought for rainfall less than or equal to 10 percent of potential evapotranspiration, severe drought for rainfall less than or equal to 25 percent of potential evapotranspiration, moderate drought for rainfall less than or equal to 50 percent of precipitation, and mild drought for rainfall less than or equal to 75 percent of evapotranspiration. While these rainfall shortages are arbitrary, they do represent the frequency of drought occurrence. The drought definition is different from the common definition of drought which is rainfall deviations from normal, in that drought is defined in terms of shortages from potential evapotranspiration. The definition of drought as used here is also related to plant water needs, therefore, in some regions there will be a high probability of drought every year.

Probabilities can be interpreted in two ways. The first is that the probability, presented as a fraction, gives the probability mat any one year will experience a drought. For example, a probability of 0.25 would mean that there is a 25 percent chance of a rainfall shortage in a given year, a probability of 0.50 is a 50 percent chance of the event occurring, and a probability of 0.75 is a 75 percent chance of the event occurring. Obviously as the fraction becomes larger the likelihood of the event occurring in a given year increases. The second way to interpret the probability is to express the likelihood of an event occurring every so many years. For example, a 0.25 probability would mean that the event can be expected once every 4 years, a 0.50 probability would mean the event could be expected once every other year (one year out of two), and a 0.75

probability that the event could be expected three years out of four. Either way of interpreting the probability gives an indication of the importance of attempting to modify the weather during any given year based on the expected or actual planting date.

Probability of Extreme Drought. When corn is planted 30 days before the normal date of planting, the highest probabilities of extreme drought occur in the silk to end of lag phase growth period where the highest probability is 0.25 (1 in 4 year) in southwest Kansas, and southwest North Dakota. Because very little corn is normally grown in southwest North Dakota, the greatest impact on corn yield would be observed in Kansas. There is a one year out of twenty probability of an extreme drought occurring in southern Illinois, Missouri, western Iowa and Minnesota, and the four western states of North and South Dakota, Nebraska, and Kansas (Figure H.1.3.9.a).

Other growth stages that show an extreme drought probability greater than 5 percent, when corn is planted 30 days before normal, include the tassel initiation to ear initiation, ear initiation to end of row set, end of row set to silk, and end of lag phase to maturity stages. During the tassel initiation to ear initiation and ear initiation to end of row set, there is a 5 percent probability (1 year out of 20) of an extreme drought in any given year throughout the region. During the growth stage from the end of row set to silk, there is a greater than 5 percent probability of an extreme drought in western Kansas, southwest Nebraska, and most of North and South Dakota. During grain fill (end of lag phase to maturity) a greater than 5 percent chance of an extreme drought exists in the panhandle of Nebraska, and the western one-half of North and South Dakota.

There is less than a 5 percent chance of an extreme drought during the planting to tassel

initiation growth stage regardless of when corn is planted. As planting is delayed the growth stages which showed drought probabilities tend to increase (Figures H.1.3.9.a-g). The most interesting changes in the areas of extreme drought probabilities occur during the silk to end of lag phase, and end of lag phase to maturity growth stages. In the silk to end of lag phase growth stage, the probability of an extreme drought in Kansas decreases as planting is delayed to 30 days after normal. From end of lag phase to maturity, the probability of an extreme drought occurring increases in the extreme west and northern regions of the North Central States.

Probability of Severe Drought. All growth stages in all planting dates from 30 days before to 30 days after normal planting, show a greater than 5 percent probability (1 year out of 20) of a severe drought occurring (O.a-g). Western Kansas, most of South Dakota and all of North Dakota show a greater than 5 percent chance of a severe drought during the planting to tassel initiation growth stage when corn is planted 30 days before normal. Most of the region shows less than a 5 percent chance of a severe drought during the planting to tassel initiation stage when the crop is planted on the normal date to 10 days after the normal date.

From tassel initiation to ear initiation the probability of a severe drought ranges from 5 percent in the northern parts of Wisconsin and Michigan, to 20 and 25 percent in southwestern Kansas when the crop is planted 20 to 30 days before normal. Across much of the rest of the region the probabilities range from 10 to 15 percent. If the crop is planted 10 days before normal, the probability of a severe drought increases to greater than 20 percent (1 year in 5) in western Kansas, central South Dakota and southeast North Dakota, and southeastern Missouri and southwest Illinois. When the crop is planted at the normal planting date or 10, 20, or 30 days after normal, a probability gradient from west to east begins to form with the highest

probabilities of a severe drought in the west. Probabilities range from 40 percent to less than 5 percent across the region in all four planting dates. In Dlinois the probability of a severe drought from tassel initiation to ear initiation ranges from 20 to 25 percent (1 in 5 years to 1 in 4 years) when the crop is planted later than the normal date of planting.

During the ear initiation to end of row set growth stage a west to east gradient of severe drought probabilities exists with all the different planting dates. The gradient becomes stronger as the date of planting is delayed from 30 days before the normal date of planting. The probability of a severe drought ranges from 10 to 30 percent when the crop is planted 30 days before normal, from 5 to 30 percent when planted 20 days before normal, from 10 to 50 percent when planted 10 days before normal, from 10 to 55 percent when planted on the normal date, from 10 to 50 percent when planted 10 days after normal, from 5 to 50 percent when planted 20 days after normal, and 5 to 55 percent when planted 30 days after normal.

From end of row set to silk, a period when rainfall had a significant effect on final grain yield, the probability of a severe drought ranged from 5 to 65 percent. The highest probability of a severe drought occurred in northwestern South Dakota and southwestern North Dakota when corn is planted 10 to 30 days after the normal date of planting. In the central part of the region (east of central Minnesota, central Iowa, and central Missouri) the probability of a severe drought ranges from 5 to 10 percent (1 year in 20 to 1 year in 10) when the crop is planted 10 to 30 days after the normal date, and from 5 to 15 percent (1 year in 20 to 2 years in 15) when the crop is planted 10 to 30 days before normal.

During pollination, silk to end of lag phase, the probability of a severe drought ranges from 5 to 70 percent. As in the end of row set to silk growth stage, the highest severe drought

probabilities occur in northwestern South Dakota, and southwestern North Dakota. When the crop is planted 30 days before normal, a severe drought can be expected 1 year out of 4 (25 percent probability) in North and South Dakota, Nebraska, Kansas and Missouri. If the crop is planted 20 days before normal the 25 percent probability area includes North and South Dakota, central Minnesota, extreme western Nebraska, Kansas, and the western one-half of Missouri. As planting is delayed to 10 days before to 20 days after normal the 25 percent probability line migrates to the east in the northern two-thirds of the region, and is relatively unchanging in Missouri. If planting is delayed to 30 days after normal, the 25 percent probability line is located along the eastern edges of North and South Dakota, Nebraska, and Kansas.

The probability of a severe drought during grain fill (end of lag phase to maturity) ranges from less than 5 percent to greater than 95 percent. The 95 percent probabilities occur in the extreme northern parts of the region when planting is delayed to 30 days after normal. In the major part of the Cornbelt (Iowa, Illinois, Indiana, Ohio, southern Wisconsin, and southern Michigan), the probability of a severe drought is generally less than 5 percent. In Nebraska and Kansas the 25 percent probability line is located in the center of the state, with a steep increasing gradient in severe drought probability to the west.

Probability of Moderate Drought. The probability of a moderate drought during the planting to tassel initiation growth stage ranges from less than 5 percent to 45 percent (1.a-g). When the crop is planted 20 to 30 days before or after normal there is a 35 percent probability of a moderate drought during the planting to tassel initiation stage in southwestern Kansas. This is contrasted to only a 15 to 20 percent chance when the crop is planted from 10 days before to 10 days after normal planting. The highest probability of a moderate drought during this growth

stage occurs in the four western states of North and South Dakota, Nebraska, and Kansas. East of these states the probability of a moderate drought is generally 5 to 10 percent when the crop is planted from 30 days before to 20 after normal. When the crop is planted 30 days after normal the probability of a moderate drought increases to 10-15 percent in the eastern part of the region during the planting to tassel initiation growth stage.

While the ear is being initiated (tassel initiation to ear initiation growth stage) there is a 15 to 75 percent chance for a moderate drought in different parts of the region. The highest drought probabilities occur in the western parts of North and South Dakota when the crop is planted from 10 days before to 30 days after normal. Across the rest of the region the probability of a moderate drought generally ranges from 15 to 30 percent across all planting dates. The major exception is in the southern two-thirds of Illinois where a 40 percent chance of a moderate drought exists when the crop is planted 10 days after the normal date of planting.

From ear initiation to the end of row set the probability of a moderate drought ranges from 15 percent to 80 percent. The highest probabilities are in the northwest parts of the region when the crop is planted 20 to 30 days after the normal date of planting. Across the major corn producing states of Iowa, Illinois, Indiana, and Ohio, the probability of a moderate drought generally ranges from 30 to 45 percent. In this major corn producing region there tends to be a minimum moderate drought probability centered over Iowa and a maximum centered over southern Illinois in all the planting dates except 10 days before and 30 days after the normal planting date.

During rapid vegetative growth (end of row set to silk growth stage) the probability of a moderate drought ranges from 15 percent in the extreme southeast to greater than 95 percent in

the west. When the crop is planted 20 to 30 days before normal there is a east-west gradient of the moderate drought probability with the higher drought probabilities to the west. This gradient has an axis that runs from the south-southwest to the north-northeast from central Kansas to central Minnesota. In the western two-thirds of Kansas, all of Nebraska and North and South Dakota, and the western one-half of Minnesota the probability of a moderate drought exceeds 50 percent (1 year out of 2). In the region east of the axis described above the probability of a moderate drought is generally in the range of 30 to 40 percent for all the planting dates from 30 days before through 30 days after normal planting.

For planting dates from 30 before the normal date of planting the probability of a moderate drought during the silk to end of lag phase stage exceeds 50 percent in the western one-half of Minnesota, all of North and South Dakota, Nebraska, and Kansas, and most of Missouri. When the crop is planted from 10 to 20 days before normal planting, the area in Missouri where there is greater than a 50 percent chance of a moderate drought shrinks to the southwest corner of the state. It then expands to include most of the state when planting is delayed to 10 days after normal planting, then again contract to the southwest as planting is delayed to 20 or 30 days after normal planting.

During grain fill, the probability of a moderate drought ranges from greater than 95 percent in the western part of the region to less than 10 percent in the extreme southeast. As planting is delayed from 30 days before the normal date of planting to 20 days after the normal date of planting the area with a moderate drought probability of 90 percent or greater tends to expand. The location of the 50 percent probability line is relatively independent of the day of planting and is located close to the eastern edge of North and South Dakota, Nebraska, and

Kansas until the planting dates after the normal date of planting when the 50 percent line moves to the west in Kansas and Nebraska.

Probability of Mild Drought. As would be expected, the probability of a mild drought is higher than other drought severities. With all the planting dates from 30 days before to 30 days after normal planting, the probability of a mild drought in each of the last four growth stages (ear initiation to end of row set, end of row set to silk, silk to end of lag phase, and end of lag phase to maturity) is greater than 50 percent (Figures H.1.3.12.a-g). All of North and South Dakota, Nebraska, and Kansas have a probability of a mild drought greater than 70 percent during the last two growth stages for all planting dates.

If planting is accomplished on or before the normal date of planting the probability of a mild drought during the period from ear initiation to the end of row set is generally between 35 and 70 percent except along the extreme western edge of the region. If planting is delayed 10 to 20 days after the normal date of planting, most of the four western states in the region have a greater than 70 percent. If, however, the date of planting is delayed to 30 days after the normal date of planting then the area with a probability of a mild drought greater than 70 percent is restricted to the western half of the four western states. In the rest of the region the probabilities of a mild drought do not change much. However, the lowest mild drought probabilities are located in the extreme eastern parts of the region.

From the end of row set to silk most of the region has a probability of a mild drought greater than 70 percent with all planting dates except when the crop is planted 30 days after the normal date of planting. The parts of the region which have less than a 70 percent chance of a mild drought are located in the northern one-half of Wisconsin and Michigan, and the eastern

one-half of Ohio. When planting is delayed until 30 days after the normal date of planting, the probability of a mild drought, in the corn producing states of Illinois, Indiana, and Ohio, decreases to less than 65 percent.

The probability of a mild drought during the growth stage of planting to tassel initiation is generally in the 20 to 40 percent range with all planting dates. For the period from tassel initiation to ear initiation, the probability of a mild drought increases to 30 to 50 percent in the eastern one-half of the region, and to 60 to 80 percent in the western one-half when planting is delayed until after the normal date of planting.

APPLICATIONS TO WEATHER MODIFICATION

Results from the two experiments conducted in this study provide the basic information that will assist decision makers in planning weather modification activities to enhance corn yields. The experiments both showed that a critical growth stage in determining final yield is the period from planting to tassel initiation. Final yield responded to both temperature and rainfall conditions during this growth stage. A major factor therefore in determining the potential returns on weather modification is determined by when the corn crop is planted. If it is planted early (before the normal planting date), air temperatures in the period from planting to tassel initiation will be lower than optimum. However, date of planting studies (Nafziger, 1994) show that the yield loss due to early planting is less than when corn is planted later than the normal date of planting. The yield loss due to colder, early air temperatures may be partially off set by more rainfall during this early growth period.

When the corn crop is planted later than normal, air temperatures become more unfavorable (too hot) and rainfall during the first growth period is less. The probability of having air temperatures greater than the optimum, and reduced rainfall is increased. Furthermore, as planting is delayed the natural cycle of rainfall results in decreasing rainfall and potential evapotranspiration is on the increase due to warmer temperatures and decreased relative humidity. Therefore, there is a greater potential for enhanced yields due to weather modification in this early growth stage when crop planting is delayed. On the negative side, the potential for enhancing yields with weather modification later in the growing season is less because of temperatures are normally greater than the optimum during the early growth stage.

The return on weather modification may be greater when the crop is planted earlier than normal because the yield potential going into the later part of the season will be greater than when the crop is planted later. Because of the higher mean rainfall observed when the crop is planted earlier than normal, the probability that weather modification can be used to enhance crop yields during the planting to tassel initiation growth stage is less than if the crop is planted later than normal when rainfall is beginning to decline and potential evapotranspiration is greater. However, when the crop is planted earlier than normal, weather modification in the later growth stages, particularly the end of row set to silk, and end of lag phase to maturity stages, may result in greater yield enhancement because of a greater yield potential due to more favorable weather in the planting to tassel initiation growth stage.

Yields are enhanced in all corn growth stages whenever water equal to potential evapotranspiration is applied to a crop compared to no rainfall during the growth stages. However, if only limited resources are available and a particular growth stage needs to be

identified to use those resources, then the growth stages which should be targeted are the planting to tassel initiation, end of row set to silk, and end of lag phase to maturity stages. Based on the probability of rainfall not exceeding potential evapotranspiration, the growth stages where rainfall enhancement is most likely to be needed are the end of row set to silk, and the end of lag phase to maturity stages. Results from this experiment show that the same results might be expected if only 50 percent of potential evapotranspiration demands are met during the end of row set to silk growth stage.

Yield expectations from corn crops that have received enhanced rainfall due to weather modification should be modified based on the air temperature during the period from planting to tassel initiation. As the mean maximum and minimum air temperature during this first growth stage increase, yield estimates should be adjusted downward. Because the mechanism for this yield decrease due to increased temperatures is not known, it is impossible to give an exact yield loss with each degree increase of temperature. Based on the slope of the regression of final yields of the soil temperature experiment on minimum air temperature, a yield loss of 0.461 Mg ha^{-1} (7.3 bu ac^{-1}) could be expected for each 1 °C minimum temperature increase. The corresponding value for maximum air temperature is a yield loss of 0.578 Mg ha^{-1} (9.2 bu ac^{-1}).

Maximum yield increases that could be expected from weather modification are 15 kg ha^{-1} mm^{-1} (6.1 bu ac^{-1} $in.^{-1}$) when applied during the planting to tassel initiation and tassel initiation to ear initiation growth stages; 8 kg ha^{-1} mm^{-1} (3.1 bu ac^{-1} $in.^{-1}$) when applied from ear initiation to end of row set and from end of row set to silk; 6 kg ha^{-1} mm^{-1} (2.4 bu ac^{-1} in^{-1}) when applied from silk to end of lag phase; and 2 kg ha^{-1} mm^{-1} (0.9 bu ac^{-1} $in.^{-1}$) when applied from end of lag phase to maturity. These values do not account for the rain that would have been received

without weather modification. Also the increases would be expected only to the extent that the total rainfall is less than the total potential evapotranspiration expected during each growth stage. It is also assumed that each additional mm or inch of rain has the same yield effect as the previous mm or inch. This may not be the case, but the experiment was restricted by available facilities such that this assumption could not be tested.

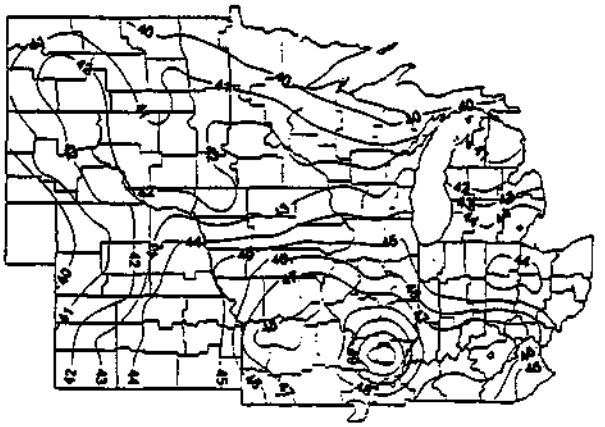

Planting to tassel initiation

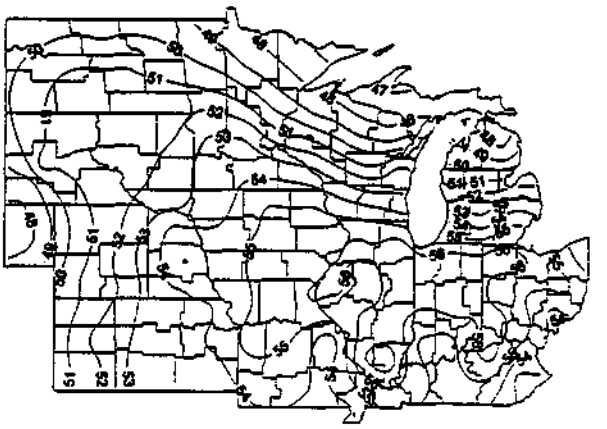

Tassel initiation to ear initiation

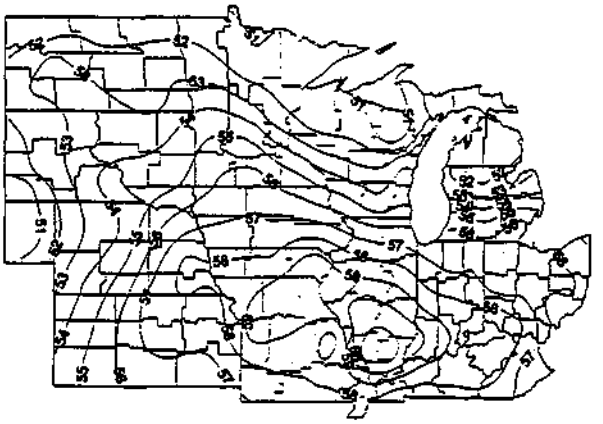

Ear initiation to end-of-row-set

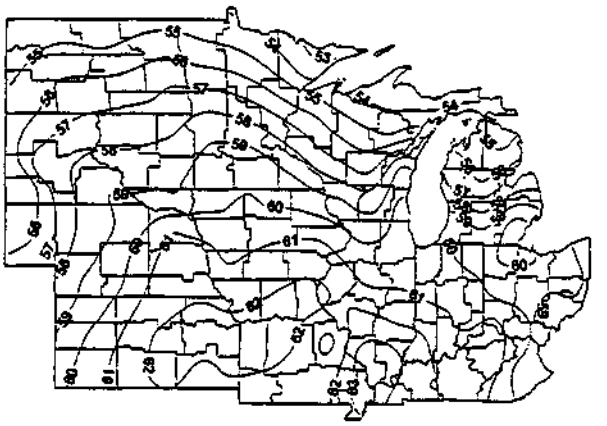

End-of-row-set to silk

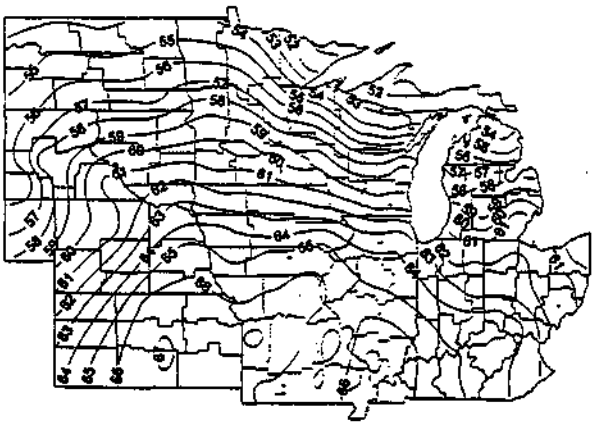

Silk to end*of-lag-phase

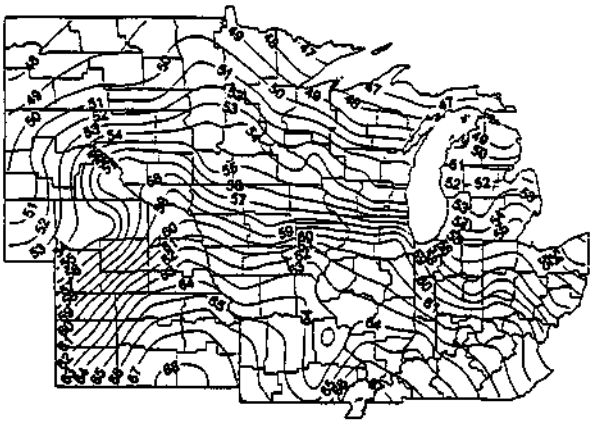

End-of-lag-phase to maturity

Figure H.1.3.5.a. Mean minimum air temperature during the different corn growth stages with a date of planting 30 days before normal. In the Central Corn Belt this represents planting in mid-April.

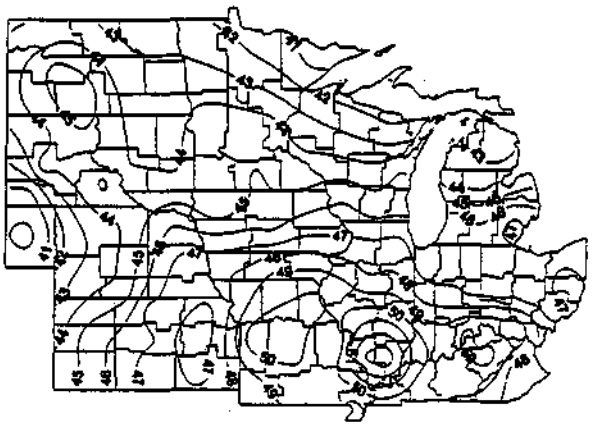

Planting to tassel initiation

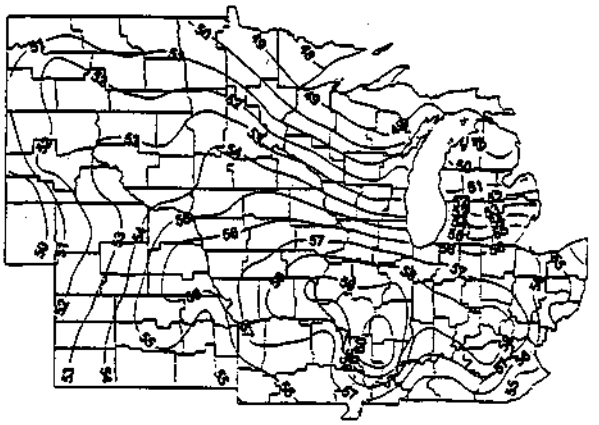

Tassel initiation to ear initiation

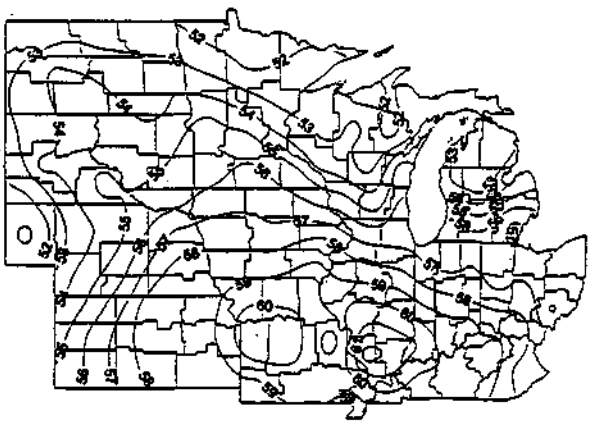

Ear initiation to end-of-row-set

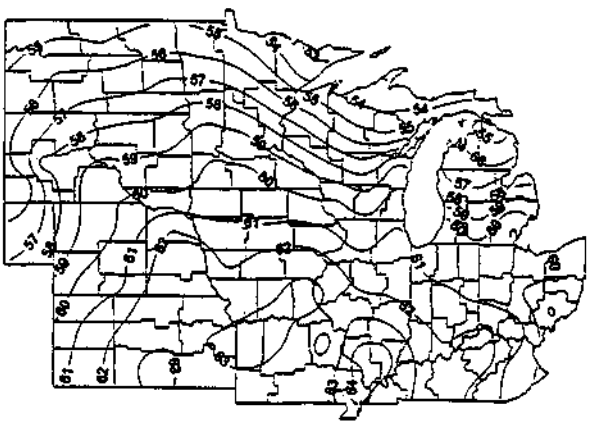

End-of-row-set to silk

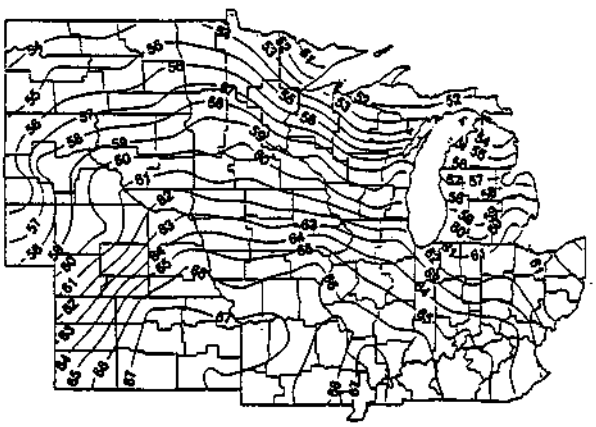

Silk to end-of-lag-phase

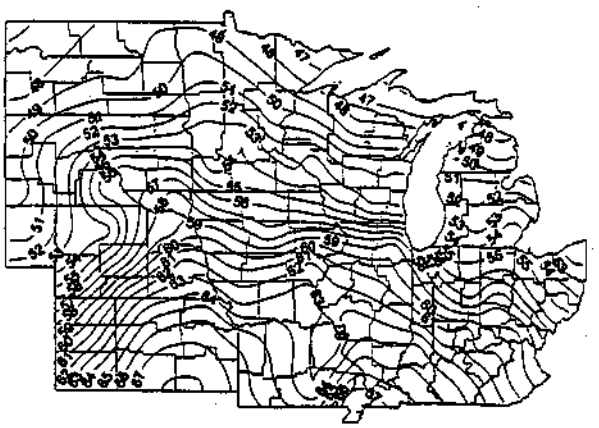

End-of-lag-phase to maturity

Figure H.1.3.5.b. Mean minimum air temperature during the different corn growth stages with a date of planting 20 days before normal. In the Central Com Belt this represents planting in late-April.

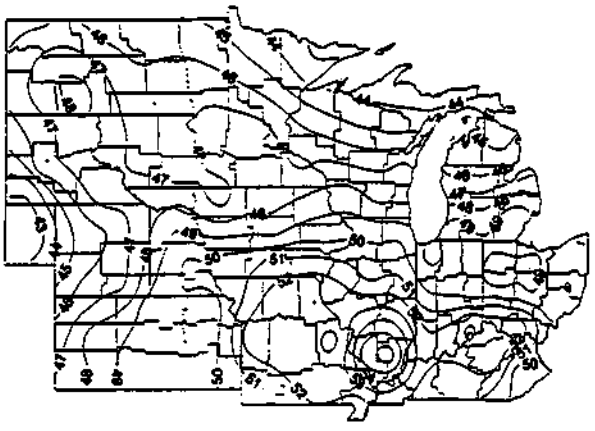

Planting to tassel initiation

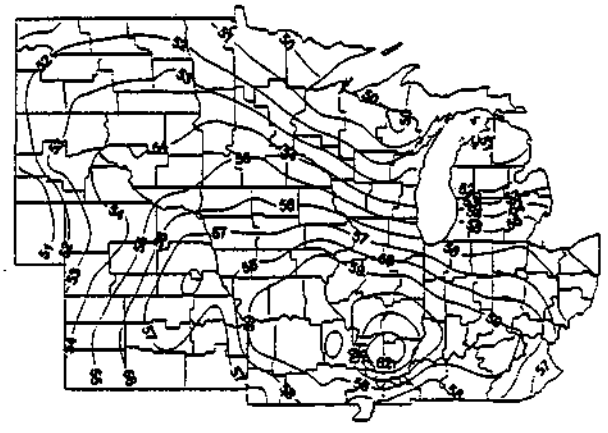

Tassel initiation to ear initiation

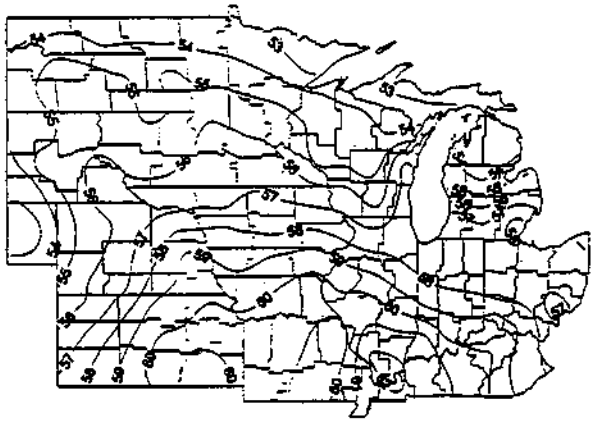

Ear initiation to end-of-row-set

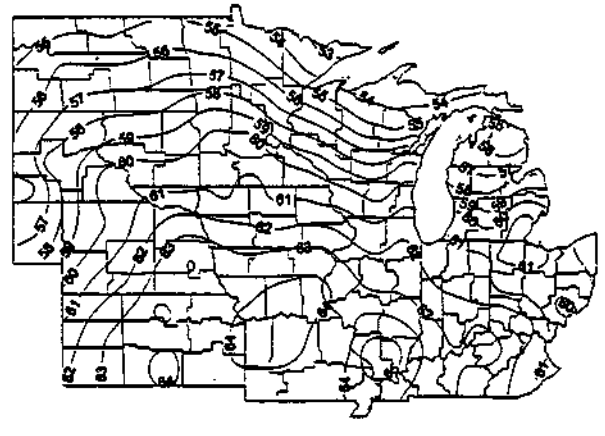

End-of-row-set to silk

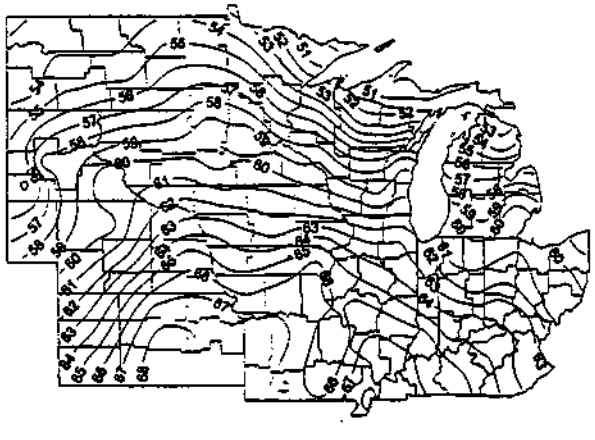

Silk to end-of-lag-phase

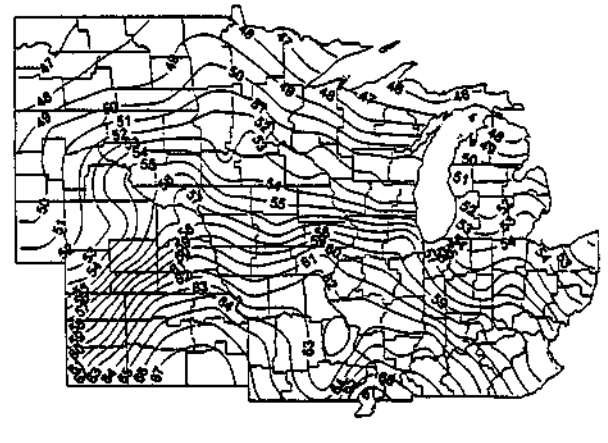

End-of-lag-phase to maturity

Figure H.1.3.5.c. Mean minimum air temperature during the different corn growth stages with a date of planting 10 days before normal. In the Central Com Belt this represents planting in early-May.

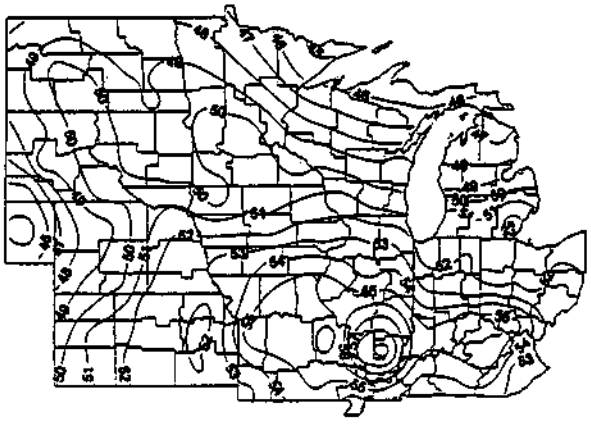

Planting to tassel initiation

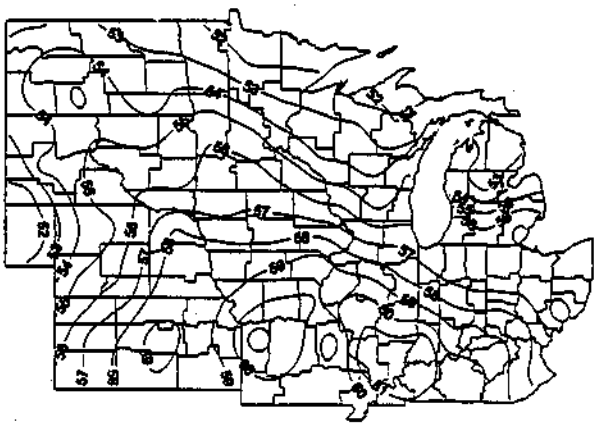

Tassel initiation to ear initiation

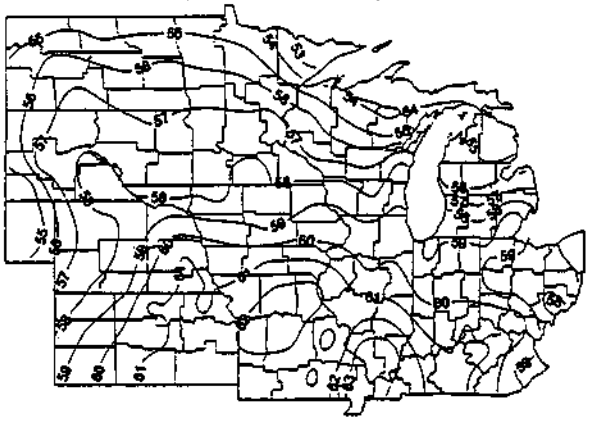

Ear initiation to end-of-row-set

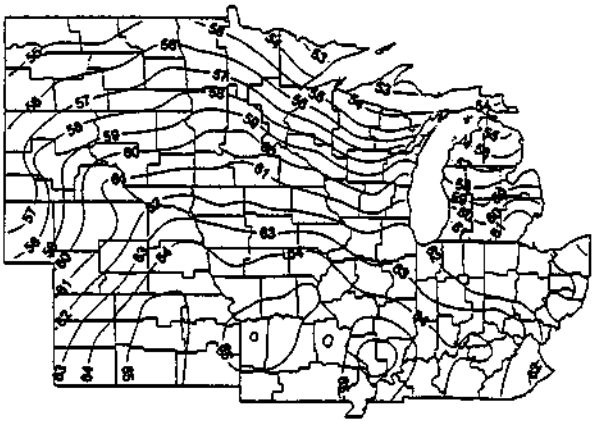

End-of-row-set to silk

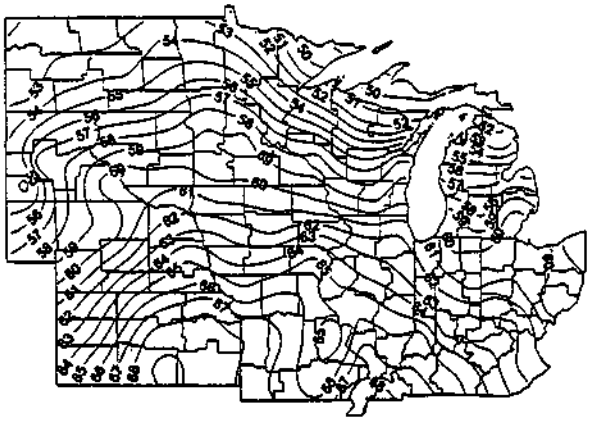

Silk to end-of-lag-phase

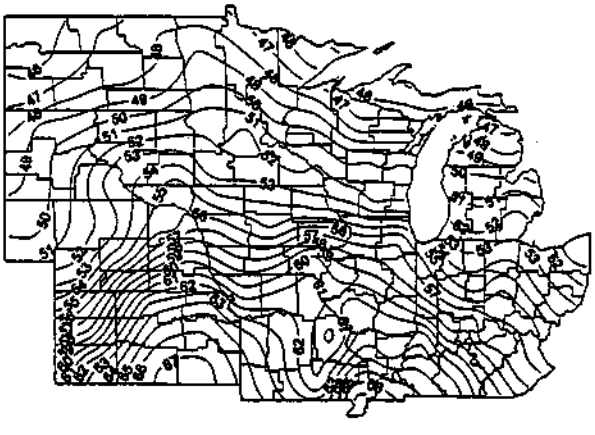

End-of-lag-phase to maturity

Figure H.1.3.5.d. Mean minimum air temperature during the different corn growth stages with a nromal date of planting. In the Central Corn Belt this represents planting in mid-May.

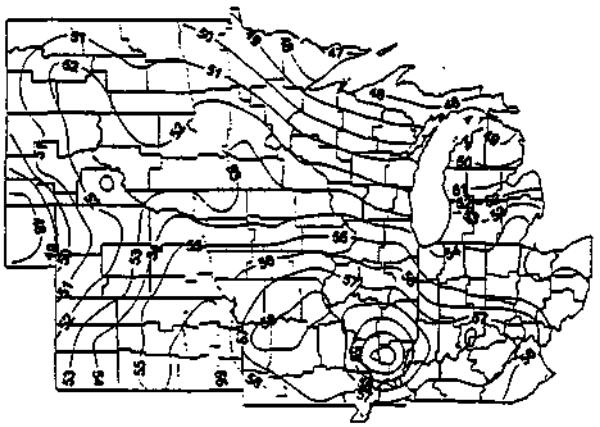

Planting to tassel initiation

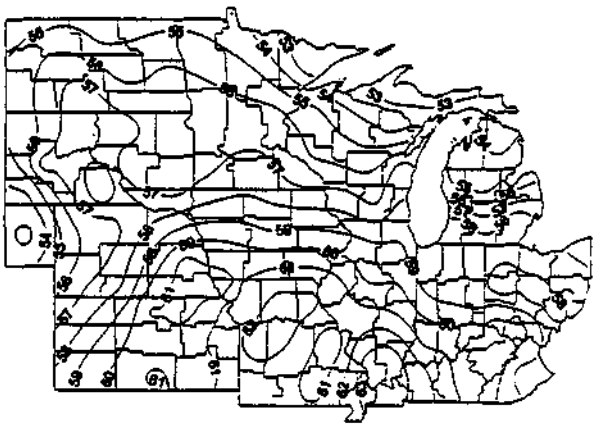

Tassel initiation to ear initiation

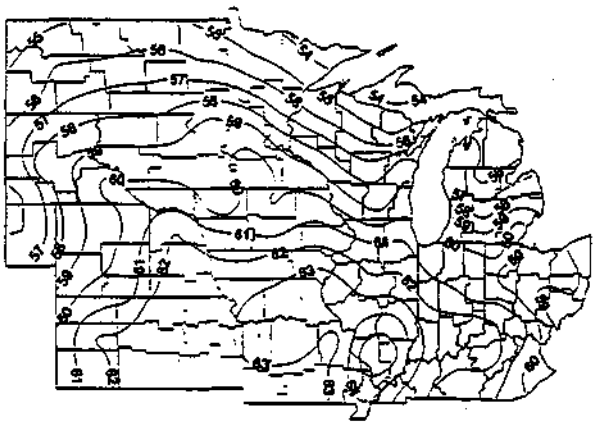

Ear initiation to end-of-row-set

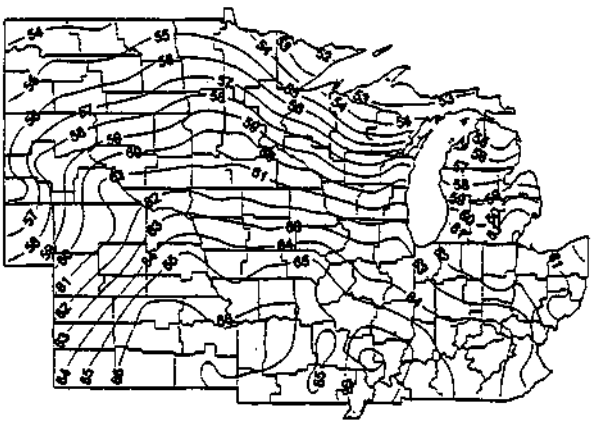

End-of-row-set to silk

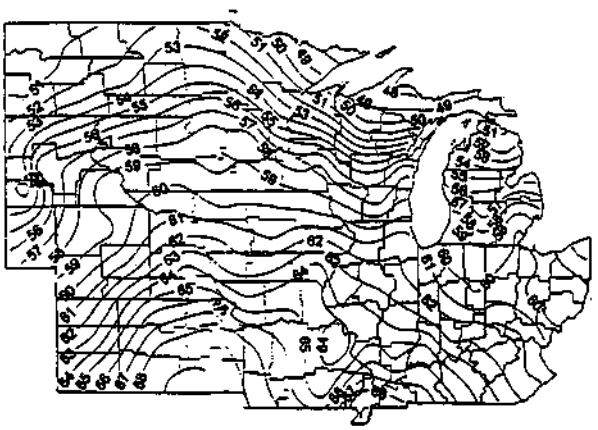

Silk to end-of-lag-phase

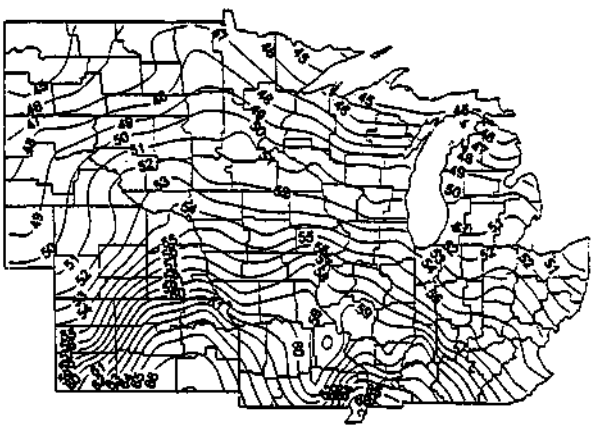

End-of-lag-phase to maturity

Figure H.1.3.5.e. Mean minimum air temperature during the different corn growth stages with a date of planting 10 days after normal. In the Central Corn Belt this represents planting in late-May.

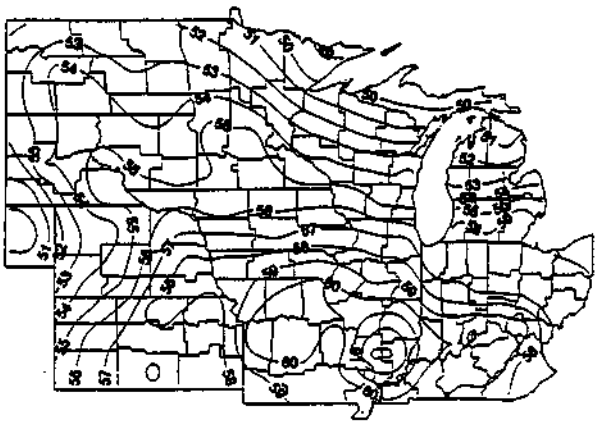

Planting to tassel initiation

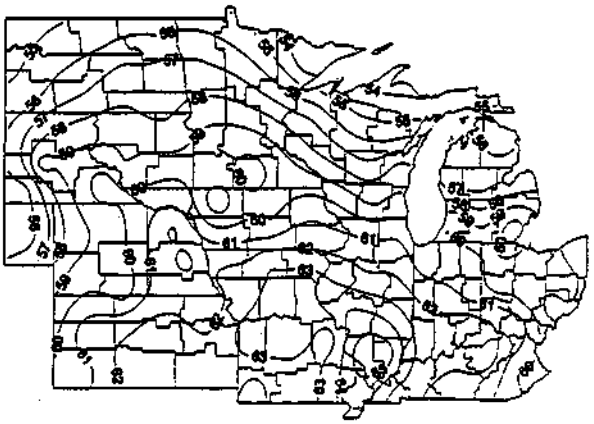

Tassel initiation to ear initiation

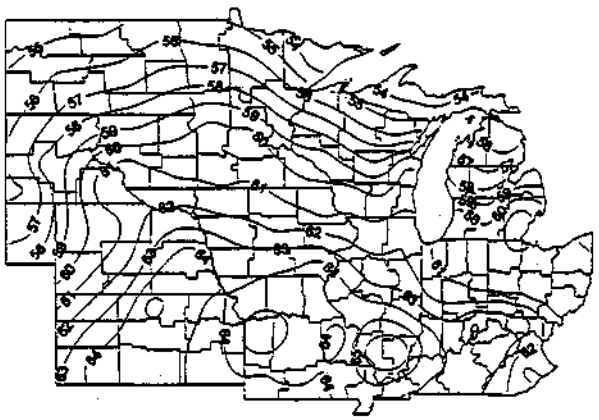

Ear initiation to end-of-row-set

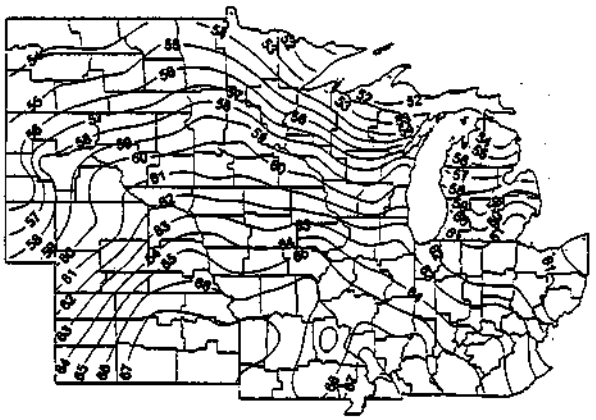

End-of-row-set to silk

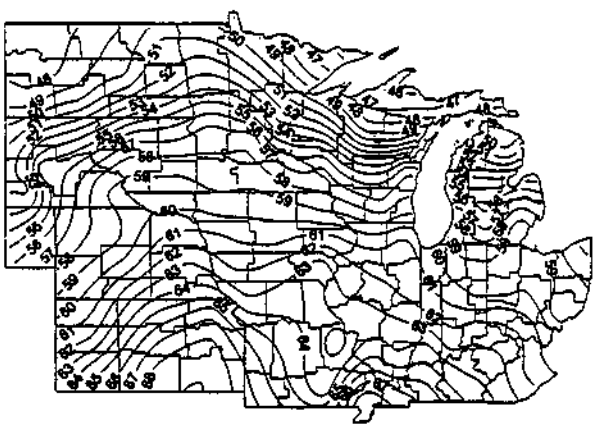

Silk to end-of-lag-phase

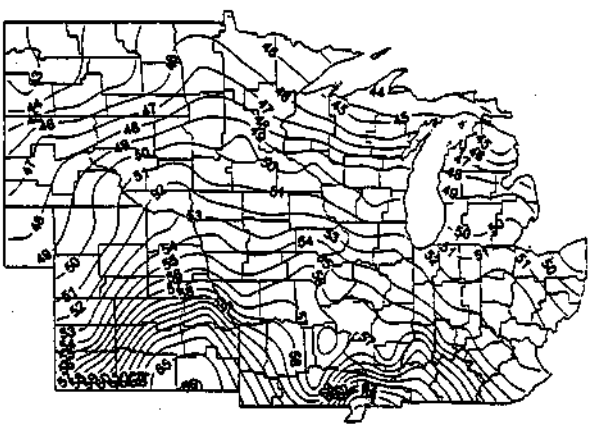

End-of-lag-phase to maturity

Figure H.1.3.5.f. Mean minimum air temperature during the different com growth stages with a date of planting 20 days after normal. In the Central Com Belt this represents planting in early-June.

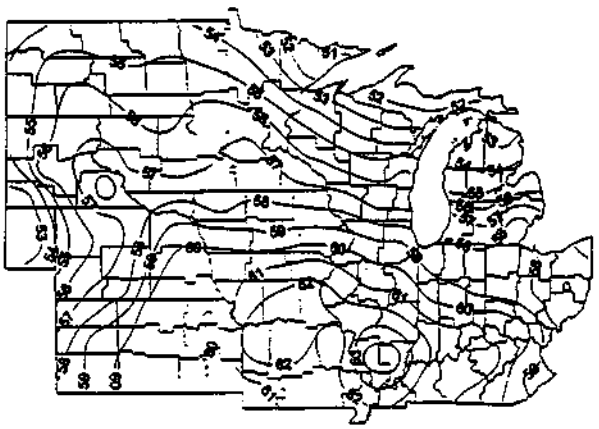

Planting to tassel initiation

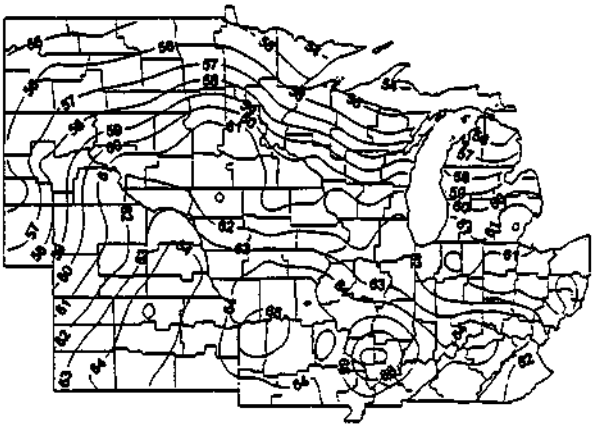

Tassel initiation to ear initiation

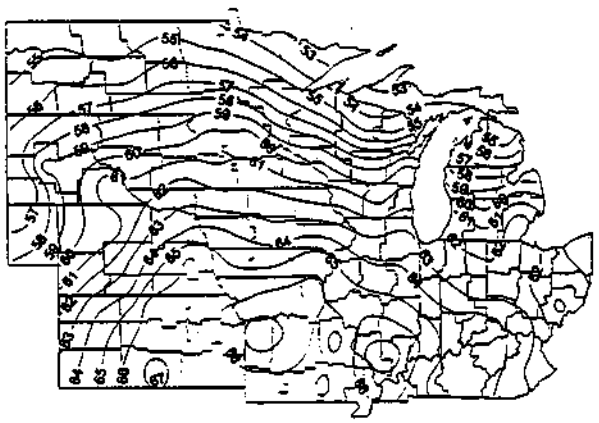

Ear initiation to end-of-row-set

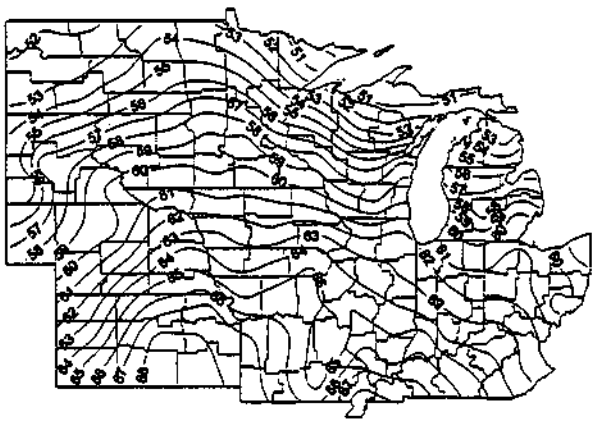

End-of-row-set to silk

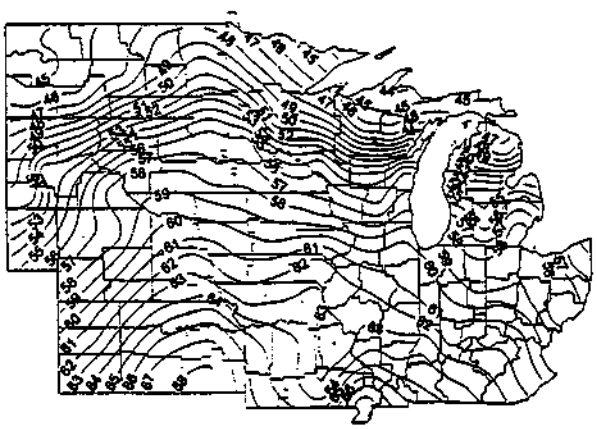

Silk to end-of-lag-phase

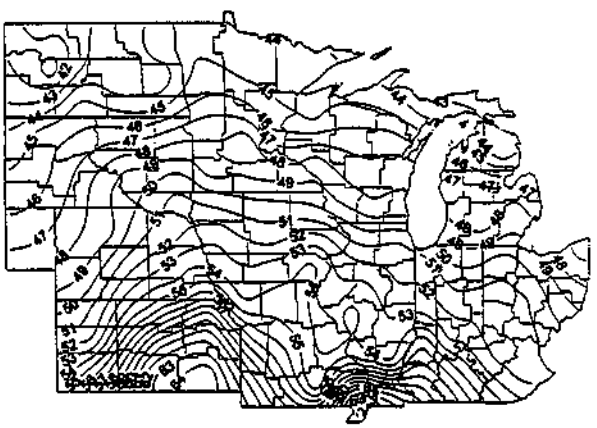

End-of-lag-phase to maturity

Figure H.1.3.5.g. Mean minimum air temperature during the different corn growth stages with a date of planting 30 days after normal. In the Central Corn Belt this represents planting in mid-June.

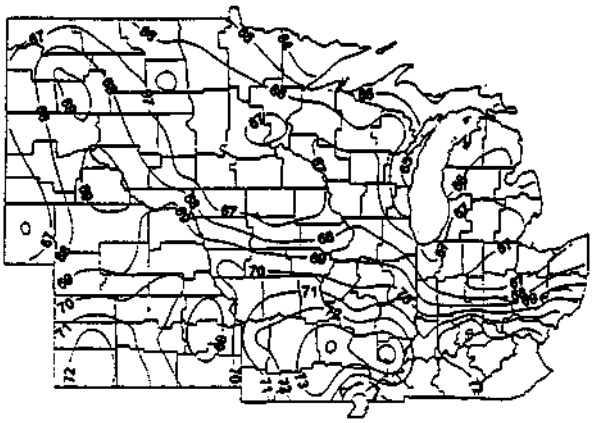

Planting to tassel initiation

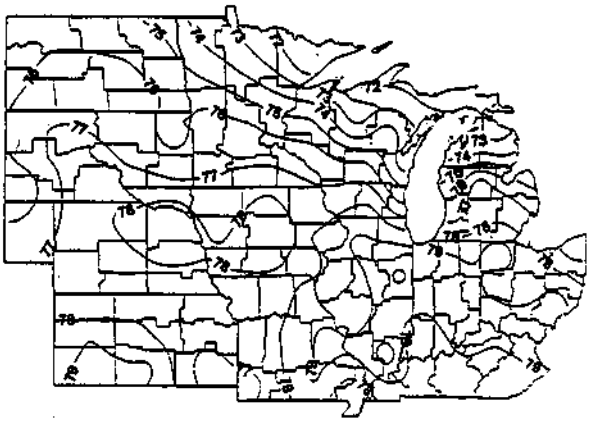

Tassel initiation to ear initiation

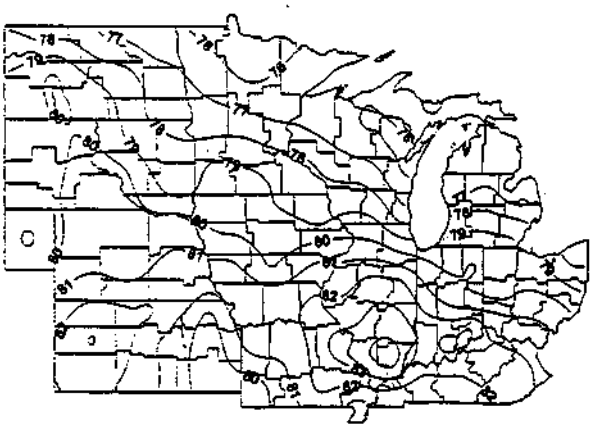

Ear initiation to end-of-row-set

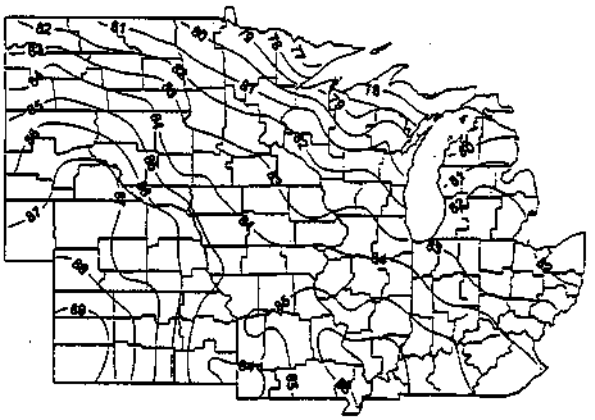

End-of-row-set to silk

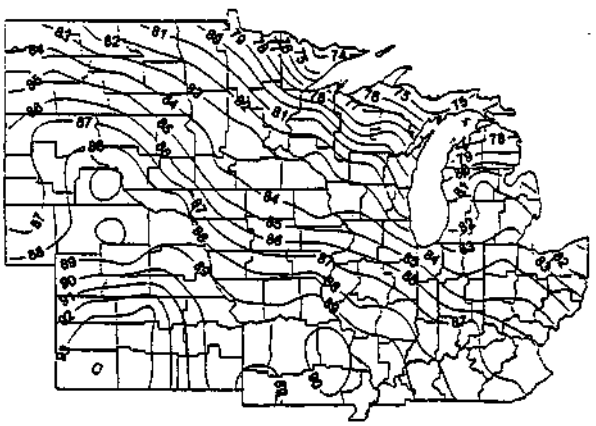

Silk to end-of-lag-phase

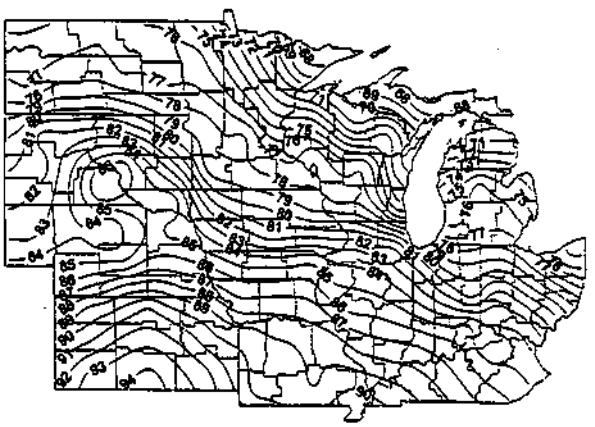

End-of-lag-phase to maturity

Figure H.1.3.6.a. Mean maximum air temperature during the different com growth stages with a date of planting 30 days before normal. In the Central Corn Belt this represents planting in mid-April.

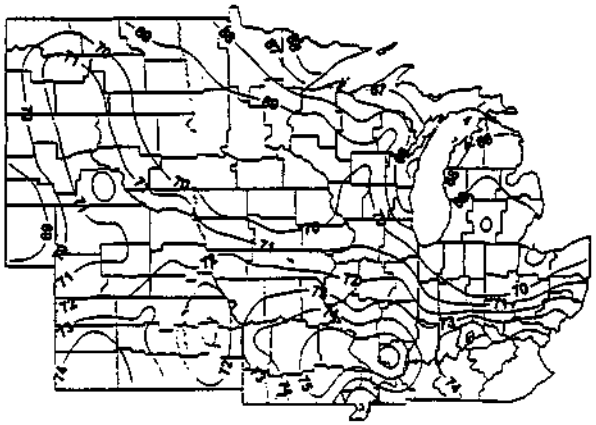

Planting to tassel initiation

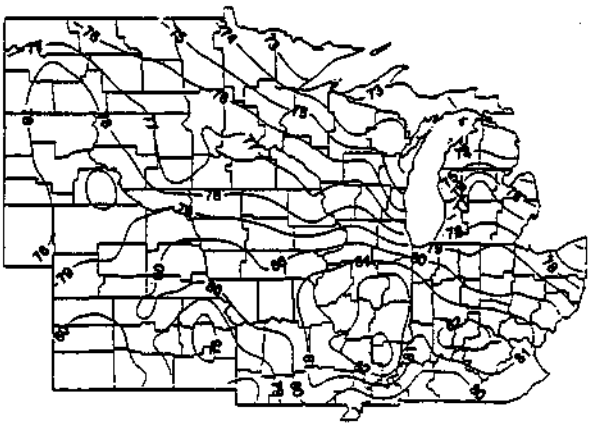

Tassel initiation to ear initiation

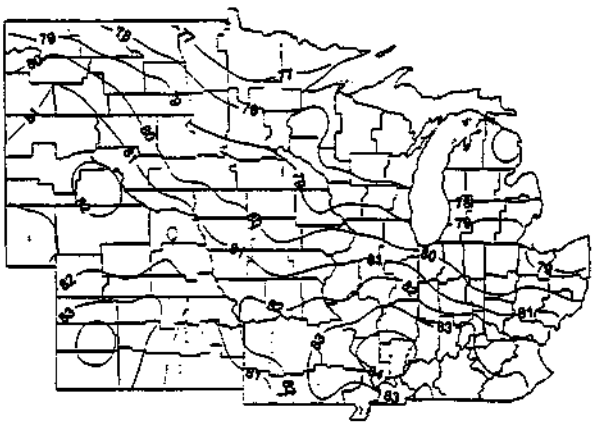

Ear initiation to end-of-row-set

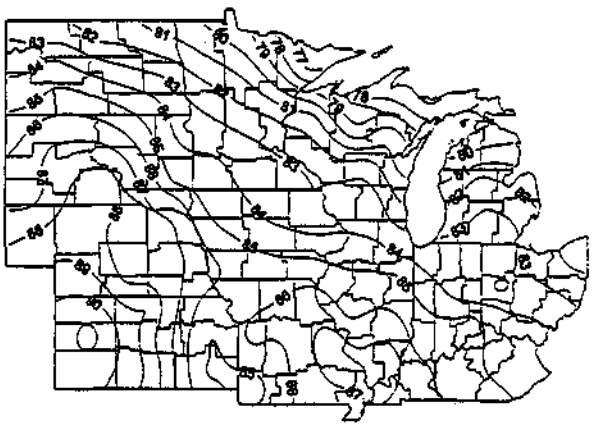

End-of-row-set to silk

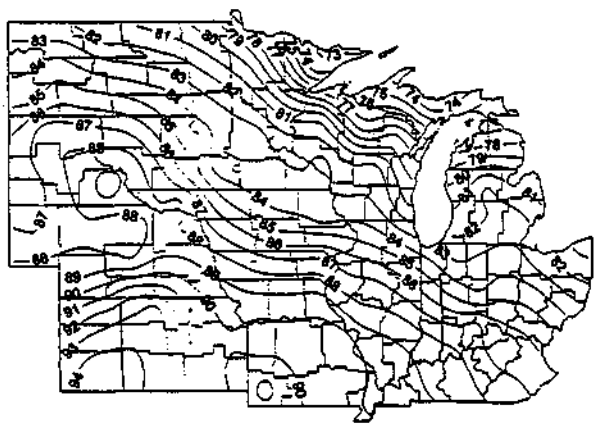

Silk to end-of-lag-phase

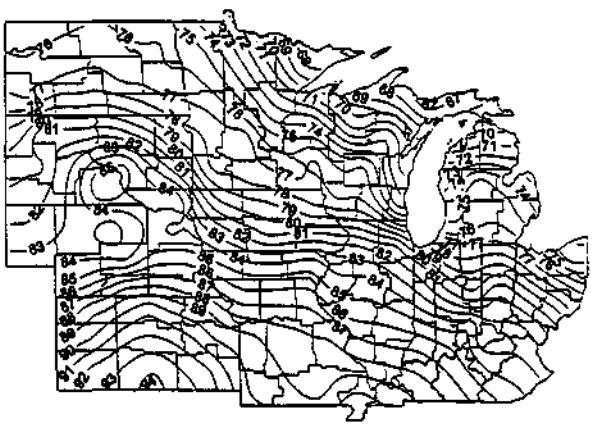

End-of-lag-phase to maturity

Figure H.1.3.6.b. Mean maximum air temperature during the different com growth stages with a date of planting 20 days before normal. In the Central Corn Belt this represents planting in late-April.

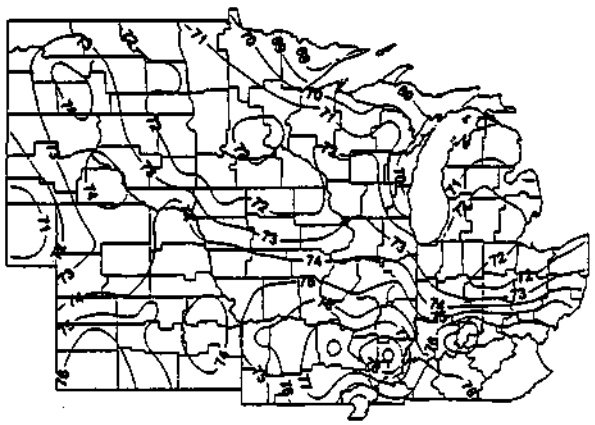

Planting to tassel initiation

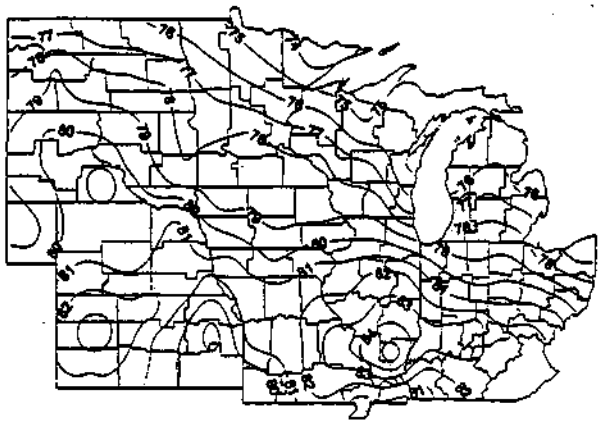

Tassel initiation to ear initiation

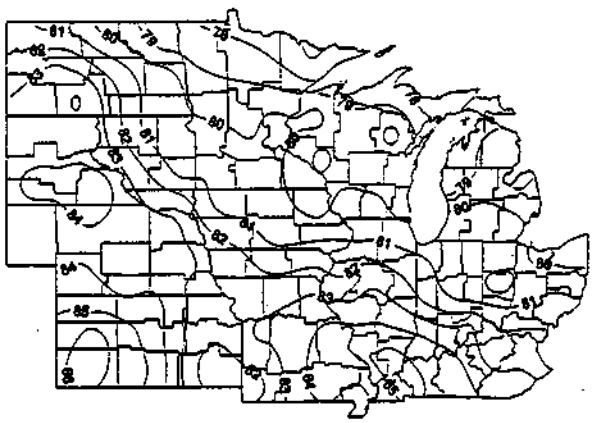

Ear initiation to end-of-row-set

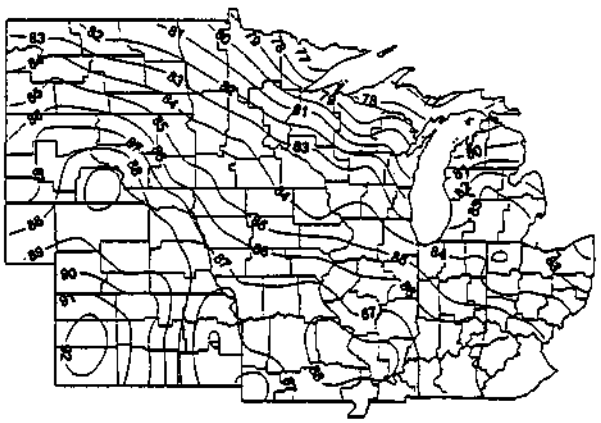

End-of-row-set to silk

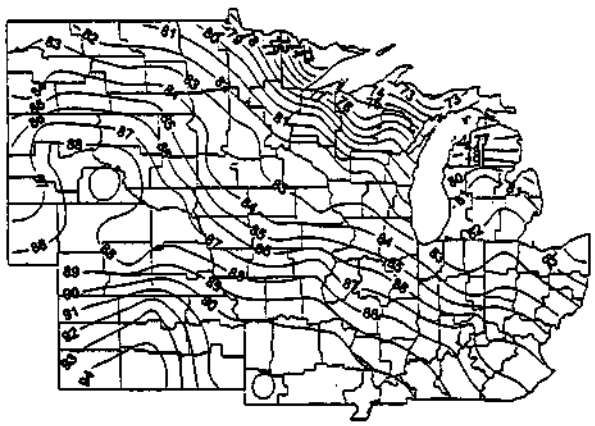

Silk to end-of-lag-phase

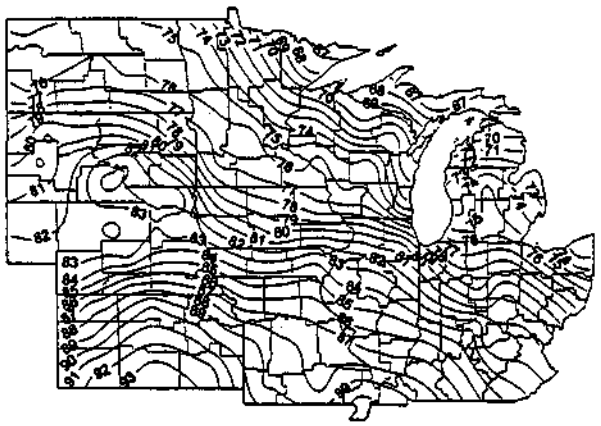

End-of-lag-phase to maturity

Figure H.1.3.6.c. Mean maximum air temperature during the different corn growth stages with a date of planting 10 days before normal. In the Central Corn Belt this represents planting in early-May.

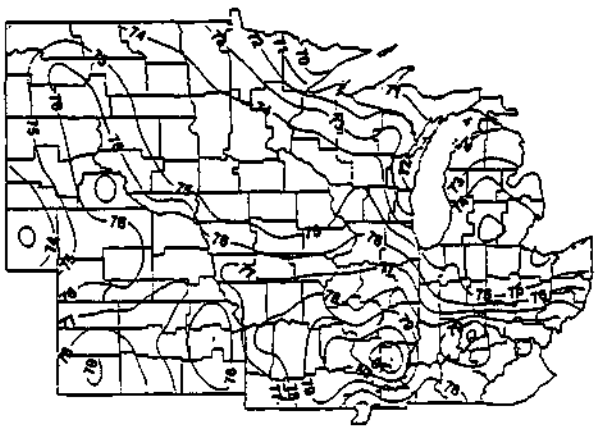

Planting to tassel initiation

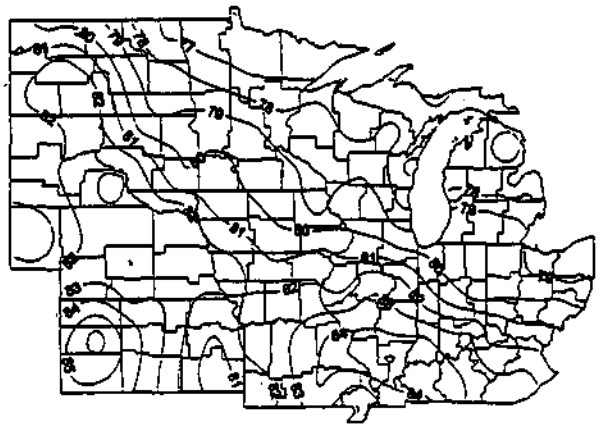

Tassel initiation to ear initiation

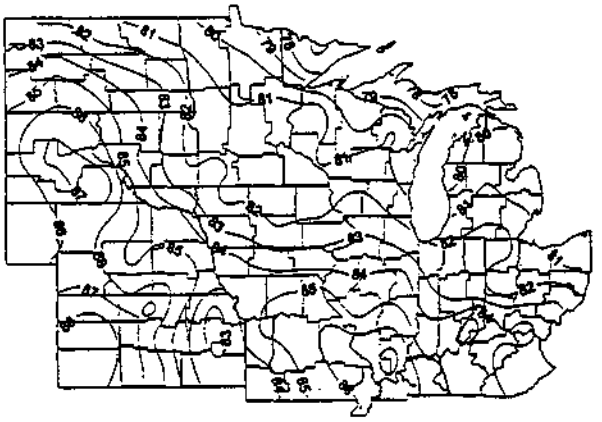

Ear initiation to end-of-row-set

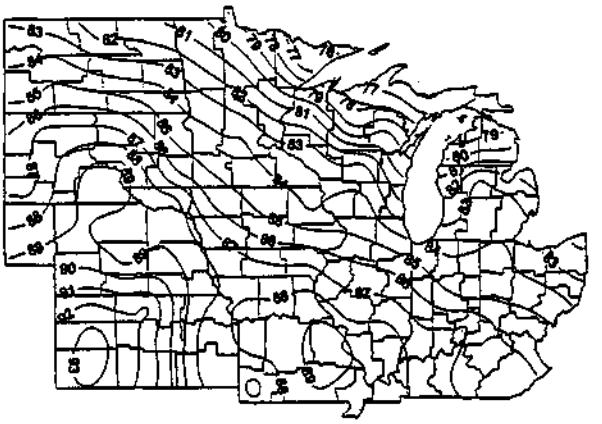

End-of-row-set to silk

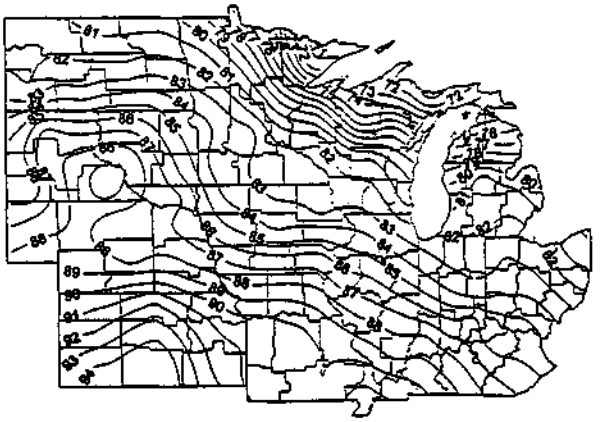

Silk to end-of-lag-phase

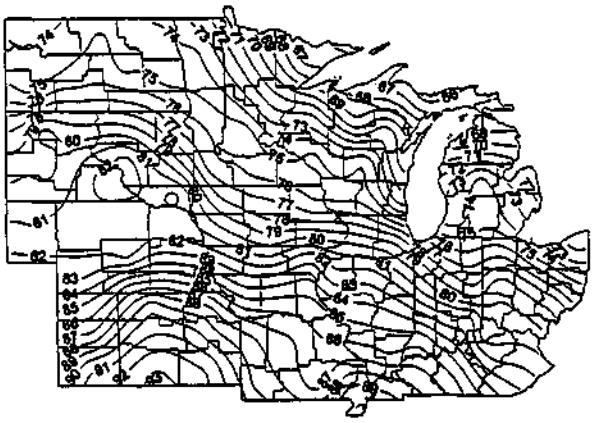

End-of-lag-phase to maturity

Figure H.1.3.6.d. Mean maximum air temperature during the different com growth stages with a nromal date of planting. In the Central Com Belt this represents planting in mid-May.

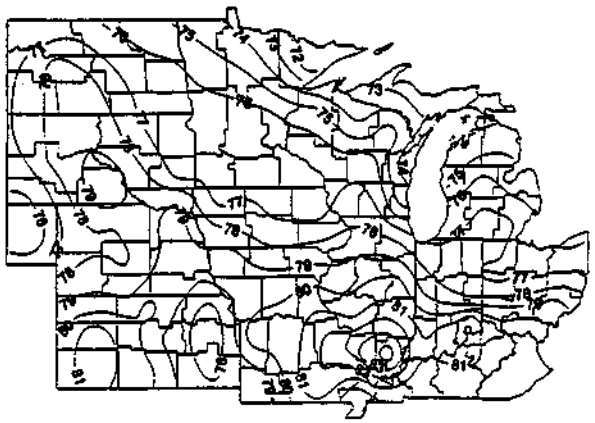

Planting to tassel initiation

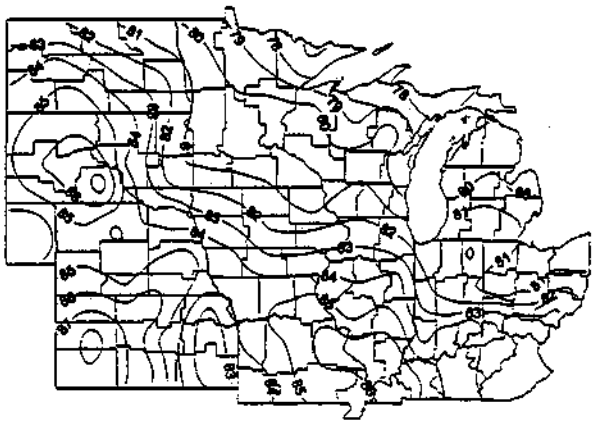

Tassel initiation to ear initiation

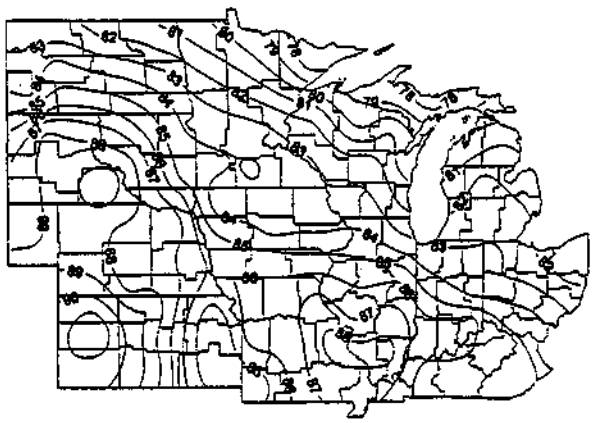

Ear initiation to end-of-row-set

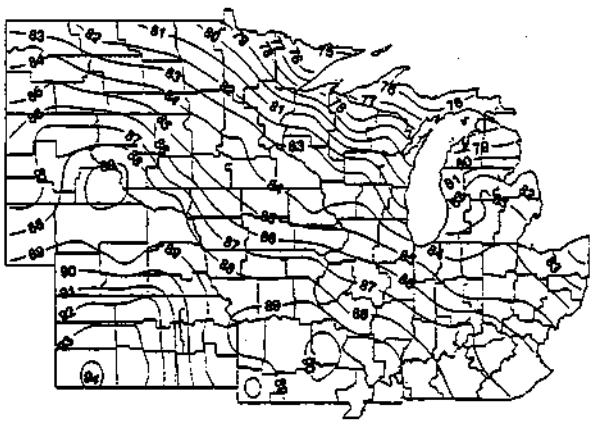

End-of-row-set to silk

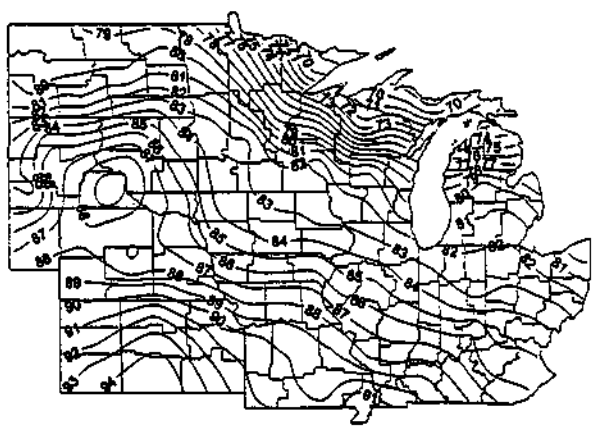

Silk to end-of-lag-phase

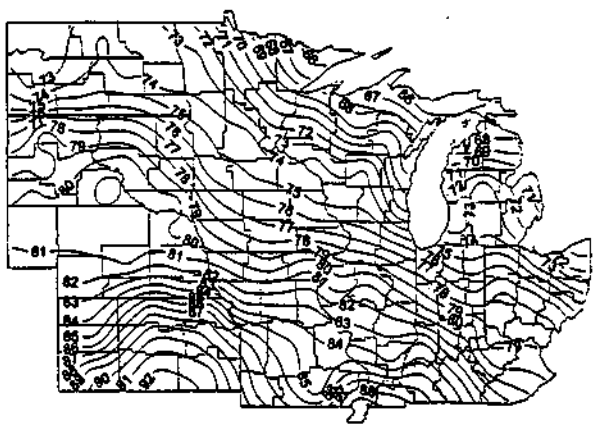

End-of-lag-phase to maturity

Figure H.1.3.6.e. Mean maximum air temperature during the different com growth stages with a date of planting 10 days after normal. In the Central Corn Belt this represents planting in late-May.

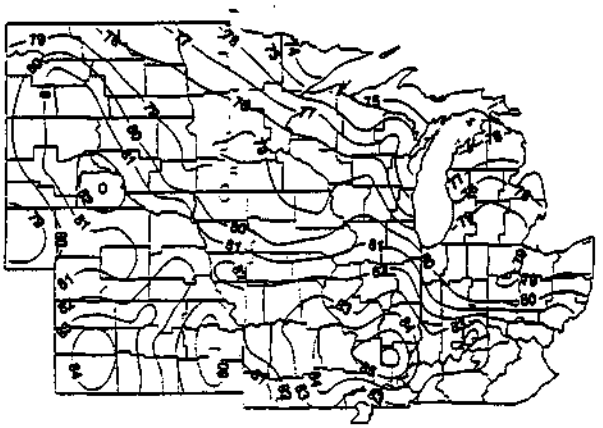

Planting to tassel initiation

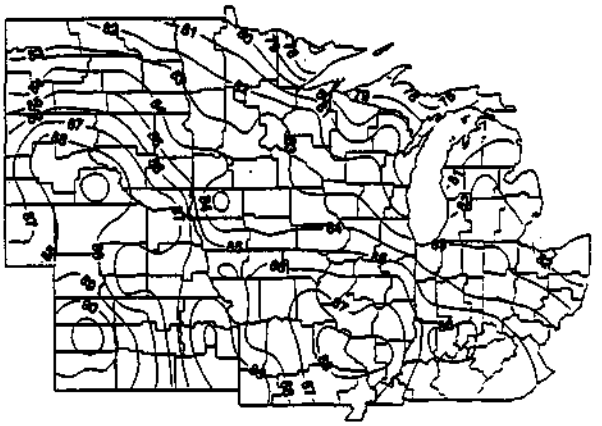

Tassel initiation to ear initiation

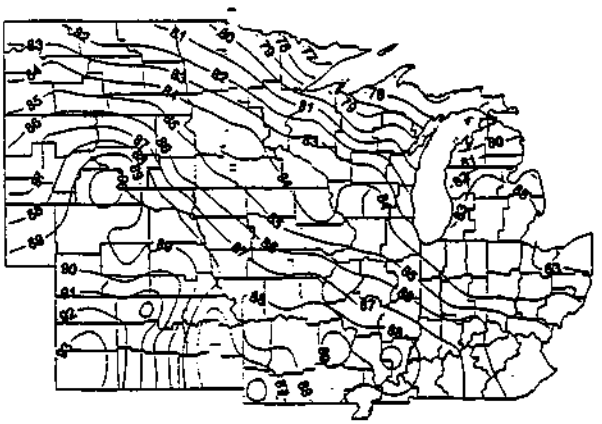

Ear initiation to end-of-row-set

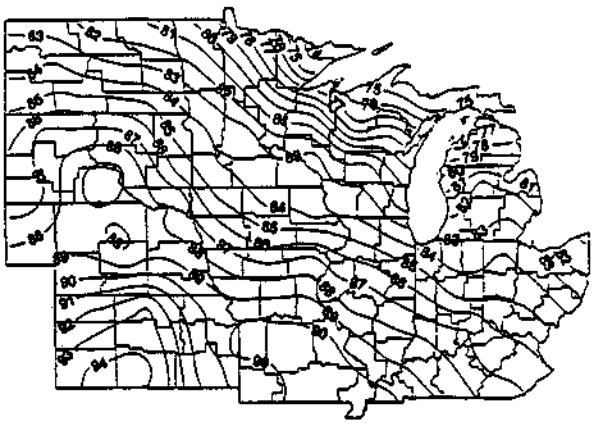

End-of-row-set to silk

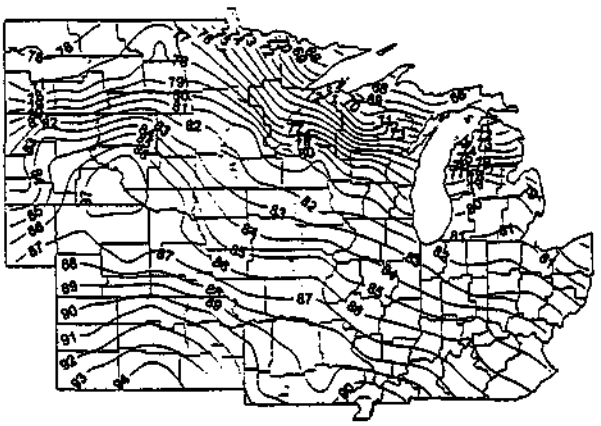

Silk to end-of-lag-phase

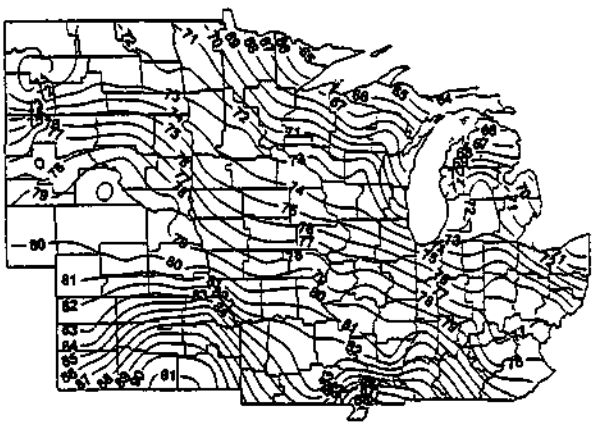

End-of-lag-phase to maturity

Figure H.1.3.6.f. Mean maximum air temperature during the different com growth stages with a date of planting 20 days after normal. In the Central Corn Belt this represents planting in early-June.

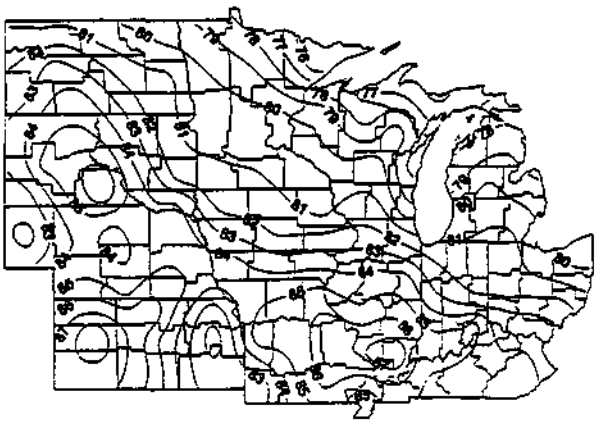

Planting to tassel initiation

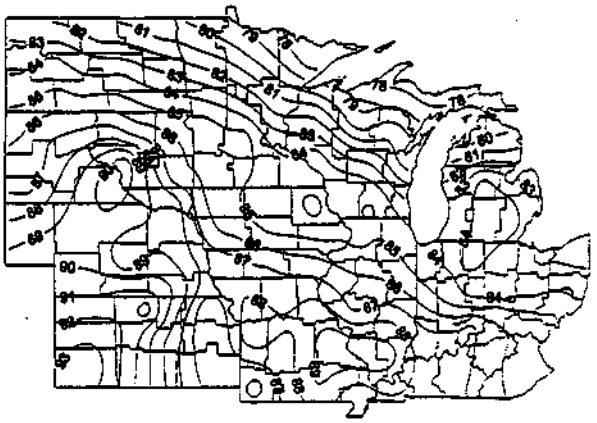

Tassel initiation to ear initiation

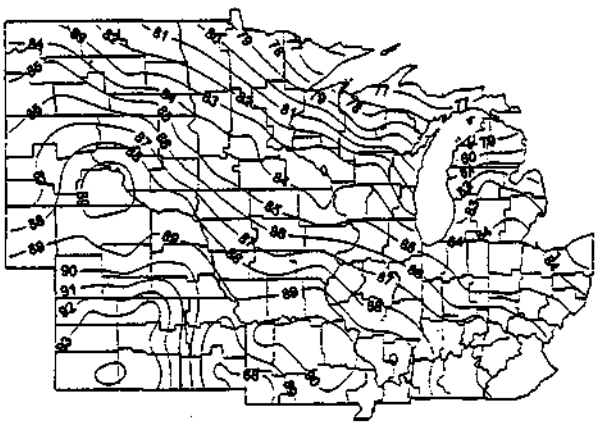

Ear initiation to end-of-row-set

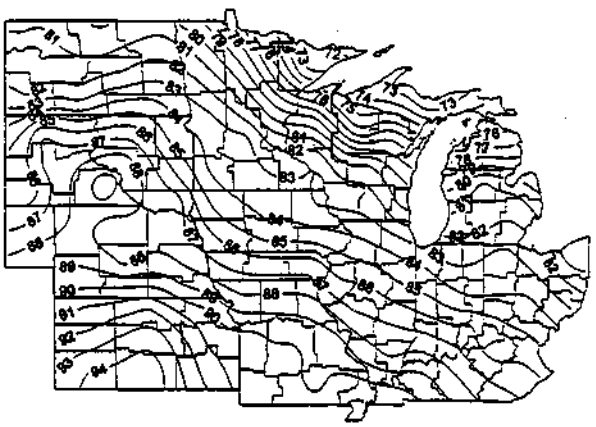

End-of-row-set to silk

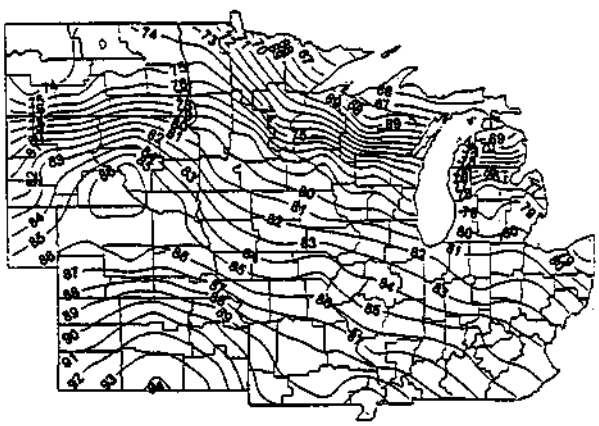

Silk to end-of-lag-phase

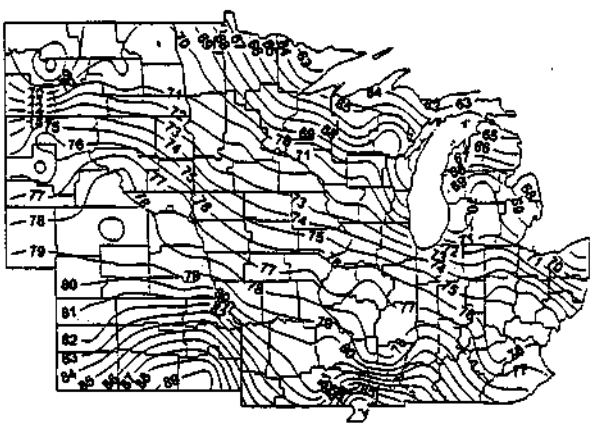

End-of-lag-phase to maturity

Figure H.1.3.6.g. Mean maximum air temperature during the different corn growth stages with a date of planting 30 days after normal. In the Central Com Belt this represents planting in mid-June.

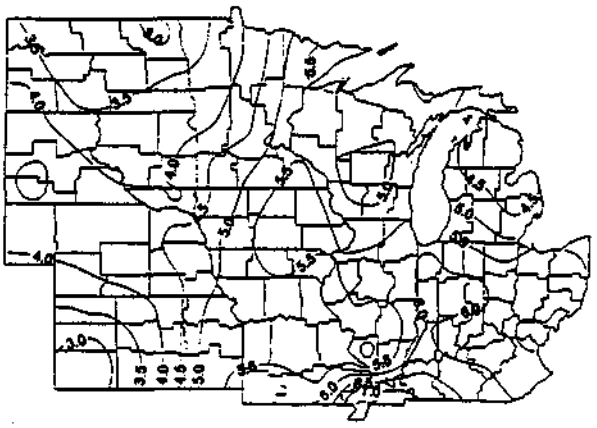

Planting to tassel initiation

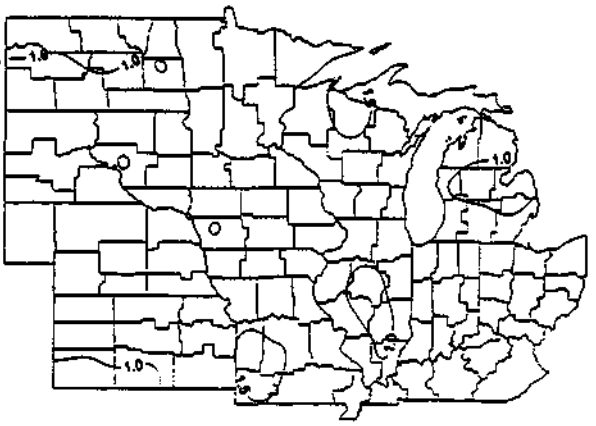

Tassel initiation to ear initiation

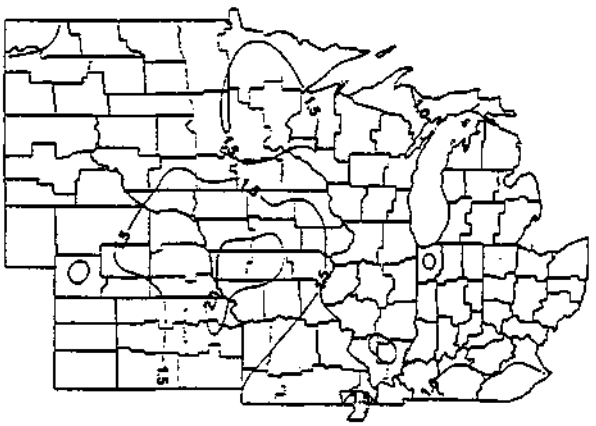

Ear initiation to end-of-row-set

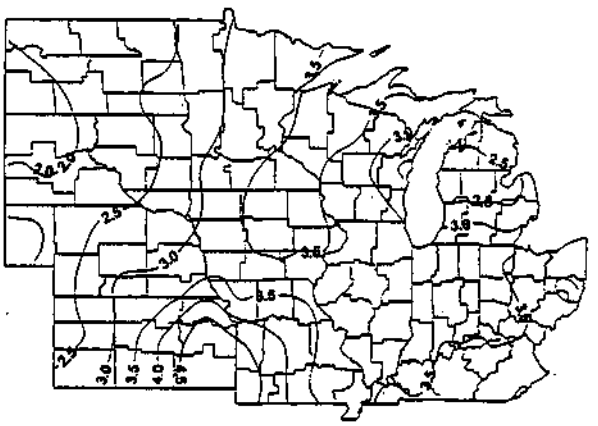

End-of-row-set to silk

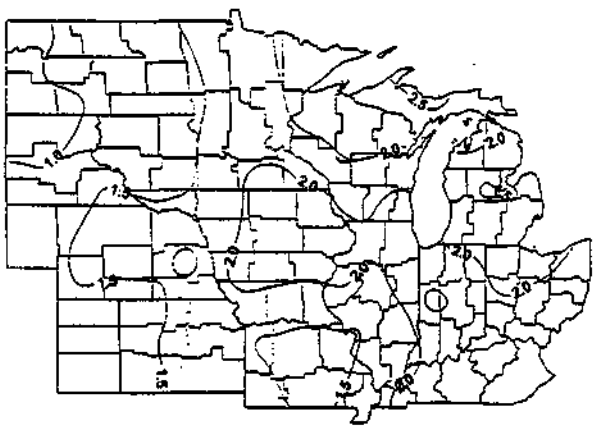

Silk to end-of-lag-phase

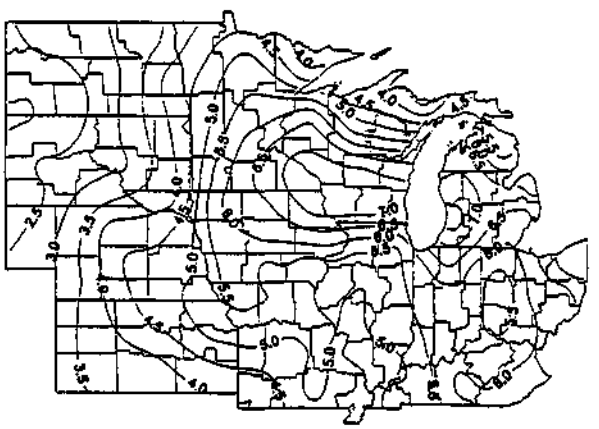

End-of-lag-phase to maturity

Figure H.1.3.7.a. Mean precipitation during the different corn growth stages with a date of planting 30 days before normal. In the Central Corn Belt this represents planting in mid-April.

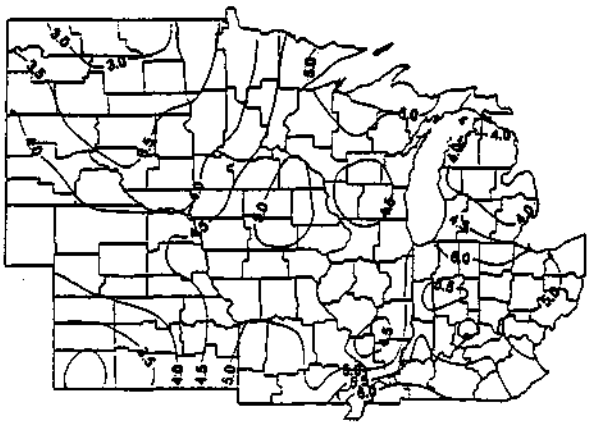

Planting to tassel initiation

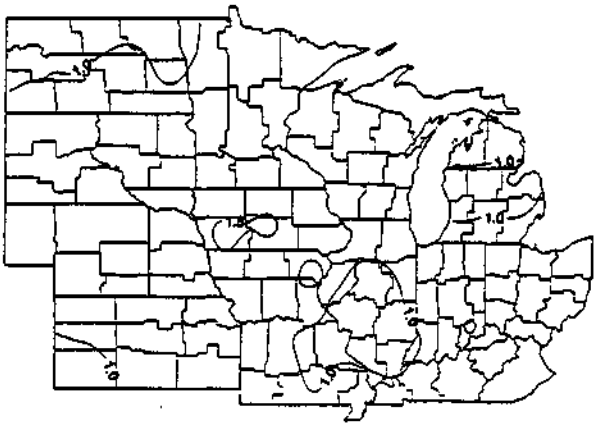

Tassel initiation to ear initiation

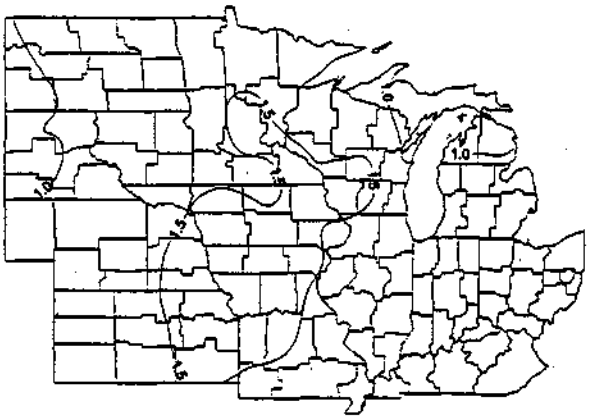

Ear initiation to end-of-row-set

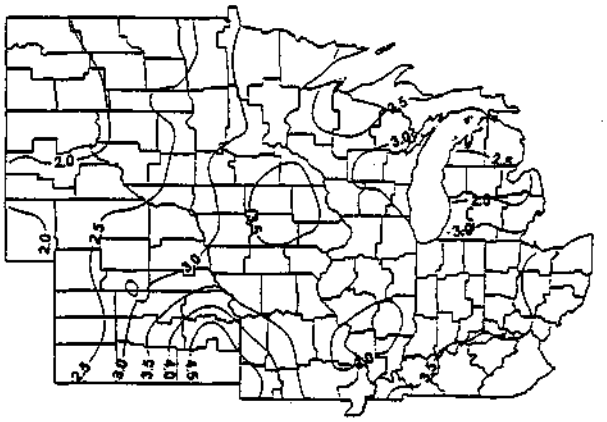

End-of-row-set to silk

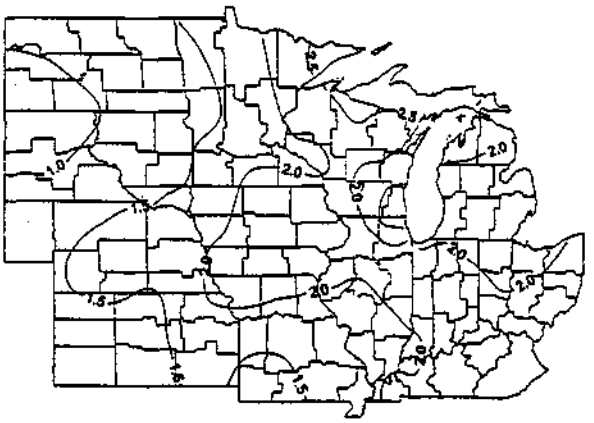

Silk to end-of-lag-phase

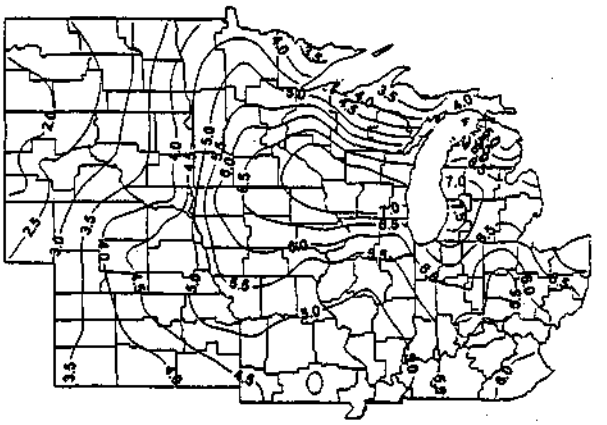

End-of-lag-phase to maturity

Figure H.1.3.7.b. Mean precipitation during the different corn growth stages with a date of planting 20 days before normal. In the Central Com Belt this represents planting in late-April.

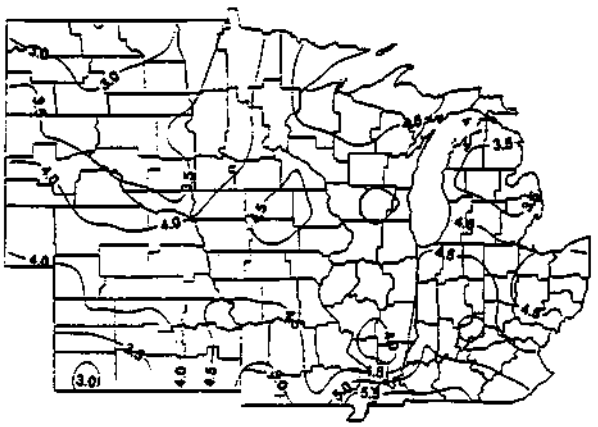

Planting to tassel initiation

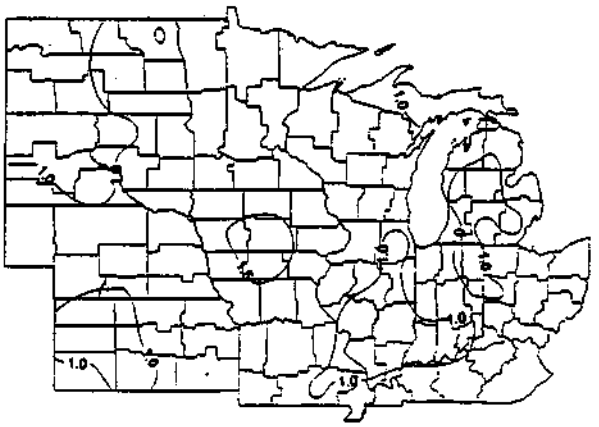

Tassel initiation to ear initiation

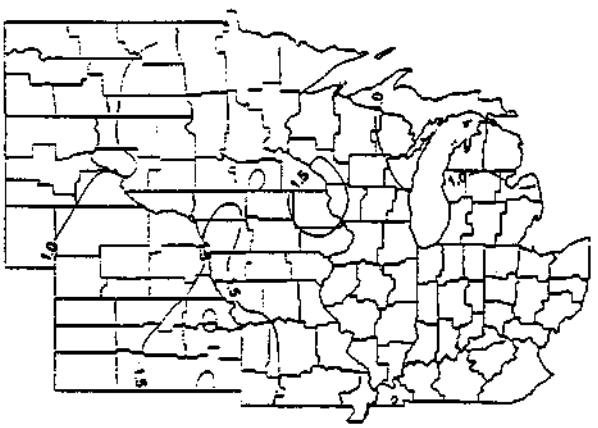

Ear initiation to end-of-row-set

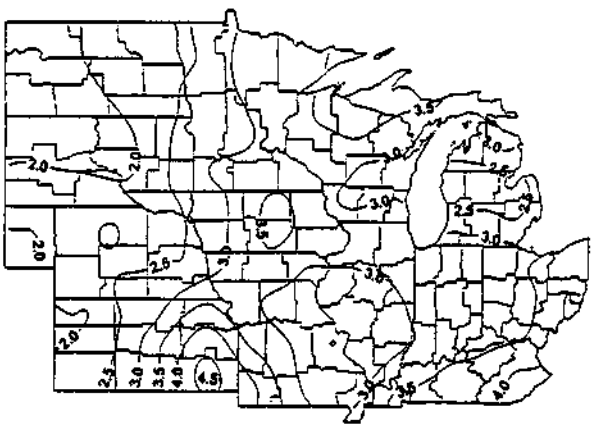

End-of-row-set to silk

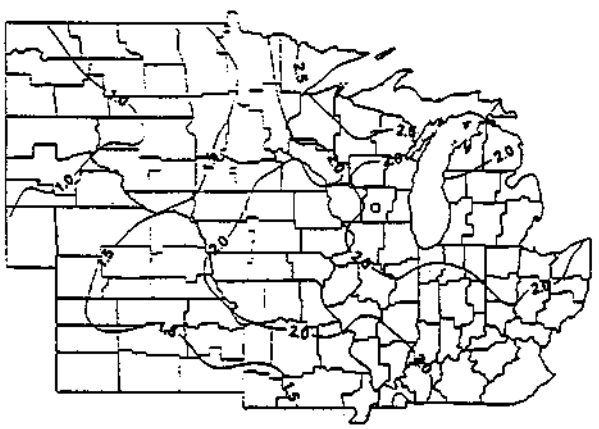

Silk to end-of-lag-phase

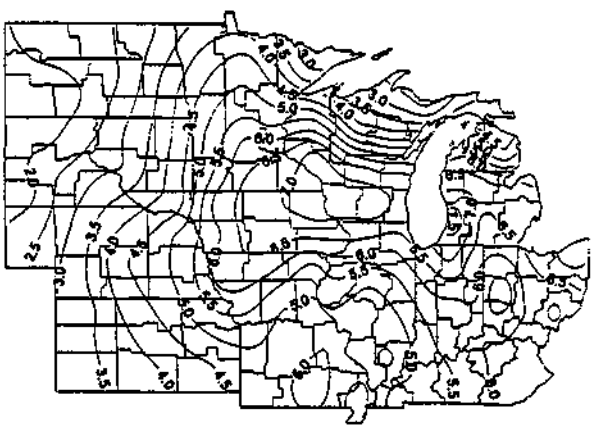

End-of-lag-phase to maturity

Figure H.1.3.7.c. Mean precipitation during the different com growth stages with a date of planting 10 days before normal. In the Central Corn Belt this represents planting in early-May.

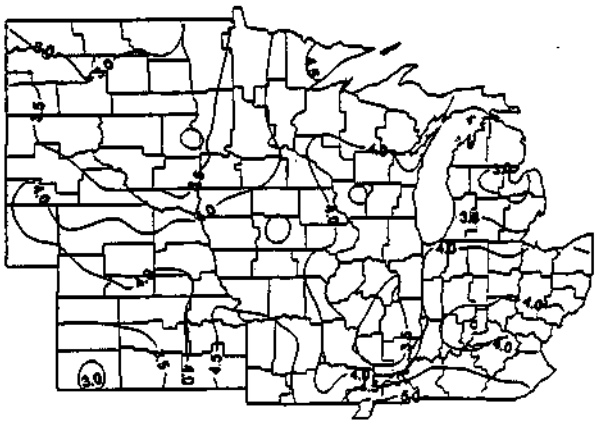

Planting to tassel initiation

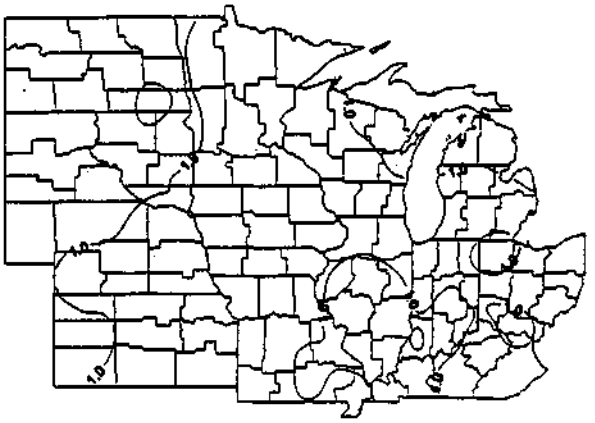

Tassel initiation to ear initiation

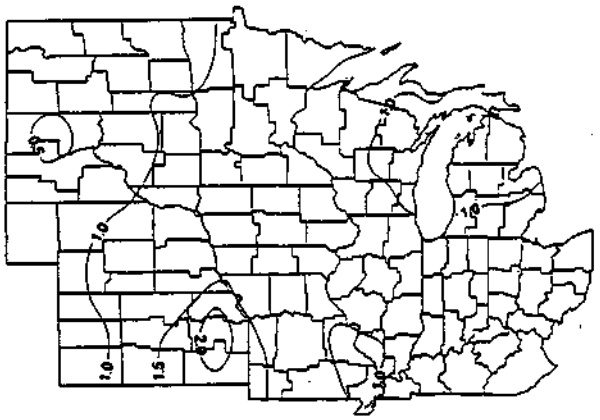

Ear initiation to end-of-row-set

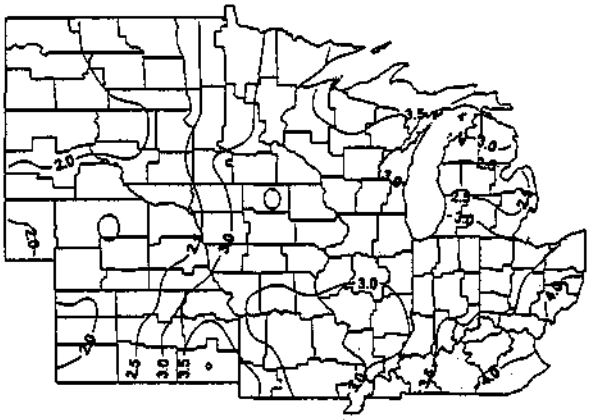

End-of-row-set to silk

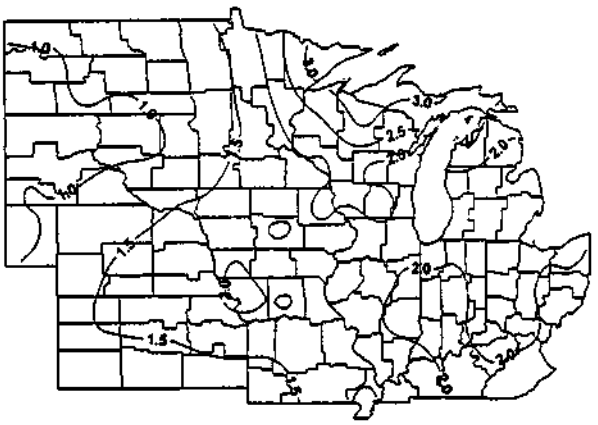

Silk to end-of-lag-phase

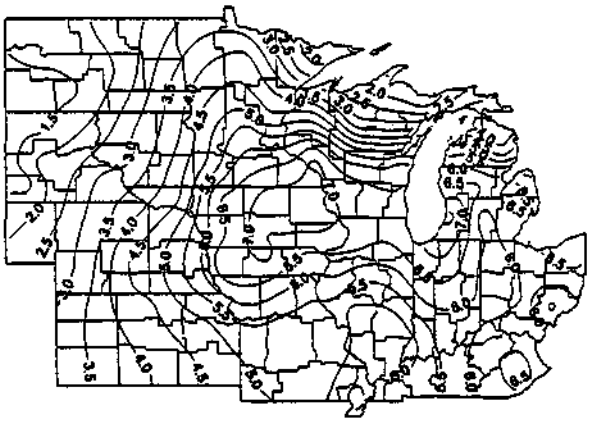

End-of-lag-phase to maturity

Figure H.1.3.7.d. Mean precipitation during the different com growth stages with a nromal date of planting. In the Central Corn Belt this represents planting in mid-May.

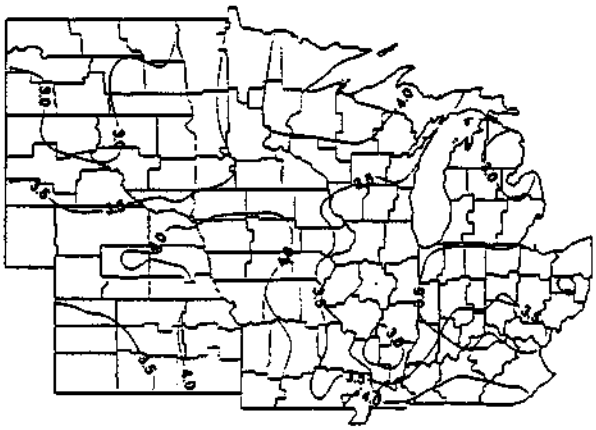

Planting to tassel initiation

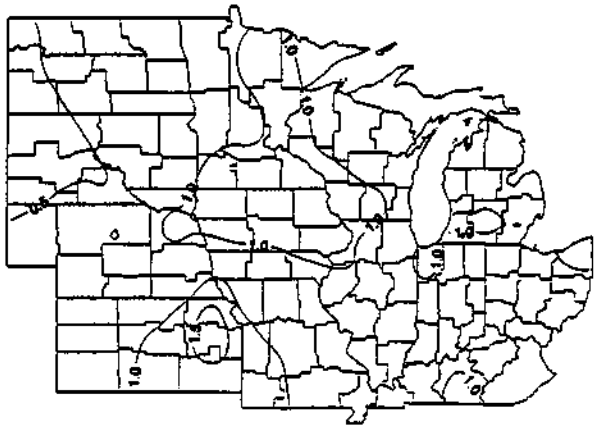

Tassel initiation to ear initiation

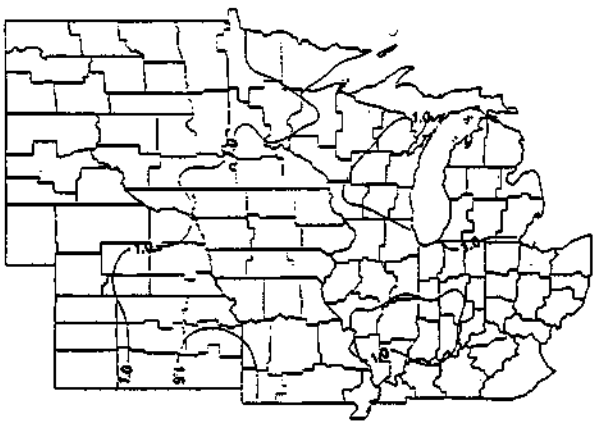

Ear initiation to end-of-row-set

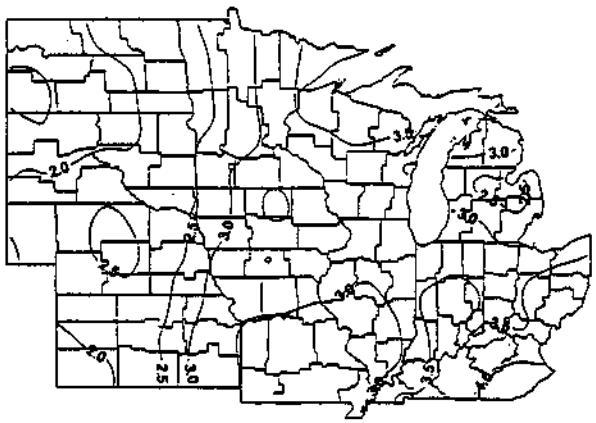

End-of-row-set to silk

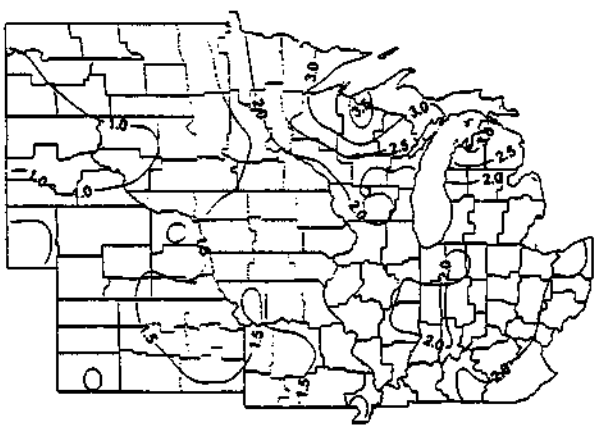

Silk to end-of-lag-phase

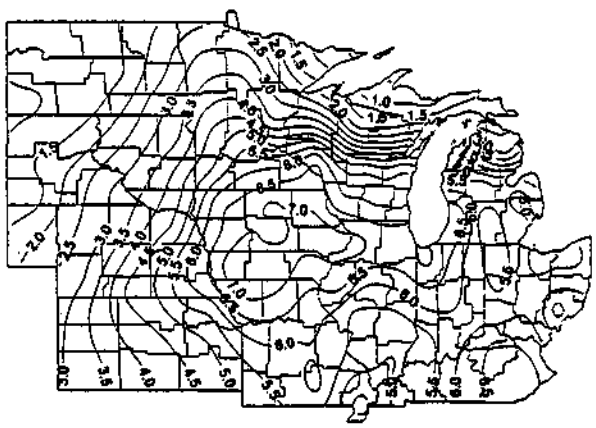

End-of-lag-phase to maturity

Figure H.1.3.7.e. Mean precipitation during the different com growth stages with a date of planting 10 days after normal. In the Central Corn Belt this represents planting in late-May.

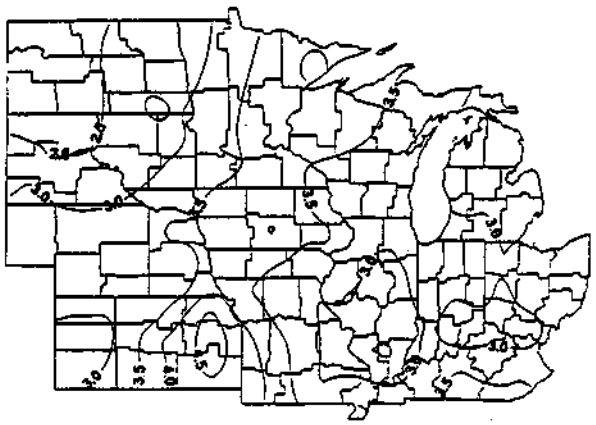

Planting to tassel initiation

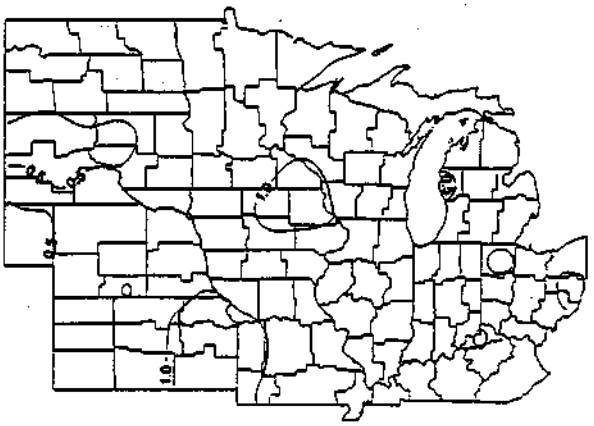

Tassel initiation to ear initiation

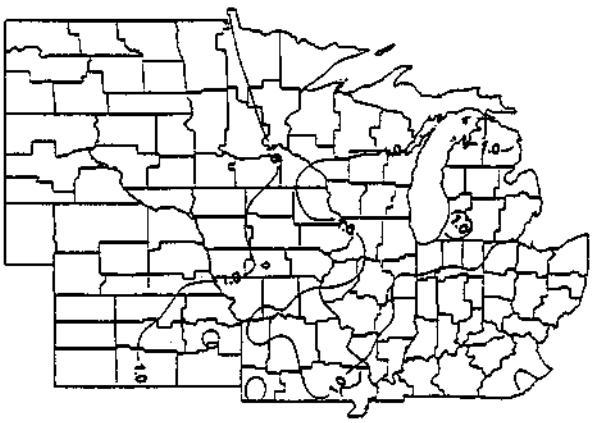

Ear initiation to end-of-row-set

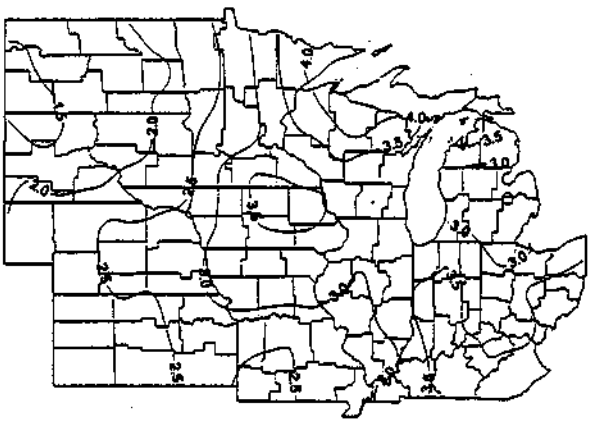

End-of-row-set to silk

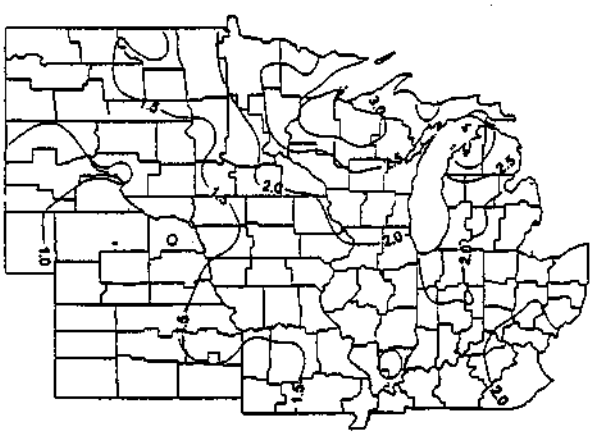

Silk to end-of-lag-phase

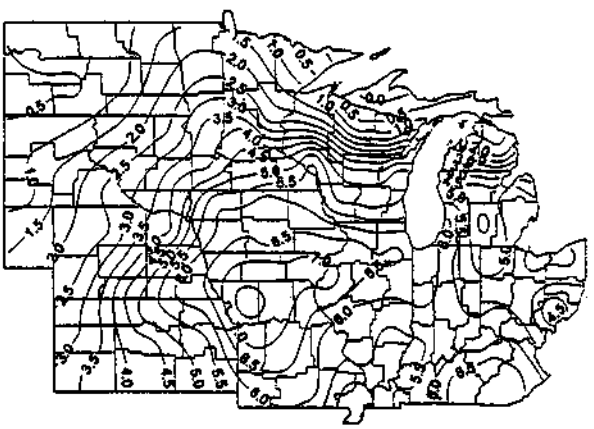

End-of-lag-phase to maturity

Figure H.1.3.7.f. Mean precipitation during the different com growth stages with a date of planting 20 days after normal. In the Central Corn Belt this represents planting in early-June.

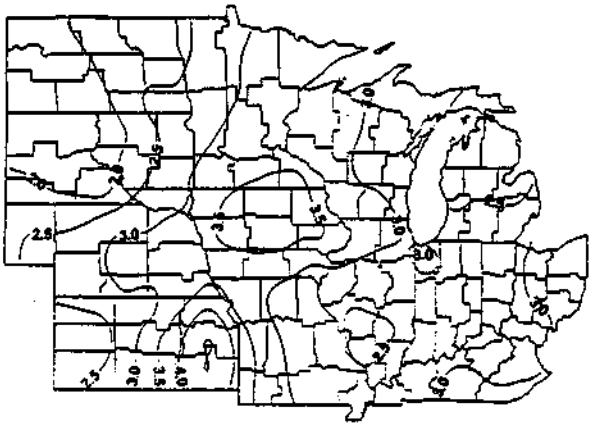

Planting to tassel initiation

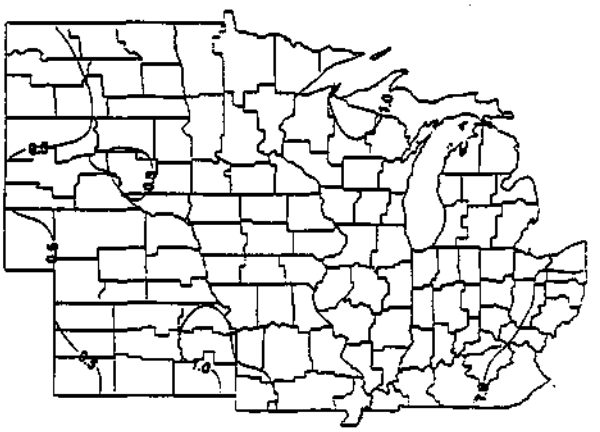

Tassel initiation to ear initiation

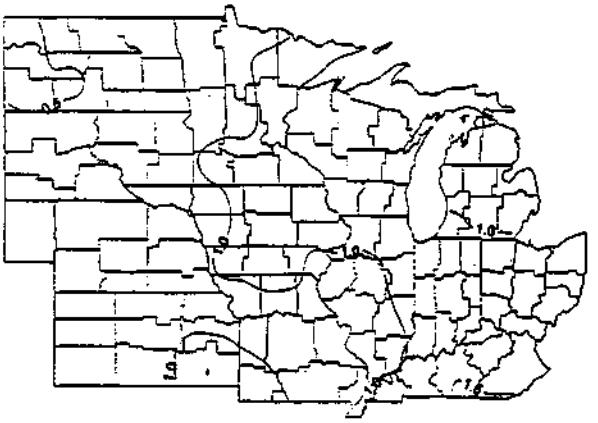

Ear initiation to end-of-row-set

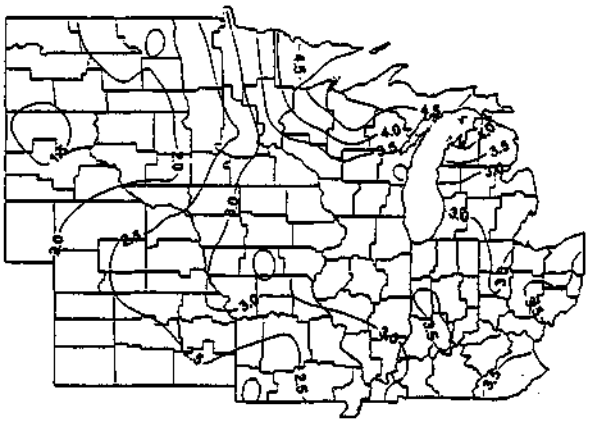

End-of-row-set to silk

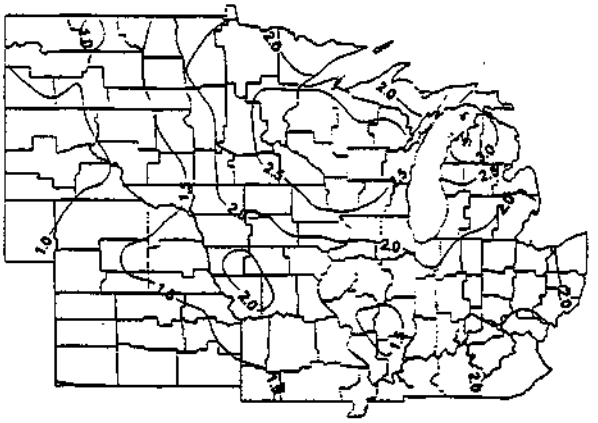

Silk to end-of-lag-phase

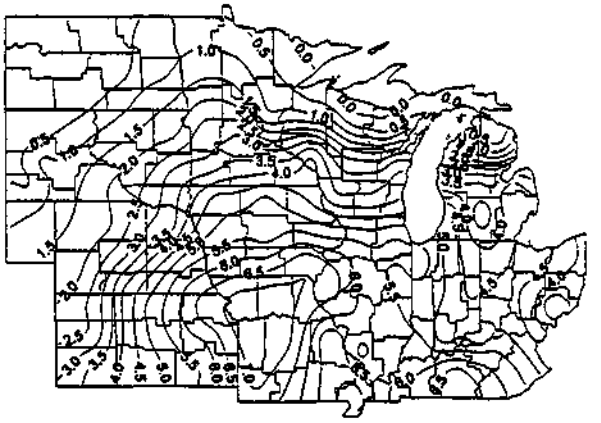

End-of-lag-phase to maturity

Figure H.1.3.7.g. Mean precipitation during the different com growth stages with a date of planting 30 days after normal. In the Central Corn Belt this represents planting in mid-June.

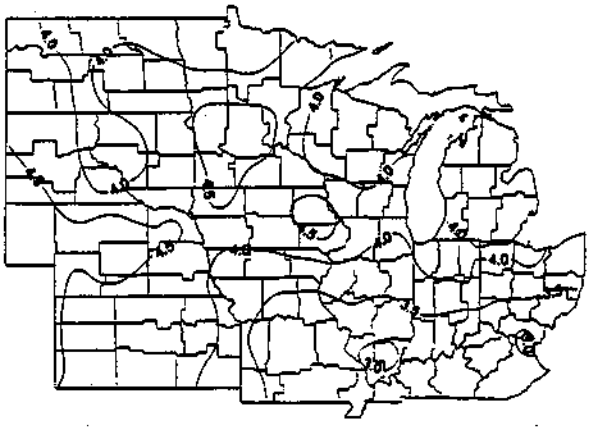

Planting to tassel initiation

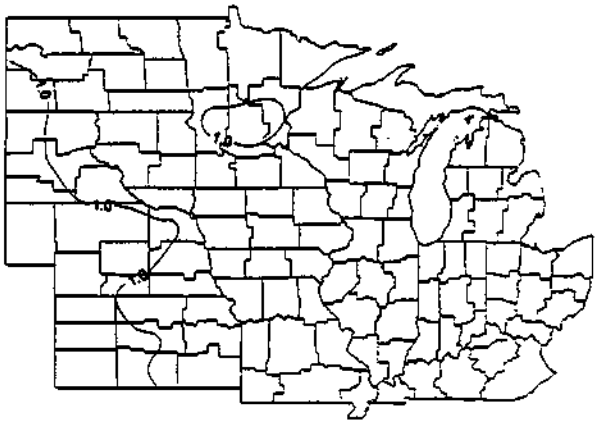

Tassel initiation to ear initiation

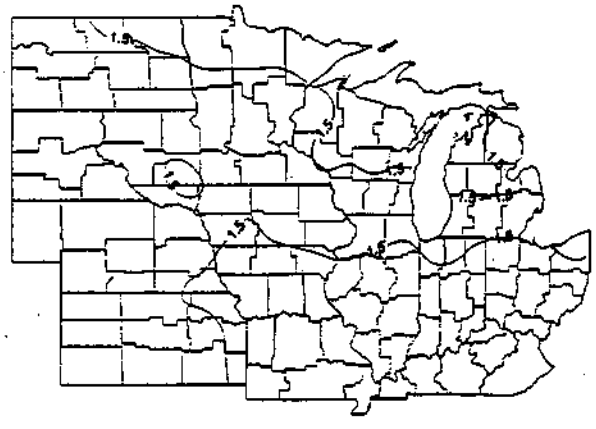

Ear initiation to end-of-row-set

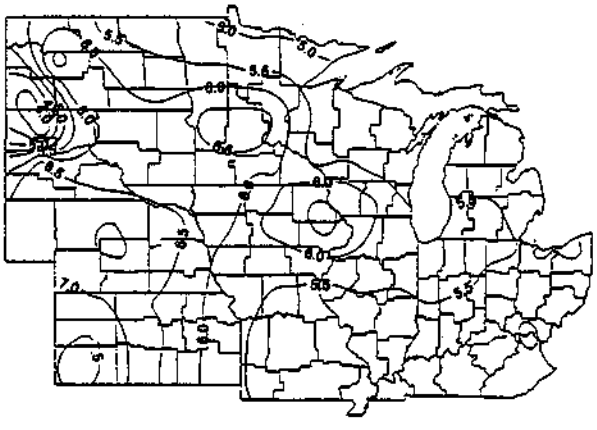

End-of-row-set to silk

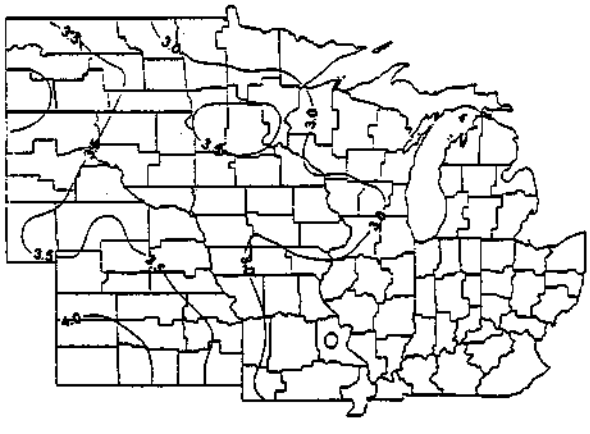

Silk to end-of-lag-phase

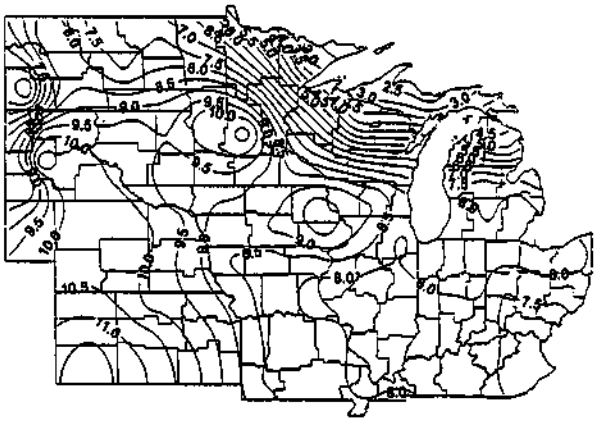

End-of-lag-phase to maturity

Figure H.1.3.8.a. Mean potenital evapotranspiration during the different com growth stages with a date of planting 30 days before normal. In the Central Corn Belt this represents planting in mid-April.

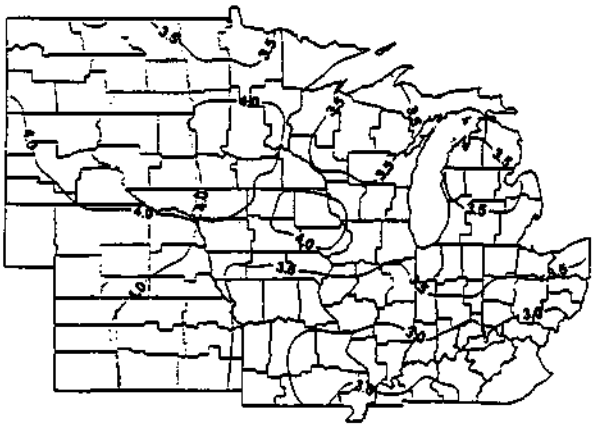

Planting to tassel initiation

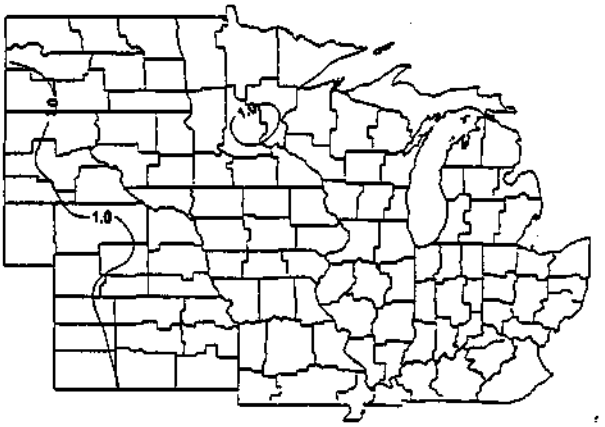

Tassel initiation to ear initiation

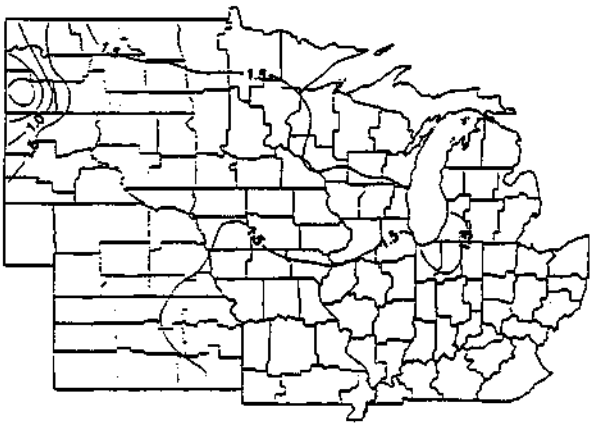

Ear initiation to end-of-row-set

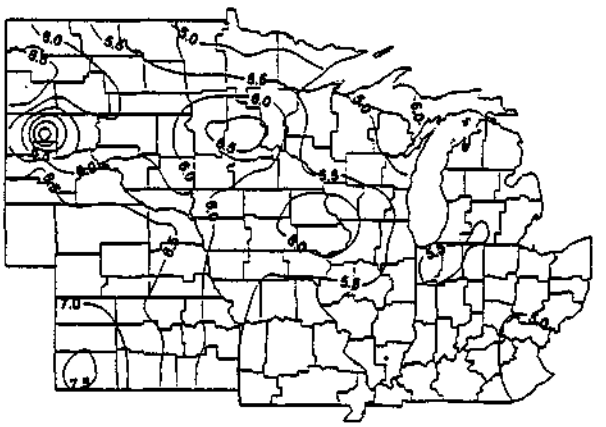

End-of-row-set to silk

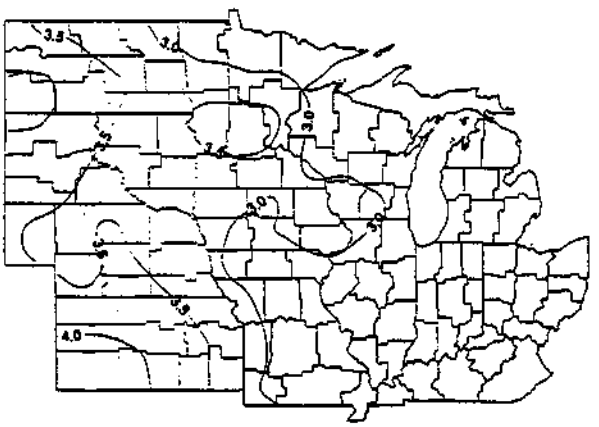

Silk to end-of-lag-phase

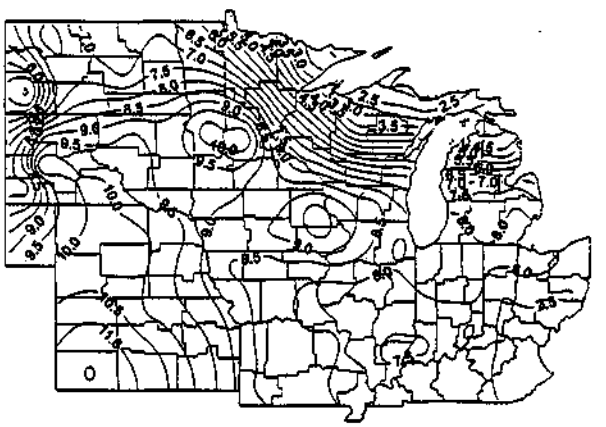

End-of-lag-phase to maturity

Figure H.1.3.8.b. Mean potenital evapotranspiration during the different com growth stages with a date of planting 20 days before normal. In the Central Com Belt this represents planting in late-April.

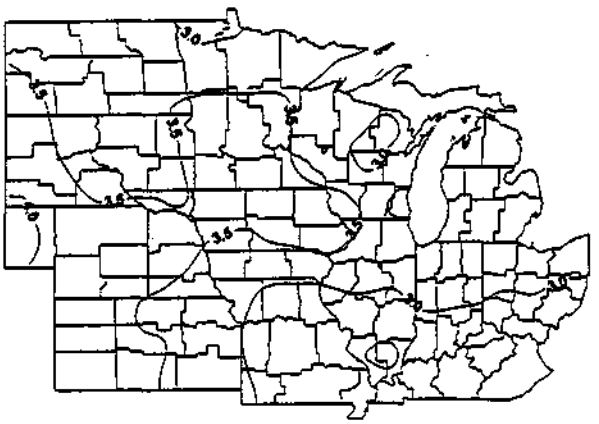

Planting to tassel initiation

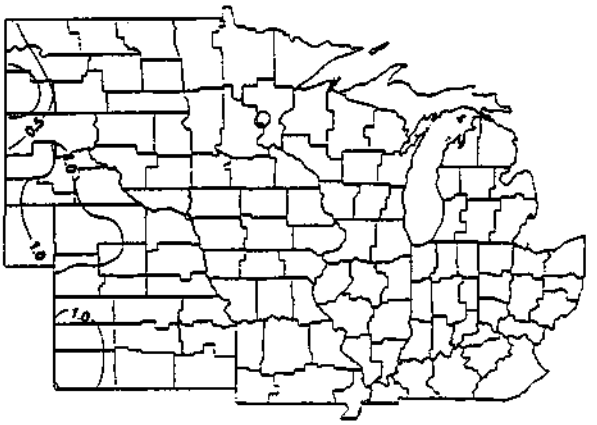

Tassel initiation to ear initiation

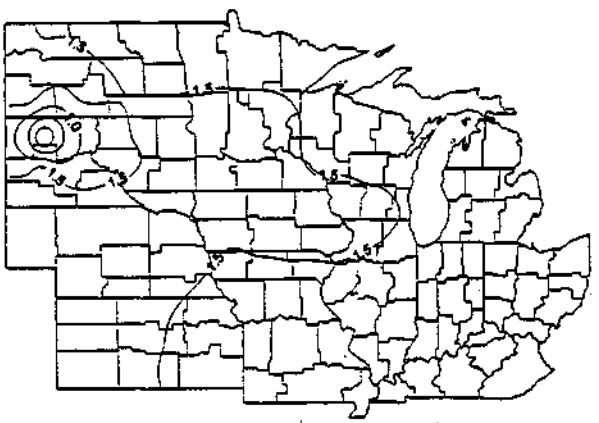

Ear initiation to end-of-row-set

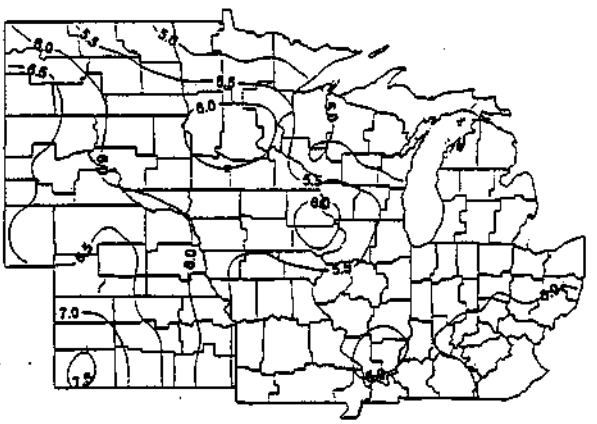

End-of-row-set to silk

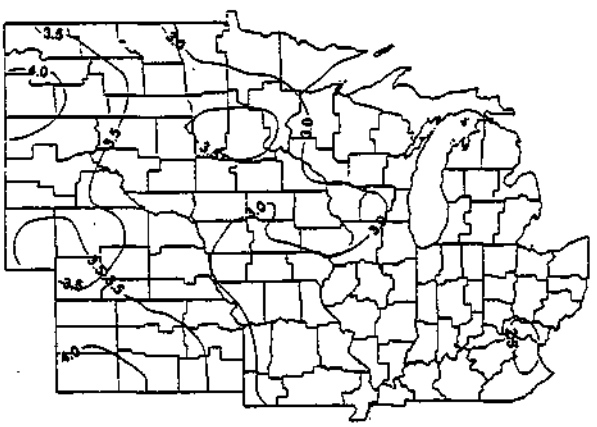

Silk to end-of-lag-phase

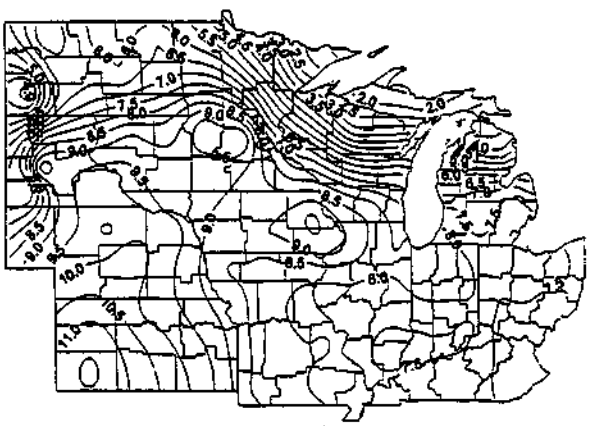

End-of-lag-phase to maturity

Figure H.1.3.8.c. Mean potenital evapotranspiration during the different corn growth stages with a date of planting 10 days before normal. In the Central Corn Belt this represents planting in early-May.

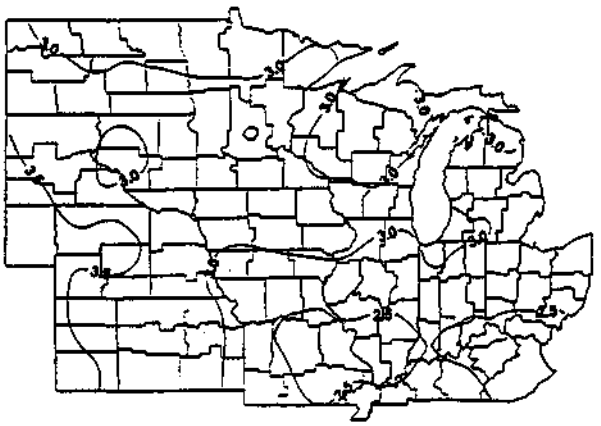

Planting to tassel initiation

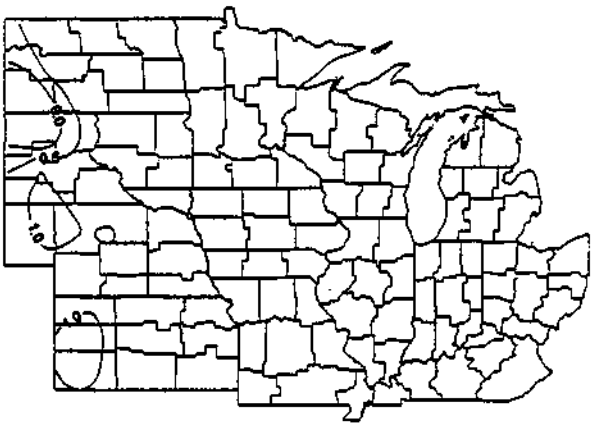

Tassel initiation to ear initiation

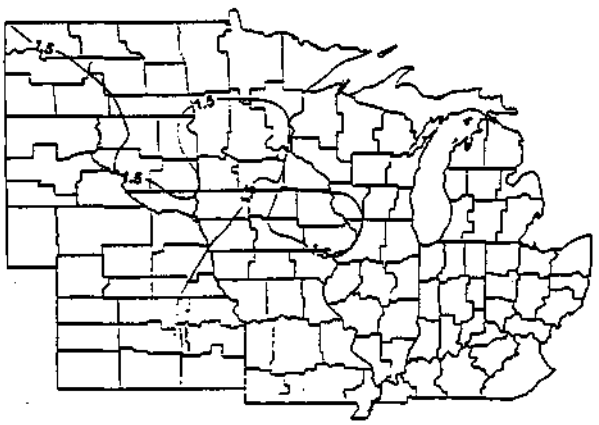

Ear initiation to end-of-row-set

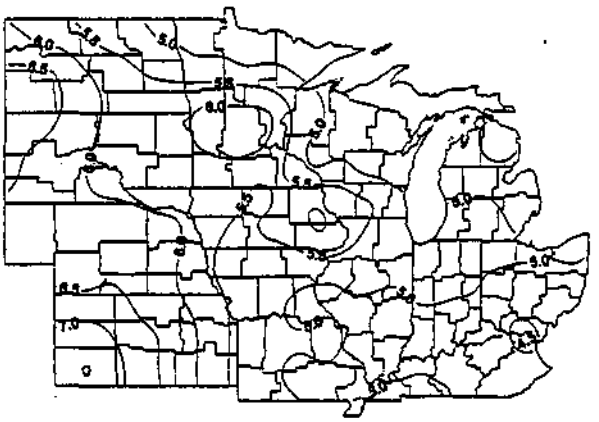

End-of-row-set to silk

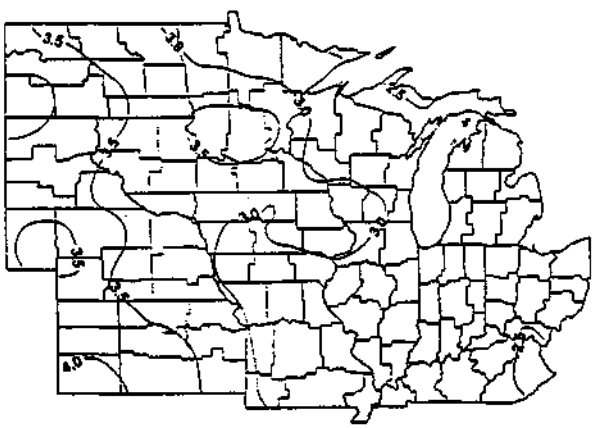

Silk to end-of-lag-phase

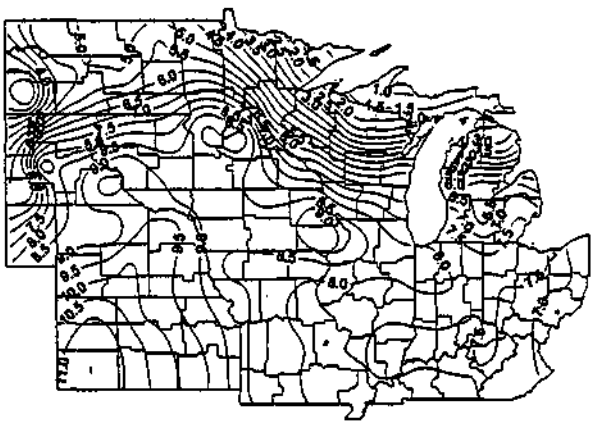

End-of-lag-phase to maturity

Figure H.1.3.8.d. Mean potenital evapotranspiration during the different corn growth stages with a nromal date of planting. In the Central Com Belt this represents planting in mid-May.

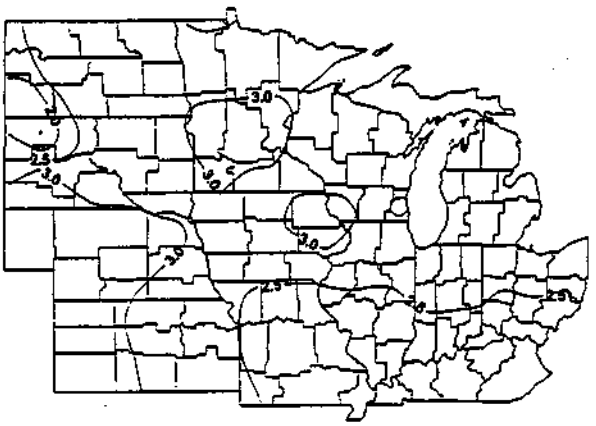

Planting to tassel initiation

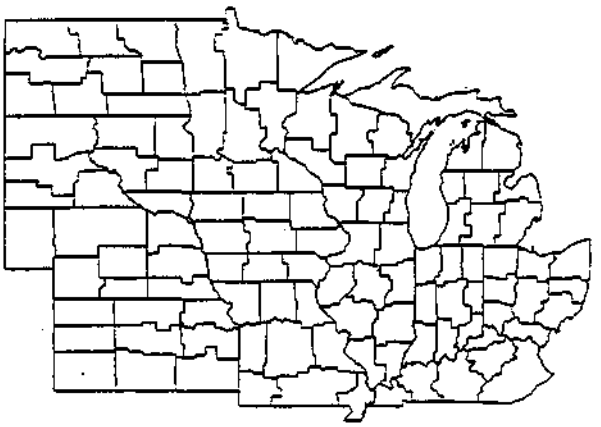

Tassel initiation to ear initiation

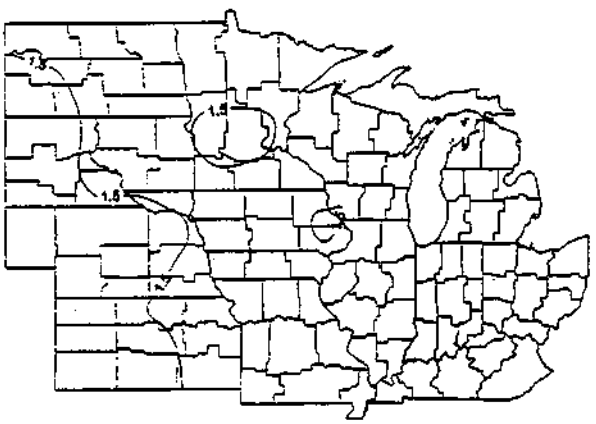

Ear initiation to end-of-row-set

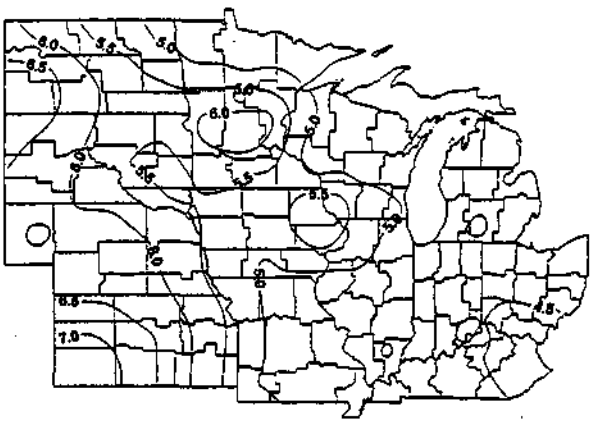

End-of-row-set to silk

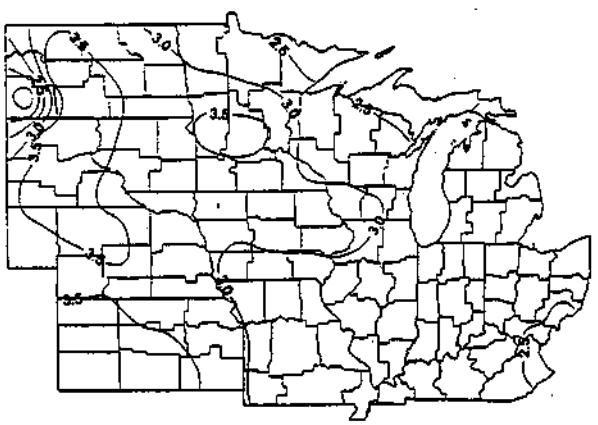

Silk to end-of-lag-phase

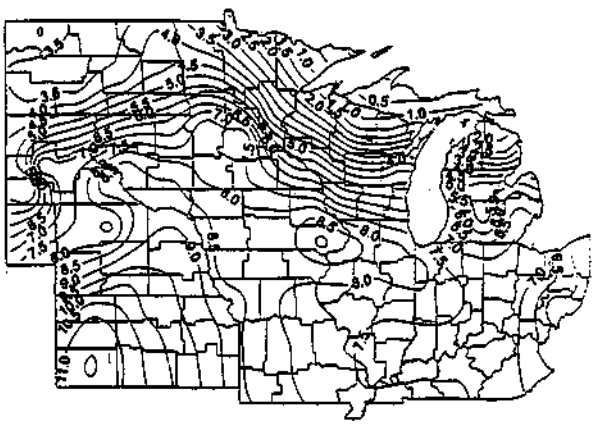

End-of-lag-phase to maturity

Figure H.1.3.8.e. Mean potenital evapotranspiration during the different corn growth stages with a date of planting 10 days after normal. In the Central Com Belt this represents planting in late-May.

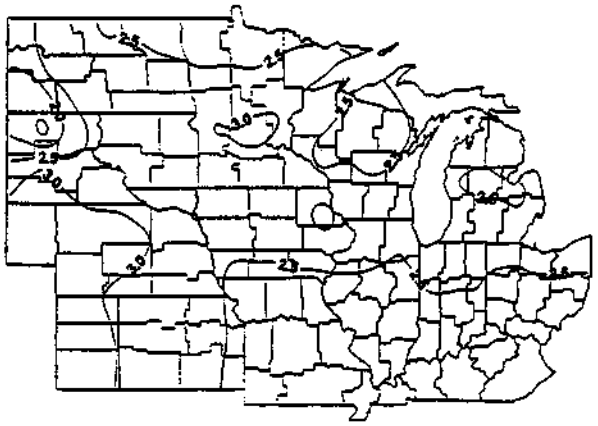

Planting to tassel initiation

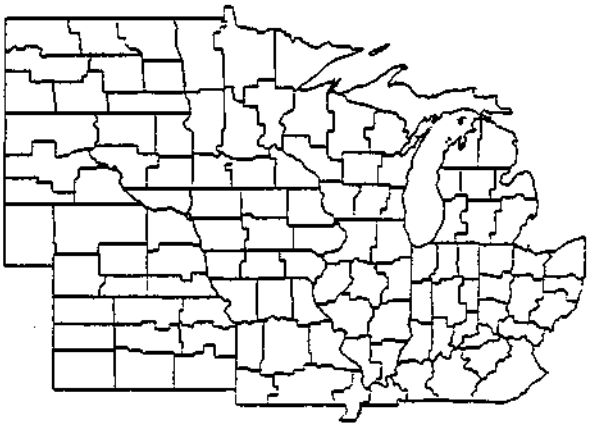

Tassel initiation to ear initiation

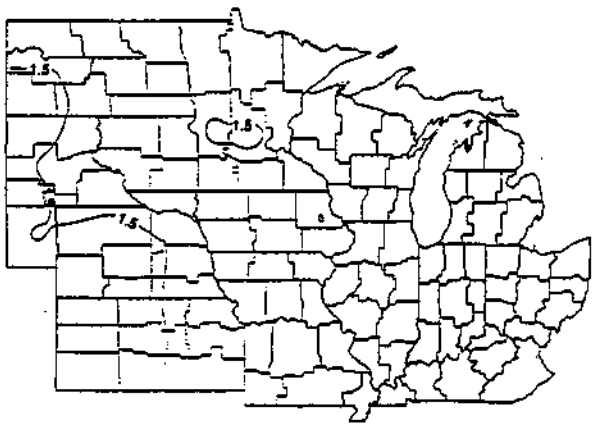

Ear initiation to end-of-row-set

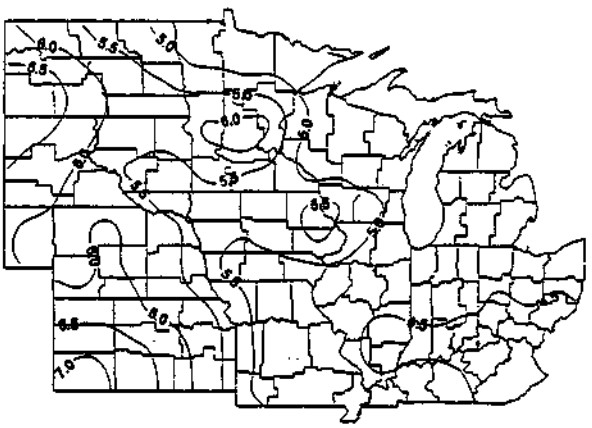

End-of-row-set to silk

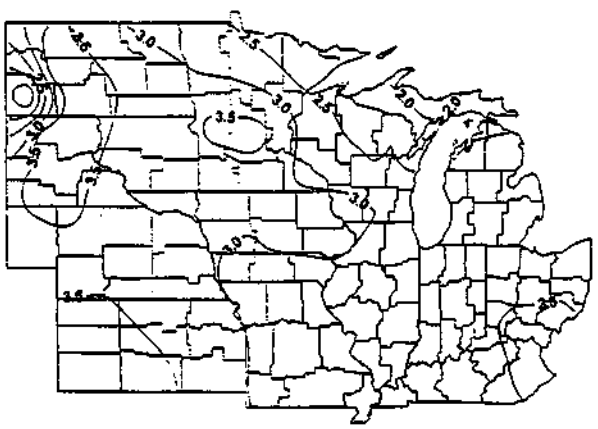

Silk to end-of-lag-phase

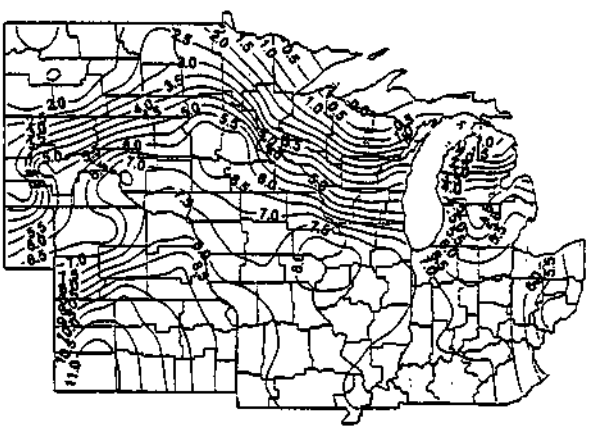

End-of-lag-phase to maturity

Figure H.1.3.8.f. Mean potenital evapotranspiration during the different com growth stages with a date of planting 20 days after normal. In the Central Corn Belt this represents planting in early-June.

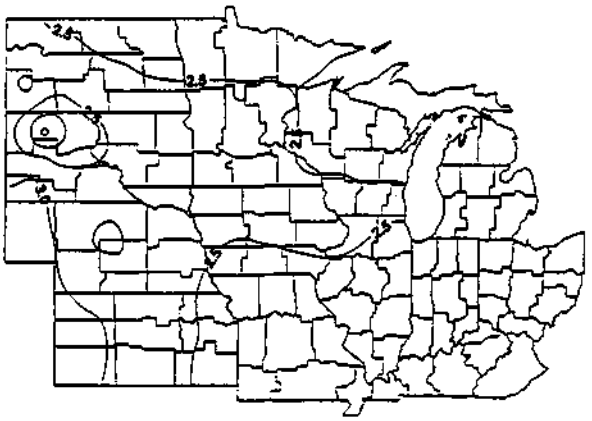

Planting to tassel initiation

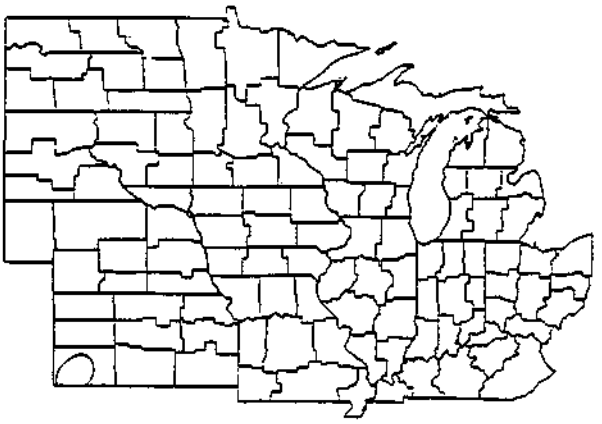

Tassel initiation to ear initiation

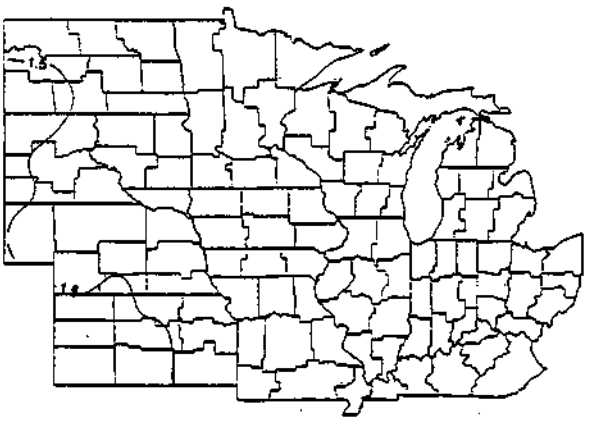

Ear initiation to end-of-row-set

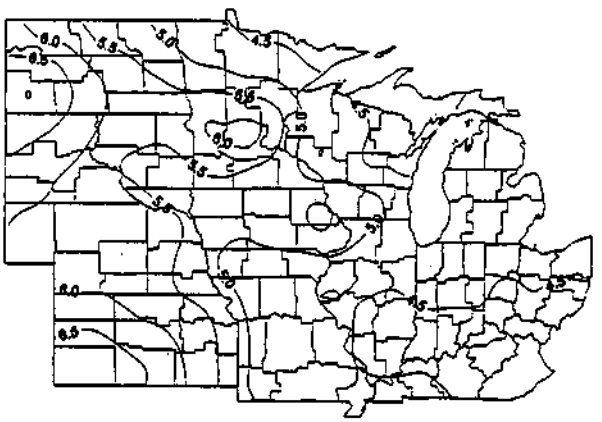

End-of-row-set to silk

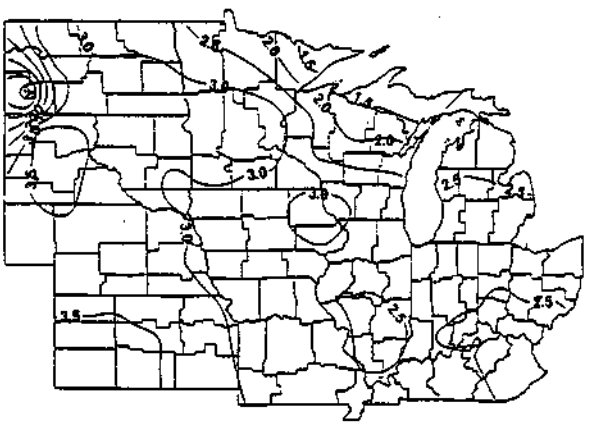

Silk to end-of-lag-phase

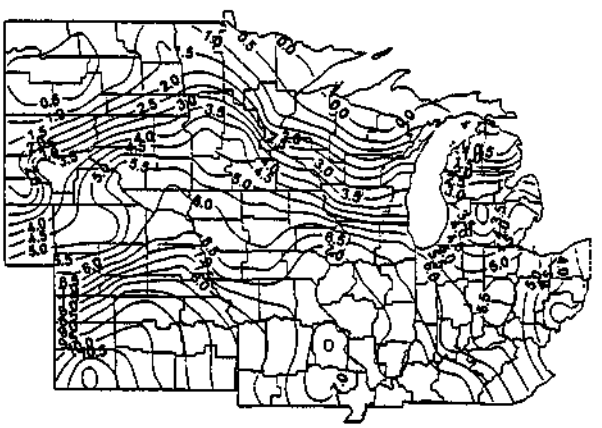

End-of-lag-phase to maturity

Figure H.1.3.8.g. Mean potenital evapotranspiration during the different corn growth stages with a date of planting 30 days after normal. In the Central Corn Belt this represents planting in mid-June.

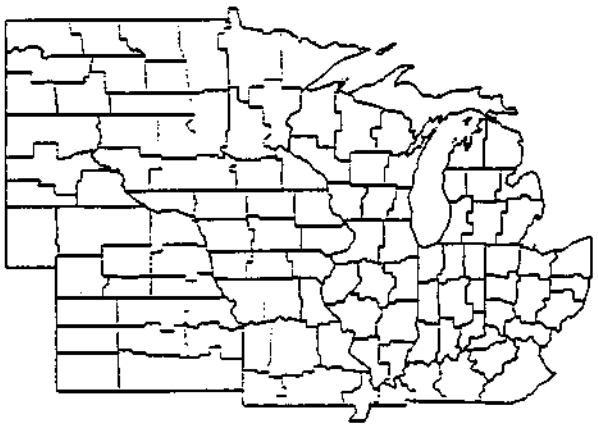

Planting to tassel initiation

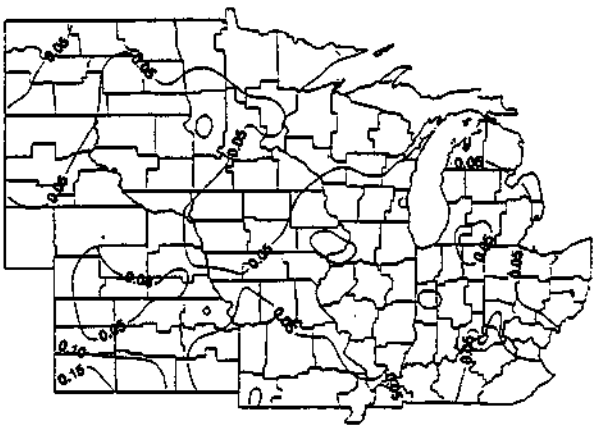

Tassel initiation to ear initiation

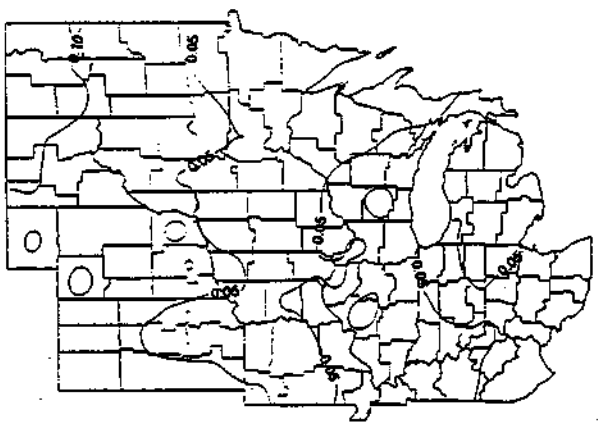

Ear initiation to end-of-row-set

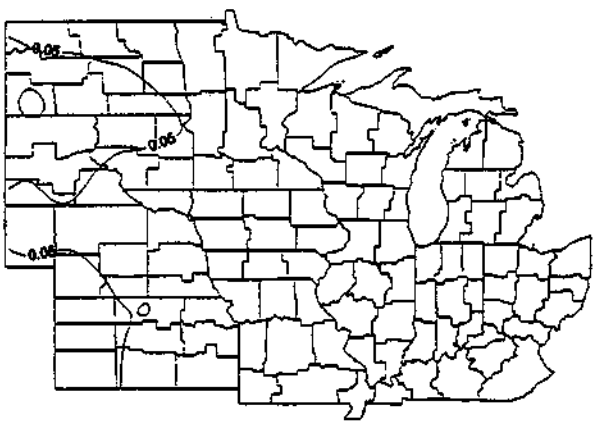

End-of-row-set to silk

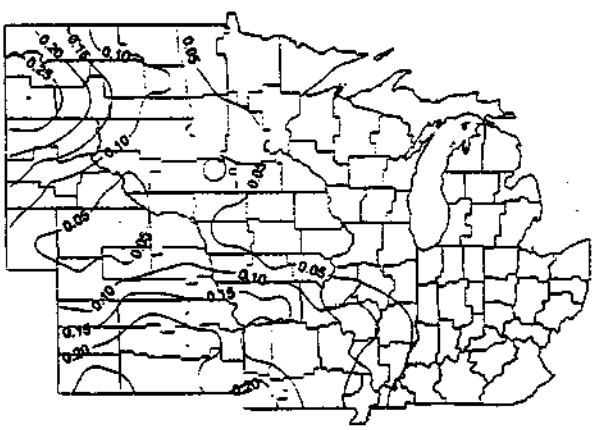

Silk to end-of-lag-phase

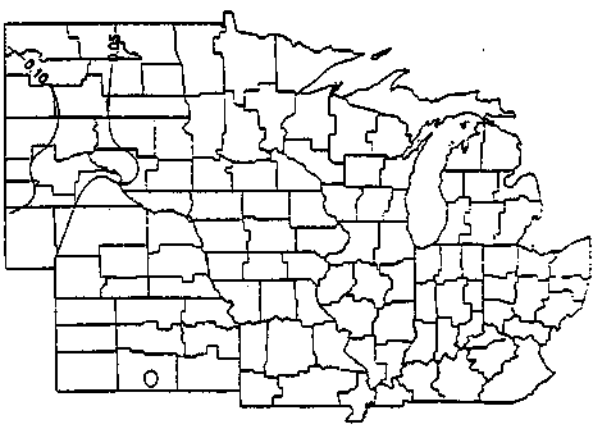

End-of-lag-phase to maturity

Figure H.1.3.9.a. Probability of rainfall less than or equal to 10 percent of potential evapotranspiration during the different com growth stages with a date of planting 30 days before normal. In the Central Com Belt this represents planting in mid-April..

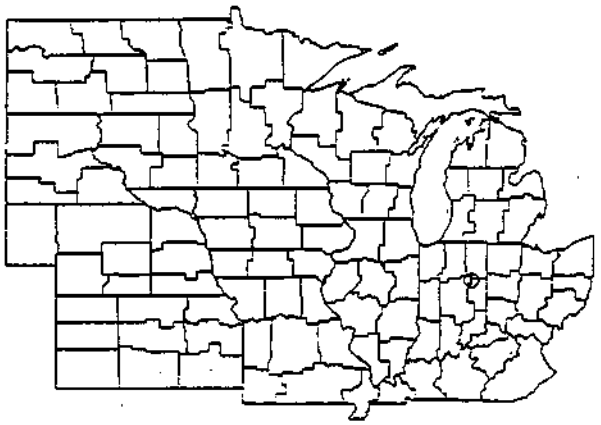

Planting to tassel initiation

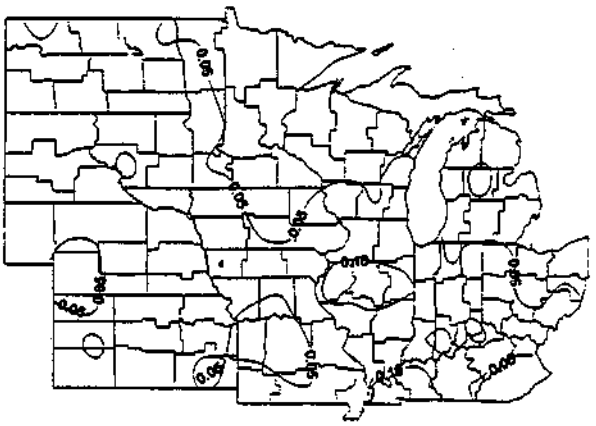

Tassel initiation to ear initiation

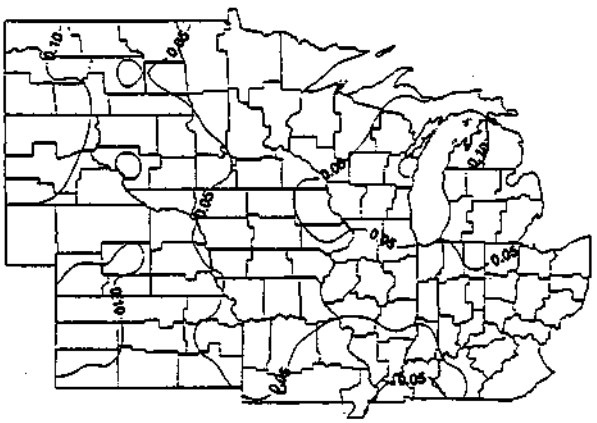

Ear initiation to end-of-row-set

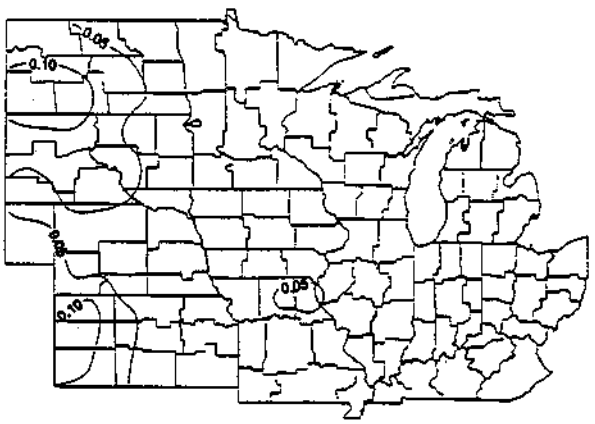

End-of-row-set to silk

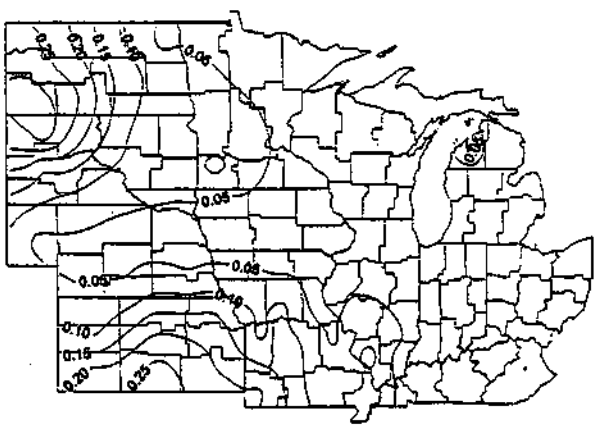

Silk to end-of-lag-phase

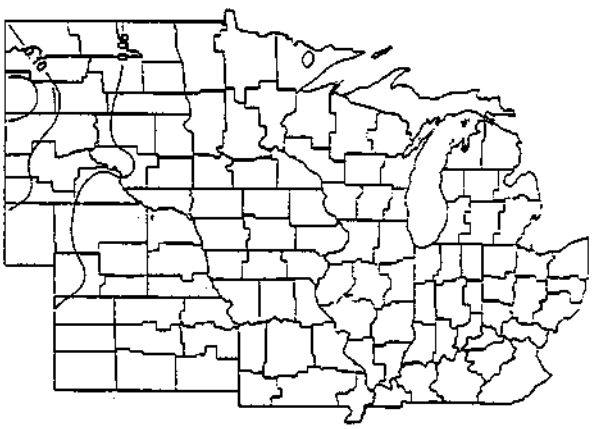

End-of-lag-phase to maturity

Figure H.1.3.9.b. Probability of rainfall less than or equal to 10 percent of potential evapotranspiration during the different com growth stages with a date of planting 20 days before normal. In the Central Com Belt this represents planting in late-April.

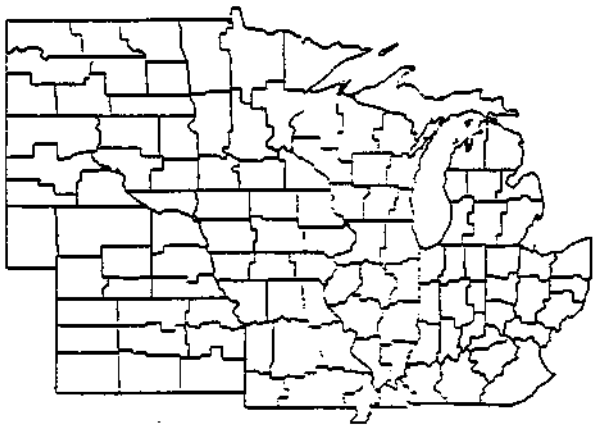

Planting to tassel initiation

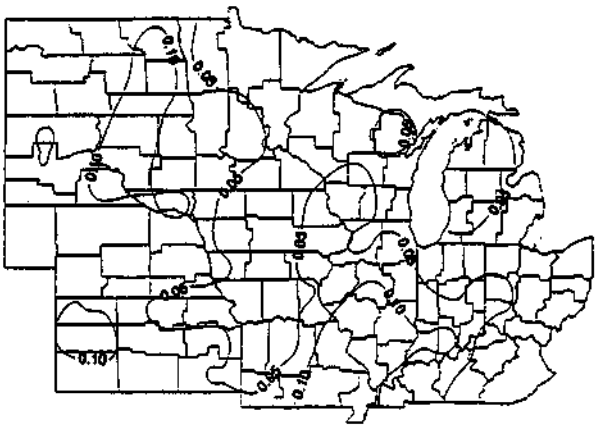

Tassel initiation to ear initiation

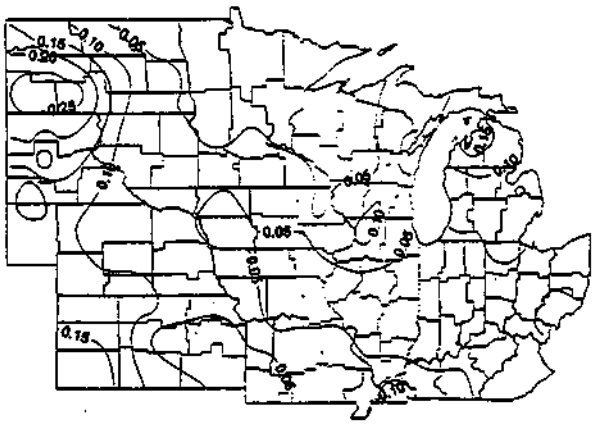

Ear initiation to end-of-row-set

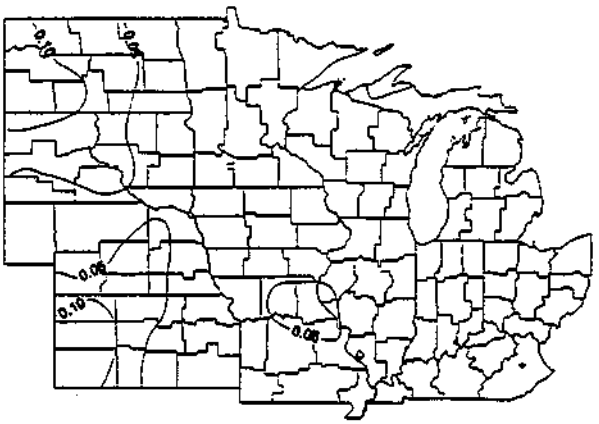

End-of-row-set to silk

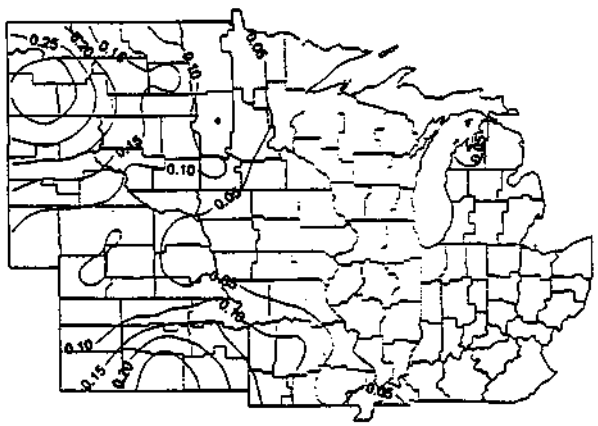

Silk to end-of-lag-phase

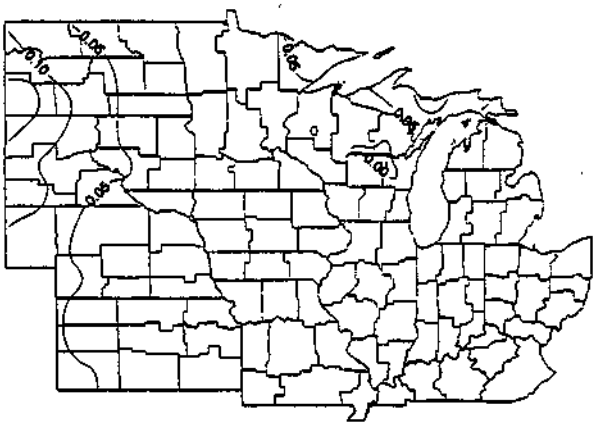

End-of-lag-phase to maturity

Figure H.1.3.9.c. Probability of rainfall less than or equal to 10 percent of potential evapotranspiration during the different corn growth stages with a date of planting 10 days before normal. In the Central Corn Belt this represents planting in early-May.

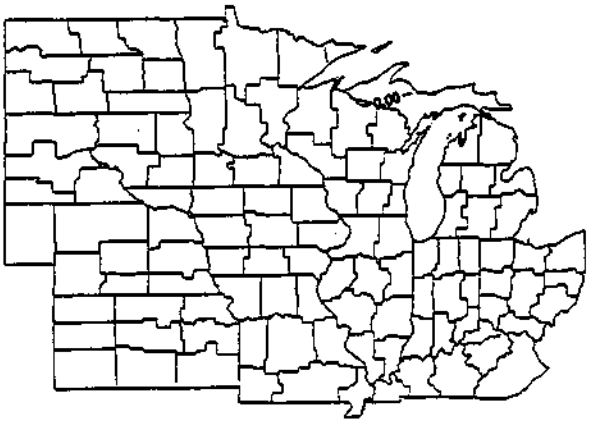

Planting to tassel initiation

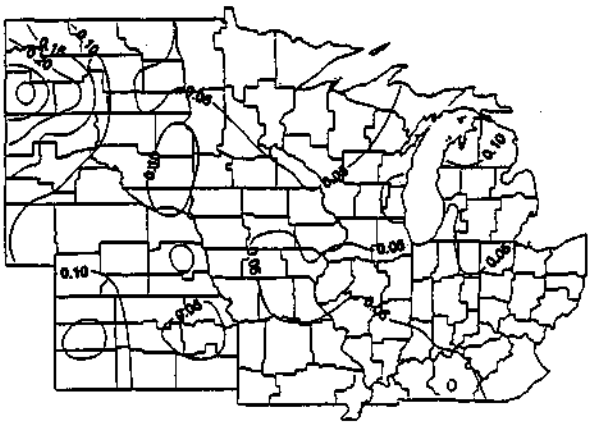

Tassel initiation to ear initiation

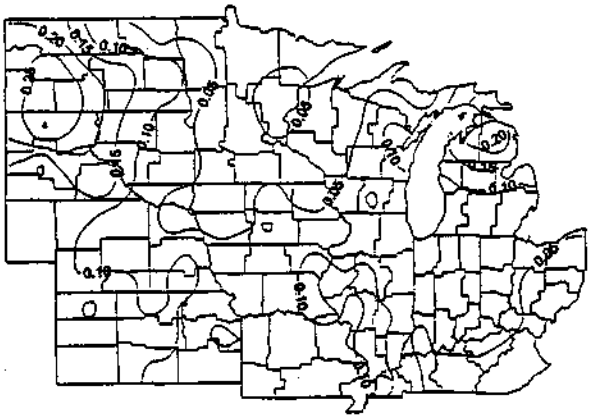

Ear initiation to end-ot-row-set

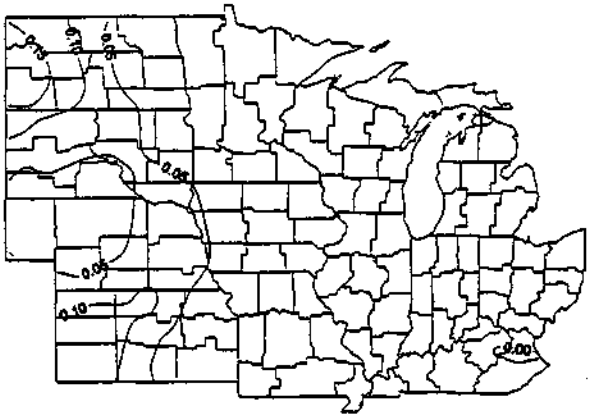

End-of-row-set to silk

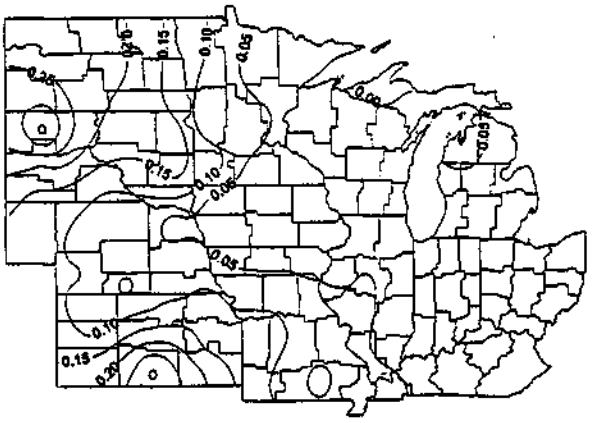

Silk to end-of-lag-phase

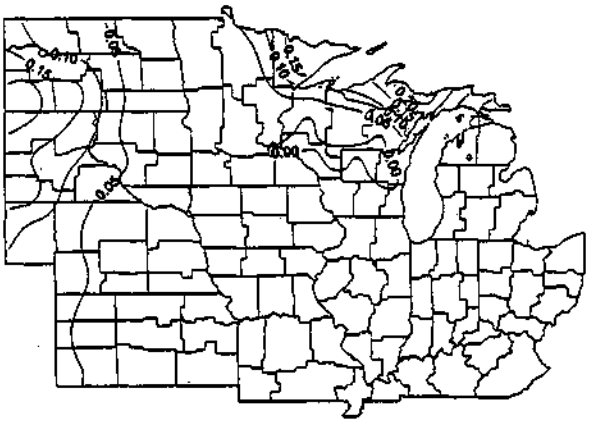

End-of-lag-phase to maturity

Figure H.1.3.9.d. Probability of rainfall less than or equal to 10 percent of potential evapotranspiration during the different corn growth stages with a nromal date of planting. In the Central Corn Belt this represents planting in mid-May.

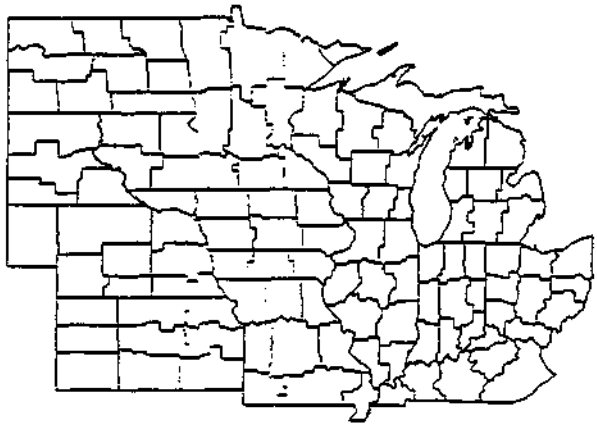

Planting to tassel initiation

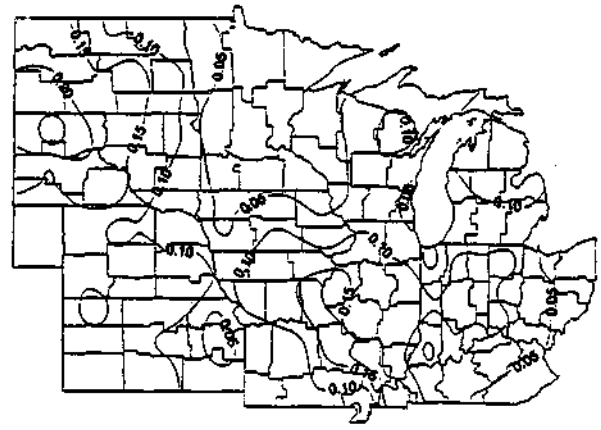

Tassel initiation to ear initiation

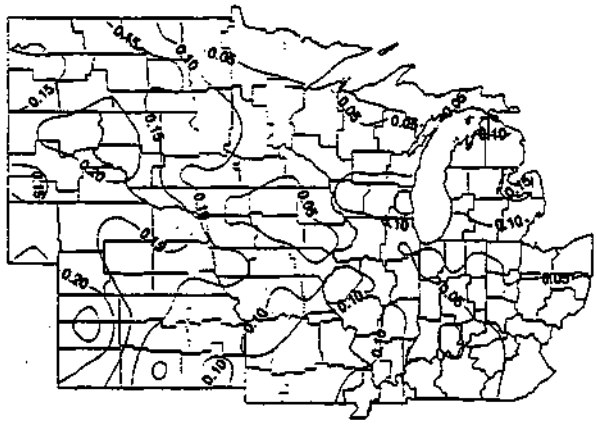

Ear initiation to end-of-row-set

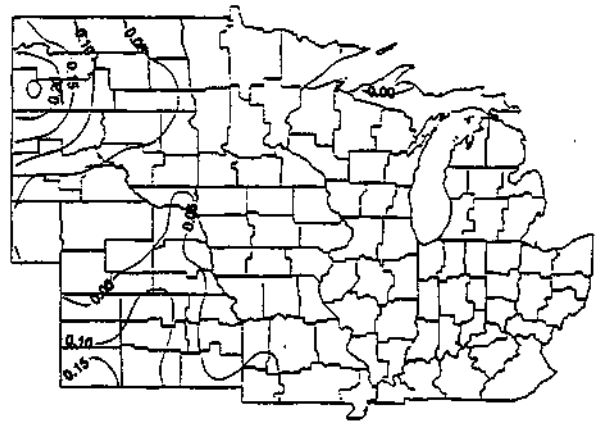

End-of-row-set to silk

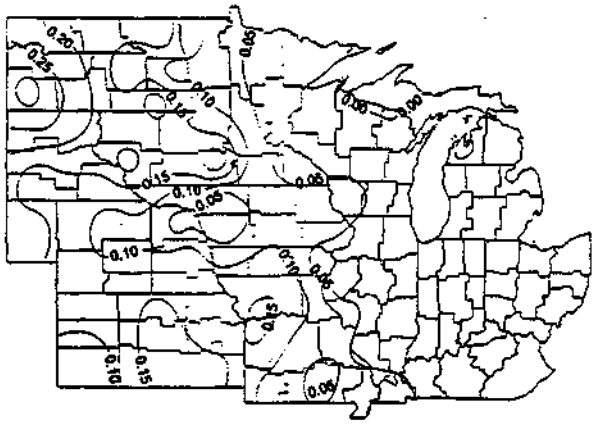

Silk to end-of-lag-phase

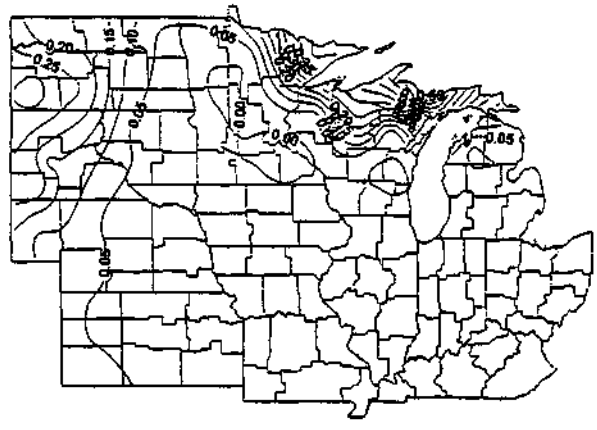

End-of-lag-phase to maturity

Figure H.1.3.9.e. Probability of rainfall less than or equal to 10 percent of potential evapotranspiration during the different corn growth stages with a date of planting 10 days after normal. In the Central Corn Belt this represents planting in late-May. .

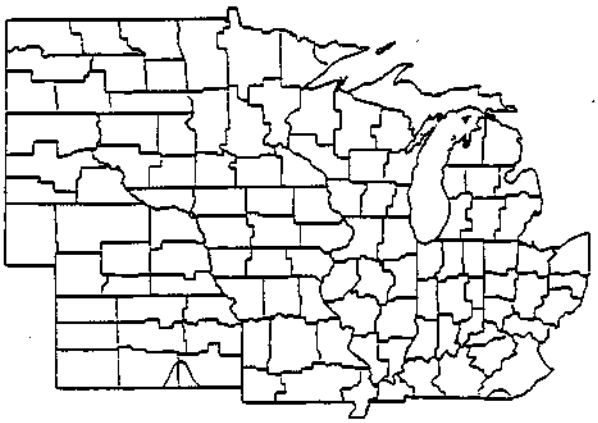

Planting to tassel initiation

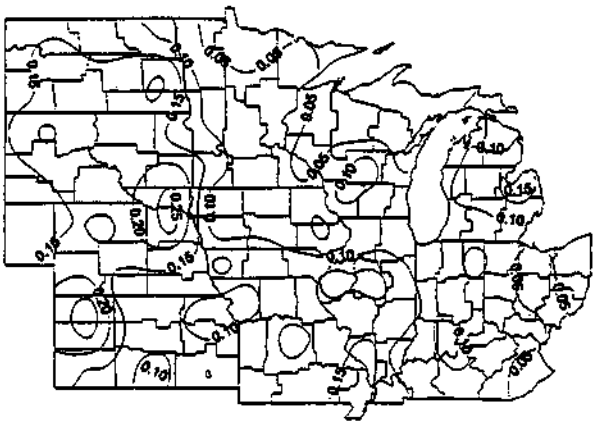

Tassel initiation to ear initiation

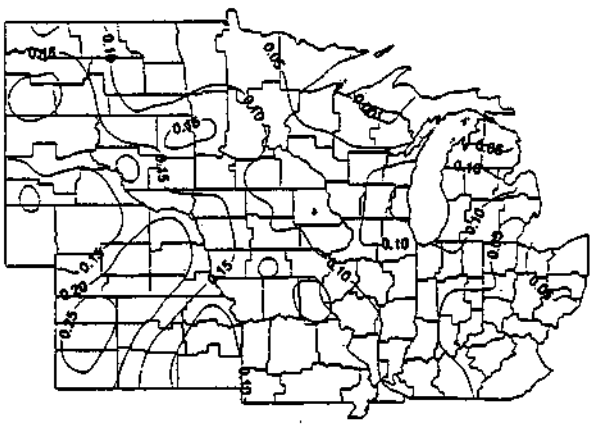

Ear initiation to end-of-row-set

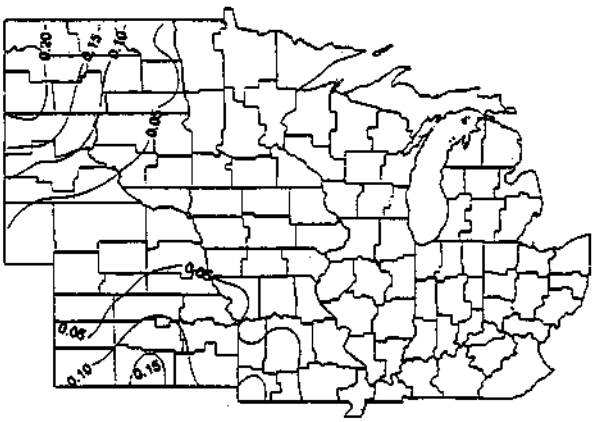

End-of-row-set to silk

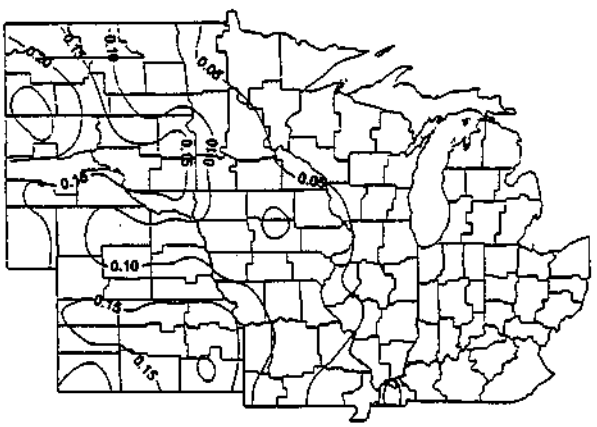

Silk to end-of-lag-phase

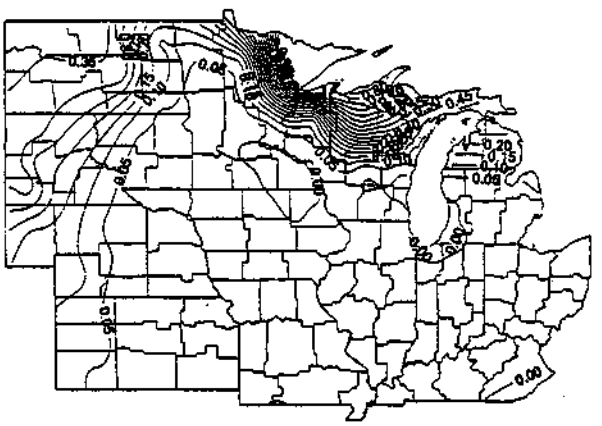

End-of-lag-phase to maturity

Figure H.1.3.9.f. Probability of rainfall less than or equal to 10 percent of potential evapotranspiration during the different com growth stages with a date of planting 20 days after normal. In the Central Com Belt this represents planting in early-June..

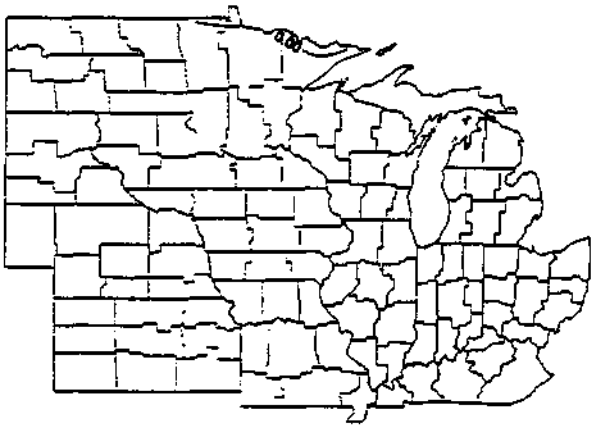

Planting to tassel initiation

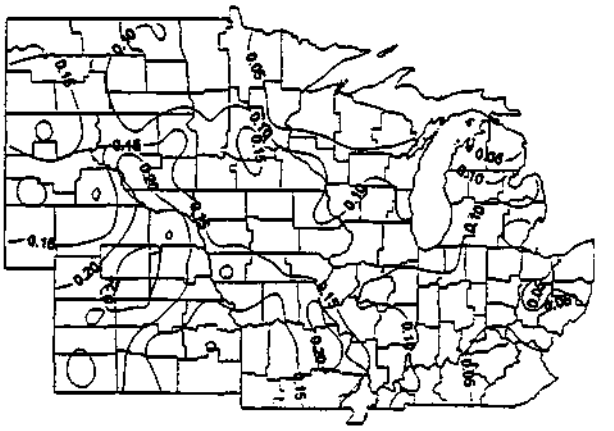

Tassel initiation to ear initiation

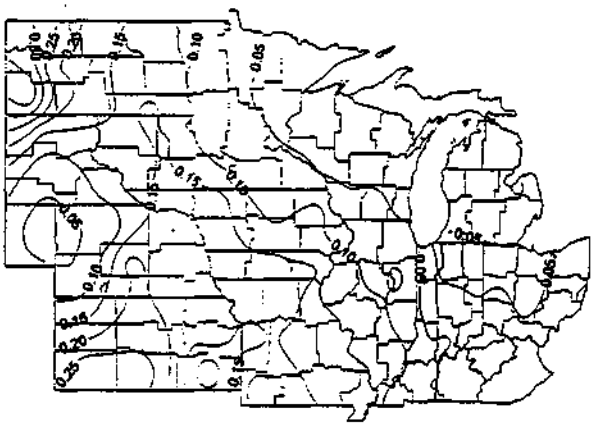

Ear initiation to end-of-row-set

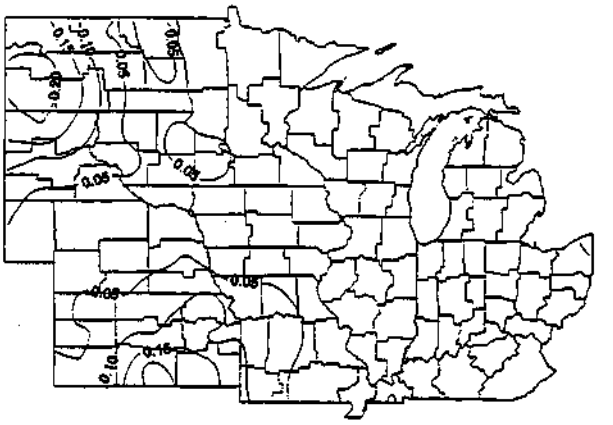

End-of-row-set to silk

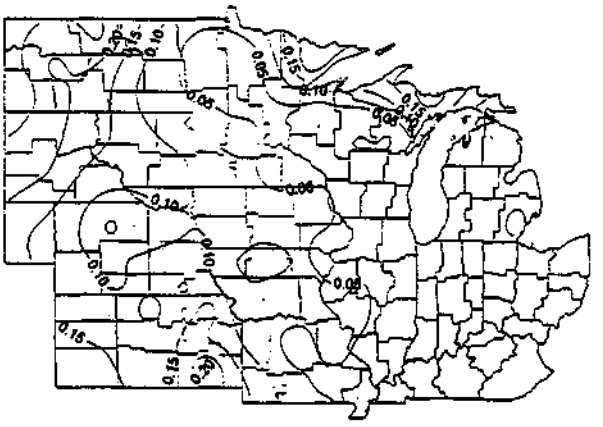

Silk to end-of-lag-phase

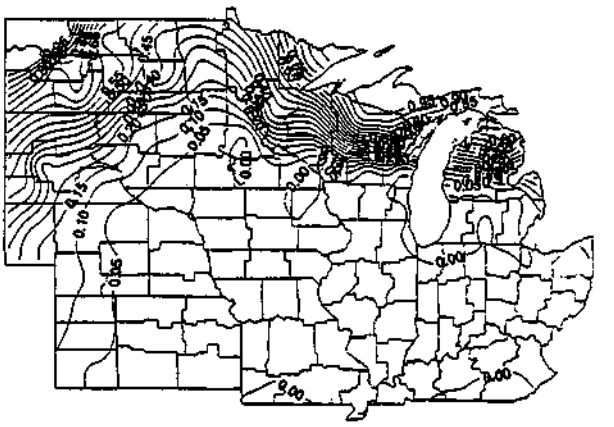

End-of-lag-phase to maturity

Figure H.1.3.9.g. Probability of rainfall less than or equal to 10 percent of potential evapotranspiration during the different corn growth stages with a date of planting 30 days after normal. In the Central Com Belt this represents planting in mid-June..

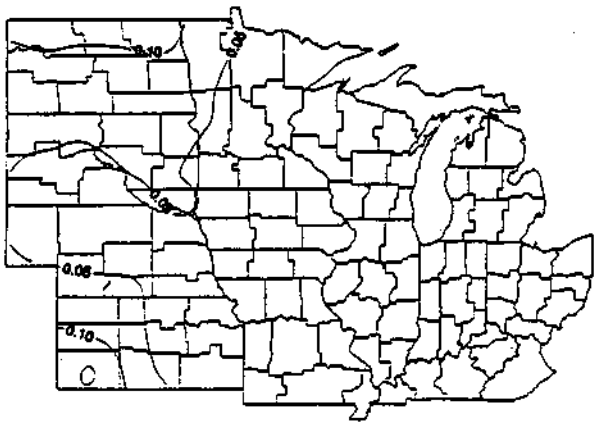

Planting to tassel initiation

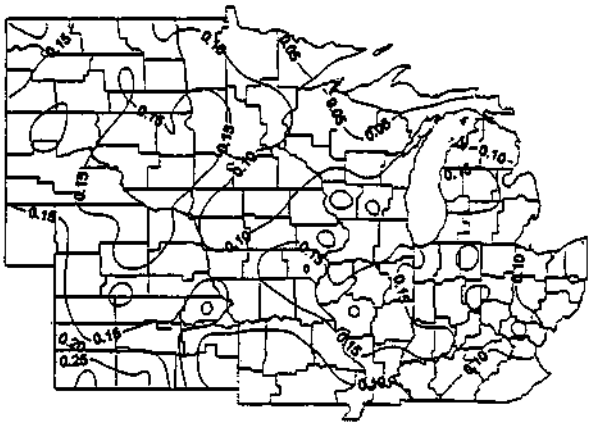

Tassel initiation to ear initiation

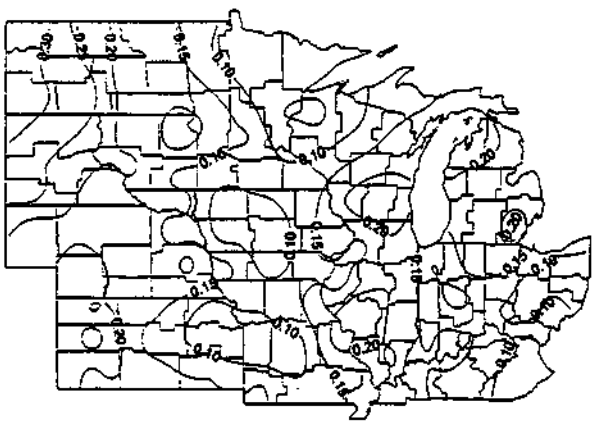

Ear initiation to end-of-row-set

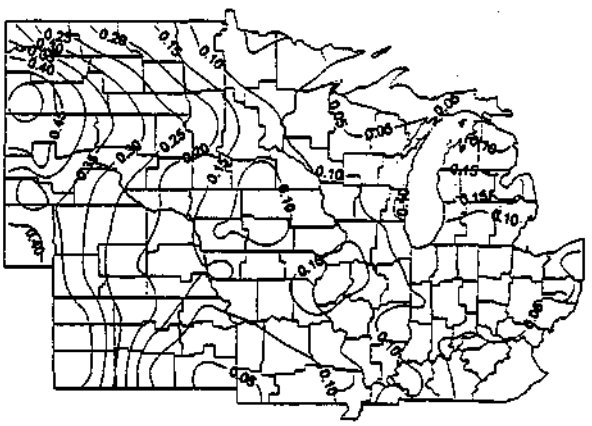

End-of-row-set to silk

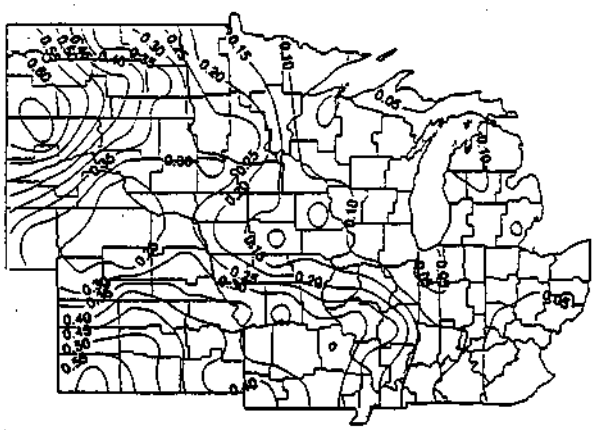

Silk to end-of-lag-phase

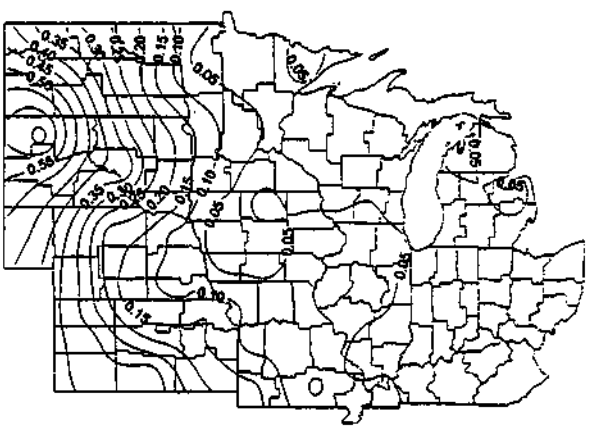

End-of-lag-phase to maturity

Figure H.1.3.10.a. Probability of rainfall less than or equal to 25 percent of potential evapotranspiration during the different com growth stages with a date of planting 30 days before normal. In the Central Corn Belt this represents planting in mid-April..

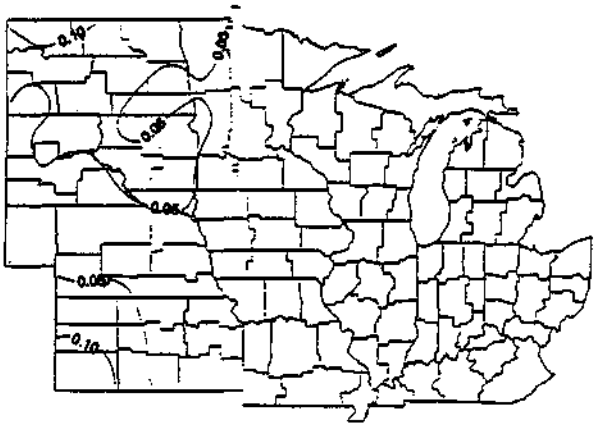

Planting to tassel initiation

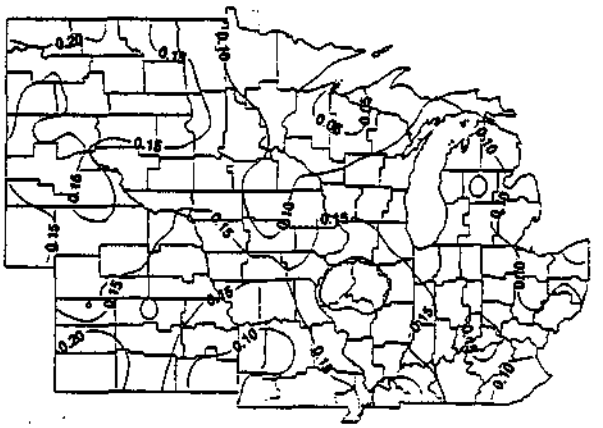

Tassel initiation to ear initiation

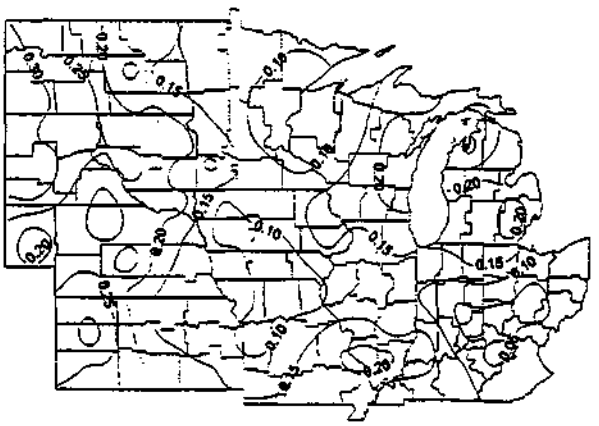

Ear initiation to end-of-row-set

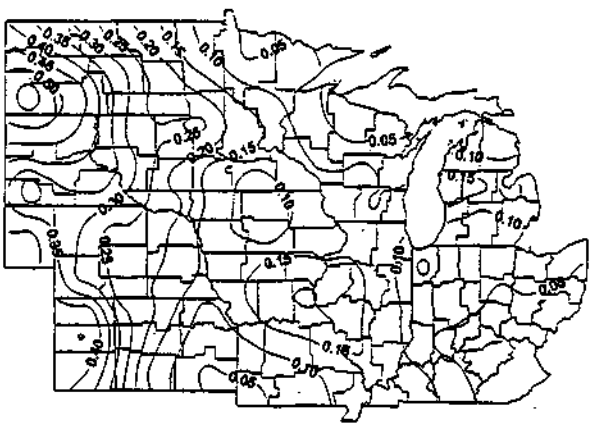

End-of-row-set to silk

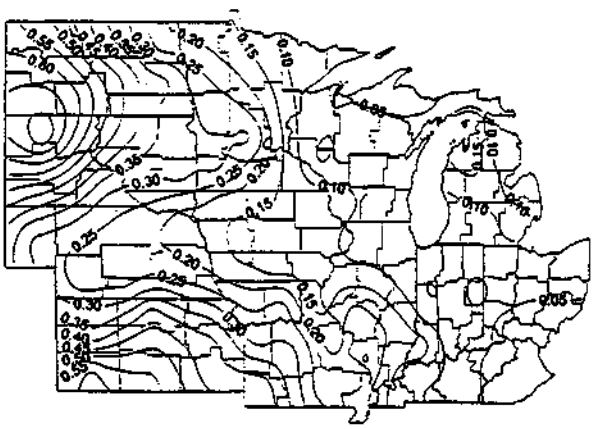

Silk to end-of-lag-phase

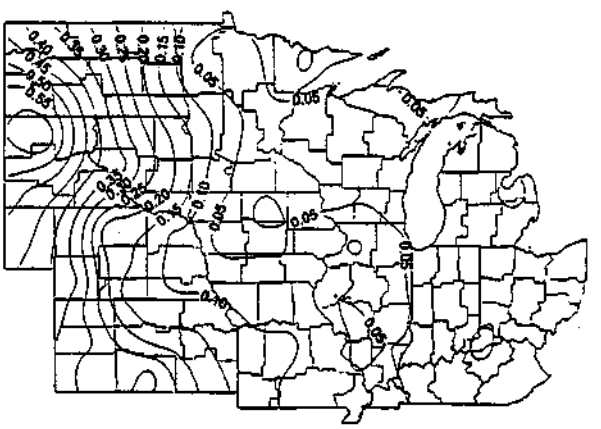

End-of-lag-phase to maturity

Figure H.1.3.10.b. Probability of rainfall less than or equal to 25 percent of potential evapotranspiration during the different com growth stages with a date of planting 20 days before normal. In the Central Corn Belt this represents planting in late-April.

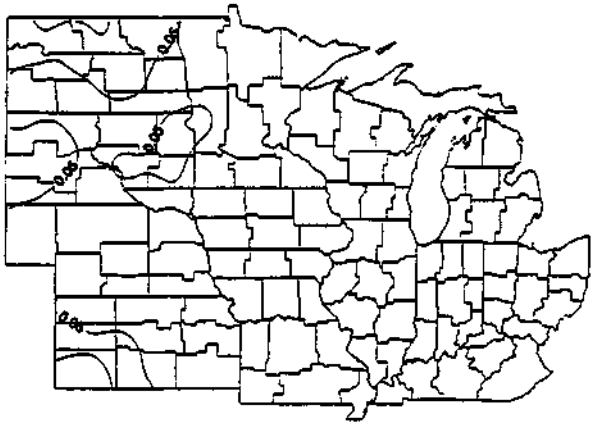

Planting to tassel initiation

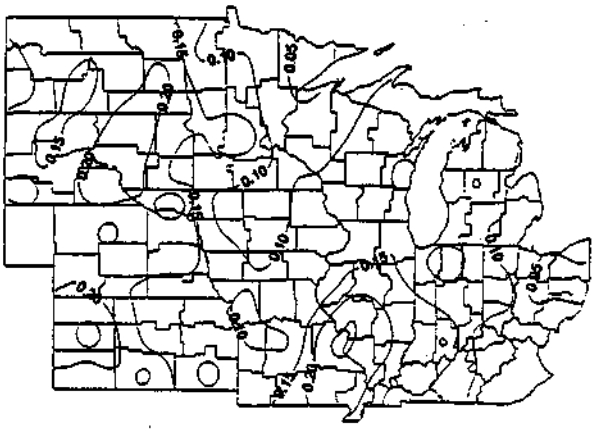

Tassel initiation to ear initiation

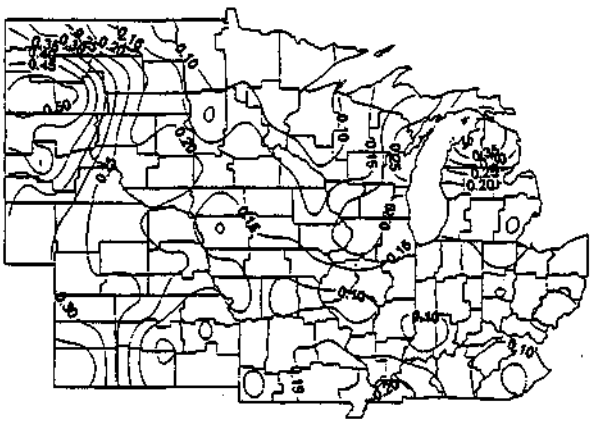

Ear initiation to end-of-row-set

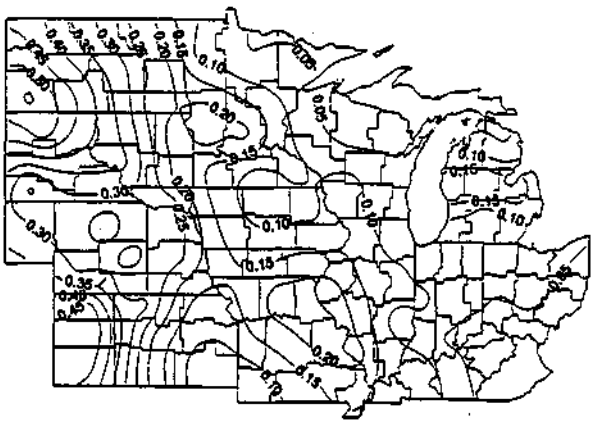

End-of-row-set to silk

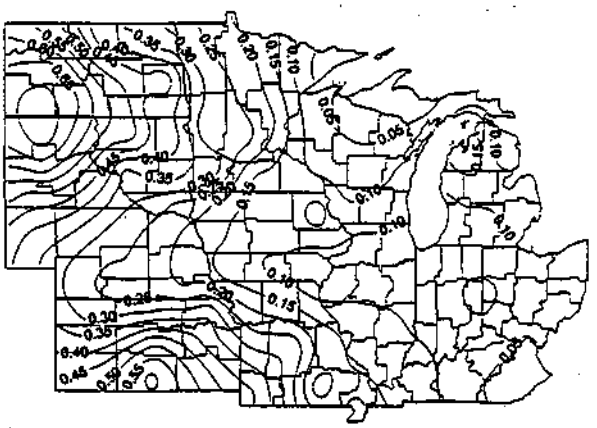

Silk to end-of-lag-phase

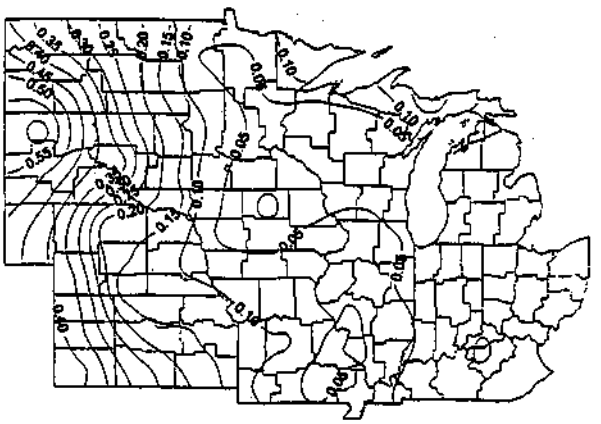

End-of-lag-phase to maturity

Figure H.1.3.10.c. Probability of rainfall less than or equal to 25 percent of potential evapotranspiration during the different corn growth stages with a date of planting 10 days before normal. In the Central Corn Belt this represents planting in early-May..

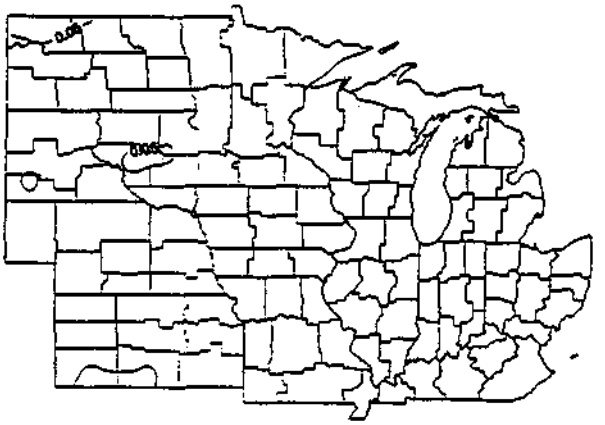

Planting to tassel initiation

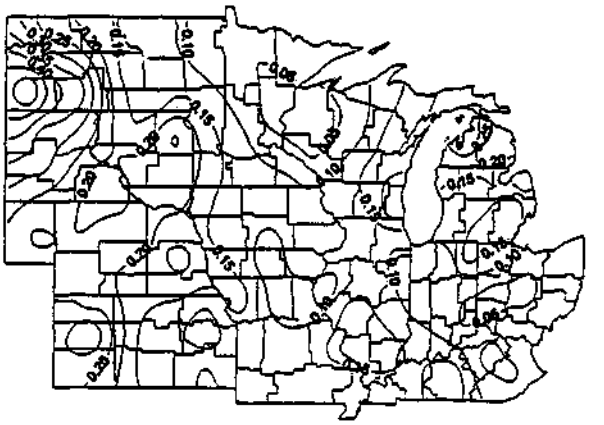

Tassel initiation to ear initiation

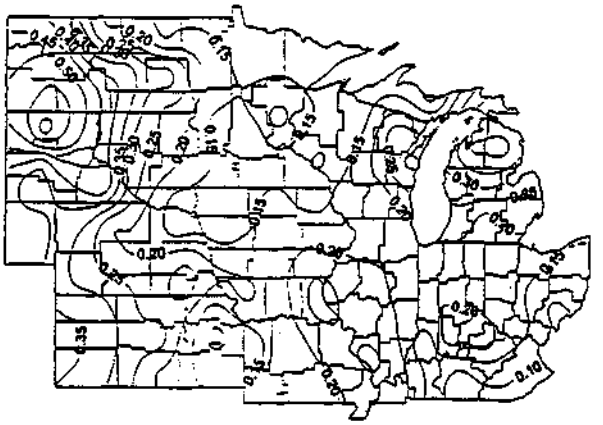

Ear initiation to end-of-row-set

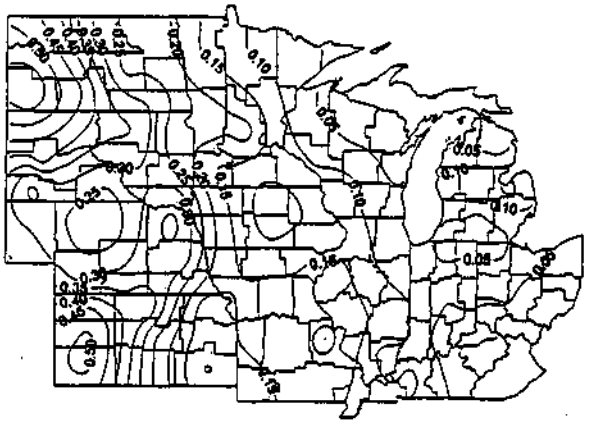

End-of-row-set to silk

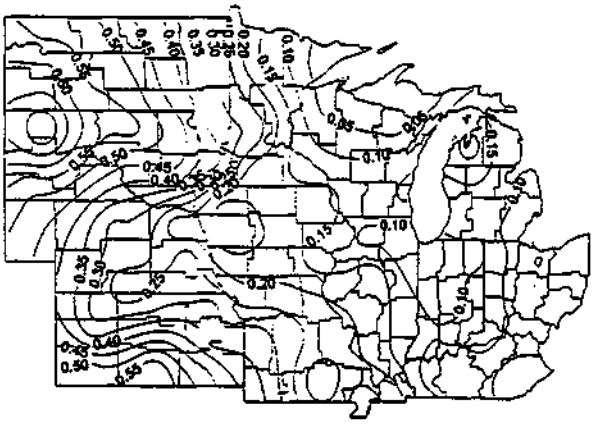

Silk to end-of-lag-phase

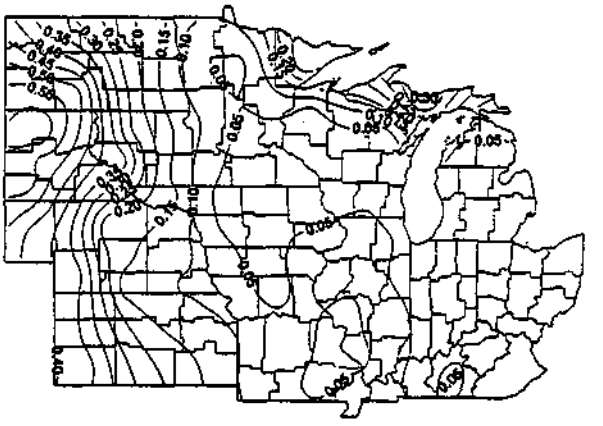

End-of-lag-phase to maturity

Figure H.1.3.10.d. Probability of rainfall less than or equal to 25 percent of potential evapotranspiration during the different corn growth stages with a nromal date of planting. In the Central Corn Belt this represents planting in mid-May.

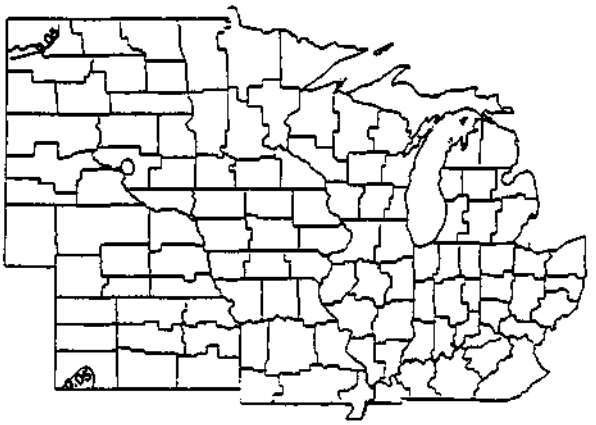

Planting to tassel initiation

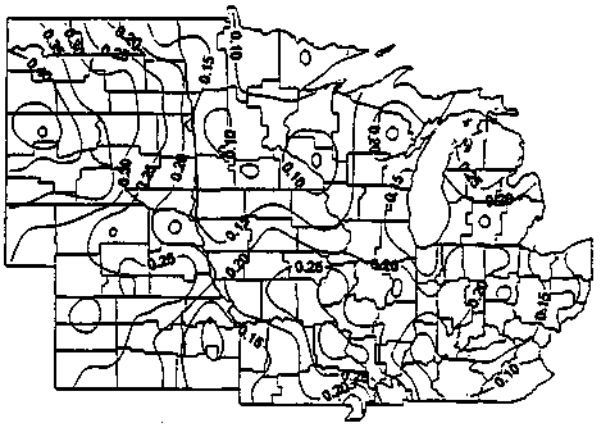

Tassel initiation to ear initiation

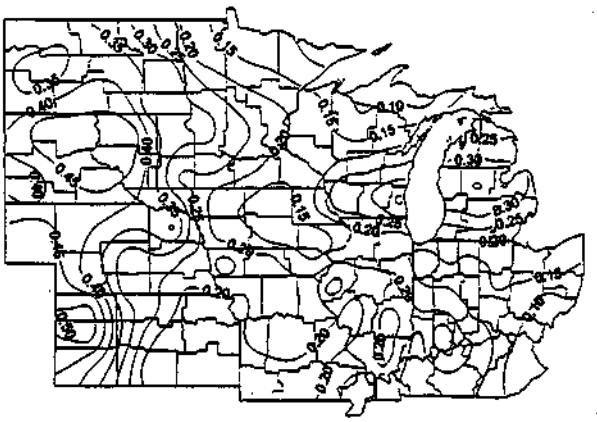

Ear initiation to end-of-row-set

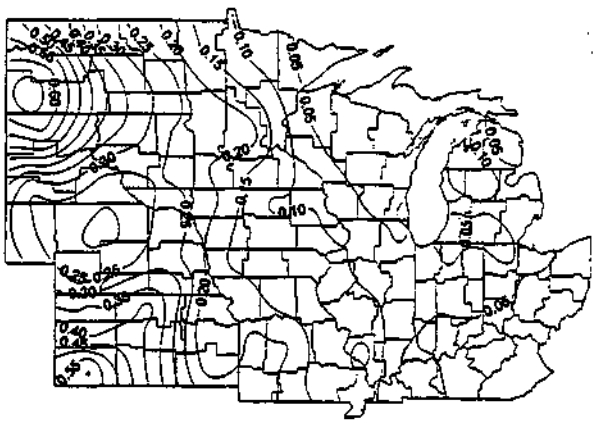

End-of-row-set to silk

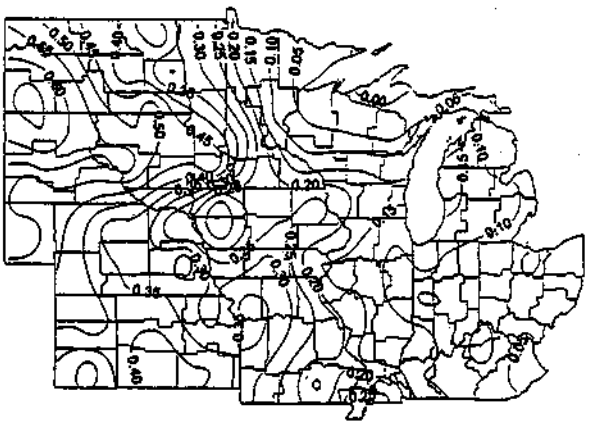

Silk to end-of-lag-phase

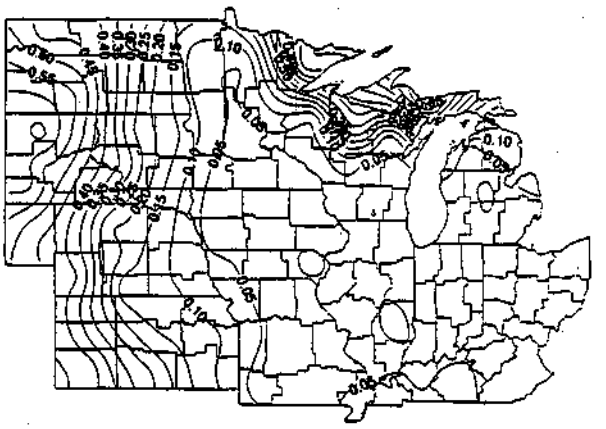

End-of-lag-phase to maturity

Figure H.1.3.10.e. Probability of rainfall less than or equal to 25 percent of potential evapotranspiration during the different corn growth stages with a date of planting 10 days after normal. In the Central Com Belt this represents planting in late-May. .

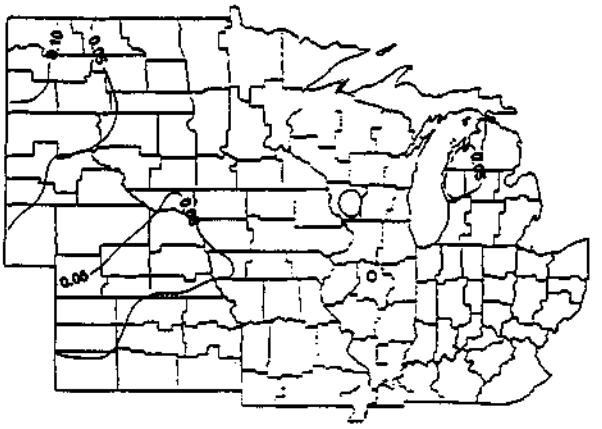

Planting to tassel initiation

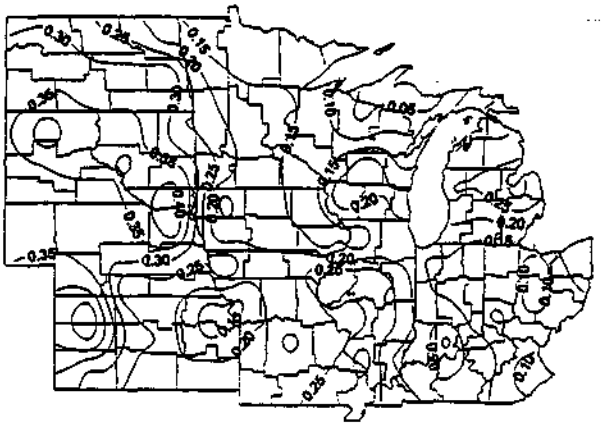

Tassel initiation to ear initiation

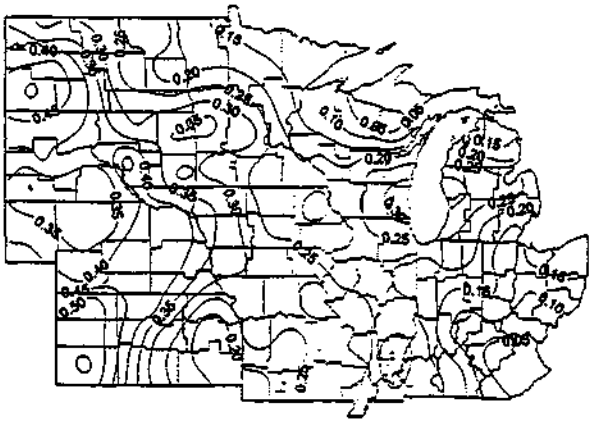

Ear initiation to end-of-row-set

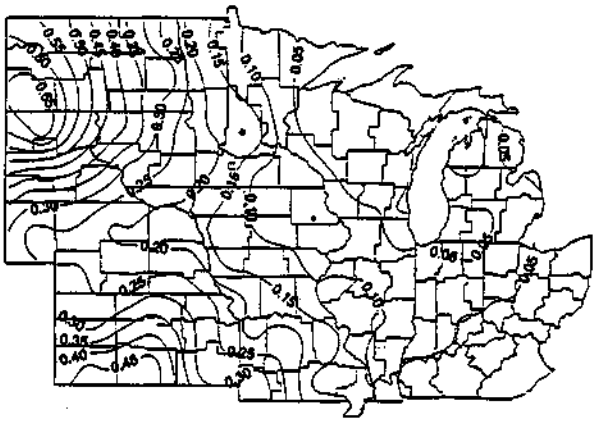

End-of-row-set to silk

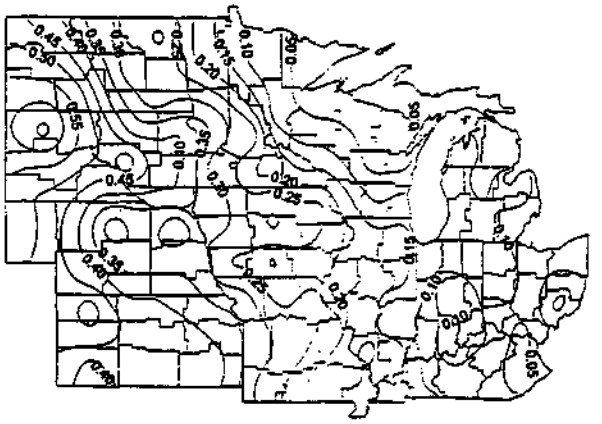

Silk to end-of-lag-phase

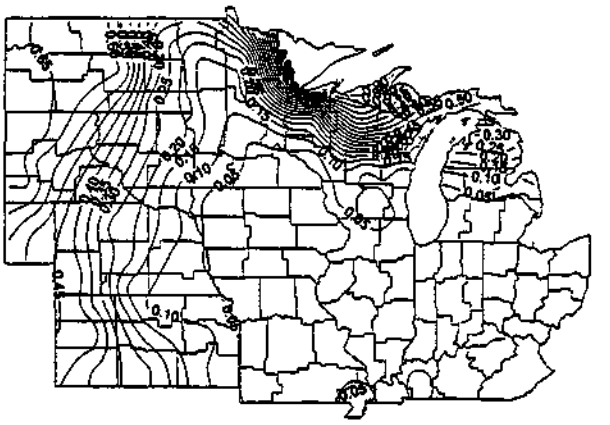

End-of-lag-phase to maturity

Figure H.1.3.10.f. Probability of rainfall less than or equal to 25 percent of potential evapotranspiration during the different corn growth stages with a date of planting 20 days after normal. In the Central Corn Belt this represents planting in early-June,

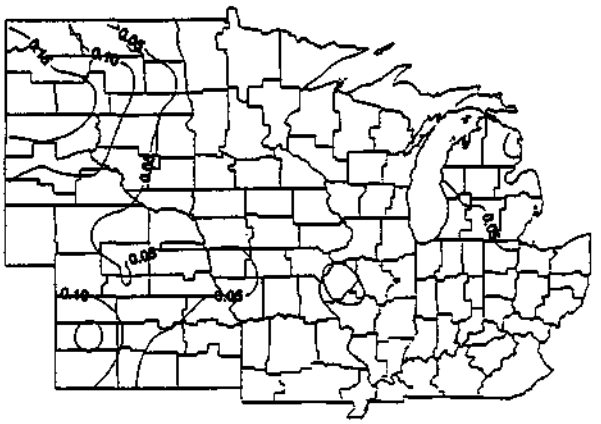

Planting to tassel initiation

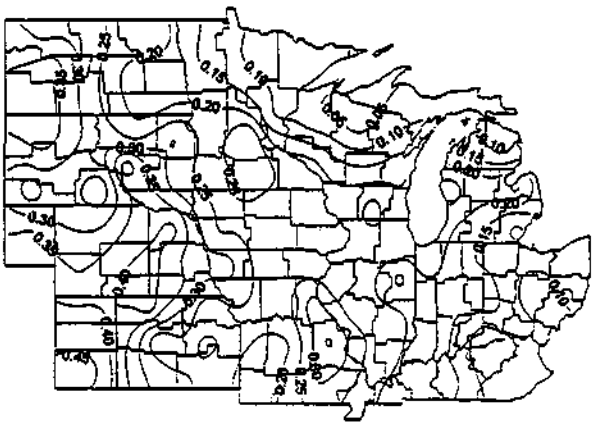

Tassel initiation to ear initiation

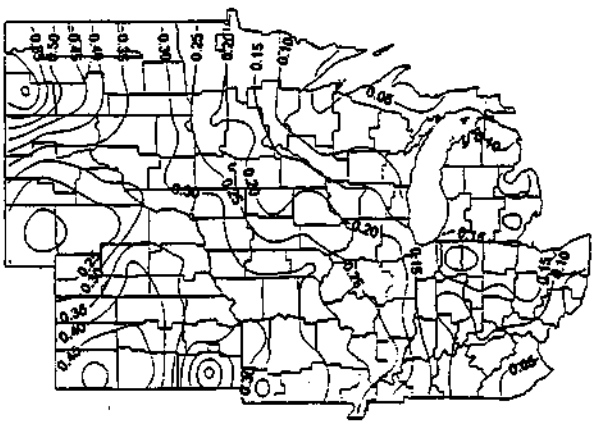

Ear initiation to end-of-row-set

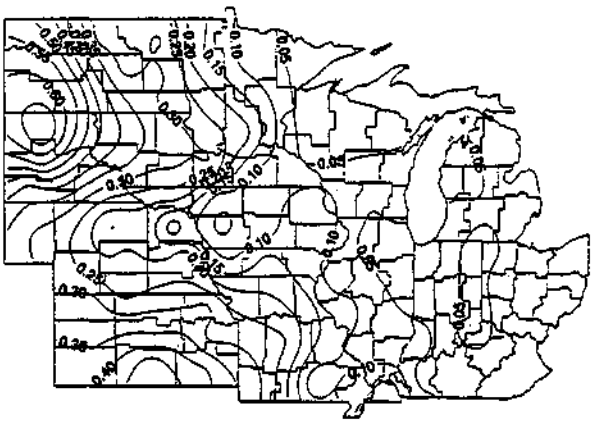

End-of-row-set to silk

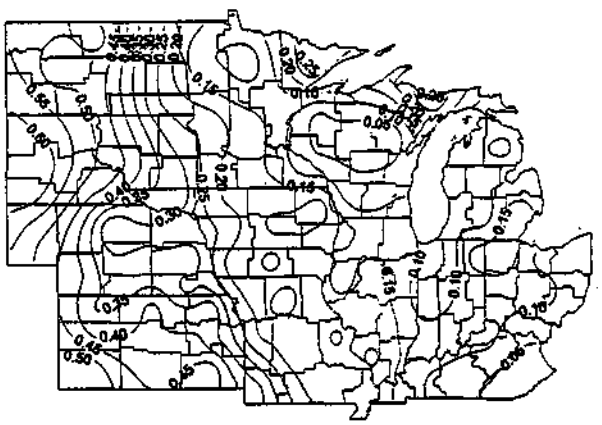

Silk to end-of-lag-phase

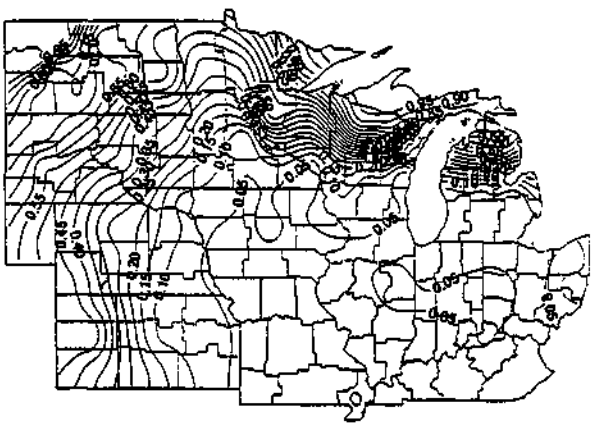

End-of-lag-phase to maturity

Figure H.1.3.10.g. Probability of rainfall less than or equal to 25 percent of potential evapotranspiration during the different corn growth stages with a date of planting 30 days after normal. In the Central Com Belt this represents planting in mid-June. .

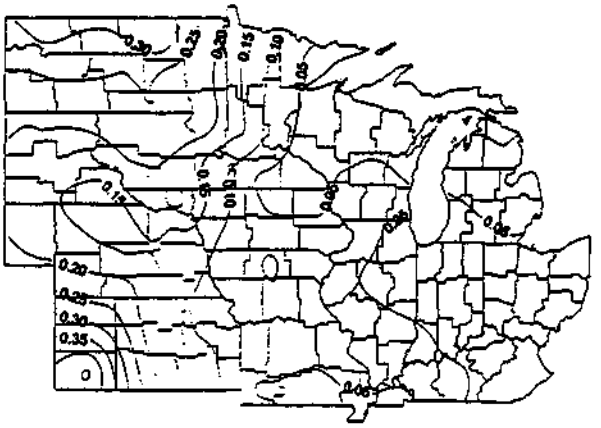

Planting to tassel initiation

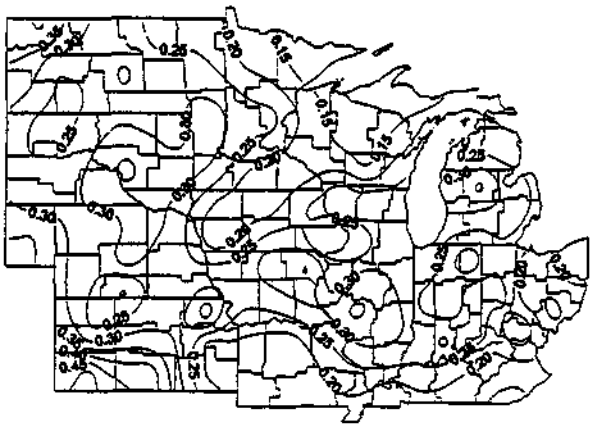

Tassel initiation to ear initiation

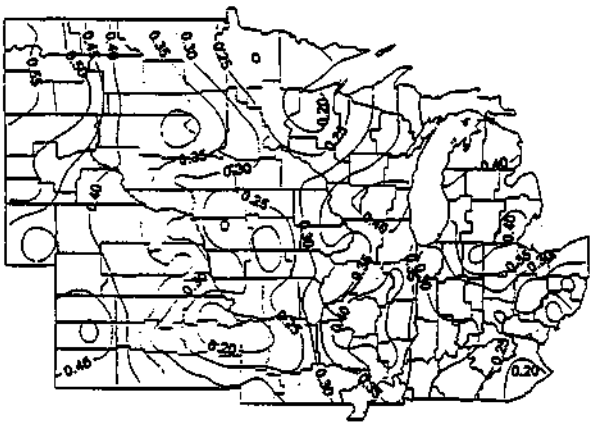

Ear initiation to end-of-row-set

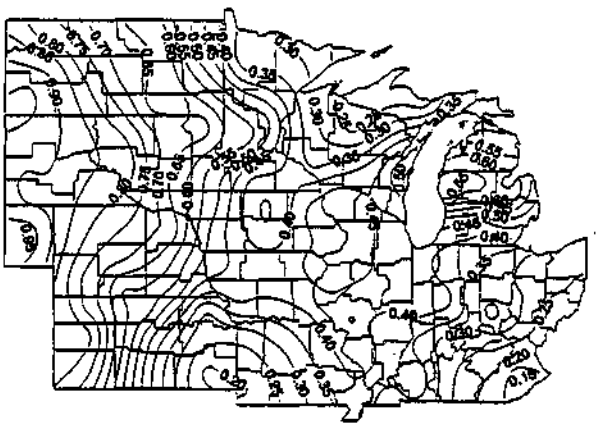

End-of-row-set to silk

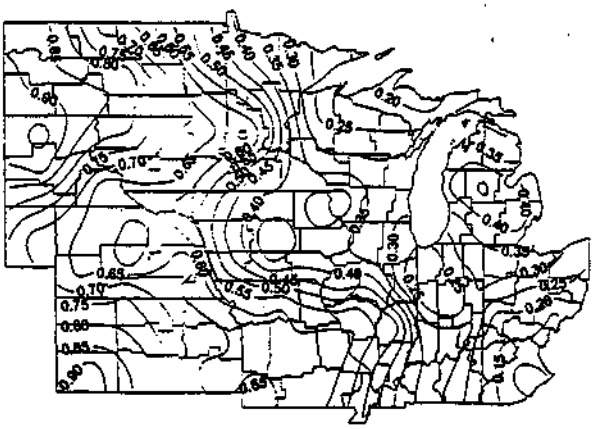

Silk to end-of-lag-phase

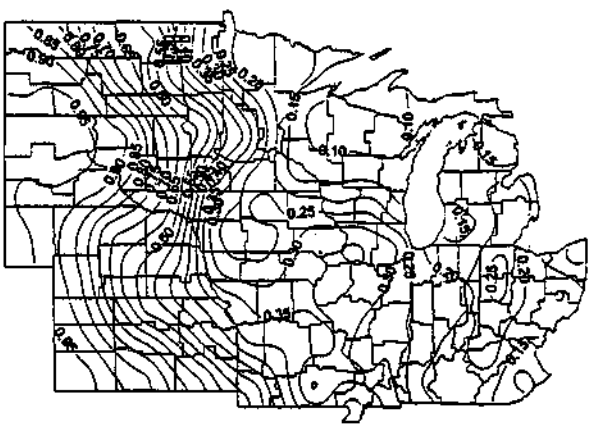

End-of-lag-phase to maturity

Figure H.1.3.11.a. Probability of rainfall less than or equal to 50 percent of potential evapotranspiration during the different com growth stages with a date of planting 30 days before normal. In the Central Corn Belt this represents planting in mid-April.

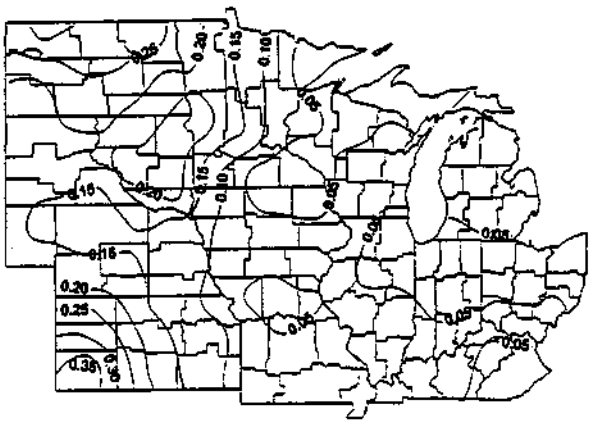

Planting to tassel initiation

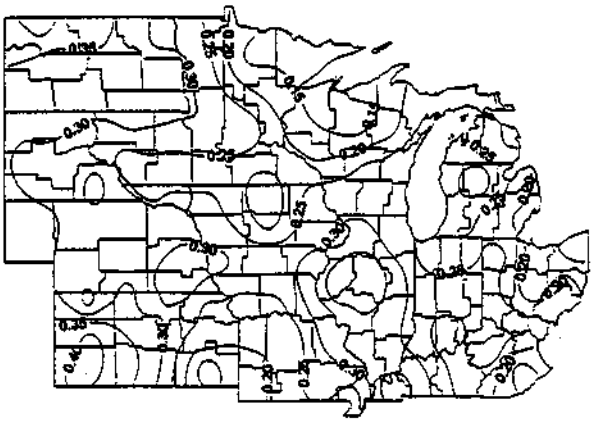

Tassel initiation to ear initiation

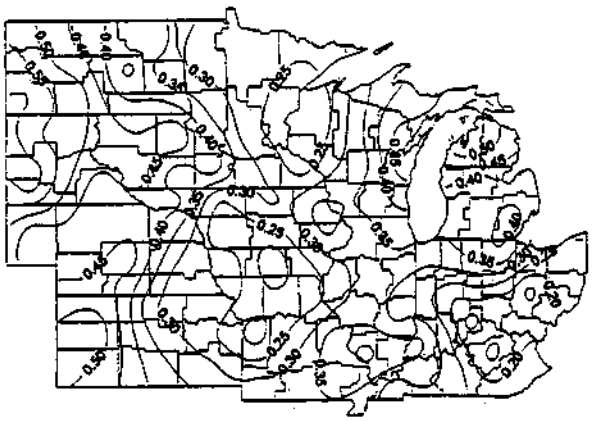

Ear initiation to end-of-row-set

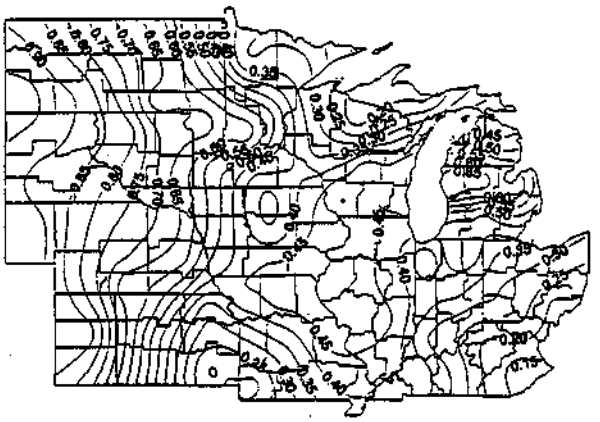

End-of-row-set to silk

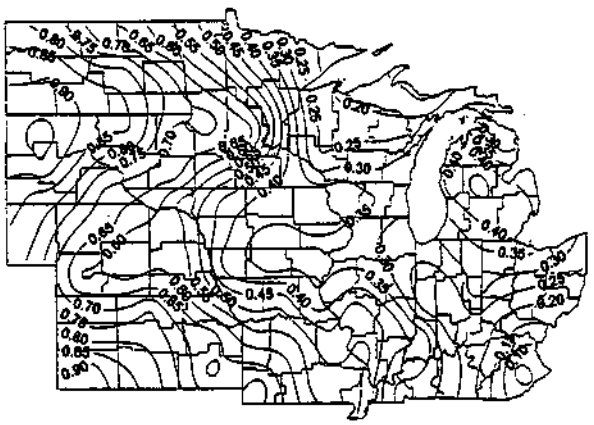

Silk to end-of-lag-phase

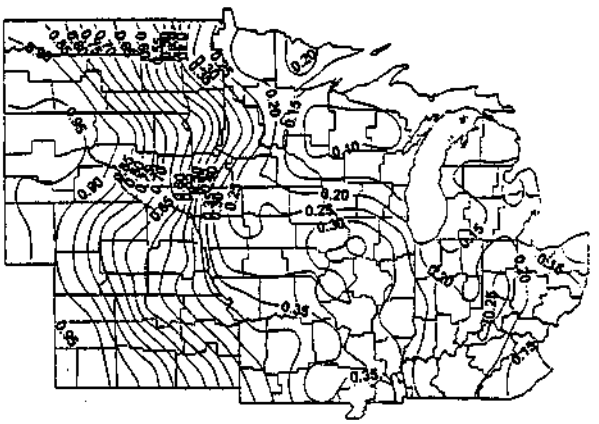

End-of-lag-phase to maturity

Figure H.1.3.11.b. Probability of rainfall less than or equal to 50 percent of potential evapotranspiration during the different corn growth stages with a date of planting 20 days before normal. In the Central Com Belt this represents planting in late-April.

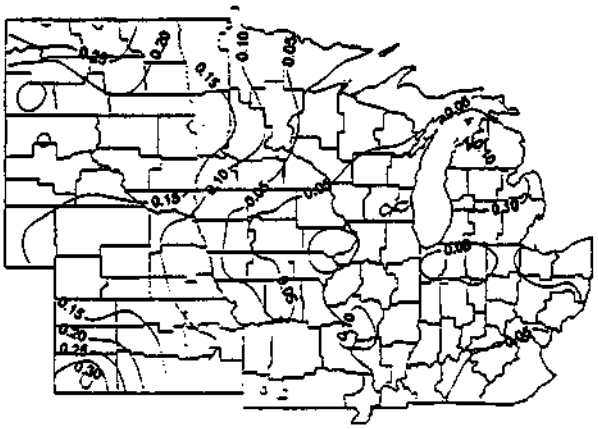

Planting to tassel initiation

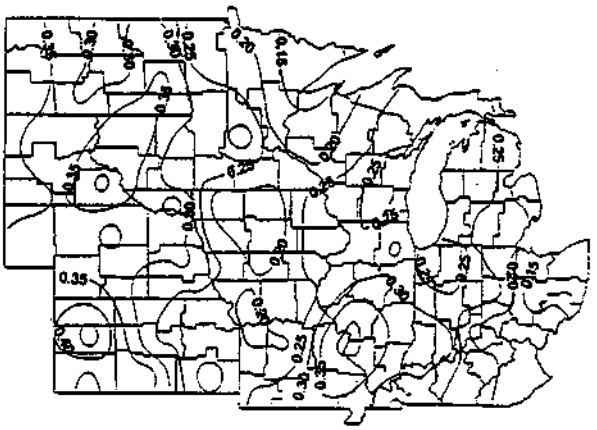

Tassel initiation to ear initiation

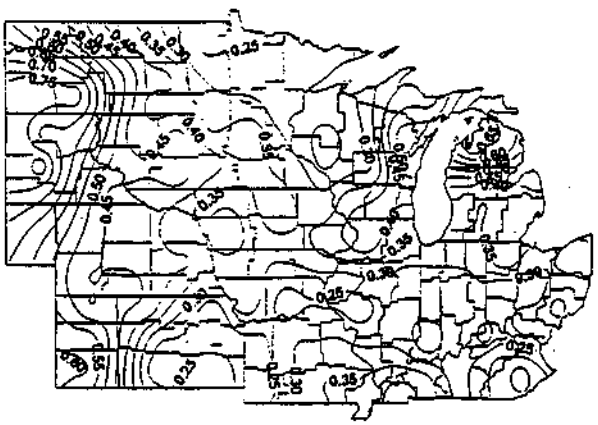

Ear initiation to end-of-row-set

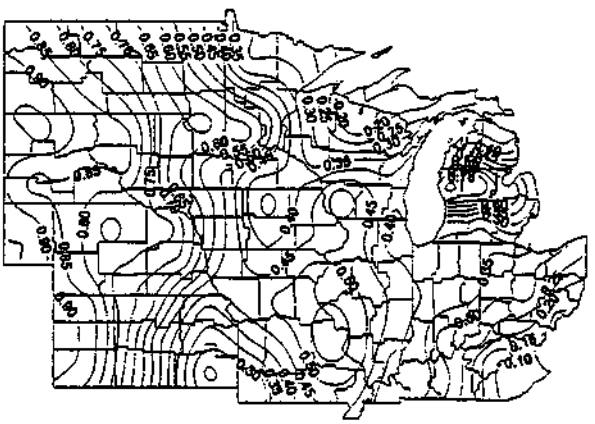

End-of-row-set to silk

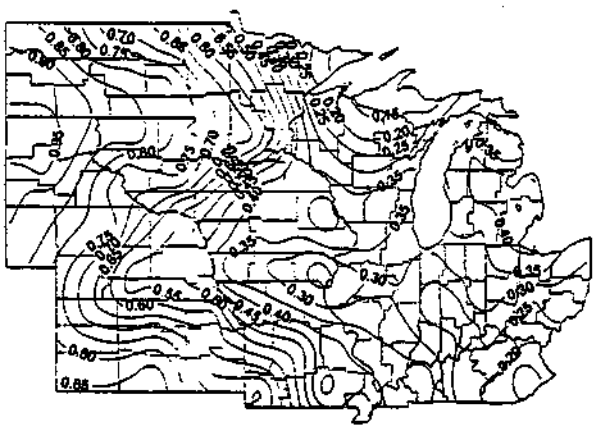

Silk to end-of-lag-phase

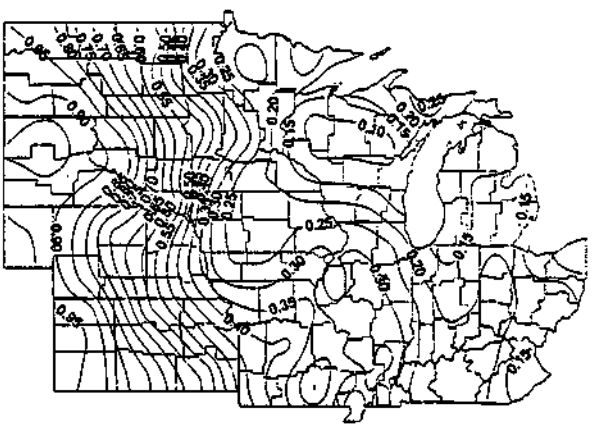

End-of-lag-phase to maturity

Figure H.1.3.11.c. Probability of rainfall less than or equal to 50 percent of potential evapotranspiration during the different corn growth stages with a date of planting 10 days before normal. In the Central Com Belt this represents planting in early-May.

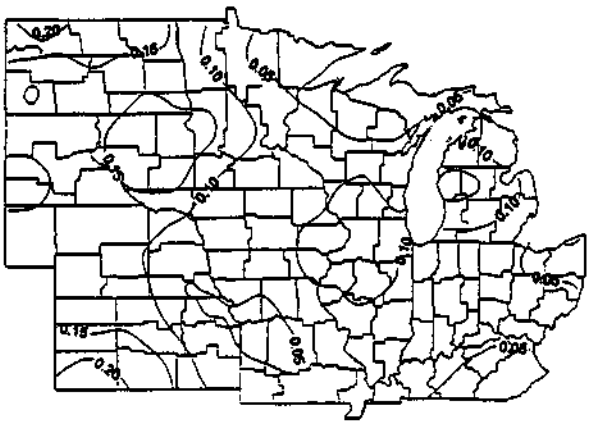

Planting to tassel initiation

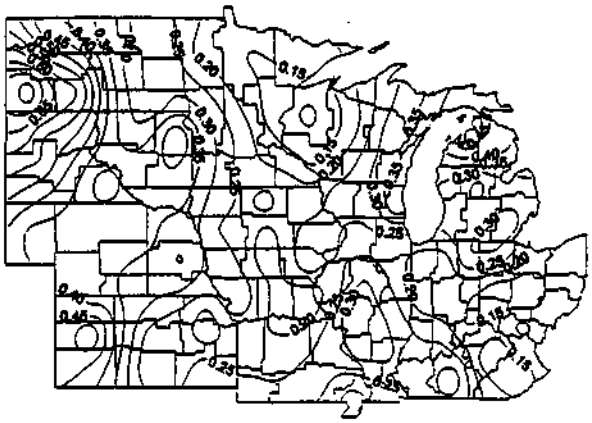

Tassel initiation to ear initiation

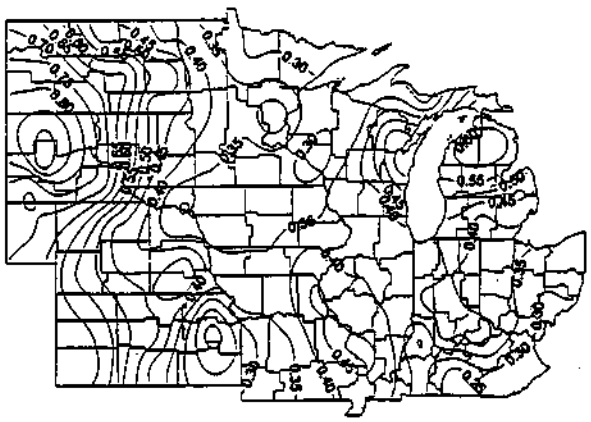

Ear initiation to end-of-row-set

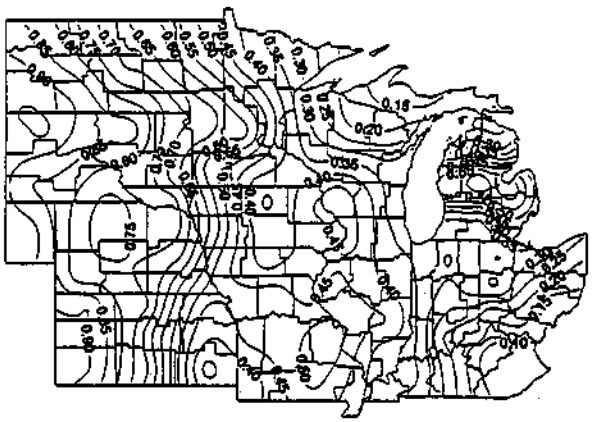

End-of-row-set to silk

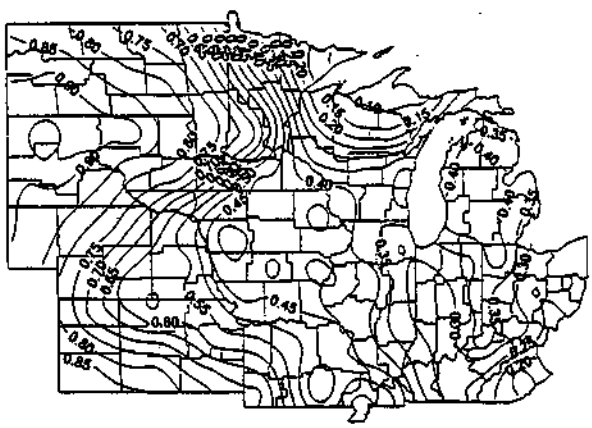

Silk to end-of-lag-phase

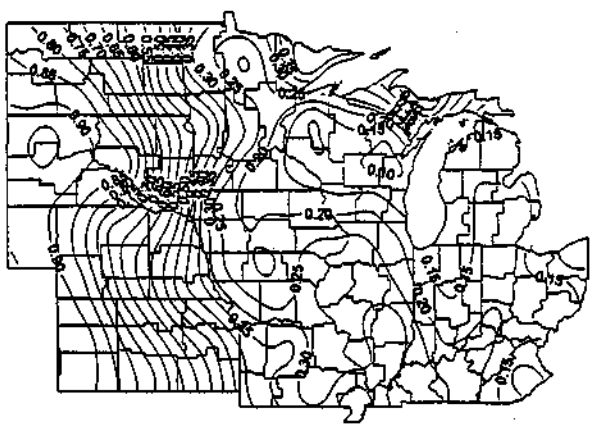

End-of-lag-phase to maturity

Figure H.1.3.11.d. Probability of rainfall less than or equal to 50 percent of potential evapotranspiration during the different com growth stages with a nromal date of planting. In the Central Corn Belt this represents planting in mid-May.

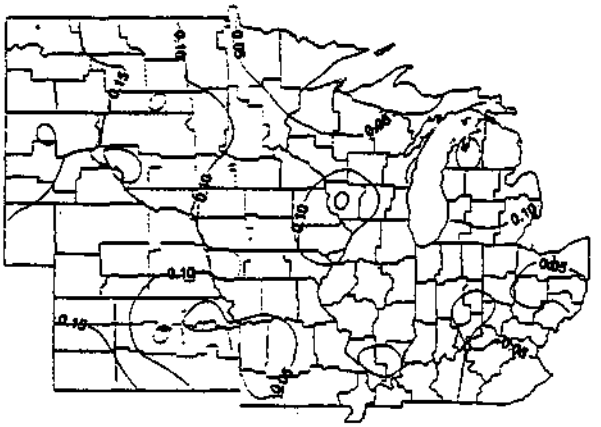

Planting to tassel initiation

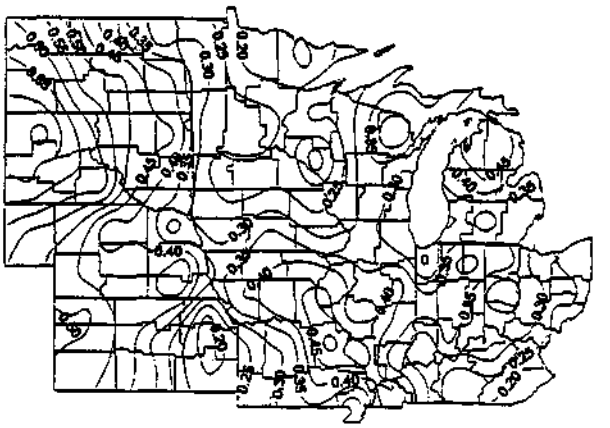

Tassel initiation to ear initiation

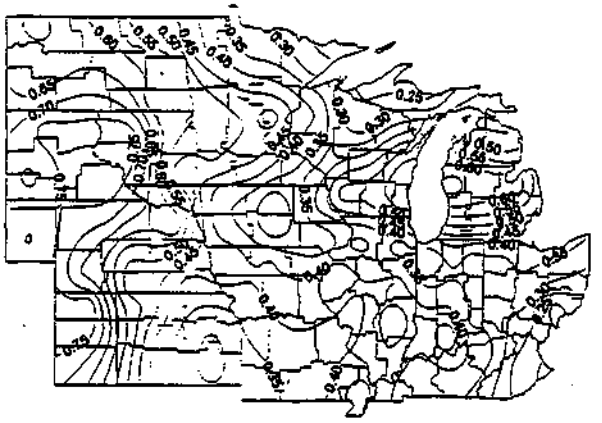

Ear initiation to end-of-row-set

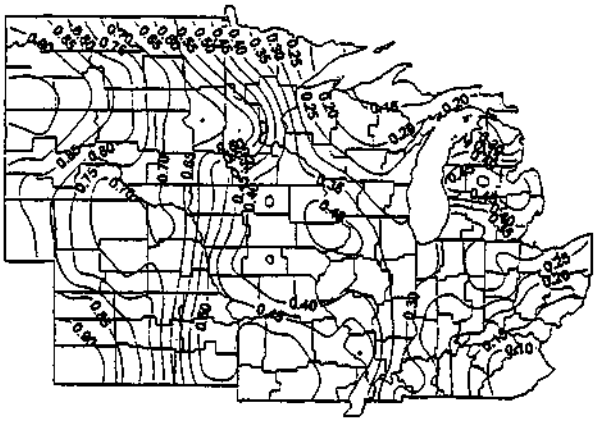

End-of-row-set to silk

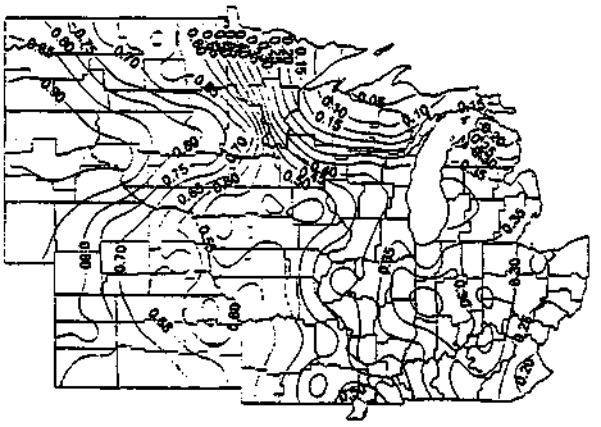

Silk to end-of-lag-phase

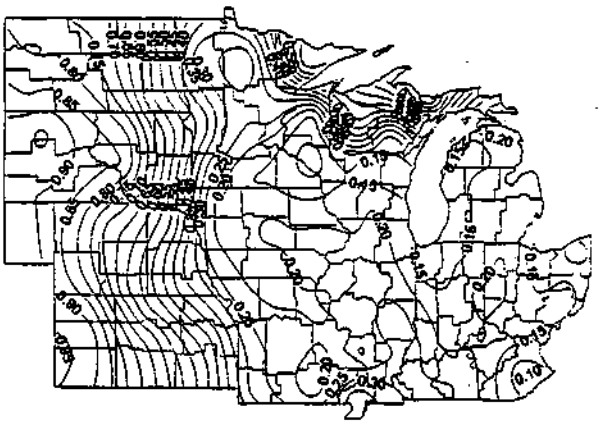

End-of-lag-phase to maturity

Figure H.1.3.11.e. Probability of rainfall less than or equal to 50 percent of potential evapotranspiration during the different com growth stages with a date of planting 10 days after normal. In the Central Com Belt this represents planting in late-May.

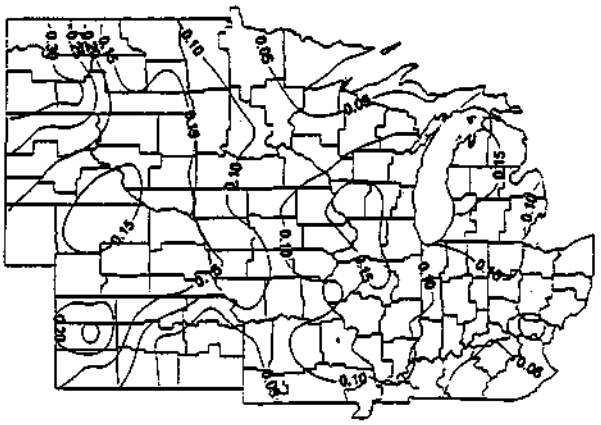

Planting to tassel initiation

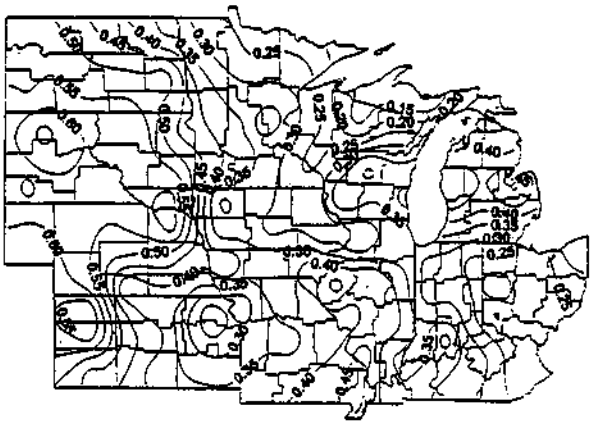

Tassel initiation to ear initiation

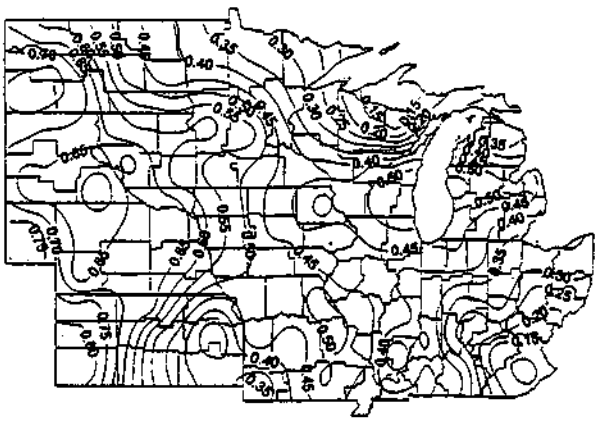

Ear initiation to end-of-row-set

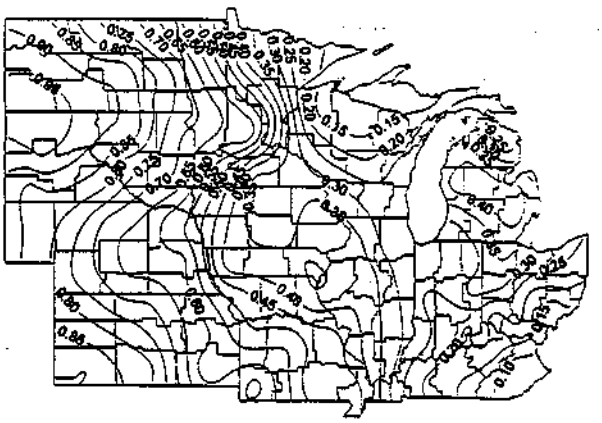

End-of-row-set to silk

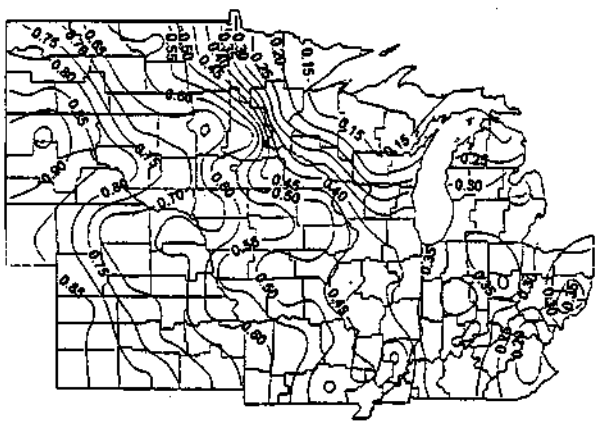

Silk to end-of-lag-phase

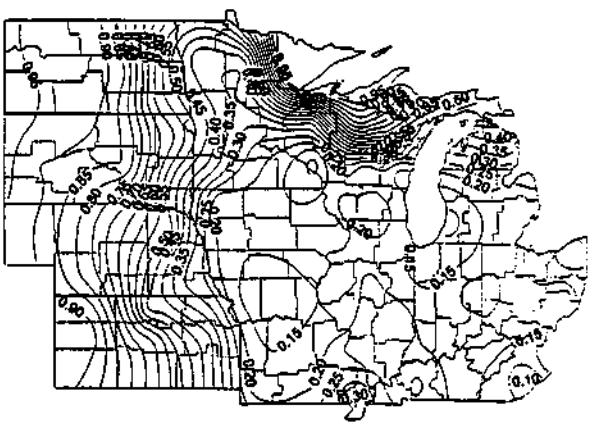

End-of-lag-phase to maturity

Figure H.1.3.11.f. Probability of rainfall less than or equal to 50 percent of potential evapotranspiration during the different corn growth stages with a date of planting 20 days after normal. In the Central Corn Belt this represents planting in early-June.

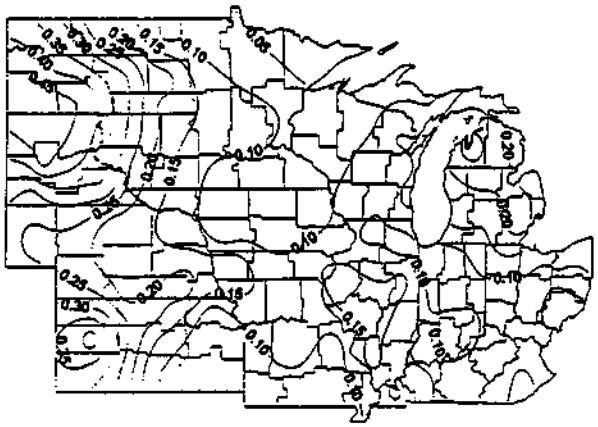

Planting to tassel initiation

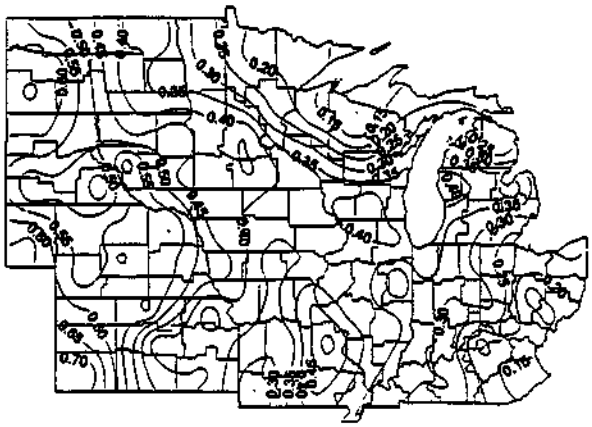

Tassel initiation to ear initiation

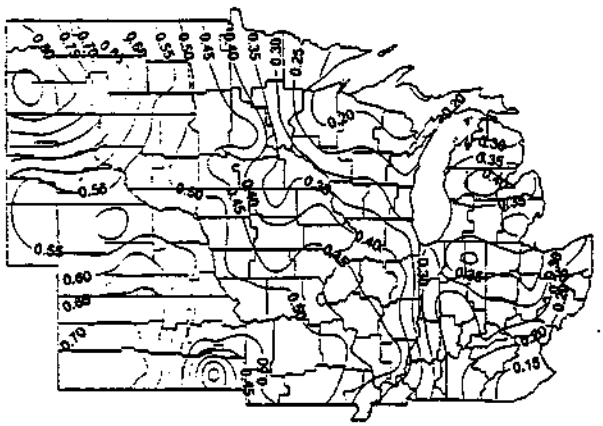

Ear initiation to end-of-row-set

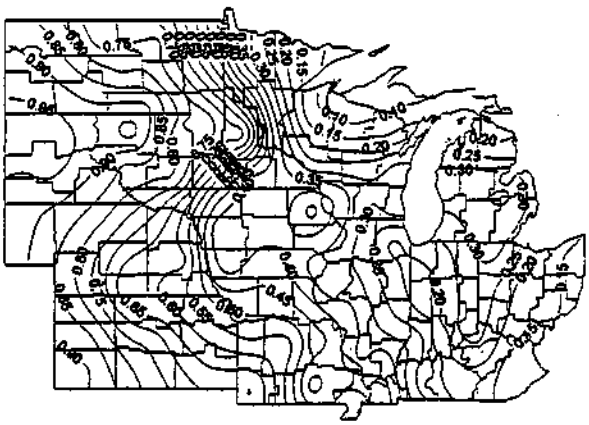

End-of-row-set to silk

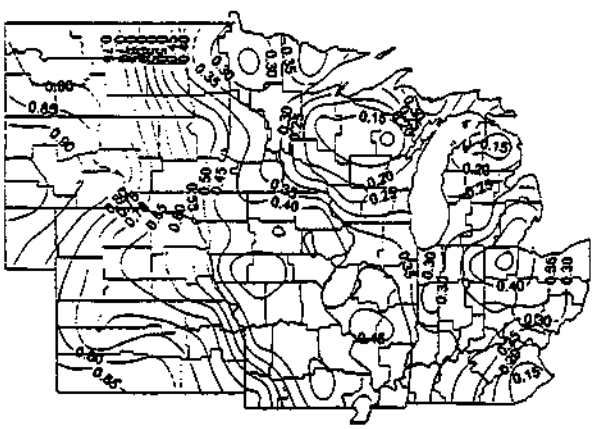

Silk to end-of-lag-phase

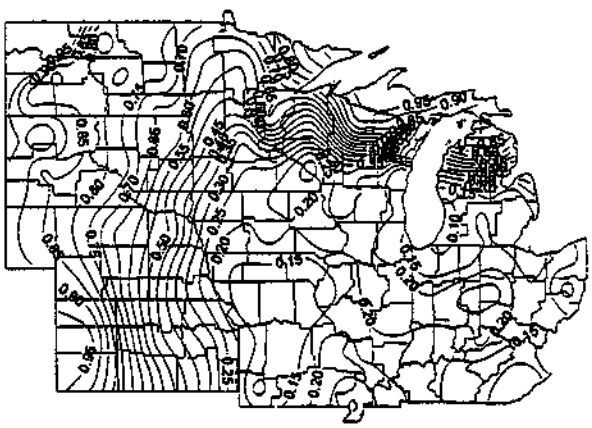

End-of-lag-phase to maturity

Figure H.1.3.11.g. Probability of rainfall less than or equal to 50 percent of potential evapotranspiration during the different corn growth stages with a date of planting 30 days after normal. In the Central Corn Belt this represents planting in mid-June.

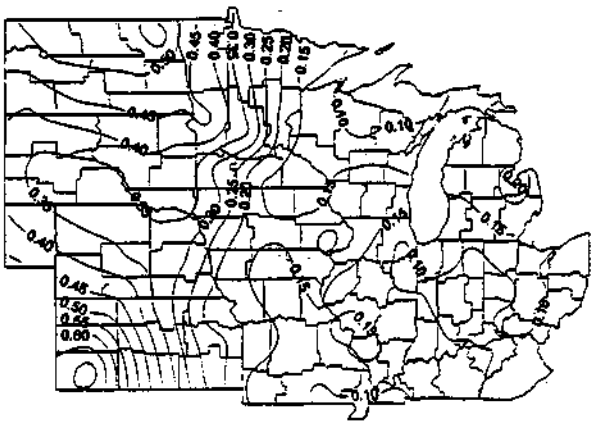

Planting to tassel initiation

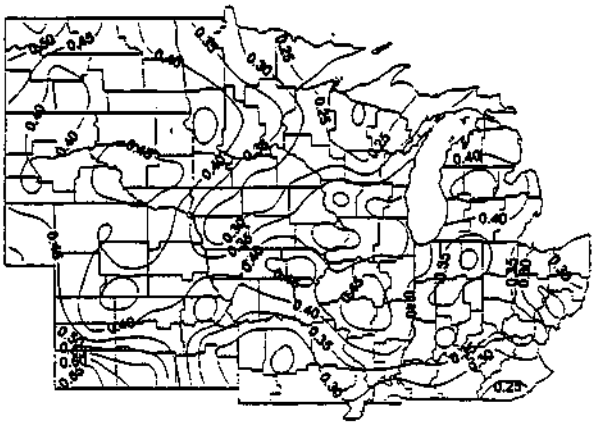

Tassel initiation to ear initiation

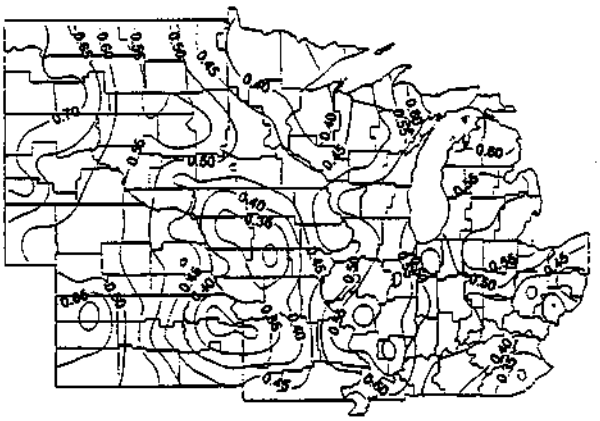

Ear initiation to end-of-row-set

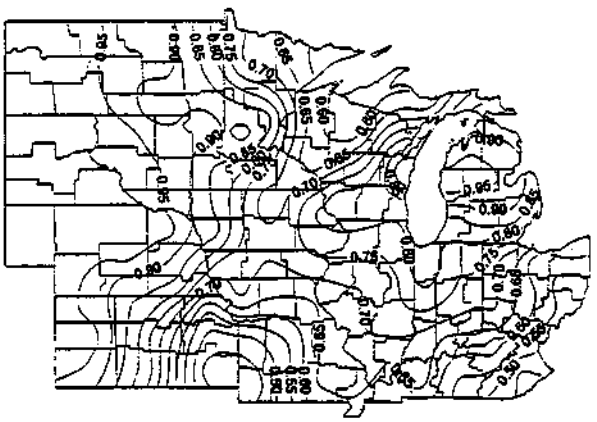

End-of-row-set to silk

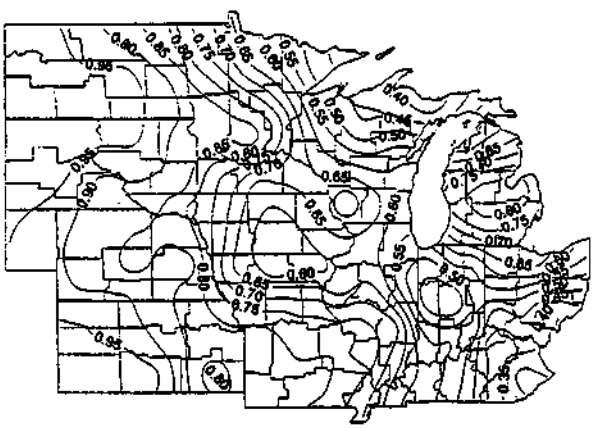

Silk to end-of-lag-phase

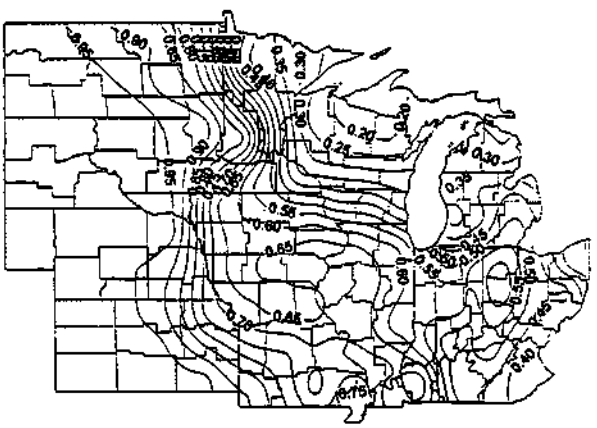

End-of-lag-phase to maturity

Figure H.1.3.12.a. Probability of rainfall less than or equal to 75 percent of potential evapotranspiration during the different corn growth stages with a date of planting 30 days before normal. In the Central Com Belt this represents planting in mid-April.

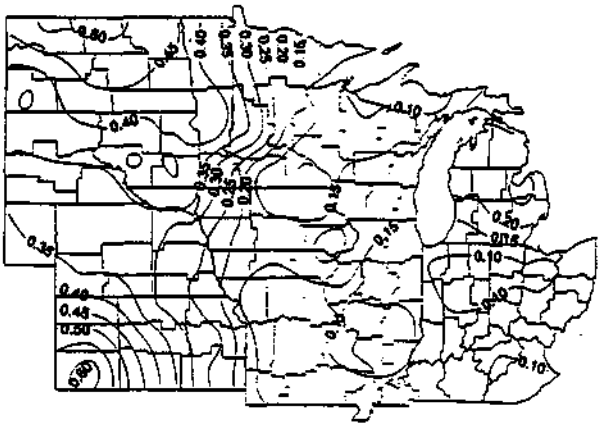

Planting to tassel initiation

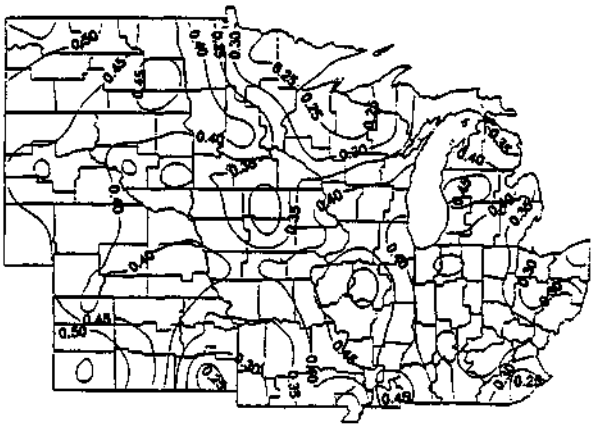

Tassel initiation to ear initiation

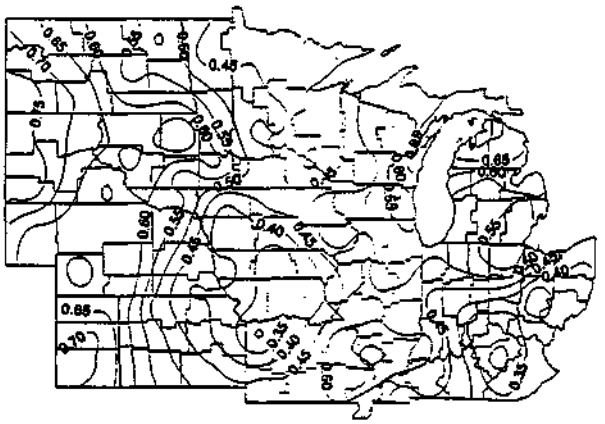

Ear initiation to end-of-row-set

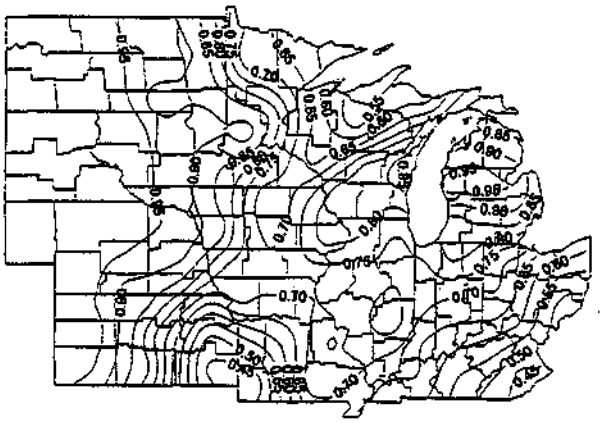

End-of-row-set to silk

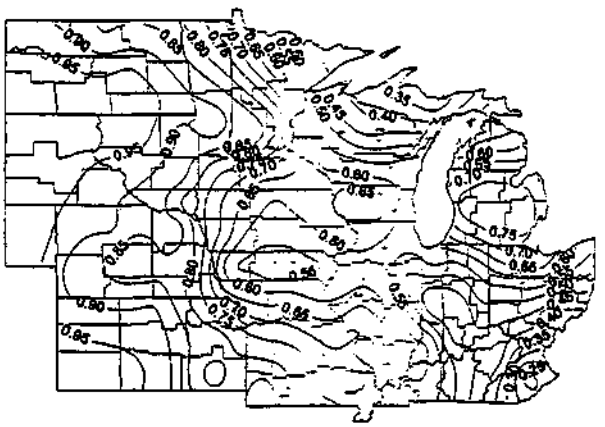

Silk to end-of-lag-phase

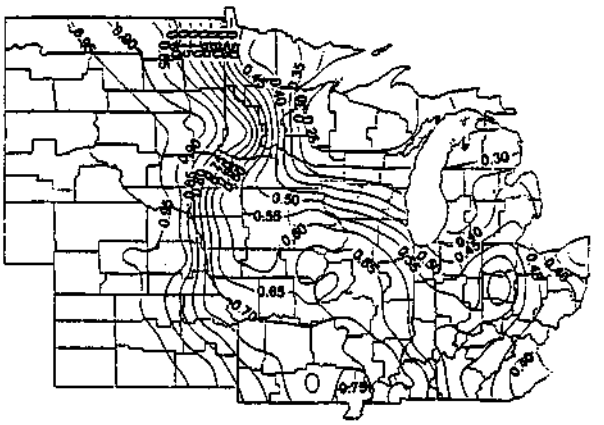

End-of-lag-phase to maturity

Figure H.1.3.12.b. Probability of rainfall less than or equal to 75 percent of potential evapotranspiration during the different corn growth stages with a date of planting 20 days before normal. In the Central Corn Belt this represents planting in late-April.

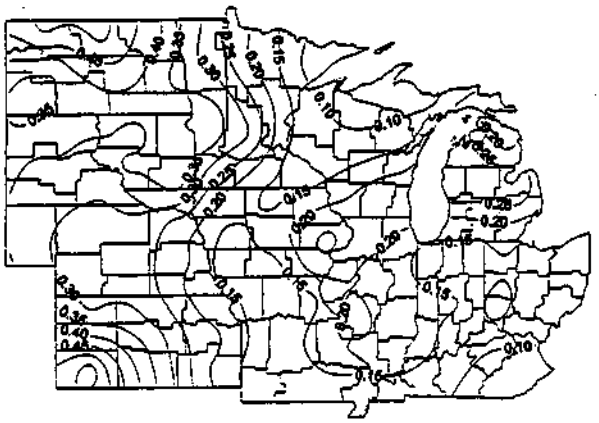

Planting to tassel initiation

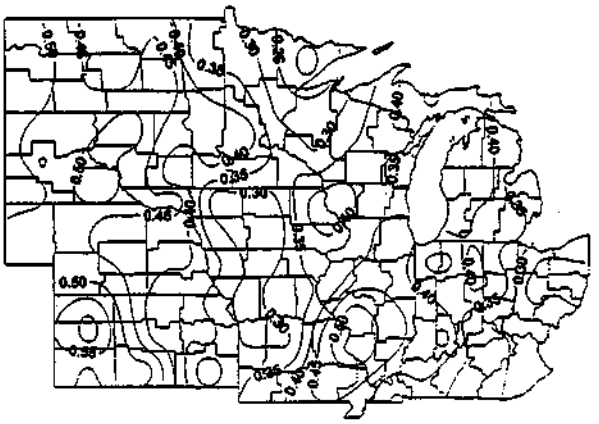

Tassel initiation to ear initiation

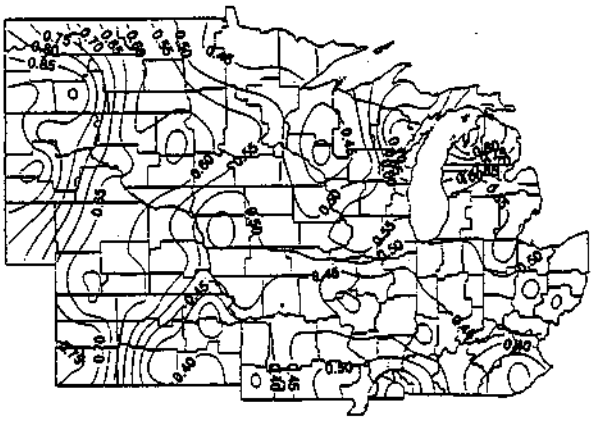

Ear initiation to end-of-row-set

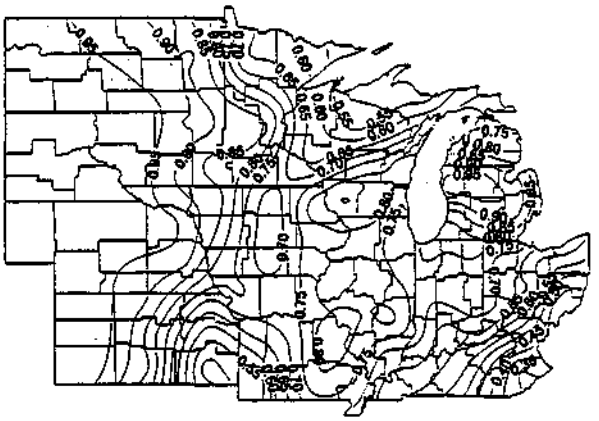

End-of-row-set to silk

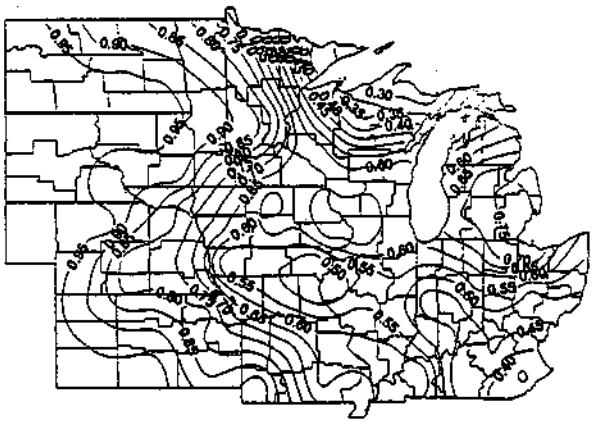

Silk to end-of-lag-phase

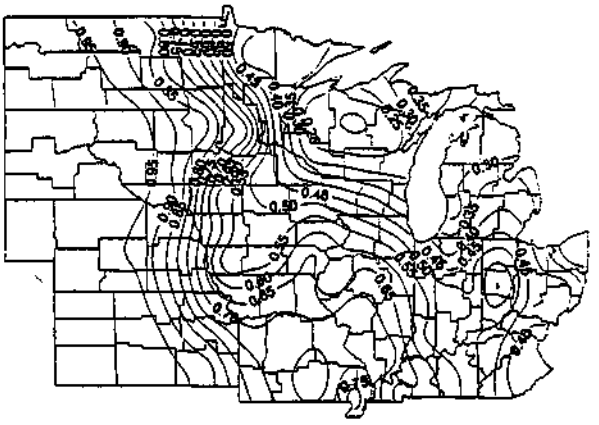

End-of-lag-phase to maturity

Figure H.1.3.12.c. Probability of rainfall less than or equal to 75 percent of potential evapotranspiration during the different corn growth stages with a date of planting 10 days before normal. In the Central Com Belt this represents planting in early-May.

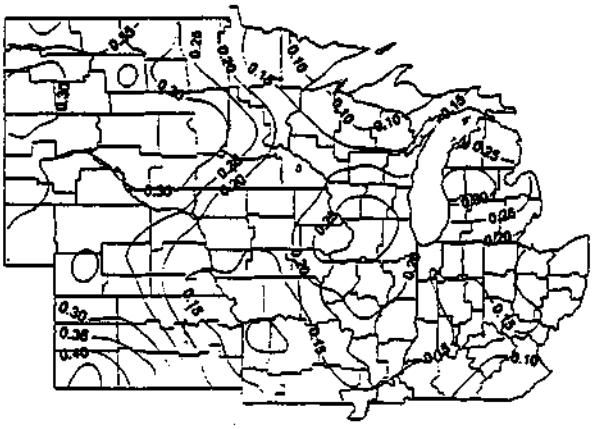

Planting to tassel initiation

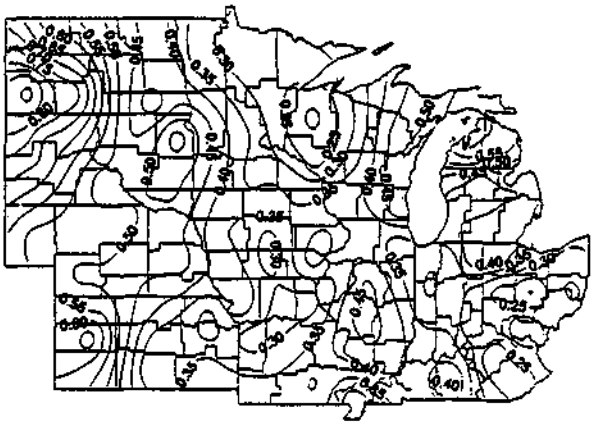

Tassel initiation to ear initiation

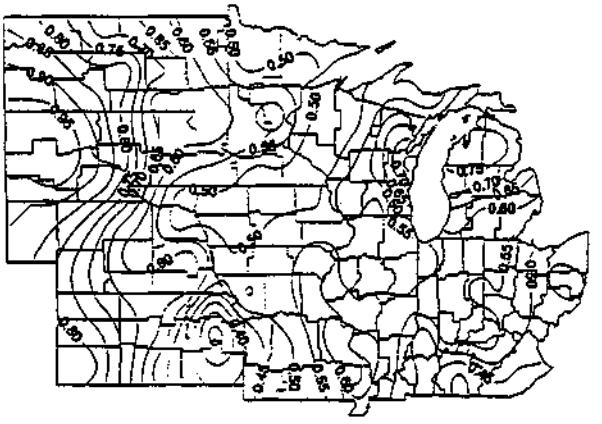

Ear initiation to end-of-row-set

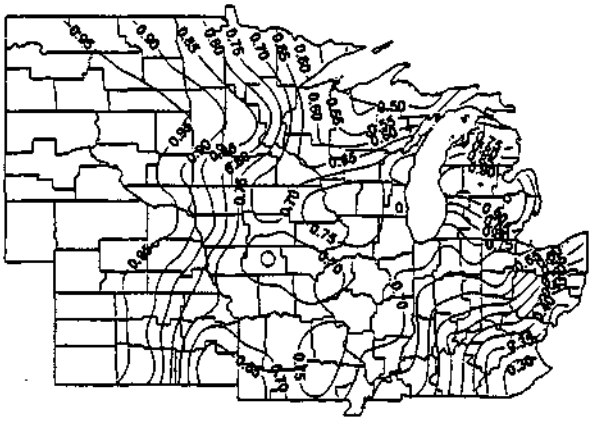

End-ot-row-set to silk

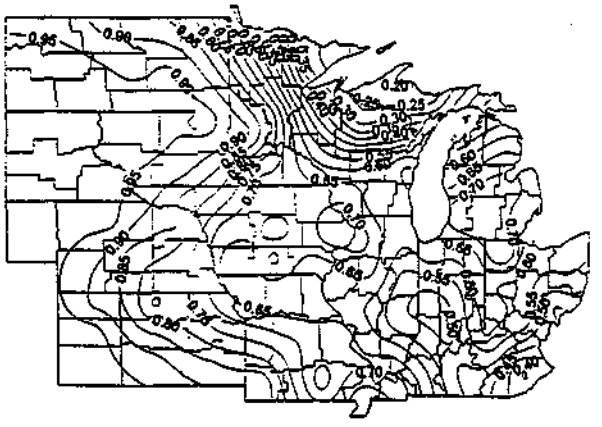

Silk to end-of-lag-phase

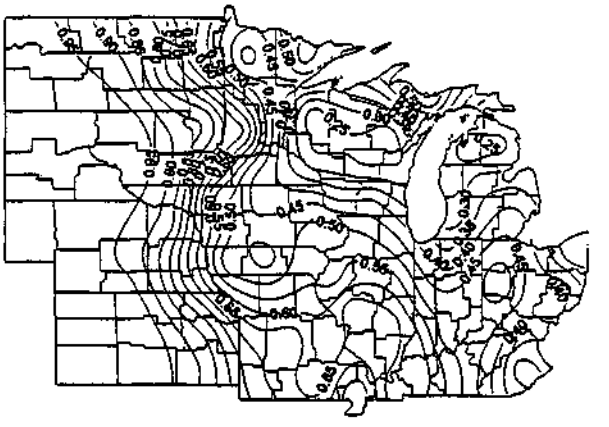

End-of-lag-phase to maturity

Figure H.1.3.12.d. Probability of rainfall less than or equal to 75 percent of potential evapotranspiration during the different corn growth stages with a nromal date of planting. In the Central Com Belt this represents planting in mid-May.

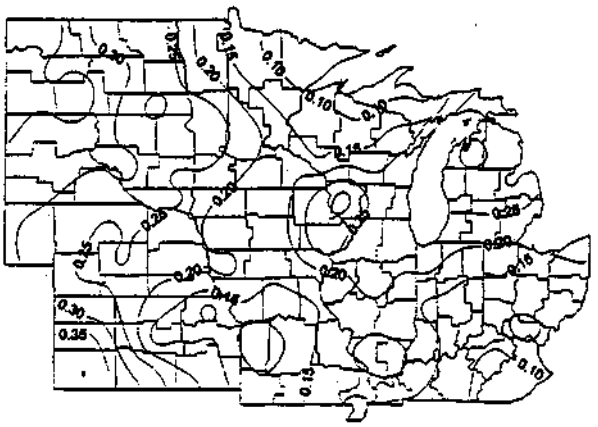

Planting to tassel initiation

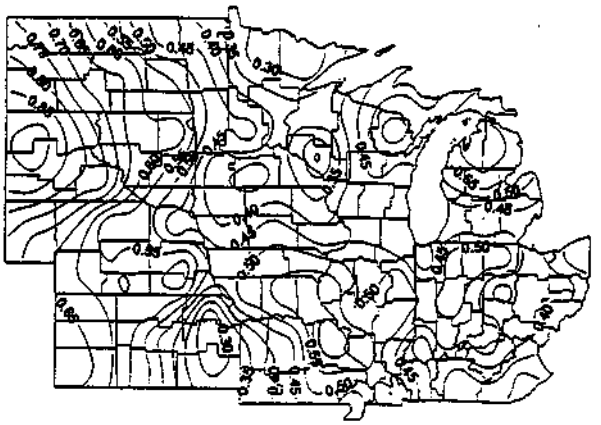

Tassel initiation to ear initiation

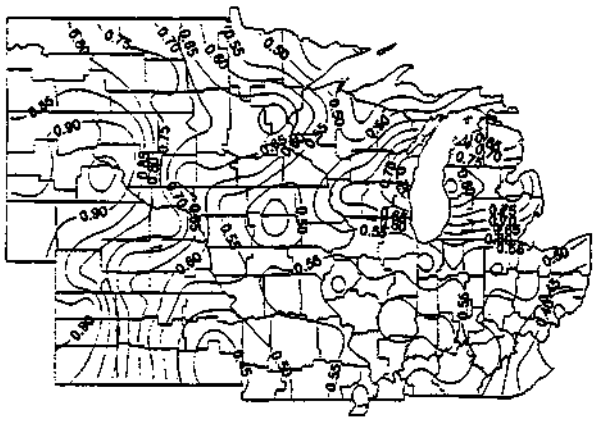

Ear initiation to end-of-row-set

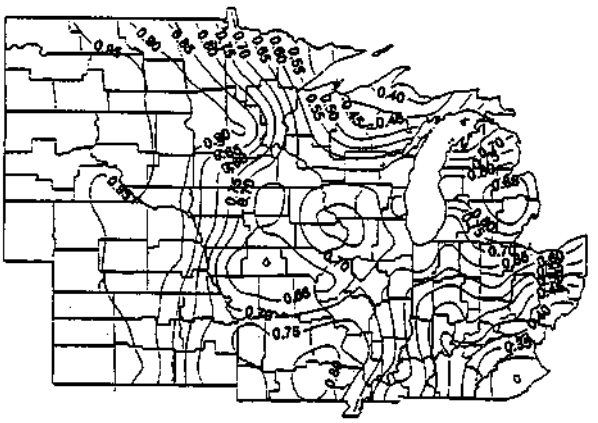

End-of-row-set to silk

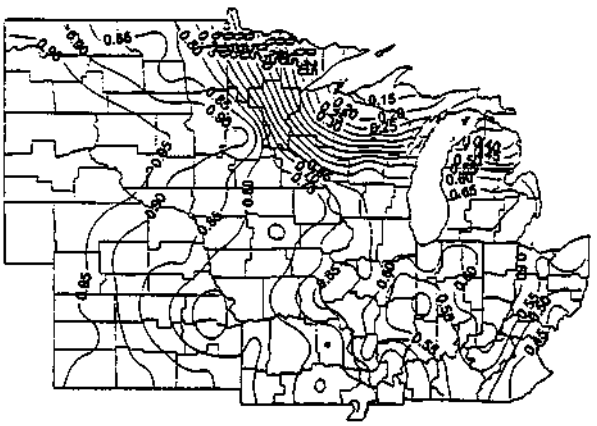

Silk to end-of-lag-phase

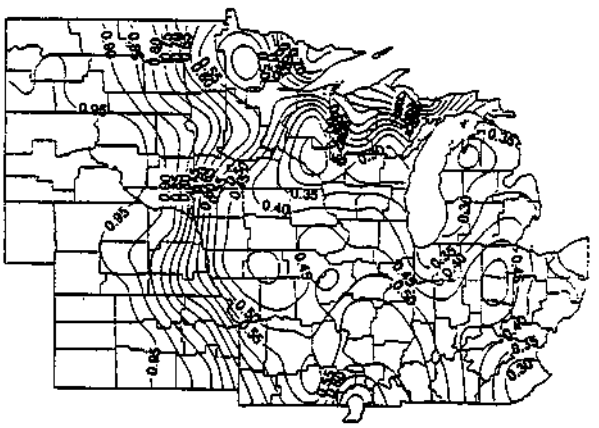

End-of-lag-phase to maturity

Figure H.1.3.12.e. Probability of rainfall less than or equal to 75 percent of potential evapotranspiration during the different corn growth stages with a date of planting 10 days after normal. In the Central Corn Belt this represents planting in late-May.

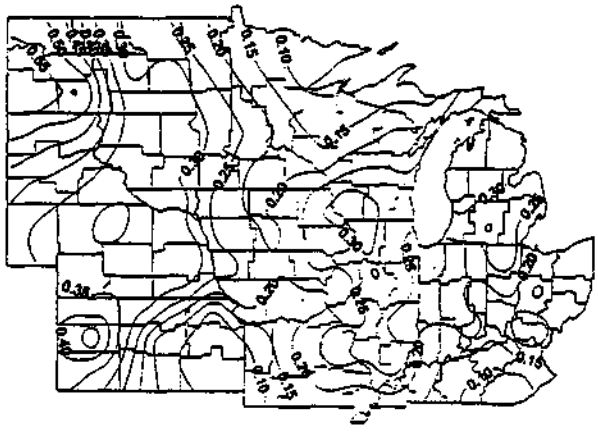

Planting to tassel initiation

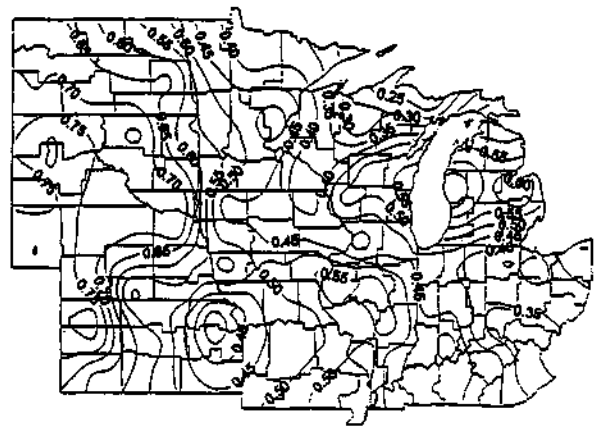

Tassel initiation to ear initiation

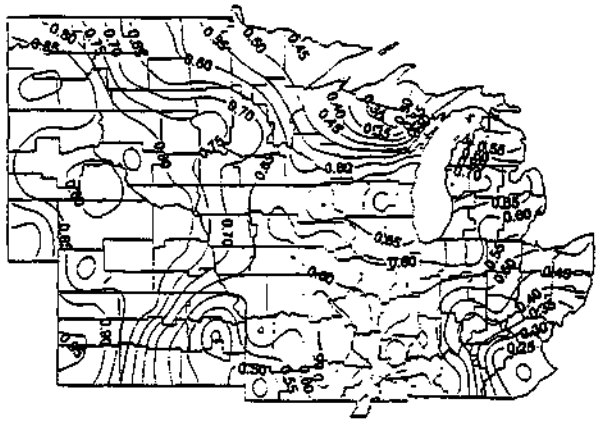

Ear initiation to end-of-row-set

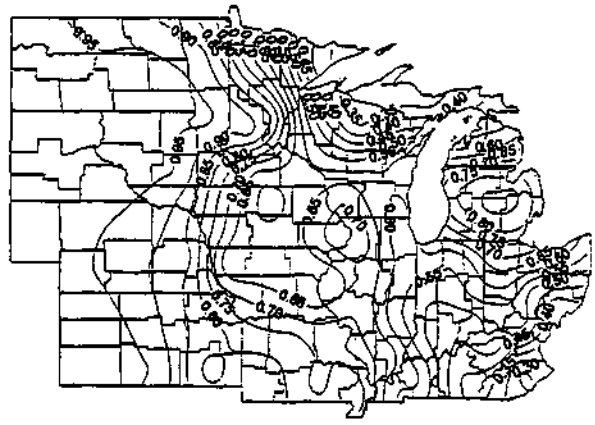

End-of-row-set to silk

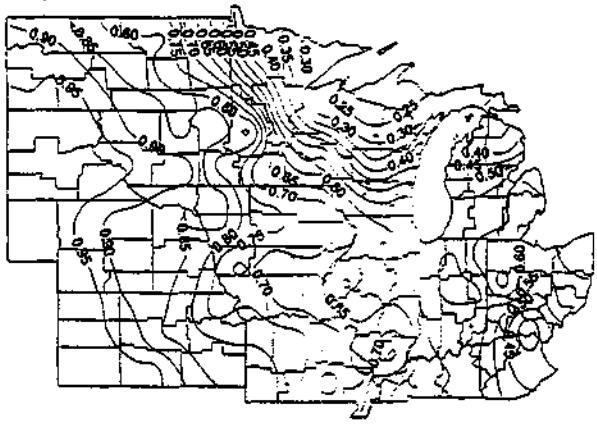

Silk to end-of-lag-phase

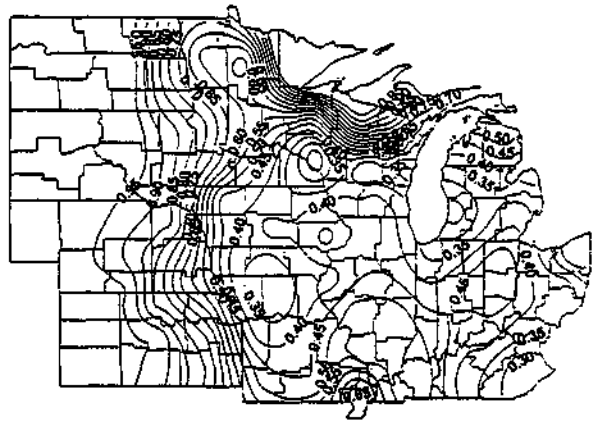

End-of-lag-phase to maturity

Figure H.1.3.12.f. Probability of rainfall less than or equal to 75 percent of potential evapotranspiration during the different corn growth stages with a date of planting 20 days after normal. In the Central Corn Belt this represents planting in earl}-June.

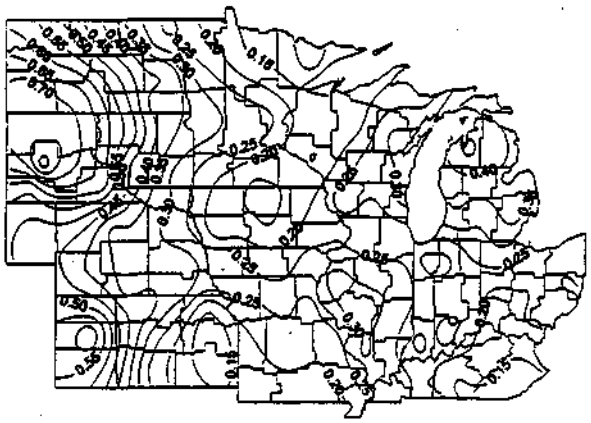

Planting to tassel initiation

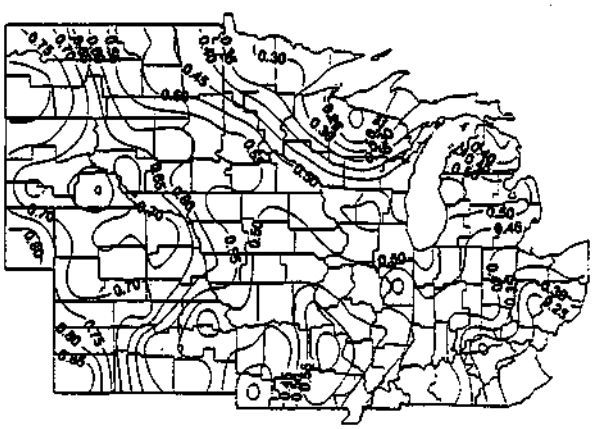

Tassel initiation to ear initiation

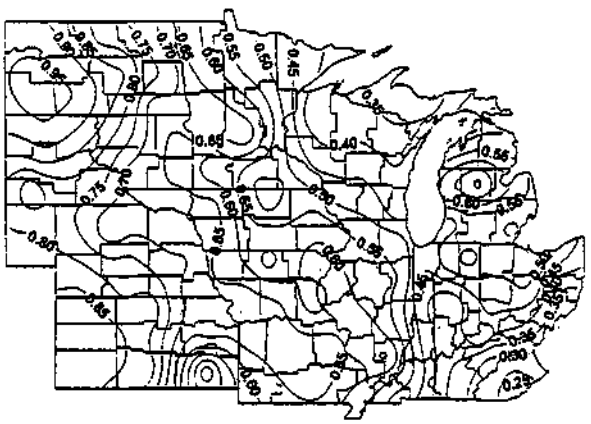

Ear initiation to end-of-row-set

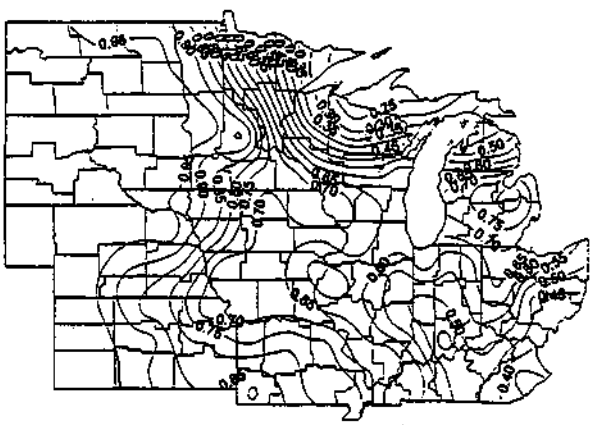

End-of-row-set to silk

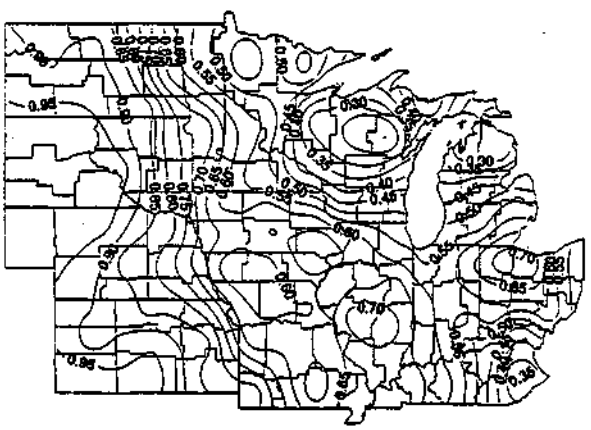

Silk to end-of-lag-phase

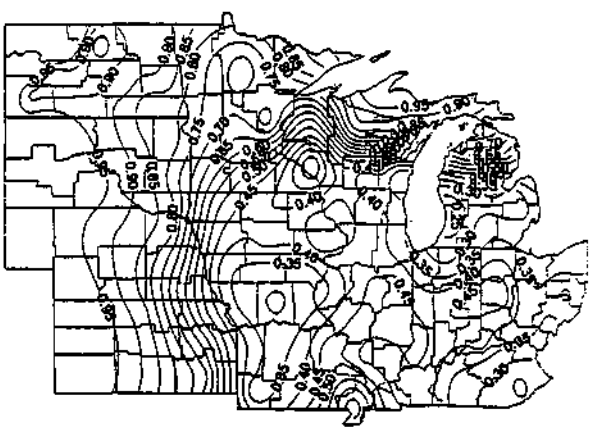

End-of-lag-phase to maturity

Figure H.1.3.12.g. Probability of rainfall less than or equal to 75 percent of potential evapotranspiration during the different corn growth stages with a date of planting 30 days after normal. In the Central Corn Belt this represents planting in mid-June.

REFERENCES

Allison, J. C. S., and D. J. Watson, 1966: The production and distribution of dry matter in maize after flowering. *Ann. Bot.*, **30**: 365-382.

Banwart, W., 1987: The acid rain test plot facility. Agric. College Rep., University of Dlinois, Agronomy Dept., Urbana, Illinois, 36 pp.

Banwart, W. L., 1988: Field evaluation of an acid rain drought stress interaction. *Environ. Pollution*, **53**, 123-133.

Bollero, G. A, 1994: The Effect of Early Season Soil Temperatures on Corn Canopy Development: A Quantitative Approach. Ph.D. Thesis, Agronomy Department, University of Illinois at Urbana-Champaign, Urbana, IL., p 193.

Changnon, S. A., and S. E. Hollinger, 1988: Use of unique field facilities to simulate effects of enhanced rainfall on crop production. *J. Weather Modification*, **20**, 60-66.

Changnon, S. A. and J. C. Neill, 1968: Mesoscale study of corn weather response on cash-grain farms. *J. Appl. Meteor.*, ***7***, 94-104.

Claassen, M. M., and R. H. Shaw, 1970: Water deficit effects on corn. I. Vegetative components. *Agron. J.*, **62**, 649-655.

Coelho, D. T., and R. F. Dale, 1980: An energy crop growth variable and temperature function for predicting corn growth and development: Planting to silking. *Agron. J.*, **72**, 503-510.

Conradsen, K., L. B. Nielsen, and L. P Prahm, 1984: Review of Weibull statistics for estimation of wind speed distributions. *J. Clim. and Appl. Meteor.*, **23**, 1173-1183.

Cross, H. Z., and M. S. Zuber, 1972: Prediction of flowering date in Maize based on different methods of estimating thermal units. *Agron. J.*, **64**, 351-355.

Dixon, B. L., S. E. Hollinger, R. Garcia, and V. Tirupattur, 1994: Estimating corn yield response models to predict impacts of climate change. *J. of Agric. and Res. Econ.*, **19**, 58-68.

Fortin, M. C, and F. J. Pierce, 1990: Development and growth effects of crop residues on corn. *Agron. J.*, **82**: 710-715.

Fortin, M. C, F. J. Pierce, and M. Edwards, 1994: Corn leaf area response to early season soil temperatures under crop residue. *Agron. J.*, **86**: 355-359.

Herrero, M. P., and R. R. Johnson, 1980: High temperature stress and pollen viability of Maize. *Crop ScL,* **30**, 796-800.

Hollinger, S. E., and S. A. Changnon, 1993: Response of corn and soybean yields to precipitation augmentation, and implications for weather modification in Illinois. Illinois State Water Survey Bulletin 73, Champaign, Illinois, pp. 95.

Huff, F. A. and S. A. Changnon, 1972: Evaluation of potential effects of weather modification on agriculture. *J. Appl. Metero.,* **11**, 376-384.

Jones, R. J., B. G. Gengenbach, and V. B. Cardwell, 1981: Temperature effects on in vitro kernel development of maize. *Crop ScL,* **21**, 761-766.

Jones, R. J., S. Ouattar, and R. K. Crookston, 1984: Thermal environment during endosperm cell division and grain filling in maize: Effects on kernel growth and development in vitro. *Crop ScL,* **24**, 133-137.

Jones, R. J., J. Roessler, and S. Ouattar, 1985: Thermal environment during endosperm cell division in maize: Effects on number of endosperm cells and starch granules. *Crop ScL,* **25**, 830-834.

Lehenbauer, R. A., 1914: Growth of maize seedlings in relation to temperature. *Physiol. Res.,* **1**, 247-288.

Ludlow, M. M., M. J. Fisher, and J. R. Wilson, 1985: Stomatal adjustments to water deficits in three tropical grasses and a tropical legume grown in controlled conditions and in the field. *Aust. J. Plant Physiol.* **13**, 33-43.

Loomis, R. S., and D. J. Connor, 1992: *Crop Ecology Productivity and management in agricultural systems.* Cambridge Univ. Press, New York, NY., pp. 538.

McKee, G. W. 1964: A coefficient for computing leaf area in hybrid corn. *Agron. J.,* **56**, 240-241.

Monteith, J. L., 1969: Light interception and radiative exchange in crop stands. In: Eastin, J. D., F. A. Haskins, C. Y. Sullivan, and C. H. M. Van Bavel, eds. *Physiological Aspects of Crop Yield.* Amer. Soc. of Agron., Crop Sci. Soc. of Amer. Madison Wisconsin, p. 89-111.

Nafziger, E. D., 1994: Corn planting date and plant population. *J. Prod. Agric,* **7**, 59-62.

Rosenberg, N. J., B. L. Blaid, and S. B. Verma, 1983: *Microclimate the Biological Environment,* 2nd ed. Wiley Interscience, New York, NY., pp 495.

Runge, E. C. A., 1968: Effects of rainfall and temperature interactions during the growing season on corn yield. *Agron. J.*, **60**, 503-507.

Warrington, I. J., and E. T. Kanemasu, 1983a: Corn growth response to temperature and photo period I: Seedling emergence, tassel initiation, and anthesis. *Agron. J.* **75**: 749-754.

Warrington, I. J., and E. T. Kanemasu, 1983b: Corn growth response to temperature and photo period II: Leaf-initiation and leaf-appearance rates. *Agron. J.* **75**: 755-761.

Watts, W. R., 1972a: Leaf extension in Zea mays L. I. Leaf extension and water potential in relation to root zone and air temperatures. *J. Exp. Bot.* **23**: 704-712.

Watts, W. R., 1972a: Leaf extension in Zea mays L. IL Leaf extension in response to independent variation of the temperature of the apical meristem, of the air around the leaves and of the root zone. *J. Exp. Bot.* **23**: 713-721.

Wilks, D. S., 1995: *Statistical Methods in the Atmospheric Sciences.* Academic Press, New York, NY., pp. 467.

APPENDIX

PROJECT PUBLICATIONS

Bolero, G. A., D. G. Bullock, and S. E. Hollinger, 1995: Modifications in corn development leaf morphology, and grain yield due to early season soil temperature. *Agron. J.*, **88**, 385-390.

Bolero, G. A., S. E. Hollinger, and D. C. Bullock, 1994: Effect of early season soil temperature on ontogeny, morphology, and grain yield on corn. *Agron. Abstr.*, p 138.

Hollinger, S. E., D. G. Bullock, G. A. Bollero, 1996: Early season soil temperature effects on a maize canopy. Abstract in the 26th Annual Crop Simulation Workshop Program, Fort Collins, CO, April 9-11, 1996.

Hollinger, S. E., G. A. Bollero, M. Belding, and D. G. Bullock, 1996: Maize yield and canopy response to early season soil temperature. Preprint: 22nd Conference on Agricultural and Forest Meteorology, 76th AMS Annual Meeting, January 1996, Atlanta, GA. AMS, Boston, MA.

Hollinger, S. E., and S. A. Changnon, 1996: Timing rainfall increases to maximize corn response. Preprint: 13th Conference on Planned and Inadvertent Weather Modification, 76th AMS Annual Meeting, January 1996, Atlanta, GA. AMS, Boston, MA.

Hollinger, S. E., 1995: Corn yield responses to rainfall during different growth stages. Agronomy Abstracts, American Society of Agronomy, Madison, WI.

SECTION I

IMPACTS AND RESPONSES TO WEATHER AND CLIMATE CONDITIONS

Relationship of Weather and Climate to Government Policies (Changnon)

Service as the Governor's Science Advisor to the Illinois Global Climate Change Task Force has involved attendance at 14 meetings, the provision of climate change information to Task Force members, and the preparation of documents on climate change. Issue papers dealing with 1) climate change research, 2) research on the impacts of climate on Illinois, and 3) research about ways to adapt to climate change were prepared for the Task Force (Changnon and Wendland, 1994). The unique activities of the Task Force were also analyzed for atmospheric scientists (Changnon, 1994).

Impacts of Climate Change on the Chicago Area (Changnon)

A series of studies have been conducted since 1990 concerning the potential effects of climate change on the Chicago metropolitan area. Recent studies focused on two topics: 1) the effects of altered summer precipitation on transportation systems in Chicago (vehicles, mass transit, and airlines - Changnon, 1996), and 2) the reactions of Chicago agencies and related institutions to the issue of climate change (Lambright, Changnon, and Hardy, 1996). Activities have also included meetings with Chicago City Committees on Transportation, Parks, and the 1995 Heat Wave.

Detection of Climate Change in Illinois (Changnon)

The Dlinois Task Force on Global Climate Change requested a study of the long-term climate conditions in Illinois. The goal was to provide the state with information about the

potential onset of climate change and its dimensions. To this end, two investigations were made.

Historical records (1901-1995) of temperatures, precipitation, and hailstorms were assessed to detect the stations in the state with quality, long-term records of these conditions. Twelve cooperative weather stations, each with records exceeding 100 years and located in small communities, were identified. Testing of the quality of their temperature and precipitation data was performed. This work will be issued as a report in 1997. Second, historical hail records from weather stations were also assessed, and 42 Illinois stations were found to have long records of quality hail data. These data were analyzed and a report prepared (Changnon, 1996). The hail incidences , temperatures, and precipitation data for 1901-1995 do not show any evidence of a change in climate related to global warming.

Shifts in Precipitation and Streamflow **(Changnon, Demissie)**

Detection of effects of changing climate on the hydrologic responses of rivers can be complicated by changes in land use, drainage, and water use. To discern effects of human-caused changes in a basin and those due to precipitation over time, a comparison was made of annual mean flows and peakflows in Midwestern basins that experienced increases in annual precipitation and heavy rain events during 1940-1990 (Changnon and Demissie, 1996). Two pairs of basins, one pair in a rural area and one pair in an urbanized area, were selected for in-pair comparisons, with one basin in each pair experiencing more land use and drainage changes during 1940-1990 than the other basin.

All four basins experienced significant upward trends in annual precipitation and annual mean flows. Human-produced changes affecting runoff in both rural basins accounted for about

two-thirds of the fluctuations found in the mean river flows, and precipitation changes accounted for the other third. However, much of the change in peakflows in the rural basin undergoing sizable changes in drainage was due to these changes (85%) versus 75% in the rural basin without comparable shifts in drainage.

The mean and peak flows of the two urban basins showed considerably more response to precipitation shifts than those of the two rural basins. The urbanized area doubled within one urban basin during 1940-1990, and these sizable land use changes explained much more of the increase in mean flows and peakflows there than in the urban basin with less change in land use. By 1990, precipitation accounted for 69% of the upward trend in mean flows since 1941 in the heavily-developed urban basin, as compared to 37% of the trend in the less settled urban basin. For purposes of assessing climate change, the precipitation changes over fifty years in all basins produced marked uptrends in basin streamflow, but the magnitude of the precipitation effect was masked by the land use and drainage changes. The results illustrate the need for careful analysis of natural basin characteristics (soils and basin shape), land use and drainage changes, and of various precipitation conditions if the influence of shifting precipitation on hydrologic conditions is to be detected, accurately measured, and correctly interpreted. For such studies the paired basin comparison techniques appears to be a valuable approach (Changnon and Demissie, 1996).

APPENDIX

PROJECT PUBLICATIONS

Changnon, S.A., 1993: Mud, flood and the Illinois River. *Proceedings, 1993 Governor's Conference on the Management of the Illinois River System*, Fourth Biennial Conference, Hotel Pere Marquette, Peoria, IL, Sept. 21 -22, pp 28-41.

Shealy, R.T., and S.A. Changnon, 1993: Value of summer season precipitation predictions in decisions about use of precipitation modification. *J. Applied Meteor*. **32(1**1): 1774-1777.

Westcott, N.E., 1993: Preliminary examination of urban/rural differences in cloud-to-ground lightning frequency for 19 central United States cities. *Preprint, AMS Conference on Atmospheric Electricity*, St. Louis, MO, American Meteorological Society, Oct. 4-8, 1993, pp. 752-755.

Changnon, S.A., and W.M. Wendland, 1994: *What Is and Is Not Known about Climate Change in Illinois: The Scientific Perspective*. Illinois State Water Survey Miscellaneous Publication 156, May 1994, 65 pp.

Changnon, S.A., R.R. Czys, and S. Hollinger, 1994: The integration of Meteorological, technological, economic, and legal factors affecting use of precipitation modification in the central United States. *Preprint*, 4 pp.

Czys, R.R., 1994: Preliminary laboratory results on the coalescence of small precipitation-size drops falling freely in a refrigerated environment. *J. of Atmos. Sci.*, **51** (21): 3209-3218.

Travis, D.J., A.M. Carleton, and S. Changnon, 1994: The radiative properties of jet contrails analyzed using AVHRR data. *Preprint, AMS Conference on Satellite Meteorology,* 1994. 2 pp.

Westcott, N.E., 1994: Merging of convective clouds: cloud initiation, bridging, and subsequent growth. *Monthly Weather Rev*. **122** (5): 780-790.

Changnon, S.A. 1995: Findings of the Illinois Global Climate Change Task Force: A Major Development of Policy at the State Level. *Preprints Sixth Symposium on Global Change Studies*, Amer. Meteor. Soc., 73-74.

Changnon, S.A., 1995: State roles in the global climate change issue. *Bulletin Amer. Meteor. Soc.*, **76**, 227-233.

Changnon, S.A., 1995: *Temporal Fluctuations of Hail in Illinois*. Misc. Publ. 167, Illinois State Water Survey, Champaign, 19 pp.

Changnon, S.A., K.R. Gabriel, N.E. Westcott, and R.R. Czys, 1995: Exploratory analysis of seeding effects on rainfall: Illinois 1989. *J. Applied Meteor*. **34**(2): 1216-1224.

Czys, R.R., 1995: Preliminary laboratory results on the mechanical nucleation of ice in bulk supercooled water. *Proceedings, AMS Conference on Cloud Physics,* Dallas, TX, American Meteorological Society, Jan. 15-20, 1995,4 pp.

Czys, R.R., 1995: Preliminary observation evidence of a collision-freezing ice initiation mechanism. *Proceedings, AMS Conference on Cloud Physics,* Dallas, TX, American Meteorological Society, Jan 15-20, 1996, 5 pp.

Czys, R.R., 1995: Progress in planned weather modification research: 1991-1994. *Reviews of Geophysics, Supplement.* pp 823-832.

Czys, R.R., S.A. Changnon, N.E. Westcott, R.W. Scott, and M.S. Petersen, 1995: Responses of warm-based, Midwestern cumulus congestus to dynamic seeding trials. *J. Applied Meteor*. **34** (5): 1194-1214.

Fortune, M.K. Labas, and N.E. Westcott, 1995: Accuracy of point rainfall estimates from an WSR-88D radar in the cool season: The Illinois Experience. *Preprint, 27th AMS Conference on Radar Meteorology,* Vail, Colorado, American Meteorological Society, Oct 3-9, 1996, pp. 614-616.

Hollinger, S.E., R.R. Reitz and R.A. Peppier, 1995: Illinois climate network site evaluation of obstructions to wind flow. *Preprints, 9th AMS Conference on Applied Climatology*, Dallas, TX, American Meteorological Society, Jan 15-20, 1996, 4 pp.

Huff, F.A., 1995: Characteristics on contributing causes of an abnormal frequency of flood-producing rainstorms at Chicago. *Water Resources Bulletin,* 31, 703-714.

Huff, F.A., 1995: Record-breaking microstorm system supports new rainfall following estimates in Illinois. *Bulletin Amer. Meteor. Soc.,* **75**, 1223-1226.

Kennedy, P.C., N.E. Westcott, and R.W. Scott, 1995: Reply. *Monthly Wea. Rev.* 123(1):235-238.

Travis, D.J., 1995: Variations in contrail morphology and relationships to atmospheric conditions. *J. Wea. Mod.,* **28**, 50-58.

Westcott, N.E., 1995: Spatial trends in lightning frequency in and around major midwestern cities. *Preprints, 9th AMS Conference on Applied Climatology,* Dallas, TX, American Meteorological Society, Jan. 15-20, 1995, pp 319-324/

Westcott, N.E., 1995: Summertime cloud-to-ground lightning activity around major midwestern urban areas. *J. of Appl. Meteor.* **34**(7): 1633-1642.

Westcott, N.E., R.W. Scott, and M. Dixon, 1995: Comparison of storms occurring during normal and dry convective rain seasons. *Preprint, 27th AMS Conference on Radar Meteorology,*

Vail, Colorado, American Meteorological Society, Oct. 3-9, 1996, 612-613.

Bollero, G.A., D.G. Bullock, and S.E. Hollinger, 1996: Soil temperature and planting date effects on corn yield, leaf area and plant development. *Agronomy J.,* **88**(3): 385-390.

Changnon, S.A., 1996: Comments on the marketing of science: Users are a key—an example of the value of scientific information. *Bulletin Amer. Meteor. Soc.,* **77**, 2729-2735.

Changnon, S.A., 1996: Effects of summer precipitation on urban transportation. *Climatic Change,* **32**, 481-494.

Changnon, S.A., 1996: Global climate change crosses state boundaries. *Forum,* **11**, 72-76.

Changnon, S.A., 1996: Impacts and responses to the 1995 Heat Wave: A focus on Chicago. *Preprints Symposium on Environmental Applications,* Amer. Meteor. Soc., 31-33.

Changnon, S.A., 1996: The Lessons from the Flood. In *The Great Flood of 1993*, Westview Press, Boulder, CO, 300-320.

Changnon, S.A., 1996: Losers and Winners: A Summary of the Flood's Impacts. In *The Great Flood of 1993*, Westview Press, Boulder, CO, 276-299.

Changnon, S.A., and M. Demissie, 1996: Detection of changes in streamflow and floods resulting from climate fluctuations and land use damage changes. *Climatic Change,* **32**, 411-421.

Changnon, S.A., and F.A. Huff, 1996: *A Scientific-Historical Review: The Atmospheric Sciences Program at the Illinois State Water Survey.* ISWS Miscellaneous Publication 171, Champaign, 341 pp.

Changnon, S.A., F.A. Huff, K.E. Kunkel, R. Scott, and N. Westcott, 1996. *Dry Periods in Illinois.* Contract Report 599, Illinois State Water Survey, Champaign, 144 pp.

Czys, R.R., R.W. Scott, and M.S. Petersen, 1996: Coalescence activity in Illinois and its relationship to choice of seeding technique. *Preprint, 13th AMS Conference on Planned and Inadvertent Weather Modification,* American Meteorological Society Annual Meeting, Atlanta, GA, American Meteorological Society, Jan. 28 - Feb. 2, 1996, 4 pp.

Hollinger, S.E., G.A. Bollero, M. Belding, and D.G. Bullock, 1996: Maize yield and canopy responses to early season soil temperature. *Preprint, 22nd Conference on Agricultural and Forest Meteorology,* American Meteorological Society Annual Meeting, Atlanta, GA, American Meteorological Society, Jan. 28 - Feb. 2, 1996, 5 pp.

Hollinger, S.E. and S.A. Changnon, 1996: Timing of rainfall increases to maximize corn response. *Preprint, 13th AMS Conference on Planned and Inadvertent Weather Modification,* American Meteorological Society Annual Meeting, Atlanta, GA, American Meteorological Society, Jan. 28 - Feb. 2, 1996, 3 pp.

Kopp, F.J, H.D. Orville, and R.R. Czys, 1996: Numerical simulations of the effects of cloud seeding on Illinois clouds. *Preprint, 13th AMS Conference on Planned and Inadvertent Weather Modification,* American Meteorological Society Annual Meeting, Atlanta, GA, American Meteorological Society, Jan. 28 - Feb. 2, 1996, 7 pp.

Lambright, W.H., S.A. Changnon, and D. Harvey, 1996: Urban reaction to the global warming issue: Agenda setting in Toronto and Chicago. *Climatic Change,* **34**, 463-478.

Scott, R.W., 1996: Summertime thermodynamic conditions in Illinois during dry periods related to weather modification. *Preprint, 13th AMS Conference on Planned and Inadvertent Weather Modification,* American Meteorological Society Annual Meeting, Atlanta, GA, American Meteorological Society, Jan. 28 - Feb. 2, 1996, 4 pp.

Scott, R.W., and S.A. Changnon, 1996: Climatic effects of the Great Lakes confound detection of inadvertent weather and climate change. *Preprint, 13th AMS Conference on Planned and Inadvertent Weather Modification,* American Meteorological Society Annual Meeting, Atlanta, GA, American Meteorological Society, Jan. 28 - Feb. 2, 1996, 4 pp.

Westcott, N.E., 1996: Land-lake differences in thunderstorm activity in the vicinity of cities near Lake Michigan. *Preprint, 13th AMS Conference on Planned and Inadvertent Weather Modification,* Atlanta, Georgia, Amer. Meteor. Soc., Jan. 28-Feb. 2, 1996, 106-109.

Westcott, N.E., 1996: The potential for candidate clouds for cloud seeding during dry summers in Illinois. *Preprint, 13th AMS Conference on Planned and Inadvertent Weather Modification,* American Meteorological Society Annual Meeting, Atlanta, GA, American Meteorological Society, Jan. 28 - Feb. 2, 1996, 4 pp.

Westcott, N.E., 1996: The potential for candidate clouds for cloud seeding during dry summers in Illinois. *Preprint, 13th AMS Conference on Planned and Inadvertent Weather Modification,* Atlanta, Georgia, American Meteorological Society, Jan 28-Feb. 2, 1996, 77-80.

Travis, D.J., A.M. Carleton, and S.A. Changnon, 1997: An empirical model to predict widespread occurrences of contrails. *J. Applied Meteoro.,* in press.

Changnon, S.A., 1997: Climate change and the water levels of the Great Lakes. *Shore and Beach,* **28**, in press.

Changnon, S.A., and F.A. Huff, 1997: Atmospheric sciences at the Illinois State Water Survey: Five decades of diverse activities and achievements. *Bulletin Amer. Meteor. Soc.,* **78**, in press.

AN ANALYSIS OF POSSIBLE CONTRAIL INFLUENCES ON DIURNAL TEMPERATURE RANGE

By

David J. Travis

Department of Geography
University of Wisconsin-Whitewater

Final Report for Subcontract - June 1, 1995- May 31, 1996*

This report also includes certain activities completed during the previous funding period of January 1, 1995- May 31, 1996

Table of Contents

Page Number

Section

Objective of the Study 289

Acquisition of Climate and Satellite Data 290

Acquisition and Scaling of Contrail Data 292

Scaling and Preliminary Analysis of Climate Data 293

Statistical Comparison of DTR to Contrail Coverage 294

Case Study Analysis of a Contrail Outbreak 308

Summary 310

References 311

Appendix 1 312

Appendix 2 314

1. Objective of the study

The primary objective of this study was to identify possible influences of jet condensation trails (contrails) on the diurnal temperature range (DTR) at the surface across the United States. This was accomplished in two ways:

The first was via an analysis of long-term trends (past 60 years) in DTR in the United States. Effects of contrails are believed to reduce DTR due to their unique microphysical characteristics and their location at relatively high altitudes in the troposphere (Beckwith, 1972). The high altitude location allows them to act similar to natural cirrus clouds and efficiently trap outgoing longwave radiation, especially at night, thus producing a "warming" effect in the atmosphere. However, this influence can at least be partially offset during the daytime since contrails efficiently absorb and/or reflect solar radiation (a "cooling" effect). The ability of contrails to efficiently block solar radiation is attributed to their relatively high optical thickness at the solar wavelengths, which is a result of the large number of small ice crystals that make up contrails, and resultant greater optical depth, compared to the relatively small number of large ice crystals that comprise natural cirrus (Mulcray, 1970). Though the net influence of these competing effects, when averaged across 24 hours, is probably close to zero (Travis, 1994), their influence on temperature *range* should result in an overall reduction of DTR.

Recent studies investigating changes in DTR have reported regional-scale decreases in the U.S. during the 20th century (e.g. Karl et. al, 1993). It is possible that contrails may have contributed to this decrease, especially within those regions that have received the greatest amount of contrail coverage (e.g. the Midwest U.S.). The present study investigated such a hypothesis by analyzing the historical temperature data for two periods, one immediately prior to

and the other immediately following the rapid increase of contrail coverage which occurred in the early 1960's (Beckwith, 1972).

The second approach utilized to study contrail influences on DTR was a case study investigation where an individual "outbreak", or large group, of contrails persisted over a specific region of the United States for an extended period (greater than 24 hours). This approach allowed a detailed determination of the influence that the contrails may have had on DTR within the affected region. The analysis was completed by studying hourly surface data and high resolution satellite imagery corresponding to the time of the contrail outbreak and the region of interest.

2. Acquisition of Climate and Satellite Data

The primary accomplishment during the first half of the funding period (June 1- December 31, 1995) was the completion of data acquisition and its preparation for analysis. This included the purchase of climatological data (both first order and cooperative stations) for the U.S. (1895-1994) and the purchase of all historical weather fields for the U.S. (1905-1994) on a total of three compact diskettes and eight magnetic tapes. The data had been archived by the National Climate Data Center from a total of 3,656 stations, including 318 National Weather Service (NWS) first order stations. Prior to purchase, all of the data had been corrected and standardized to remove potential biases related to (1) differences in observation times, (2) missing observations, and (3) inhomogeneous records primarily related to stations relocating within the period of record. Additional correction factors had been applied to many of the NWS first order stations to account for variations in urban influences on the station record (e.g. urban heat island,

exposure, etc.). Such adjustments ensured maximum consistency between the first order stations and the cooperative stations.

Two periods of climatological data were of greatest interest for this study. These were the periods 1931 -1960 and 1961-1990. These periods were selected for comparison because they represent the two climatological "normal" periods closest to the early 1960's. By comparing the "normals" for the 1931-1960 period with those of the 1961-1990 period, and considering where contrail coverage was greatest during the 1961-1990 period (see Section #3 below), it was possible to test the aforementioned hypothesis. Also, by comparing data from two adjacent periods the influences of other anthropogenic (e.g. global warming, land use changes, etc.) or natural sources of climate change were likely to be of less importance.

Additional periods of interest were the mid-season months of 1987 (January, April, July, October). These months were selected for case study analysis due to the availability of twice daily high resolution satellite imagery for each. The data consisted of daily hard copy swaths of Defense Meteorological Satellite Program (DMSP) high resolution imagery (2.6 km) and Advanced Very High Resolution Radiometer digital imagery (AVHRR) (1.1 km). The DMSP data were inspected manually for "candidate outbreaks" and then the AVHRR analyzed in more detail on computer when a candidate was selected for further analysis. Approximately 3-5 images (of DMSP and AVHRR combined) per day were available.

When a candidate outbreak was selected from the satellite imagery for further analysis it was also necessary to extract the corresponding surface climate data from compact disk. This primarily consisted of hourly observations from first order NWS stations. The data were then analyzed in correspondence with the timing of the outbreaks, as viewed on the satellite imagery,

to determine possible contrail effects on DTR. A minimum of 24 hours of data (including at least one nighttime and one daytime period) were analyzed for each selected case study.

3. Acquisition and Scaling of Contrail Data

A final data acquisition task was to obtain the contrail "climatology" data from the DeGrand (1991- Indiana University M.S. Thesis) study. These data represented the only comprehensive analysis of contrail coverage available for the U.S. and were completed for the mid-season months of 1977-79 using high resolution DMSP (1.6 km) hard copy imagery. Prior to arrival the data had been summarized in 1 × 1 degree (latitude/longitude) grids covering the entire U.S. and adjacent coastal waters in units of the number of contrails per grid per day. Each grid value had also been standardized by considering the number of satellite image swaths available for inspection per grid per day (DeGrand, 1991).

Once the data were obtained it became necessary to scale them up to a 3 × 3 degree grid resolution. This was done to maximize spatial consistency with the climate data which did not have a sufficient density of stations to complete statistical analyses at a 1 1 degree resolution. Moreover, the typical size of contrail outbreaks tends to be closer to a 3 × 3 degree grid size (Carleton and Lamb, 1986). Since contrail *outbreaks* are more likely to modify DTR rather than individual contrails, this was deemed a more appropriate scale to complete the analysis. Following the scaling procedure, a total of 99 grid values of contrail coverage were available for the U.S. and adjacent coastal waters for comparison with the climate data.

The value of contrail coverage calculated for each grid was assumed to be representative of the typical amount of coverage for that grid for the entire 1961-1990 period. Though it is

likely that the actual amounts of coverage per grid had increased with the increase in jet traffic throughout the period, the fact that the DeGrand (1991) study was completed for the period 1977-1979, which is approximately half way through the 1961 -1990 period, allowed an assumption that the values represented a fair estimate of contrail coverage for the entire period. More importantly, the spatial variations in contrail coverage were likely to have remained consistent throughout the period since the flight corridors that most high altitude aircraft follow had changed little. This was confirmed by inspecting current and historical high altitude flight navigation charts (e.g. FAA, 1996). In addition, the results of a similar study by Travis (1994) for the mid-season months of 1987 demonstrated very close agreement with the spatial distribution of contrails found in the DeGrand (1991) study, even though it analyzed data for nearly 10 years later.

4. Scaling and Preliminary Analysis of Climate Data

To ensure consistency with the contrail data it was also necessary to calculate 3 × 3 degree grid averages of the climate data. To accomplish this task, each of the 3,656 stations included in the analysis were assigned to one of the corresponding 99 "contrail" grids based on their latitude and longitude. Once all stations were assigned a grid the values for stations within each grid were averaged to determine an overall grid value for each observation. Each of the 99 grids contained at least one station with the majority having between 30-40 stations.

Following the scaling of the climate data, average grid values of DTR were obtained for both the 1931-1960 and 1961-1990 periods. The DTR values were calculated by subtracting the average daily maximum and average daily minimum temperature value (listed by year and month

on the CD) for each grid and then averaged to obtain a "normal" DTR value for each period. The DTR values for the two periods were then subtracted from corresponding grids to obtain a change in DTR value for each grid. This provided a new variable labeled ADTR which is the measure of climate change that was used throughout this study.

5. Statistical Comparison of ADTR to Contrail Coverage

a. Pearson Correlation Tests

To test the hypothesis that contrail coverage had reduced DTR, it was necessary to complete statistical tests between ADTR and the scaled contrail data set (DeGrand, 1991). The statistical tests were completed in two ways. The first utilized Pearson correlation tests to determine if trends in the ADTR were negatively correlated with the amount of contrail coverage for each grid. This analysis was completed first by considering all of the grids for the U.S., and then second by stratifying the data set according to region (northeast, northwest, southeast, southwest) by season. The "regions" were determined by subdividing the contiguous U.S. into four approximately equal quarters divided by the 40° N latitude parallel and the 100°W longitude meridian with no specific consideration for physical boundaries. The "seasons" were defined using the standard 3-month meteorological definition for each (i.e. Winter: January, February, March; Spring: April, May, June; etc.)

Table 1 provides the results of the Pearson correlation analysis and level of significance (Prob > IRI) of the relationships between contrail coverage and ADTR for all seasons combined and stratified by season. Corresponding scatterplots for each can be seen in Figures 1-5. The

relationship is strongest for the Summer and Fall seasons. The greater abundance of days with clear sky conditions that exists over a large portion of the U.S. during those seasons is likely responsible for the increased importance of contrails during that time of the year. Without the influence of contrails (i.e. prior to 1960) there would have been a higher percentage of cloudfree days (and nights) and a greater likelihood for a large DTR. Hence, the Summer and Fall seasons were more sensitive to the influence of a contrail-induced increase in cloud cover than the Winter and Spring seasons where a large abundance of natural cloudiness tended to already exist. These results concur with those found by Changnon (1981) where he also showed the influence of contrails over the Midwest United States to be greatest during the Fall season and attributed this to the same explanation as that offered above.

Though all relationships between contrail coverage and ADTR are negative, which supports the primary hypothesis of this study, the r-values for the Winter and Spring seasons are low and not statistically significant. Nevertheless, the overall association when all seasons are combined is reasonably good and still statistically significant (Prob > IRI is less than 0.05). Scatterplots of contrail coverage versus ADTR stratified by region (and repeated for the entire U.S.) can be seen in Figures 6-9 with corresponding statistics summarized in Table 2. In all cases but the "southeast" region, there is a negative slope to the relationship, thus, once again supporting the hypothesis that increased contrail coverage has produced a decrease in DTR for much of the U.S. However, not all of the relationships are statistically significant.

The best association between ADTR and contrail coverage is for the "southwest" region of the U.S., with a relatively weak but still statistically significant negative fit when all regions are combined. The strong association between ADTR and contrail coverage for the "southwest"

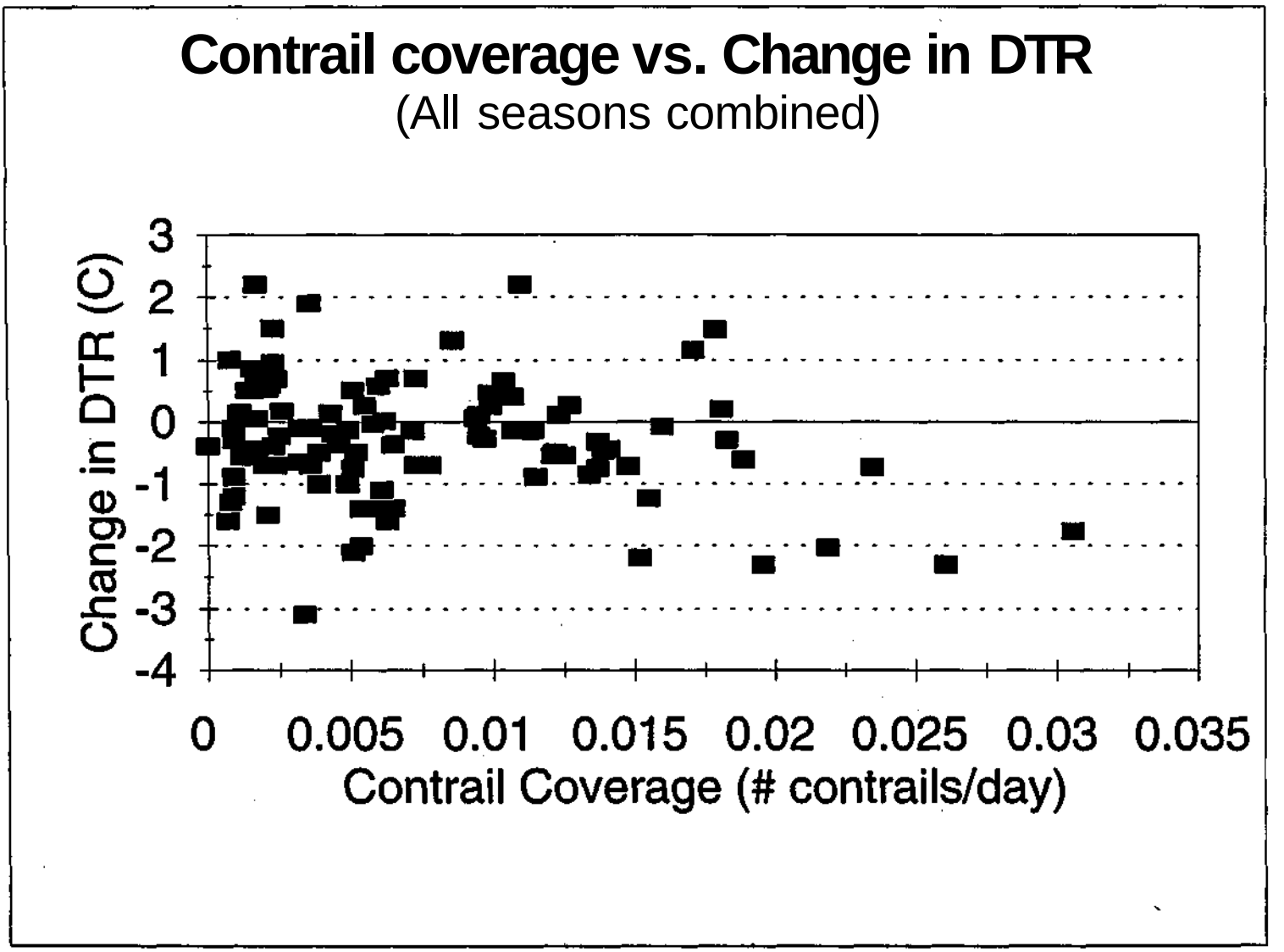

FIGURE 1: Scatterplot of the relationship between contrail coverage and ΔDTR for all seasons.

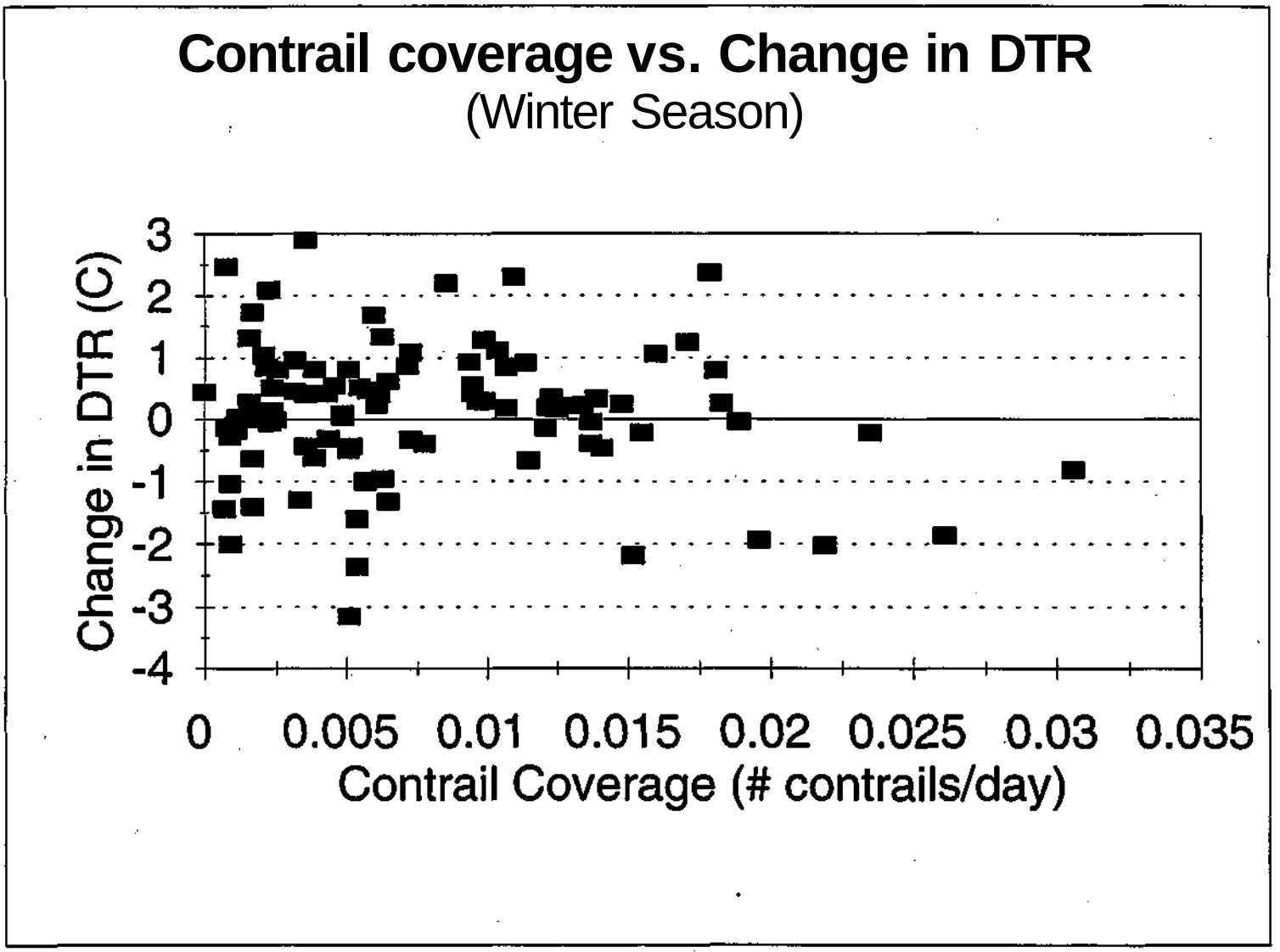

FIGURE 2: Same as Figure 1 but for Winter season only.

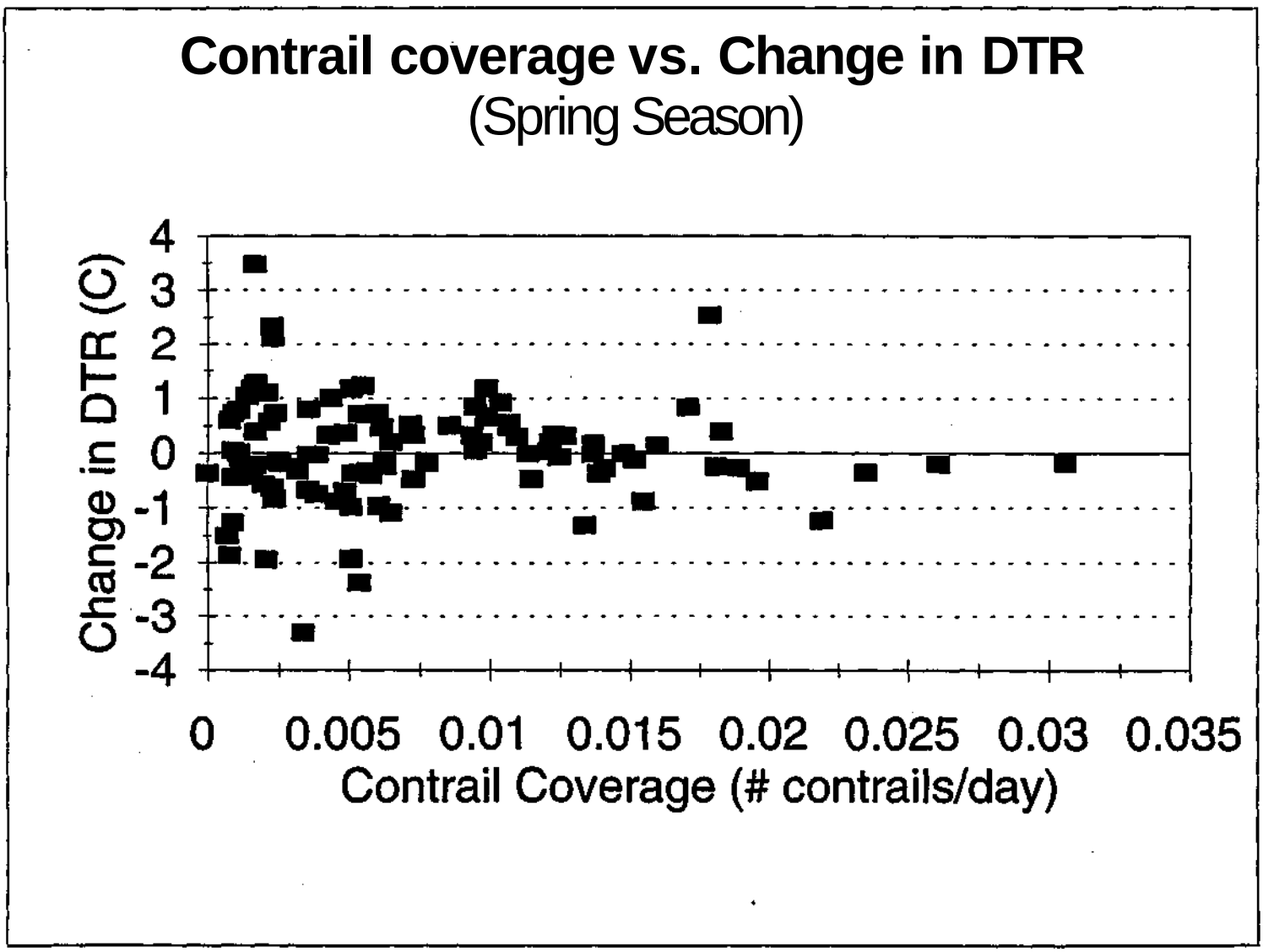

FIGURE 3: Same as Figure 2 but for Spring season only.

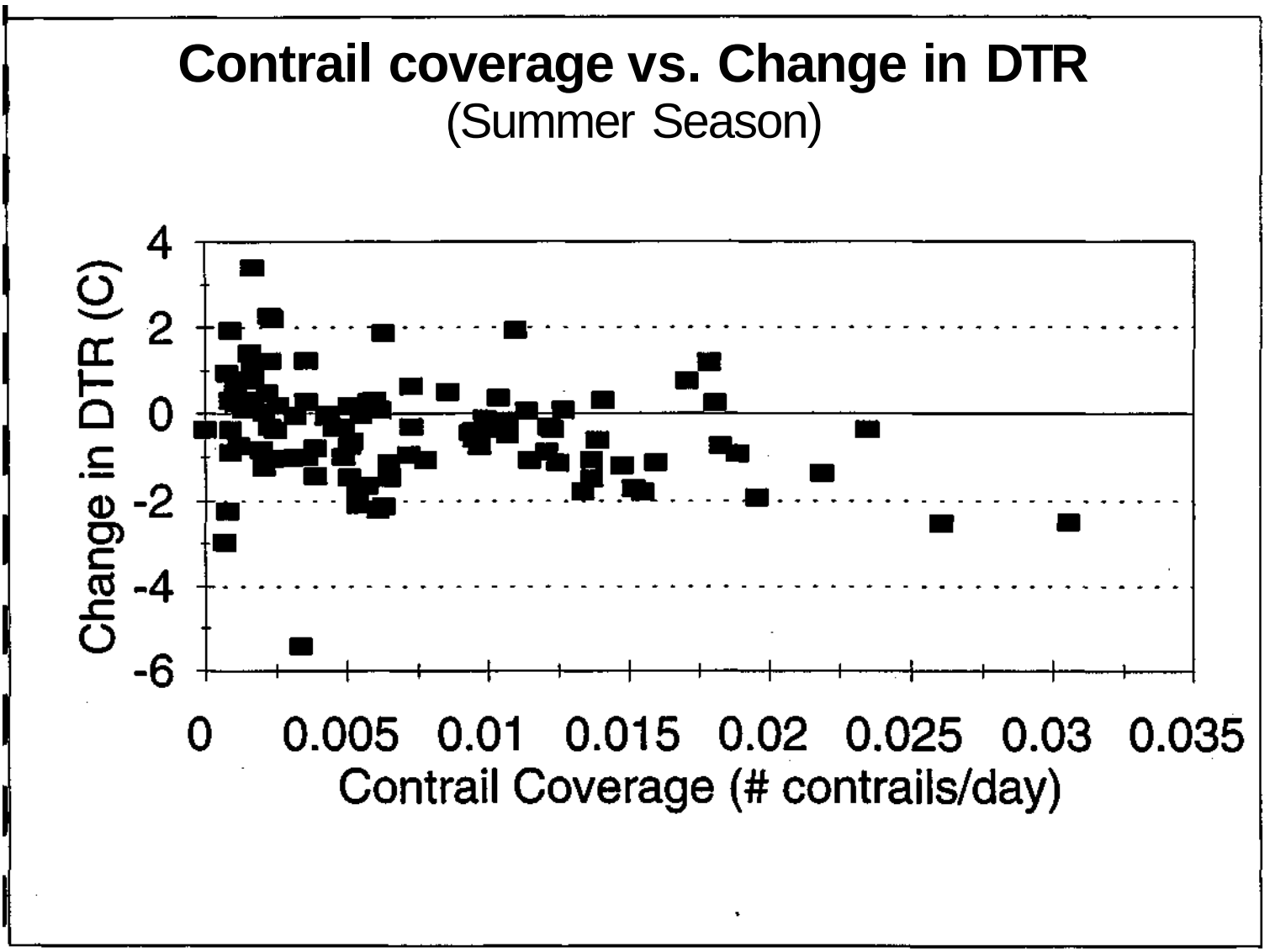

FIGURE 4: Same as Figure 3 but for Summer season only.

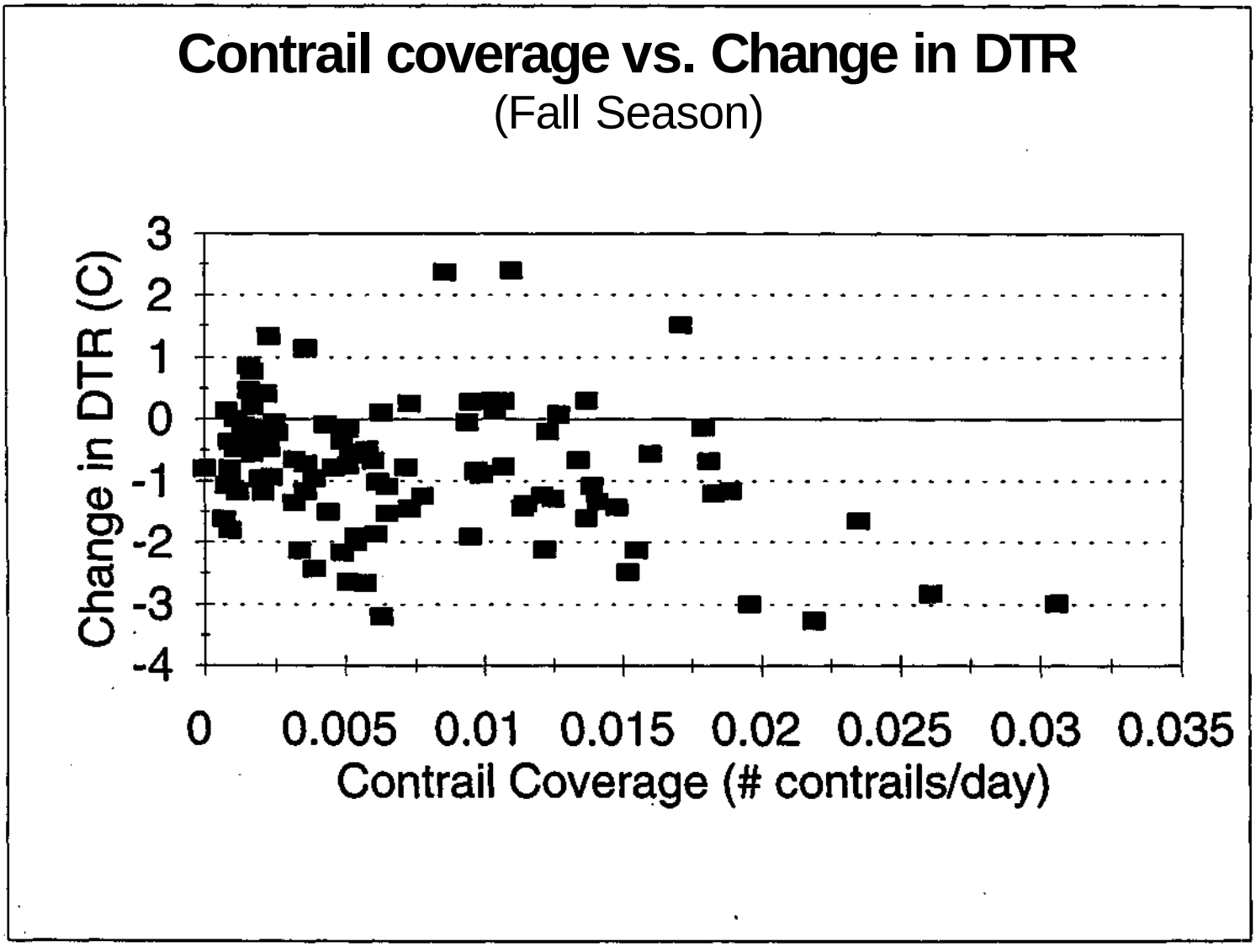

FIGURE 5: Same as Figure 4 but for Fall season only.

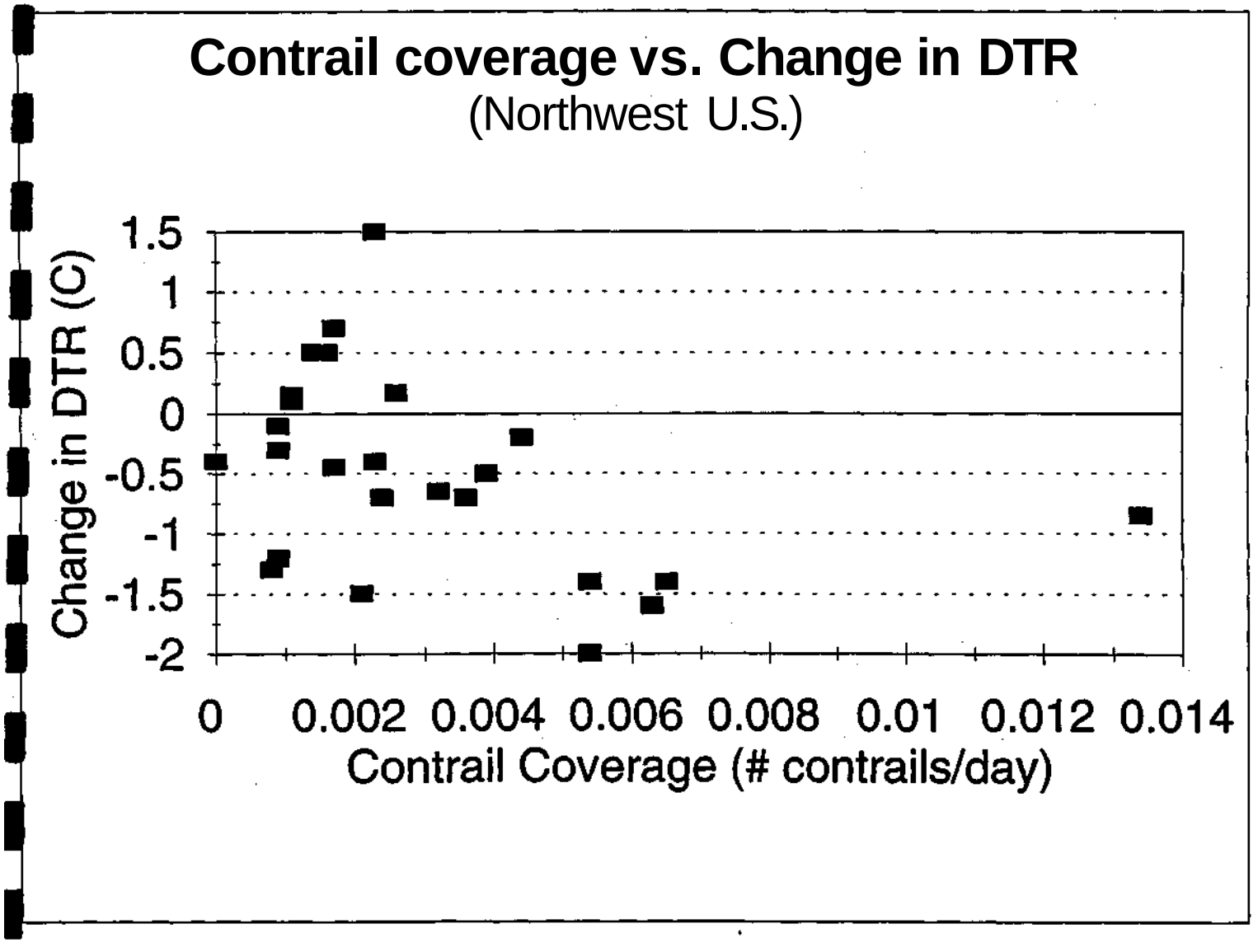

FIGURE 6: Same as Figure 5 but for the Northwest U.S. region only.

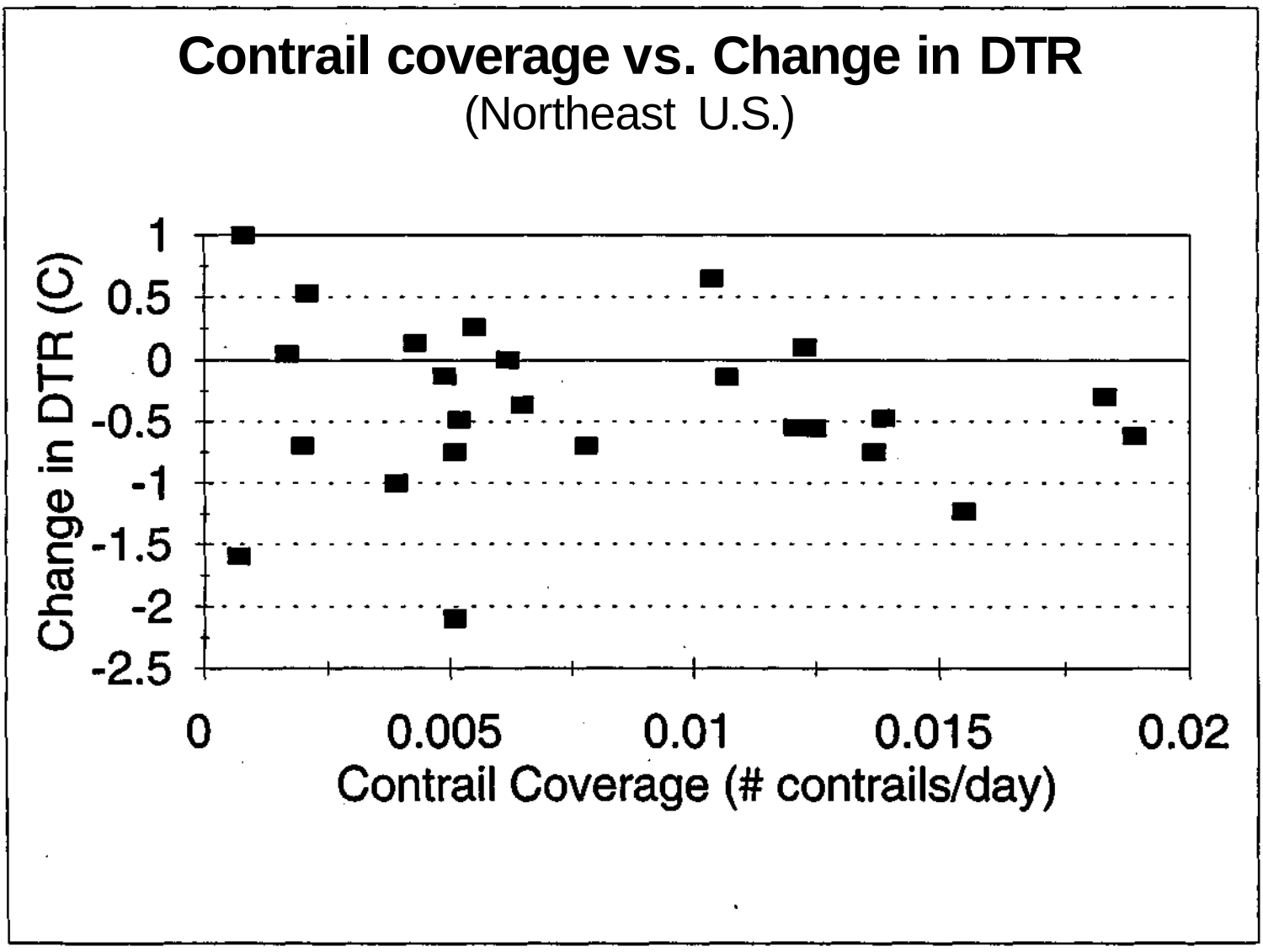

FIGURE 7. Same as Figure 6 but for the Northeast U.S. region only.

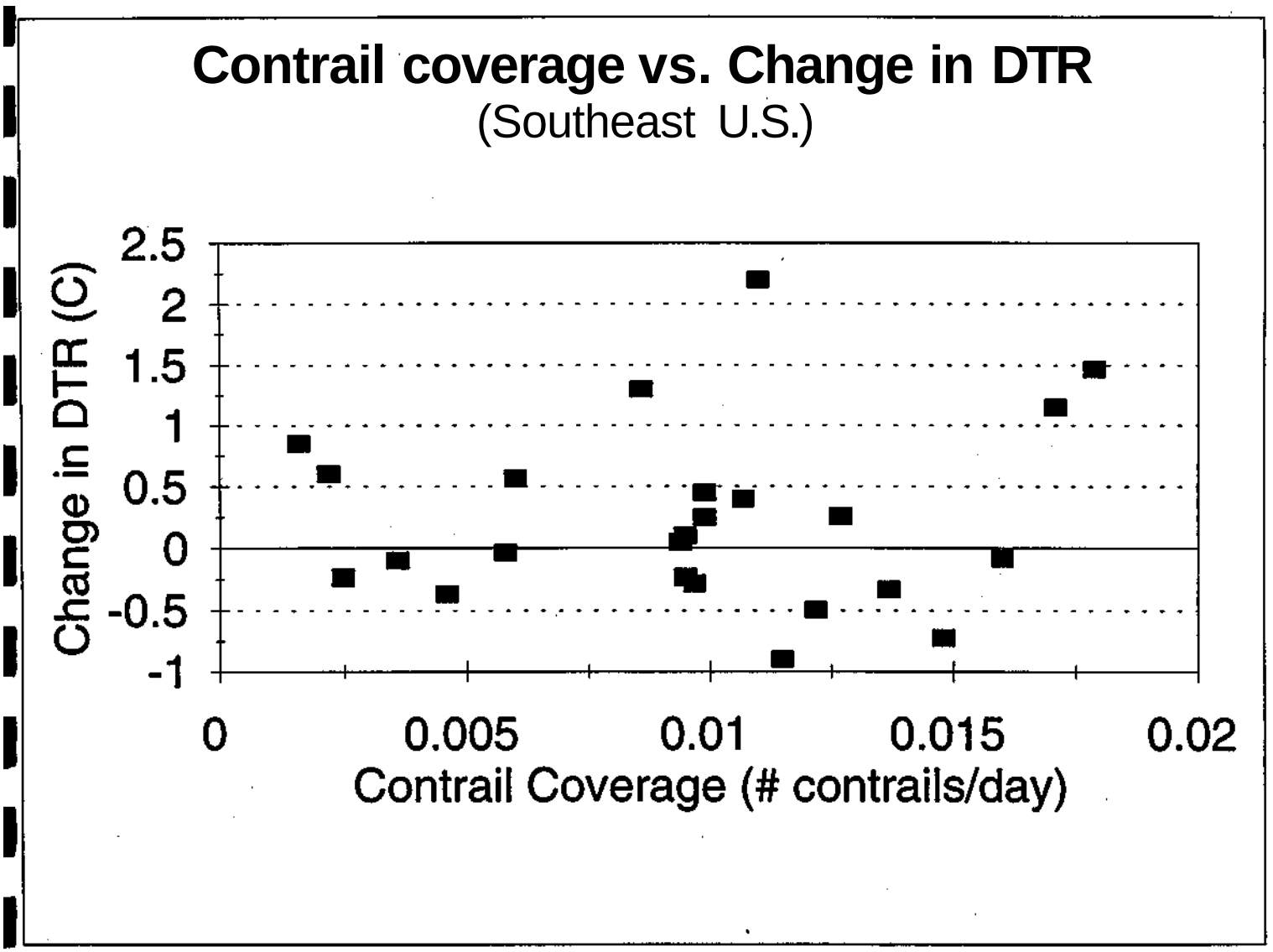

FIGURE 8: Same as for Figure 7 but for the Southeast U.S. region only.

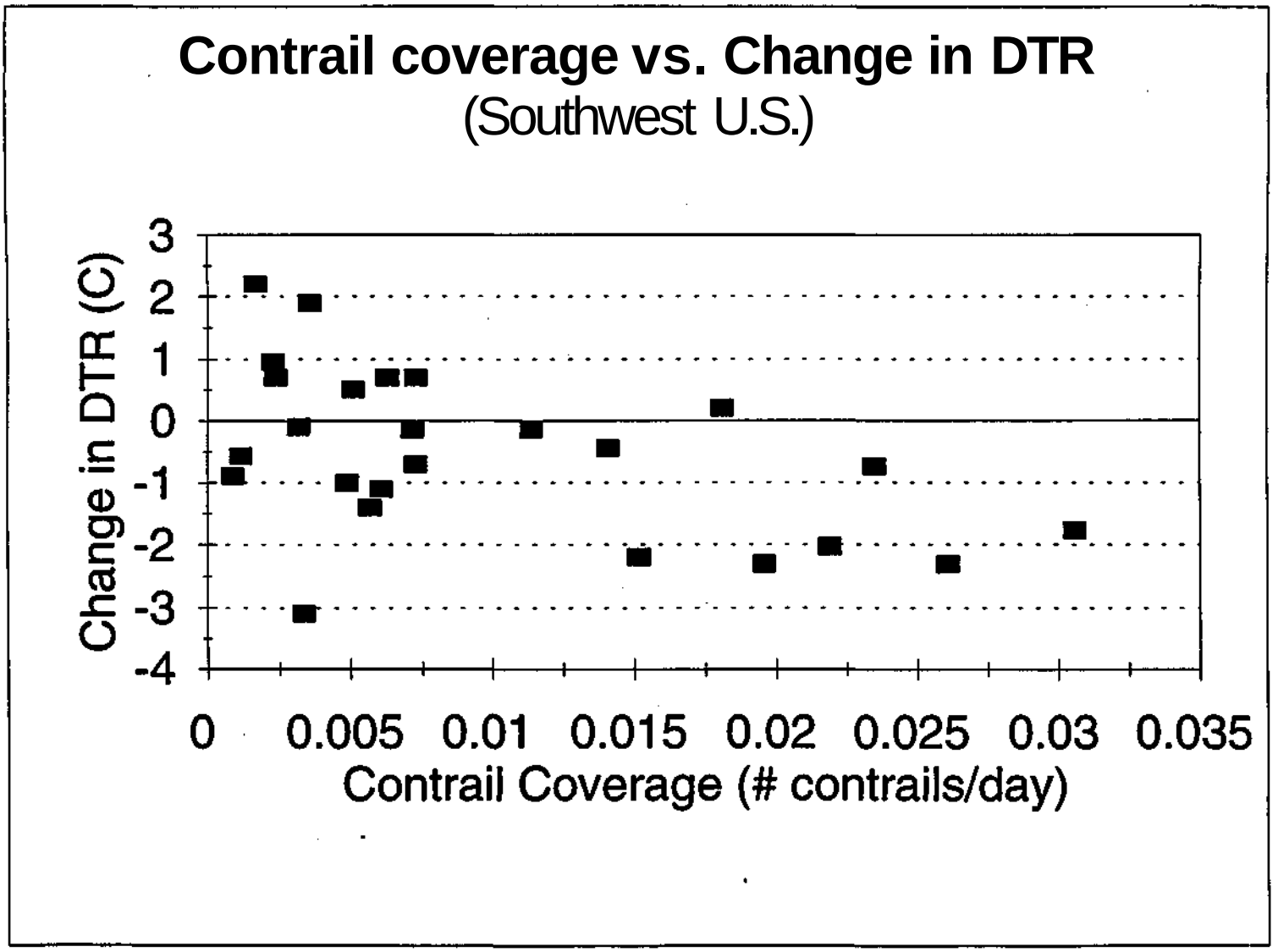

FIGURE 9: Same as Figure 8 but for the Southwest U.S. region only.

Table 1. Results of the Pearson correlation analysis by season.

Season	R-value	Prob > |R|	N
All	-0.22	0.03	99
Winter	-0.11	0.30	94*
Spring	-0.01	0.90	99
Summer	-0.27	0.01	99
Fall	-0.29	0.01	99

* The winter season data had 5 missing values.

region can be explained once again by the abundance of clear sky conditions that tend to prevail in that region of the U.S. where typically large values of DTR would be expected to naturally occur. The region would also, therefore, be most sensitive to any increase in clouds provided by jet contrail coverage. A similar effect would also be expected in the "northwest" portion of the U.S., at least during the warm season, which is usually accompanied by an extended period of dry conditions. This region too would, therefore, be more sensitive than other regions to any increase in clouds provided by jet contrail coverage. This may explain the relatively high r-value between contrail coverage and DTR corresponding to that region (-0.35).

This lack of a distinct dry season characterized by a large number of cloudfree days for the remainder of the U.S. provides a possible explanation for the relatively poor fit of the two eastern regions of the U.S. which are dominantly influenced by moisture from the Gulf of Mexico and/or

Table 2. Results of the Pearson correlation analysis by region.

Region	R-value	Prob > |R|	N
All	-0.22	0.03	99
NW	-0.35	0.09	24
NE	-0.12	0.58	25
SE	0.07	0.71	24
SW	-0.48	0.01	26

the Atlantic Ocean throughout most of the year. Additional consideration must also be given to the inability of the model to account for the influences of other climate change variables (e.g. natural variability, land use changes, global warming, etc.) which likely have also modified DTR and were not completely accounted for in the data standardizations (see Section #2). Nevertheless, the negative fit and the weak but consistent associations between contrail coverage and ADTR for a majority of the U.S. suggest that a relationship exists and supports the primary hypothesis of this study.

b. Difference of Means Testing

A second statistical method utilized to assess possible influences of contrail coverage on DTR was difference-of-means testing. This was done by simply determining the mean ADTR for each 3 × 3 degree grid (see section 4) containing significant contrail coverage and comparing that

value to the mean ADTR for those grids containing either no contrail coverage, or a small, insignificant amount. In this study a "significant amount" of contrail coverage was defined as 0.01 or greater contrails/grid/day. This threshold value was determined by comparing the average amount of contrail coverage in each of the peak regions in the U.S., as identified in the DeGrand (1991) study, to that amount found in other "non-peak" regions. Each of the peak areas contained values in excess of 0.01 contrails/grid/day, while most other areas that contained contrails had significantly less than that amount. Though contrails can occur anywhere in the U.S., it is unlikely that they will have a significant climatic influence unless they occur regularly and in clusters. The cutoff of 0.01 contrails/grid/day provided the largest statistical separation between the peak areas and the remainder of the U.S. Using this method, a total of 69 grids were placed into the non-contrail category with the remaining 30 grids classified as having significant contrail coverage (i.e. greater than 0.01 contrails/grid/day).

The average value of ADTR for grids containing greater than 0.01 contrails/day, and for those containing none or an insignificant amount, is summarized by season (and for the entire U.S.) in Table 3 along with standard deviation values (in parentheses). Since the overriding hypothesis of this study states that significant contrail coverage should only produce a *decrease* in DTR, a one-tailed t-test was completed only for those seasons where the ADTR was less (more negative or less positive) for the contrail grids than for the non-contrail grids. As a result, no tests were completed for the Winter and Spring seasons. The only significant difference of means was found for the Fall season ($p > t = 0.05$) with a moderately strong difference between contrail and non-contrail grids for the Summer season. Though the direction of the annual value of ADTR supports the hypothesis at -0.37, the difference is not statistically significant due to the poor

Table 3. Results of the Differences of Means Testing By Season.

Season	DTR Change (°C) for Grids with Insignificant Contrail Coverage	DTR Change (°C) for Grids with Significant Contrails Coverage	t-value Between Grids	p > t Between Grids
Annual	-0.26 (0.95)	-0.37 (1.03)	0.50	0.30
Winter	0.08 (1.10)	0.21 (1.13)	-	-
Spring	-0.02 (1.08)	0.09 (0.67)	-	-
Summer	-0.31 (1.34)	-0.62 (0.98)	1.29	0.10
Fall	-0.71 (0.94)	-1.07 (1.36)	1.54	0.05

relationship found for the Winter and Spring seasons. This follows previous results since those seasons are typically the cloudiest in the U.S. and contrails should not be expected to have a significant influence on DTR during that time of year.

The strength of the Summer and Fall results reinforces the importance of considering the contrail influence on DTR from a seasonal perspective rather then just on annual time scales. Moreover, these results, when considered in combination with those of the previous section, support the contention that subsequent investigations into contrail-DTR relationships should focus on arid or semi-arid regions during dominantly cloudfree seasons.

6. Case Study Analysis of A Contrail Outbreak

To investigate the contrail influence on surface climate from a case study perspective, it is important to find cases which permit, as clear as possible, a separation of the influence of contrails

from that of natural clouds or other factors which can influence DTR (e.g. soil moisture, mesoscale winds, etc.). The original objective of this study was to find a minimum of five case studies during the mid-season months of 1987 and complete a case study analysis of each. A total of 18 "candidate" outbreaks were identified on the DMSP occurring during the mid-season months. Though a sufficient number of candidates were identified, only one case matched the preset determined specifications for inclusion into the study (Table 4). The case study that qualified for analysis was an outbreak of contrails that occurred in the Midwest (centered over Illinois) on April 17-18, 1987. This outbreak persisted over the 5-state region surrounding Illinois

Table 4. Summary of Qualifications for a Contrail Outbreak to be Included in the Analysis

CHARACTERISTIC OF OUTBREAK	QUALIFICATION LEVEL
Duration	> 24 Hours
Size	> 300 km Diameter
Amount of Natural Cloud	< 25% of Total Cloud/Contrail Combined
Time of Last Precipitation Event	> 48 Hours

for approximately 30 hours, which increased the potential for the contrails to modify the diurnal temperature range within the region due to their persistence and widespread coverage. The location and density of the contrail coverage was identified using 5 AVHRR digital satellite images and 2 DMSP hard copy image swaths taken during the time of coverage. Moreover, the

persisting contrails were confirmed from surface observations of high clouds from hourly observations of first order NWS stations located within the outbreak region. A summary of the methods and results of this case study are provided in Appendix 1 (reprinted from Travis, 1996).

7. Summary

This study has provided circumstantial evidence suggesting a possible link between jet contrail coverage and a decrease in DTR in the U.S. since the early 1960's. The relationship is strongest for the "southwest" and "northwest" regions of the U.S. and most dominant during the Summer and Fall seasons. Though the influence of contrails on DTR is not statistically significant for the other regions of the U.S., nor during other seasons, the consistency of a negative relationship between contrail coverage and changes in DTR in nearly all cases provides justification for further investigation. Moreover, the influences of other climate change variables (e.g. urban heat island, global warming, etc.) which likely have had a more dominant impact on DTR than contrails were not assessed in this study. Future studies could potentially find better statistical results once the influences of these other variables are filtered out.

Acknowledgments

The principle investigator expresses appreciation to Maren Overby and Trent Blank, both undergraduate students at UW-Whitewater, for their assistance in the climatological data preparation and case study data collection of this project. The principle investigator also thanks Stanley Changnon for his assistance in preparation of this final report.

References

Beckwith, W.B. (1972). Future patterns of aircraft operations and fuel burnouts with remarks on contrail formation over the United States. *Preprints of the International Conference on Aerospace and Aeronautical Meteorology,* Amer. Met. Soc., Boston, MA, 422-426.

Changnon, S.A. (1981). Midwestern cloud, sunshine, and temperature trends since 1901: possible evidence of jet contrail effects. *J. Appl. Meteor.,* 20:496-508.

DeGrand, J.Q. (1991). A satellite-derived mid-season climatology of jet condensation trails: April 1977- October, 1979. *Unpub. M.A. thesis,* Dept. of Geography, Indiana University. 117 pp. plus appendices.

Detwiler, A. and R. Pratt (1984). Clear-air seeding: Opportunities and strategies. *J. Wea. Mod.,* 16: 46-60.

FAA (1996). *IFR enroute high altitude,* U.S., Dept. of Defense, Federal Aviation Administration, Dept. of Commerce, single maps.

Murcray, W.B. (1970). On the possibility of weather modification by aircraft contrails. *Mon. Wea. Rev.,* 98:(10)745-748.

Travis, D.J. (1994). Jet aircraft condensation trails: their radiative impacts and association with atmospheric conditions. *Unpublished Ph.D. Dissertation.* Indiana University, 118 pp.

Travis, D.J. (1996). Diurnal temperature range modifications induced by contrails. Preprints of the *Thirteenth Conference on Planned and Inadvertent Weather Modification,* pp. 110-111, Atlanta, GA, Jan. 28- Feb. 2.

APPENDIX 1

4.6 DIURNAL TEMPERATURE RANGE MODIFICATIONS INDUCED BY CONTRAILS

David J. Travis

University of Wisconsin-Whitewater
Whitewater, WI

I. INTRODUCTION

The potential for jet condensation trails (contrails) to modify surface climate has been speculated for much of the latter half of this century (e.g. Murcray, 1970; Carleton and Lamb, 1986). This is especially true for regions favored by a high density of jet traffic (e.g. the U.S. Midwest) where "outbreaks" of contrails can occur and persist in large groups continuously for a day or more. During such situations, contrails have been reported to obscure a majority of the sky. More recent observations from satellite data have confirmed their ability to modify the radiation budget (Goethe and Grassl, 1993, Travis *el al.*, 1994).

Contrails contain a high density of relatively small ice crystals (< 100 μrn) (Murcray, 1970), which creates a higher albedo than is characteristic of most high clouds and, therefore, a greater ability to decrease the amount of solar radiation reaching the surface (Goethe and Grassl, 1993). Hence, contrails are suspected to produce a "cooling" effect during the daylight hours. At night, contrails are assumed to act similar to most other natural clouds and "warm" the surface by trapping outgoing infrared radiation. Over a 24-hour period, the influence of contrails would, therefore, be expected to result in a reduction in the diurnal temperature range (DTR).

Asymmetric variations in DTR have recently been noted for the 20th century, with significant decreases in some areas of the U.S. (Karl *et al.*, 1994). Though jet contrail coverage is not considered sufficient to have a significant radiative influence on a global scale, they may play an important regional-scale role where they are most abundant. Similarities in the regional-scale nature of the DTR decreases and the peak locations of contrail occurrence suggests a link may exist between the two.

The present study investigates the surface climate influences of a single outbreak of contrails that occurred over the U.S. Midwest on April 18, 1987. A combination of satellite and National Weather Service (NWS) data are analyzed. The primary objective is to determine if the , presence of the contrail outbreak modified the diurnal temperature range within the area subjected to persistent contrail coverage.

2. DATA AND METHODS

The location of the outbreak of contrails was determined by analyzing a combination of one Defense Meteorological Satellite Program (DMSP) "hard copy" image and three Advanced Very High Resolution Radiometer (AVHRR) digital images, all for April 18, 1987. Both the DMSP (2.7km) and the AVHRR (1.1km) imagery provide sufficient pixel resolution to study persisting contrails (Carleton and Lamb, 1986). Images from each satellite overpass (8:50am, 10:00am, 3:15pm, and 8:10pm local time) were utilized to identify the location of contrails and then composited to determine the overall area influenced by jet contrails on this particular day (Fig. 1). It was possible to "enhance" the contrail signal for two of the AVHRR images by utilizing the "split-window IR" method (Lee, 1989).

Hourly temperature values were extracted for all available first order NWS stations located within the contrail outbreak region. Diurnal temperature range values were determined from the hourly values. Continuous data, for all 24 hours, was available from 31 NWS stations (Fig. **1).**

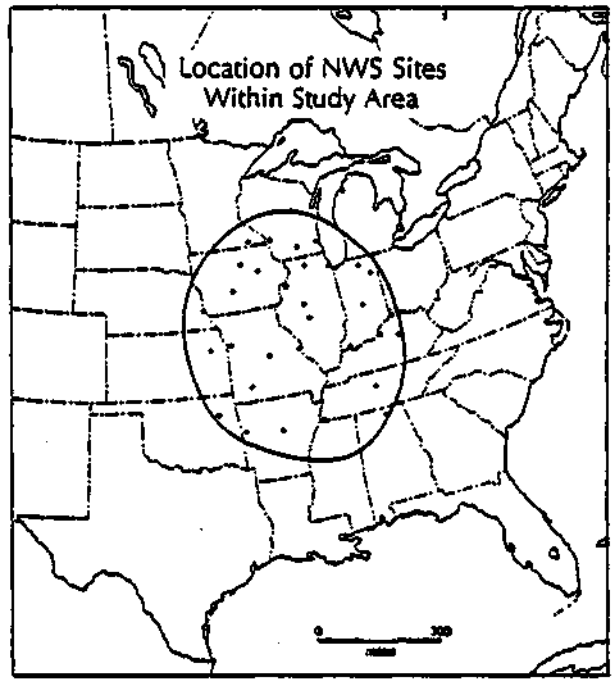

Figure 1. Locations of the contrail "outbreak" region and available NWS stations for April 18,1987.

To minimize the potential bias introduced by the clustering of NWS stations, point values of DTR were transformed into 3" × 3° grid values for the study area. When more than one NWS station was located within a single grid, the average DTR value was calculated from all point values within the grid. A total of 16 grid values were determined, with at least one NWS station located within each. Contouring was then completed, at a 1° C interval, from the midpoint of each grid.

3. RESULTS

a. Synoptic Conditions for the Study Area

Before identifying the influence of the contrails on DTR, it is appropriate to analyze the upper air conditions to better understand why contrail formation and persistence was so extensive for this particular time and location. Owing to it's close proximity to the center of the contrail areal coverage, data from the 12:00z sounding for Salem, IL (38.4° N 88.6° W) is selected for analysis (Table **1).**

Pressure (mb)	Height (m)	Temp (°C)	Dewpt. (°C)	Wind Dir. (Speed) (Deg.) (kts.)
1000	57	3.8	1.2	288 (3)
900	903	-0.7	-3.1	325 (9)
800	2143	-7.3	-9.7	303 (14)
700	3864	-14.3	-16.8	305 (15)
600	4531	-22.9	-29.9	281 (20)
500	5319	-34.5	-43.5	271 (23)
400	6859	-41.9	-	233 (21)
300	8779	-46.1	-	223 (37)
200	11469	-47.5	-	240 (31)

TABLE 1: Summary of sounding data for Salem, IL.

The data indicate that conditions within the 500-300mb layer, which is the most common altitude for contrail occurrence, are typical of those known to favor contrail formation and persistence (Travis *et al,* 1994). Wind shear associated with warm air advection is evident within this layer as well as a temperature generally between -35° C and -45° C. Though dewpoint information is unavailable above the 500mb level, there is apparently sufficient ambient moisture to support the persistence and growth of contrails following their initial formation from the jet exhaust.

b. Contrail Influence on DTR

A contour map of the DTR for April 18, 1987 for the study area is presented in Fig. 2. Results indicate that the smallest DTR occurred near the center of the study area with a gradual increase in DTR away from the center, especially to the north and south. By assuming that the overall coverage of contrails, during the entire 24-hour period, is most likely to have been greatest near the center of the study area, this result seems to support the hypothesis that the radiative influence of contrails reduces DTR.

To ensure that the pattern of DTR is not simply **a** result of **natural** cloud cover, a Pearson correlation calculation was completed between total (24 hour) cloud amount (determined from hourly observations) and DTR for each individual NWS station. No significant correlation was found ($R=0.04$; $p<0.81$). Hence, these results provide strong circumstantial evidence of a contrail influence on DTR.

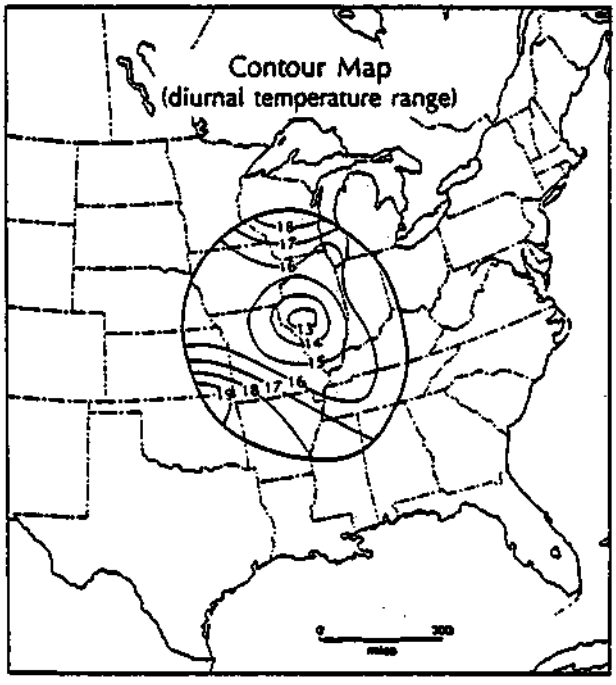

Figure 2: Contour map of DTR (at 1° C intervals).

Acknowledgement

This research funded by NOAA grant #NA47RA0225 via subcontract with the Illinois State Water Survey.

4. REFERENCES

Carleton, A.M. and P.J. Lamb (1986). Jet contrails and cirrus cloud: a feasibility study employing high resolution satellite image. *Bull. Amer. Met. Soc.*, 67:301-309.

Gothe, MB. and H. Grassl (1993). Satellite remote sensing of the optical depth and mean crystal size of thin cirrus and contrails. *Theor. App. Clim.*, 48:101-113.

Karl, T.R., Jones, P.D., Knight, R.W., Kukla, G., Plummer, N., Razuvayev, V., Gallo, K.P., Lindseay, J., Charlson, R.J., and T.C. Peterson (1993). Asymmetric trends of daily maximum and minimum temperature. *Bull. Am. Met. S*oc.,74(6):1007-1023.

Lee, T.F. (1989). Jet contrail identification using the AVHRR infrared split window. *J. App. Met.*, 28:993-995.

Murcray, W.B. (1970). On the possibility of weather modification by aircraft contrails. *Mon. Wea. Rev.*, 98:(10) 745-748.

Travis, D. J., Carleton, A.M., and S.A. Changnon (1994). The radiative properties of jet contrails analyzed using AVHRR data. *Seventh Conference on Satellite Meteorology and Oceanography*, Monterey, CA. pp. 283-284.

Appendix 2- Publications and Conference Presentations Supported by this Project

Publications

Travis, D.J., Carleton, A.M. and S.A. Changnon (In Review). An Empirical Model to Predict Widespread Occurrences of Contrails. *Jour. of Appl. Met.,* 23 page manuscript.

Travis, D.J. (1996). Variations in contrail morphology and relationships to atmospheric conditions. *Jour. of Wea. Mod.,* 28: 50-58.

Travis, D.J. (1996). Diurnal temperature range modifications induced by contrails. Preprints of the *Thirteenth Conference on Planned and Inadvertent Weather Modification,* pp. 110-111, Atlanta, GA, Jan. 28- Feb. 2.

Conference Presentations

Travis, D.J. (1995). Travis, D.J. (1995). "An Assessment of the Radiative Influence of Jet Contrails on Surface Climate", *44th Annual Meeting of the Weather Modification Association,* Durango, CO, May, 1995.

Travis, D.J. (1996). Diurnal temperature range modifications induced by contrails. *Thirteenth Conference on Planned and Inadvertent Weather Modification,* pp. 110-111, Atlanta, GA, Jan. 28- Feb. 2.


ILLINOIS
DEPARTMENT OF
NATURAL
RESOURCES